

**DEFORMATION CHARACTERISTICS OF SCALY CLAY
SUBJECT TO TROPICAL WEATHERING**

A thesis submitted to the
University of London
(University College London)
for the degree of Doctor in Philosophy
in the
Department of Geological Sciences

by

Chen-Hui Fan.

September, 1994

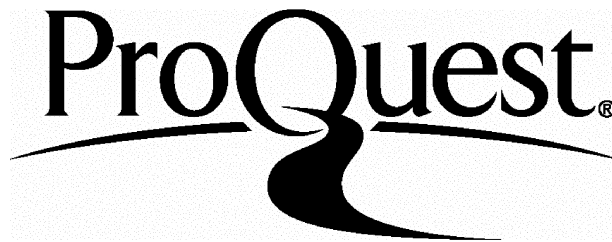
ProQuest Number: 10045519

All rights reserved

INFORMATION TO ALL USERS

The quality of this reproduction is dependent upon the quality of the copy submitted.

In the unlikely event that the author did not send a complete manuscript and there are missing pages, these will be noted. Also, if material had to be removed, a note will indicate the deletion.



ProQuest 10045519

Published by ProQuest LLC(2016). Copyright of the Dissertation is held by the Author.

All rights reserved.

This work is protected against unauthorized copying under Title 17, United States Code.
Microform Edition © ProQuest LLC.

ProQuest LLC
789 East Eisenhower Parkway
P.O. Box 1346
Ann Arbor, MI 48106-1346

*In memory of my Father,
and
to my dearest Mum,
the rest of my family
and Rita*

ABSTRACT

Scaly clay is an argillaceous sediment, with a pervasive fabric of lenticular, highly polished, curved, slickensided surfaces and is commonly associated with mélange formations. In regions subject to tropical weathering regimes outcrops of scaly clay erode rapidly, giving rise to extensive badlands topography. Islands such as Barbados lose considerable areas of land to badlands evolution each year and associated landslides disrupt settlements and communications.

The effects and implications of tropical weathering on scaly clay sediments have been examined. A programme of laboratory studies has been completed to characterise the physical, mineralogical and mechanical properties of undisturbed samples of the materials. The samples, collected from different depths within weathering profiles, between ground surface and fresh, unweathered materials at depth were each subject to similar experiments. The results provide a picture of how mechanical properties and physical characteristics vary with depth into the weathering profile.

Two materials were selected: the Joe's River Formation from Barbados, a scaly clay of Upper Eocene age; and the Lichi mélange of Taiwan, a Pliocene-Pleistocene scaly clay. The outcrops of these two materials experience similar climate and weathering regimes and are both characterised by frequent landslides, badlands development and loss of agricultural land.

Physical parameters, clay mineralogy and chemical composition were determined and a series of triaxial deformation experiments were conducted to gain a better understanding of how the mechanical behaviour of the sediments changes with depth into the weathering horizon. The data illustrate important changes during weathering, including destruction of the original sedimentary structure, a large increase in pore volume and variations in geotechnical characteristics. The experimental results demonstrate that mechanical changes caused by tropical weathering are an important factor in the development of the badlands which are common to scaly clay terrains.

ACKNOWLEDGEMENT

I have been thinking of how should this acknowledgement be written since four years ago when I first started my life in England. Now, the day has come and I still don't know how to write it because there are too many people who have contributed tremendously to this work and it is not possible to list all those names. However, the following deserve a special mention.

First of all, I would like to thank Professor Hongey Chen who I was working with before I came to this country, and it is him who introduced me to the Sediment Deformation Research group and then I had the opportunity to do this research.

The experimental study of this work required various types of testing and therefore technical support is substantial. I would like to thank all the technicians at University College London. They are: Steve Boon, Richard Rabe, John Bowles and Neil Hughes who helped me in the machinery and rescued it whenever was needed; Tony Osborn, Steve Hiron and Arthur Beer who helped me in the XRD analysis; Andy Beard and Jim Davy who gave me great assistance when I was doing the SEM; Mike Gray and Toby Stiles for their excellent service in all my photograph processing and; Sean Houlding and John Huggett for being nice friends to talk to half past three in the afternoon. Special thank also goes to Dr. Rita Gardner and her assistant, Aysen, at the Department of Geography, King's College London, who kindly allowed me to use the SediGraph for the particle analysis.

I was very lucky to be able to work in an incredibly interesting as well as highly successful laboratory, Sediment Deformation Research. Many ideas, character building and a lot of fun have been given to me by people who are (were) working in the lab. They are Mike Leddra (Mr. Aircraft), Nils Kågeson-Loe (Mr. Tall Shark), David Petley (Coventry), Catherine Stafford (Undergrad's Favourite) and Spence Willis (Cliff Hanger). Nils in particular, has always helped me stopping leaks for my little cell. Many thoughts were initiated through conversation with him. Thanks, Nils!

During my four years in England, I met quite a few friends, namely Eric Tsai, Jeannie Fan, Joyce Huang, Grace Yeh, Teresa Chang, Xiau-Lu Too and Anita Lin. I would like to give my sincere thank you to them for their encouragement and the most warm friendship. Two people deserve a special mention. They are Jia-Hou Jiang and Yuang-Ming Chang, two best friends of mine in Taiwan, who were always willing to give me their hands whenever I needed any special geological data from Taiwan.

A special thank you should go to Dr. Bob Allison, my supervisor at University of Durham, who has given me a great help both in terms of research and life in this country. Without his encouragement I, as an overseas student, could have had more problems in concentrating on my work and in fitting in the environment.

This work could not have been completed without Dr. Mervyn Jones, my supervisor. During my stay in Britain, including the very first day of my arrival, he and his family (Jane, Katie and Blue) have treated me as a member of their family which makes me don't feel like being thousands miles away from home. His unstinting help and great suggestions through the research and the unbelievable patience in correcting my English have to be specially acknowledged.

Finally, I would give my greatest thank to my family, Mum, Grand Mum, Wendy, Raine, Rossane, Frank, Alex, Dale, Sue and Jane. Their endless encouragement and warmest support allow me to complete this study. Without them none of this work would have been possible. My thank to them can never be enough.

LIST OF CONTENTS

TITLE.....	1
ABSTRACT.....	3
ACKNOWLEDGEMENT.....	4
LIST OF CONTENTS.....	6
LIST OF FIGURES.....	9
LIST OF PLATES.....	15
LIST OF TABLES.....	16
CHAPTER ONE: INTRODUCTION.....	18
1.1 Introduction.....	18
1.2 Research background.....	19
1.3 Research objectives.....	21
1.4 Arrangement of the thesis.....	23
CHAPTER TWO: WEATHERING.....	24
2.1 Introduction.....	24
2.2 Weathering processes.....	25
2.3 Weathering products.....	27
2.4 Weathering profile.....	30
2.5 Weathering in tropical humid environment.....	33
2.6 Mechanical behaviour and weathering of clays.....	36
CHAPTER THREE: SCALY CLAY AND ITS NATURAL OCCURRENCE.....	47
3.1 Introduction.....	47
3.2 Scaly clay.....	47
3.2.1 Origin of the scaly fabric.....	47
3.3 Field areas.....	51
3.3.1 Barbados.....	51
3.3.1.1 Climate.....	51
3.3.1.2 Geology.....	52
3.3.1.3 Tectonic setting.....	57
3.3.1.4 Joe's River Formation.....	59
3.3.2 Taiwan.....	63
3.3.2.1 Climate.....	63
3.3.2.2 Geology.....	65
3.3.2.3 Tectonic setting.....	71
3.3.2.4 Lichi Mélange.....	74
3.4 Sample collection.....	77
CHAPTER FOUR: PHYSICAL AND CHEMICAL CHARACTERISATION.....	80
4.1 Introduction.....	80

4.2 Procedures and sample preparation	80
4.2.1 Particle size distribution.....	80
4.2.2 Porosity, moisture content and bulk density	82
4.2.3 Plasticity index	84
4.2.4 Clay mineralogy	87
4.2.5 Micro-structure	92
4.2.6 Chemical composition	92
4.3 Results	93
4.3.1 Barbados.....	93
4.3.1.1 Particle size distribution	93
4.3.1.2 Porosity, natural water content and bulk density.....	96
4.3.1.3 Plasticity index.....	96
4.3.1.4 Clay mineralogy	97
4.3.1.5 Micro-structure.....	101
4.3.1.6 Chemical analysis.....	108
4.3.2 Taiwan.....	109
4.3.2.1 Particle size distribution	109
4.3.2.2 Porosity, natural water content and bulk density.....	113
4.3.2.3 Plasticity index.....	113
4.3.2.4 Clay mineralogy	114
4.3.2.5 Micro-structure.....	120
4.3.2.6 Chemical analysis.....	127
4.4 Discussion	127

CHAPTER FIVE: MECHANICAL CHARACTERISTICS OF THE TWO SCALY CLAYS

CHAPTER FIVE: MECHANICAL CHARACTERISTICS OF THE TWO SCALY CLAYS	133
5.1 Introduction	133
5.2 Methodology.....	134
5.2.1 Test equipment.....	135
5.2.2 Test specimen preparation	140
5.2.3 Test procedures.....	146
5.3 Reference state concept	149
5.4 Experimental results	149
5.4.1 Joe's River Formation, Barbados	149
5.4.1.1 Least weathered sample experiments.....	150
5.4.1.2 Partially weathered sample experiments.....	159
5.4.1.3 Most weathered sample experiments	166
5.4.1.4 Mud flow material experiment.....	172
5.4.2 Lichi Mélange, Taiwan	176
5.4.2.1 Least weathered sample experiments.....	177
5.4.2.2 Slightly weathered sample experiments.....	181
5.4.2.3 Partially weathered sample experiments.....	185
5.4.2.4 Most weathered sample experiments	189
5.5 Discussion	194
5.5.1 Barbados.....	194
5.5.1.1 Consolidation.....	194
5.5.1.2 Undrained triaxial deformation.....	198
5.5.1.3 Summary of the mechanical behaviour of the Joe's River Formation scaly clay.....	213

5.5.2 Taiwan	214
5.5.2.1 Consolidation	214
5.5.2.2 Undrained triaxial deformation	215
5.5.2.3 Summary of the mechanical behaviour of the Lichi Mélange scaly clay	224
CHAPTER SIX: DISCUSSION AND CONCLUSIONS	225
6.1 Introduction	225
6.2 General discussion on the physical-chemical characteristics	225
6.2.1 Porosity	225
6.2.2 Particle size distribution	228
6.2.3 Atterberg limits	232
6.2.4 X-ray diffraction study	233
6.2.5 Chemical analyses	234
6.2.6 Micro-fabric study	235
6.3 General discussion on the mechanical behaviour	239
6.3.1 Consolidation behaviour	239
6.3.2 Undrained triaxial deformation characteristics	244
6.4 Summary of the similarities and differences	262
6.4.1 Similarities	262
6.4.2 Differences	264
6.4.3 Conclusion	267
6.5 Implication on the evolution of badlands topography	268
REFERENCES	272
APPENDIX I: SOIL MECHANICS THEORIES	289
AI.1 Effective stress concept	289
AI.2 Consolidation theory	290
AI.3 Critical state model	293
AI.4 Skempton's pore pressure parameters	303
APPENDIX II: SEDIGRAPH 5100, SEDIMENTATION THEORY	304
APPENDIX III: CHEMICAL ANALYSIS	307
APPENDIX IV: CALIBRATION OF TRANSDUCERS	310
APPENDIX V: UNDRAINED DEFORMATION PROCESS	325

LIST OF FIGURES

- Figure 2.3.1 The silicon-oxygen tetrahedron and tetrahedral sheet
Figure 2.3.2 The cation-oxygen octahedron and the octahedral sheet
Figure 2.4.1 Four layered model
Figure 2.5.1 Intensity of chemical weathering in relation to rainfall and temperature
Figure 2.5.2 Diagram suggesting the relative importance of various types of weathering under various temperature and rainfall conditions
Figure 2.6.1 Diagram showing single plate "card-house" structure
Figure 2.6.2 Diagram showing plates aggregated face to face
Figure 2.6.3 Results of shear tests conducted on samples from Walton's Wood
- Figure 3.2.1 A schematic representation of the fracture pattern in a shear zone
Figure 3.2.2 Block diagrams showing fracture pattern described by Skempton (1966)
Figure 3.3.1 Map of the Caribbean islands
Figure 3.3.2 Geological map of Barbados
Figure 3.3.3 Regional tectonic unit of the south-eastern Caribbean
Figure 3.3.4 Tectonic setting of Barbados
Figure 3.3.5 Geological map of the study area in Barbados
Figure 3.3.6 Geomorphologic map of the study area in Barbados
Figure 3.3.7 Map of south-east Asia
Figure 3.3.8 Geological map of Taiwan
Figure 3.3.9 Seismicity of Taiwan
Figure 3.3.10 Geological units of Taiwan
Figure 3.3.11 Principal tectonic features and structural elements in the Ryukyu-Taiwan-Philippine island arc chain
Figure 3.3.12 Tectonic setting of Taiwan
Figure 3.3.13 Geological map of the study area in Taiwan
- Figure 4.2.1 Casagrande apparatus for Liquid limit determination
Figure 4.2.2 Diagram illustrating Liquid Limit test
Figure 4.2.3 The diffraction of X-rays
Figure 4.2.4 X-ray diffractogram of oriented mount of clay sediment
Figure 4.3.1 Particle size distribution curve for least weathered sample, Barbados
Figure 4.3.2 Particle size distribution curve for partially weathered sample, Barbados
Figure 4.3.3 Particle size distribution curve for most weathered sample, Barbados
Figure 4.3.4 X-ray diffractogram of the least weathered sample, Barbados
Figure 4.3.5 X-ray diffractogram of the partially weathered sample, Barbados

Figure 4.3.6 X-ray diffractogram of the most weathered sample, Barbados
Figure 4.3.7 Particle size distribution curve for least weathered sample, Taiwan
Figure 4.3.8 Particle size distribution curve for slightly weathered sample, Taiwan
Figure 4.3.9 Particle size distribution curve for partially weathered sample, Taiwan
Figure 4.3.10 Particle size distribution curve for most weathered sample, Taiwan
Figure 4.3.11 Particle size distribution curve for top surface sample, Taiwan
Figure 4.3.12 X-ray diffractogram of the least weathered sample, Taiwan
Figure 4.3.13 X-ray diffractogram of the slightly weathered sample, Taiwan
Figure 4.3.14 X-ray diffractogram of the partially weathered sample, Taiwan
Figure 4.3.15 X-ray diffractogram of the most weathered sample, Taiwan
Figure 4.3.16 X-ray diffractogram of the top surface sample, Taiwan

Figure 5.2.1 The triaxial deformation cell used in the study
Figure 5.2.2 Sample in the membrane with a strain belt, which enables radial strain to be monitored
Figure 5.2.3 Schematic diagram of the drainage board
Figure 5.2.4 Soil lathe used to produce cylindrical specimen for triaxial testing
Figure 5.2.5 Sample in the membrane
Figure 5.2.6 Typical consolidation curve for using side drainage and reconstructed consolidation path.
Figure 5.2.7 Relationships among soil phase: (a) element of natural soil; (b) element separated into phases.
Figure 5.4.1 Consolidation path of experiment BDL-100
Figure 5.4.2 Consolidation path of experiment BDL-100
Figure 5.4.3 Consolidation path of experiment BDL-200
Figure 5.4.4 Consolidation path of experiment BDL-200
Figure 5.4.5 Consolidation path of experiment BDL-400
Figure 5.4.6 Consolidation path of experiment BDL-400
Figure 5.4.7 Stress-strain curves for BDL experiments
Figure 5.4.8 Stress paths for BDL experiments
Figure 5.4.9 Effective horizontal-vertical stress relationships for BDL experiments
Figure 5.4.10 Pore fluid pressure development during undrained compression for BDL experiments
Figure 5.4.11 Diagram showing relationship between deviatoric stress and pore fluid pressure during undrained compression for BDL experiments
Figure 5.4.12 Consolidation path of experiment BDP-50
Figure 5.4.13 Consolidation path of experiment BDP-50
Figure 5.4.14 Consolidation path of experiment BDP-100

Figure 5.4.15 Consolidation path of experiment BDP-100
Figure 5.4.16 Consolidation path of experiment BDP-400
Figure 5.4.17 Consolidation path of experiment BDP-400
Figure 5.4.18 Stress-strain curves for BDP experiments
Figure 5.4.19 Stress paths for BDP experiments
Figure 5.4.20 Effective horizontal-vertical stress relationships for BDP experiments
Figure 5.4.21 Pore fluid pressure development during undrained compression for BDP experiments
Figure 5.4.22 Consolidation path of experiment BDM-100
Figure 5.4.23 Consolidation path of experiment BDM-100
Figure 5.4.24 Consolidation path of experiment BDM-200
Figure 5.4.25 Consolidation path of experiment BDM-200
Figure 5.4.26 Consolidation path of experiment BDM-400
Figure 5.4.27 Consolidation path of experiment BDM-400
Figure 5.4.28 Stress-strain curves for BDM experiments
Figure 5.4.29 Stress paths for BDM experiments
Figure 5.4.30 Effective horizontal-vertical stress relationships for BDM experiments
Figure 5.4.31 Pore fluid pressure development during undrained compression for BDM experiments
Figure 5.4.32 Consolidation path for experiment BDR-100
Figure 5.4.33 Consolidation path for experiment BDR-100
Figure 5.4.34 Stress-strain curve for experiment BDR-100
Figure 5.4.35 Stress path for experiment BDR-100
Figure 5.4.36 Effective horizontal-vertical stress relationship for experiment BDM-100
Figure 5.4.37 Pore fluid pressure development during undrained compression for experiment BDR-100
Figure 5.4.38 Consolidation path of experiment TWL-400
Figure 5.4.39 Consolidation path of experiment TWL-400
Figure 5.4.40 Stress-strain curves for TWL experiments
Figure 5.4.41 Stress paths for TWL experiments
Figure 5.4.42 Effective horizontal-vertical stress relationships for TWL experiments
Figure 5.4.43 Pore fluid pressure development during undrained compression for TWL experiments
Figure 5.4.44 Consolidation path of experiment TWS-400
Figure 5.4.45 Consolidation path of experiment TWS-400
Figure 5.4.46 Stress-strain curves for TWS experiments
Figure 5.4.47 Stress paths for TWS experiments
Figure 5.4.48 Effective horizontal-vertical stress relationships for TWS experiments

Figure 5.4.49 Pore fluid pressure development during undrained compression for TWS experiments

Figure 5.4.50 Consolidation path of experiment TWP-400

Figure 5.4.51 Consolidation path of experiment TWP-400

Figure 5.4.52 Stress-strain curves for TWP experiments

Figure 5.4.53 Stress paths for TWP experiments

Figure 5.4.54 Effective horizontal-vertical stress relationships for TWP experiments

Figure 5.4.55 Pore fluid pressure development during undrained compression for TWP experiments

Figure 5.4.56 Consolidation path of experiment TWM-400

Figure 5.4.57 Consolidation path of experiment TWM-400

Figure 5.4.58 Stress-strain curves for TWM experiments

Figure 5.4.59 Stress paths for TWM experiments

Figure 5.4.60 Effective horizontal-vertical stress relationships for TWM experiments

Figure 5.4.61 Pore fluid pressure development during undrained compression for TWM experiments

Figure 5.5.1 Consolidation paths for experiments BDL-400, BDP-400 and BDM-400

Figure 5.5.2 Consolidation paths for experiments BDL-400, BDP-400 and BDM-400

Figure 5.5.3 Isotropic compression of kaolin clay. (a) Loading-unloading-reloading path in linear scale. (b) Same data plotted in logarithmic scale.

Figure 5.5.4 Expected undrained test stress paths for samples at different degrees of overconsolidation

Figure 5.5.5 Normalised stress paths for undrained tests on overconsolidated samples of kaolin clay

Figure 5.5.6 Deviatoric stress-Skempton pore pressure parameter A relationships for BDL experiments

Figure 5.5.7 Isotropic compression of quartz sand

Figure 5.5.8 Stress paths in $q : p'$ and $v : p'$ space for undrained tests on dense and loose specimens of sand

Figure 5.5.9 Normalised stress paths in $q/p'_e : p'/p'_e$ space for drained and undrained tests on loose and dense samples of sand

Figure 5.5.10 Deviatoric stress-Skempton pore pressure parameter A relationships for BDP experiments

Figure 5.5.11 Comparison between BDM experiments and expected normally consolidated material tests

Figure 5.5.12 Deviatoric stress-Skempton pore pressure parameter A relationships for BDM experiments

Figure 5.5.13 Stress paths for both TWL and TWS experiments

- Figure 5.5.14 Stress-strain curves for both TWL and TWS experiments
- Figure 5.5.15 Deviatoric stress-Skempton pore pressure parameter A relationships for TWL experiments
- Figure 5.5.16 Deviatoric stress-Skempton pore pressure parameter A relationships for TWS experiments
- Figure 5.5.17 Deviatoric stress-Skempton pore pressure parameter A relationships for TWP experiments
- Figure 5.5.18 Deviatoric stress-Skempton pore pressure parameter A relationships for TWM experiments

- Figure 6.2.1 Particle size distribution curves for the Barbados samples
- Figure 6.2.2 Particle size distribution curves for the Taiwan samples
- Figure 6.3.1 Consolidation paths for experiments BDL-400, BDP-400 and BDM-400
- Figure 6.3.2 Consolidation paths for experiments BDL-400, BDP-400 and BDM-400
- Figure 6.3.3 Consolidation paths for experiments BDL-100, BDP-100, BDM-100 and BDR-100
- Figure 6.3.4 Consolidation paths for experiments BDL-100, BDP-100, BDM-100 and BDR-100
- Figure 6.3.5 Three families of stress paths for samples from Joe's River Formation scaly clay, Barbados
- Figure 6.3.6 Three families of stress paths for samples from Lichi Mélange scaly clay, Taiwan
- Figure 6.3.7 Expected undrained test stress paths for samples at different degrees of overconsolidation
- Figure 6.3.8 (a) Stress-strain behaviour of the BDM samples
(b) Pore fluid pressure development during undrained loading for the BDM experiments.
- Figure 6.3.9 Stress paths and failure envelopes for the Barbados experiments
- Figure 6.3.10 Stress paths and failure envelopes for the Taiwan experiments
- Figure 6.3.11 Comparison between the stress - strain curves from experiments BDM-100 and BDR-100
- Figure 6.3.12 Comparison between the stress paths from experiments BDM-100 and BDR-100
- Figure 6.3.13 Comparison between the effective horizontal-vertical stress relationship from experiments BDM-100 and BDR-100
- Figure 6.3.14 Comparison between the pore fluid pressure development during undrained compression from experiments BDM-100 and BDR-100
- Figure 6.3.15 Stress paths for TWP and TWM families

Figure 6.3.16 Stress paths for the three Barbados experiments at effective confining pressure of 100 kPa

Figure 6.3.17 Stress paths for the three Taiwan experiments at effective confining pressure of 400 kPa

Figure 6.3.18 Stress-strain curves for BDL experiments

Figure 6.3.19 Stress-strain curves for BDM experiments

Figure 6.4.1 Consolidation paths for experiments BDP-400 and BDM-400

Figure 6.4.2 Consolidation paths for experiments BDP-400 and BDM-400

Figure 6.4.3 Diagram illustrating the effect of weathering on the mechanical behaviour of scaly clay

Figure 6.5.1 Suggested model for badlands evolution

Figure AI.1 Consolidation model

Figure AI.2 Undrained response to increase in total stress

Figure AI.3 Consolidation as pore water drains and pore water pressure equilibrates

Figure AI.4 Normal consolidation line in $v - p'$ space

Figure AI.5 Normal consolidation line in $v - \ln p'$ space

Figure AI.6 Normal consolidation line in $q - v - p'$ space

Figure AI.7 Critical state line in $q - p'$ space

Figure AI.8 Critical state line in $v - p'$ space

Figure AI.9 Critical state line in $q - v - p'$ space

Figure AI.10 Roscoe surface in $q - p'$ space

Figure AI.11 Roscoe surface in $q - v - p'$ space

Figure AI.12 Hvorslev surface in $q - p'$ space

Figure AI.13 Hvorslev surface in $q - v - p'$ space

Figure AI.14 Complete critical state model

Figure AI.15 Diagram explaining wet & dry of critical

Figures AIV Calibration of the system

LIST OF PLATES

Plate 1.2.1 Typical badlands topography

Plate 3.3.1 Joe's River Formation scaly clay

Plate 3.3.2 Aerial photograph of Taiwan

Plate 3.3.3 Lichi badlands topography

Plate 3.3.4 Sampling technique

Plate 4.3.1 SEM photographs for the least weathered sample, Barbados

Plate 4.3.2 SEM photographs for the partially weathered sample, Barbados

Plate 4.3.3 SEM photographs for the most weathered sample, Barbados

Plate 4.3.4 SEM photographs for the least weathered sample, Taiwan

Plate 4.3.5 SEM photographs for the partially weathered sample, Taiwan

Plate 4.3.6 SEM photographs for the most weathered sample, Taiwan

Plate 5.2.1 The triaxial deformation cell used in the present study

Plate 5.2.2 Setting up experiment

Plate 5.5.1 Sample BDL-200, the experiment was terminated early. Photograph showing the clearly defined shear failure plane

Plate 6.2.1 Photograph demonstrating strongly preferred orientation of clay particles along the scaly surface

Plate 6.2.2 Photograph showing random arrangement of clay particles away from the scaly surface

Plate 6.2.3 Photograph demonstrating some original preferred particle orientation in the partially weathered scaly clay

Plate 6.2.4 Photograph demonstrating pore enlargement in the highly weathered scaly clay

Plate 6.5.1 Photograph showing widespread gulley system in badlands area

Plates AV A series of photographs demonstrating the undrained deformation process

LIST OF TABLES

- Table 2.2.1 Functions of water in the weathering processes
- Table 2.3.1 Some common iron minerals occur during weathering
- Table 2.4.1 Classification of weathered mudrocks
- Table 2.6.1 Weathering scheme for Keuper Marl
- Table 2.6.2 Engineering grade classification of weathered mudrocks
- Table 2.6.3 Weathering scheme for the London Clay at South Ockendon
- Table 2.6.4 Strength parameters of the Bangkok Clays
-
- Table 3.3.1. The climate data of Taitung from 1981 to 1990
- Table 3.4.1 Classification of weathering
-
- Table 4.2.1 X-ray identification of the principal clay minerals ($< 2 \mu\text{m}$) in an oriented mount.
- Table 4.3.1 Summary of the porosity, natural water content and bulk density of the Barbados samples
- Table 4.3.2 Summary of the Liquid and Plastic Limits and Plasticity Index of the Barbados samples
- Table 4.3.3 The clay mineralogy of the Barbados materials
- Table 4.3.4 The chemical composition of the Barbados materials
- Table 4.3.5 Summary of the porosity, natural water content and bulk density of the Taiwan samples
- Table 4.3.6 Summary of the of the Plastic and Liquid Limits and Plasticity Index of the Taiwan samples
- Table 4.3.7 Summary of the main clay mineralogy of the of the Taiwan samples
- Table 4.3.8 The chemical composition of the Taiwan samples
-
- Table 5.1.1 The experiments conducted in the study
- Table 5.2.1 Types of transducer used in the study
- Table 5.4.1 Initial dimensions and porosities of the Barbados specimens
- Table 5.4.2 Summary of the deviatoric stress, mean effective stress and pore pressure states at the beginning of dilation and end of the BDL experiments
- Table 5.4.3 Summary of the deviatoric stress, mean effective stress and pore pressure at the beginning of dilation and the end of test for BDP experiments
- Table 5.4.4 Summary of the deviatoric stress, mean effective stress and pore pressure at the beginning of dilation and the end of test for BDM experiments
- Table 5.4.5 Testing condition of the naturally remoulded sample

- Table 5.4.6 Initial dimensions and porosities of the Taiwan specimens
- Table 5.4.7 Summary of the deviatoric stress, mean effective stress and pore pressure at the beginning of dilation and the end of test for TWL experiments
- Table 5.4.8 Summary of the deviatoric stress, mean effective stress and pore pressure at the beginning of dilation and the end of test for TWS experiments
- Table 5.4.9 Summary of the deviatoric stress, mean effective stress and pore pressure at the beginning of dilation and the end of test for TWP experiments
- Table 5.4.10 Summary of the deviatoric stress, mean effective stress and pore pressure at the beginning of dilation and the end of test for TWM experiments
- Table 5.5.1 Typical A values at failure for materials with different consolidation states
-
- Table 6.2.1 Summary of the porosity, natural water content and bulk density of the test materials
- Table 6.2.2 Liquid limits, plastic limits and plasticity index of the samples examined
- Table 6.3.1 Some strength parameters for materials with various degrees of weathering
- Table 6.4.1 Effects of tropical weathering on the physical-chemical and mechanical characteristics of scaly clay
-
- Table AIII.1 The chemical composition of the Barbados samples (raw data)
- Table AIII.2 The chemical composition of the Taiwan samples (raw data)
-
- Tables AIV Calibration data of the system

Chapter One: Introduction

1.1 Introduction

This thesis presents and discusses work concerning the influence of tropical weathering on the deformation characteristics of some argillaceous rocks. The thesis reports the results of research undertaken to examine some of the significant changes which take place to the geotechnical properties of scaly clays, an argillaceous mudrock with a well developed, pervasive fabric, under tropical weathering conditions. The study aims to gain a better understanding, both qualitatively and quantitatively, of how weathering, particularly in tropical environments, alters the physical and chemical properties and subsequently the mechanical behaviour of the material. To accomplish the study representative sites are needed. Two localities from two different parts of the world have been chosen to undertake the research. One is Barbados, in the Caribbean, and the other is Taiwan, in Southeast Asia. The reason for choosing these two places is their many similarities in terms of the environment and the materials that characterise both locations.

A naturally developed landform may have reached its present shape by one of several routes. It is the result of the interaction between the long-term action of a set of denudation processes, still active at the present day and the physical characteristics of the near-surface materials which are exposed to those particular conditions (Bromhead, 1986). To understand landform development, not only is an insight into the characteristics of the processes and the properties of the material needed, but a knowledge of the interaction between the two is particularly important.

As described above, the study material is scaly clay, an argillaceous rock with well developed, randomly oriented micro-fabrics. The micro-fabrics seldom considered an important feature in terms of significance in promoting weathering (Brenner *et al.*, 1981). In studies of cemented rock masses, such as sandstones and limestones, it is accepted that discontinuity properties such as density, orientation and continuity are important controls on material behaviour (Farmer, 1983; Selby, 1993). Smaller scale fractures which manifest themselves as a micro-fabric are also likely to be significant in many respects regarding material properties and the consequences of weathering. Cracks will act as lines along which weathering will be preferentially active. As a consequence, those variables which are important with the larger rock mass discontinuities may also be significant at the smaller, macro- and micro-scales (Ebuck *et al.*, 1990) if the discontinuities are sufficiently permeable.

The project consists of two major parts. One is the field observation and sampling. The other is laboratory testing. The field observation provides a description of the landform and preliminary information on the nature of the material. Laboratory testing provides a more precise measure of the physical and geotechnical properties of the material. The laboratory experimental program in this research was designed to allow study of the interaction of the materials and earth surface processes through examination of physical, chemical, mineralogical and mechanical properties of the materials and how they change during tropical weathering. In the examination of the mechanical characteristics of the materials a series of standard consolidated undrained triaxial experiments were employed. Since mudrocks often exhibit low permeability, it seems to be reasonable to monitor their failure behaviour under undrained conditions (Wu *et al.*, 1990)

1.2 Research background

At some specific places on the surface of the Earth, due to the combination of a warm, humid climate, tectonic activity and soft, argillaceous sedimentary rocks, it is possible to detect the effects of weathering over a relatively short period of time. Rocks displaying little or no sign of weathering may exist quite close to those materials which are exposed at the ground surface and which have been significantly altered by various surface processes. Sometimes the visual differences between the two are so great that it is difficult to accept that the two materials are of the same lithologic unit. Such abrupt profiles indicate that only short durations are required for freshly exposed sediments to alter to highly weathered materials. For argillaceous sediments, scaly clay in this instance, weathering processes usually promote a large increase in pore volume (Terzaghi, 1936; Chandler & Apted, 1988), an appreciable change in material structure and associated changes to mechanical properties of the material (Barden, 1972b; El-Sohby *et al.*, 1990).

As mentioned previously, the rates of landform development and the characteristics of landforms are strongly associated with weathering processes and rock type. Furthermore landform evolution is directly controlled by the physical properties and mechanical characteristics of the rocks that crop out in the area. With the above description in mind, understanding the effects of weathering on the physical and mechanical characteristics of the materials becomes the key to understanding landform evolution, one of the major aims of the study. In order to have a more thorough understanding of landform development it is necessary to investigate the physical and mechanical properties of the

materials. Studies which try to establish the relationship between weathering, rock materials and resulting landform often need to examine *in situ* rock outcrops (Caine, 1979; Motteshead, 1989) and recover undisturbed samples with different degrees of weathering for laboratory testing (Chandler & Apted, 1988). Quantitative measures of the effects of weathering tend to be based on rock disintegration.

Weathering is the collection of processes which modify and change properties of near surface materials (Ollier, 1984). During weathering the geotechnical properties of rock materials are changed and the consequence of the changes is the disintegration of the rock mass (Aires-Barros & Mouraz-Miranda, 1989). In particular, weathering in tropical environments is generally much more severe than anywhere else due to the warm temperature and high humidity (Birkeland, 1984). There is hardly any other place where the interactions between weathering processes, materials and landforms are so significantly evident as in tropical environments where argillaceous rocks are exposed. Additionally, tectonic activity may accelerate the weathering rate as rapid uplift provides a more unstable environment which enables weathering to proceed more easily. Because of the continuous uplifting and surface lowering (erosion) there is potential to examine the effects of weathering on rock exposures displaying little or no signs of alteration and directly compare this to those which have become highly altered within a relatively shallow depth profile.

In tropical argillaceous rock terrains, one of the characteristics is the high frequency of surface mud flows and shallow landslides. As a result, vegetation has difficulty sustaining a presence on some slopes, resulting in a very distinctive type of landscape known as "badlands". Badlands topography characterises both the chosen localities. The characteristics of badlands are steep slopes with little or no vegetation and numerous gullies. Typical badlands topography is shown in Plate 1.2.1. Badlands frequently develop on materials comprising a massive muddy matrix with no perceptible bedding, one of the characteristics of *mélange* formation (Ho, 1975). Examples are found in the island of Nias, Indonesia (Moore & Kraig, 1980), Cyprus (Hsu, 1971), Barbados (Enriquez-Reyes *et al.*, 1990) and Taiwan (Hsu, 1956). One thing the above places have in common is the occurrence of *mélange* sediments. Most of the work that has been done on badlands development has concentrated on the qualitative field description and observation such as climate, vegetation and rock types (Yen & Chen, 1990) or on the significance of material properties (Solé *et al.*, 1992). Little work was focused on quantitative analysis in terms of the mechanical characteristics and engineering behaviour and how weathering changes the properties of the materials. It is hoped that by combining field observation and the laboratory experimental data of undisturbed samples

recovered from the selected sites, the whole evolutionary of sequence badlands development can be better understood.

From a practical view point such as agricultural development and land use, the high frequency of slope instabilities, the frequent surface erosion and the consequent land loss often lead to a tremendous problem for human activities resulting in enormous physical and economical loss in both study areas. In Southern Taiwan, for example, the frequent and massive surface erosion in regions where argillaceous badlands topography develop causes large volume of sediments to be deposited in reservoirs, shortening their life expectancy, results in damages to roads causing problems in communication as well as a loss of farm land. This leads to difficulties in developing the area. It is therefore an important task to improve the situation caused by this developmentally unfriendly geological condition in places like Taiwan where over-population and lack of easily-usable land places significant pressures on land use.

Minimise the risks associated with widespread and rapid landscape denudation, it is essential to have a full knowledge of landform development. Once the evolutionary sequence of the landscape is understood, proper solutions and constructional plans can then be designed. It is hoped that the results of the study and the conclusions drawn from the data will provide quantitative information which can aid geotechnical design and subsequently contribute to developing a feasible technique for slope stabilisation.

1.3 Research objectives

Having described the background and motives for this research, the main research objectives are:

- *To examine the physical, chemical, mineralogical and especially mechanical properties of the scaly clays, and the changes of the properties through tropical weathering.*
- *To understand the importance of the micro-fabric in terms of controlling the mechanical behaviour and engineering performance, and the role played by the fabric during weathering in tropical environments.*
- *To investigate the interactions between the changes in deformation characteristics of the scaly clay induced by weathering and the resulting badlands evolution.*



Plate 1.2.1 Typical badlands topography

- *To use the laboratory experimental data combined with information on environmental conditions such as climate to establish a model for the landform development.*

The landform development model can subsequently be used to develop more suitable land management practises in scaly clay terrains.

1.4 Arrangement of the thesis

Similar to many other laboratory based geological thesis, this piece of work consists of a literature review, field work, experimental results, a discussion and conclusion. Chapters Two and Three include an introduction to weathering and weathering processes, a literature review of mechanical behaviour and weathering of clays, a description of scaly clay and a description of the study areas. Laboratory experimental results are presented in Chapters Four and Five. Chapter Four contains a presentation of the inherent properties of the material including physical, chemical and mineralogical characterisations. Chapter Five describes the triaxial test results. Each of the two chapters describes test procedure and sample preparation and presents results. Following the results is a discussion focused on the main theme of the chapter. A general discussion is given in Chapter Six, synthesising the two sets of results and other relevant information to assemble a general pattern of the effects of tropical weathering on scaly clays. A proposed model of badlands evolution is also presented.

Chapter Two: Weathering

2.1 Introduction

Most earth materials exposed at and immediately beneath the ground surface, are in an environment which is quite different to that where they formed in terms of temperature and pressure conditions. As a consequence, when subject to the near surface environment, materials are no longer in an equilibrium state. The physical and chemical alteration processes result in rock weathering. Weathering can therefore be defined as the processes by which rocks and minerals adjust themselves to more stable forms under the various conditions of moisture, temperature and biological activity that prevail at the ground surface (Brunsden, 1979; Ollier, 1984). In other words, weathering is the breakdown and/or alteration of minerals near the Earth surface to products that are more stable under the newly imposed physical-chemical conditions.

Since weathering is the response of materials to the surface environment (Keller, 1957; Birkeland, 1984; Gerrard, 1988; Chesworth, 1992), the nature and rate of weathering will depend on several variables including climate, rock forming materials and biological organisms. The variables combine through time to alter the basic properties of the weathering mantle (Carroll, 1970b; Brunsden, 1979). Jenny (1941) noted that the five basic factors, which control the weathering processes and thus soil formation, are climate, topography, parent material, organisms and time which combine to yield the soil properties.

Because of the totally different nature of the five basic factors, weathering processes may vary significantly from one location to another. Generally speaking, however, there are some tendencies common to all weathering processes.

1. Weathering is a movement toward a more stable state where mineral assemblages, formed under conditions of subsurface temperature and pressure, adjust to new environmental conditions, atmospheric pressure and lower temperatures at the Earth surface.
2. Weathering causes an irreversible change of rock and mineral from a massive to a clastic or plastic state as breakdown proceeds.

3. Weathering changes the volume, density, grain size, surface area, permeability, consolidation and shear characteristics of the material.

2.2 Weathering processes

The specific nature of weathering processes is essentially dependent on the prevailing climatic conditions (Ollier, 1984). It is generally difficult to isolate the nature of the climatic parameters that control the main weathering processes (Birkeland, 1984; Chesworth, 1992). Usually it is only possible to relate generalised climatic parameters to broad concepts of weathering process. The most important controls are the availability of water and the prevailing temperature conditions. The intensity, frequency and duration of precipitation-evaporation events are important in weathering processes since the supply of water is essential for many of the main chemical changes such as hydration, hydrolysis and solution (Trudgill, 1983). Characteristics of precipitation/evaporation events are also important in the leaching and removal of soluble constituents thereby enhancing further reactions (Pedro & Sieffermann, 1979). Water is essential to control the concentration of hydrogen ions, organic content and oxidation-reduction conditions (Berner, 1970), and to control the distribution of clay minerals and the zonation of the weathering profile (Chesworth, 1972; Velde, 1985). The functions of water in the physical and chemical weathering processes are summarised in Table 2.2.1.

Table 2.2.1 Functions of water in the weathering processes (after Chesworth, 1992)

Functions of water in physical weathering processes
<ol style="list-style-type: none"> 1. Agent of physical transport on both macro- and micro-scale. 2. Medium through which reactants diffuse at reaction sites, such as at the solid-liquid interface. 3. Exerts partial pressure, which is directly associated with chemical potential and activity. 4. May help physical disintegration of solids, such as the freeze-thaw mechanism.
Function of water in chemical weathering processes
<ol style="list-style-type: none"> 1. Most able solvent in the natural world. 2. Necessary component of all the typical reactions of the weathering zone, such as hydration/dehydration, solution/precipitation, etc. 3. Important constituent of the principal new phases formed during weathering, such as clays. 4. Acts as a chemical buffer.

Although it is difficult to differentiate or isolate the weathering processes, two main types of weathering can be recognised in terms of the mechanisms of rock material alteration. One is physical weathering and the other is chemical weathering (Birkeland, 1974). A third class, biological weathering, is also recognised but this can be regarded as being partly a physical and partly a chemical process (Ollier, 1984).

Physical weathering is the disintegration of rock into smaller-sized fragments, with no appreciable change in chemical or mineralogical composition. The mechanism common to all physical weathering is the establishment of sufficient stress within the rock to enable it to break (Birkeland, 1984). In other words, physical weathering occurs when the material is stressed in some way and the material breaks up under stress along lines of weakness. Rock fragments may be produced, or the rock may be split into individual minerals, or minerals may fragment along crystal cleavage planes.

The most common examples of physical weathering are unloading of rocks by removing the overburden, expansion of fluid in cracks or along grain boundaries by wetting and drying, freezing water, crystallisation of salts and possibly thermal expansion and contraction of the constituent minerals (Ollier, 1984). Wetting and drying, for instance, is one of the most important physical weathering processes, especially in tropical areas (Gerrard, 1988; Nahon, 1991). Appreciable stress can be introduced into a rock by alternate and frequent wetting and drying. Minerals will expand when they take up water (known as hydration) into their crystal structures and contract when this water is subsequently removed from the structure (dehydration). Hydration can result in considerable stress and is thought to be a principal cause of the mechanical disintegration of rocks (Trudgill, 1983). With alternate hydration and dehydration there will be alternate expansion and contraction, which will consequently lead to the weakening of crystals. Eventually, the minerals tend to break along lines of weakness.

Beside the absorption of water by crystal structures, water may also be absorbed on to the surface of some minerals, especially clays. This surface water will accelerate chemical reactions and diffusions (Chesworth, 1992). Swelling may frequently accompany these processes.

Chemical weathering, on the other hand, is the alteration of the chemical and/or mineralogical composition of the original rock and minerals. Usually chemical weathering occurs because rocks and minerals are not chemically in equilibrium with near surface moisture, temperature and pressure conditions (Nahon, 1991). Broadly speaking,

chemical weathering is active in most areas where temperatures are high, since an increase in temperature often accelerates chemical reactions (Brunsden, 1979).

Alteration by chemical weathering can also be the expression of the minerals of a rock adjusting to equilibrium under new environmental conditions (Carroll, 1970b). This alteration is fundamentally a chemical process in which the original minerals are affected by inorganic and organic solutions that form within the weathering mantle. Specific reactions are governed by the laws of chemical solution and equilibrium, free energy and redox potentials (Ollier, 1984).

2.3 Weathering products

After experiencing different types of weathering processes, rocks become altered physically and/or chemically to new materials, termed weathering products. Since physical weathering does not alter the chemical or mineralogical composition of the material appreciably, the weathering products introduced here are mostly the products from chemical weathering.

Materials released during chemical weathering are either removed from the system by leaching or react in the system to form a variety of crystalline and amorphous products (Carroll, 1970b). The most commonly observed reaction products are the clay minerals and hydrous oxides of aluminium and iron (Evans, 1992). The common clay minerals are hydrated silicates of aluminium, iron and magnesium arranged in various combinations of layers. They are termed layer silicates or phyllosilicates. Two kinds of sheet structures, the tetrahedral and the octahedral (Figures 2.3.1 & 2.3.2), make up the clay minerals, and variations in combinations of the structures and in their chemical makeup give rise to the multitude of clay minerals (Evans, 1992). The basic difference between the two sheet silicate structures is in the geometrical arrangement of Si, Al, Fe, Mg cations with respect to the O and OH anions. The arrangements differ with the cation because it is the size of the cation that determines how many O or OH ions surround it.

Although most clay minerals are by-products of weathering, it is possible that one clay mineral can be transformed into another clay mineral if the present environmental conditions are different from those which the minerals experienced previously (Deer *et al.*, 1966). Glenn and Nash (1964) demonstrated a sequential alteration caused by weathering where by mica can be altered to become chlorite and then kaolinite or gibbsite. Burial is also one of the usual explanations for clay minerals alteration (Gerrard,

1988). Kaolinitic weathering, a process during which other minerals weather to kaolinite, is also common (Thomas, 1974). Most kaolinite is formed by the acid leaching of alkaline rocks, primarily the feldspars and micas. However, practically any silicate rock or mineral will alter to kaolinite if leaching conditions are suitable for a sufficiently long period of time (Weaver & Pollard, 1975). Montmorillonite, for example, is often weathered to kaolinite (Deer *et al.* 1966; Weaver & Pollard, 1975).

Other than clay minerals, hydrous oxides of aluminium and iron are also common as weathering products (Birkeland, 1984). Some are crystalline, such as gibbsite ($\text{Al}(\text{OH})_3$), and some are non-crystalline, such as Allophane ($\text{Al}_2\text{O}_3\text{-}2\text{SiO}_2\text{-}n\text{H}_2\text{O}$). Table 2.3.1 presents some common iron oxide minerals formed during weathering.

Table 2.3.1 Some common iron minerals occur during weathering
(after Schwertmann & Taylor, 1977)

Minerals	Formula	Colour
Goethite	$\alpha\text{-FeOOH}$	yellowish to brown
Lepidocrocite	$\gamma\text{-FeOOH}$	orange
Hematite	$\alpha\text{-Fe}_2\text{O}_3$	bright red
Ferrihydrite	$\text{Fe}_5\text{HO}_8\text{-}4\text{H}_2\text{O}$ or $\text{Fe}_5(\text{O}_4\text{H}_3)_3$	reddish to brown

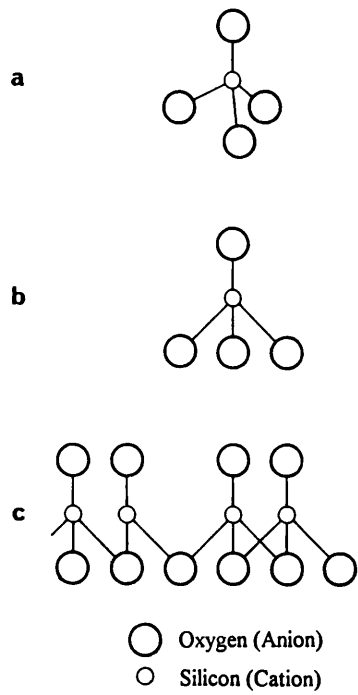


Figure 2.3.1 The silicon-oxygen tetrahedron and tetrahedral sheet
(after Deer *et al.*, 1966)

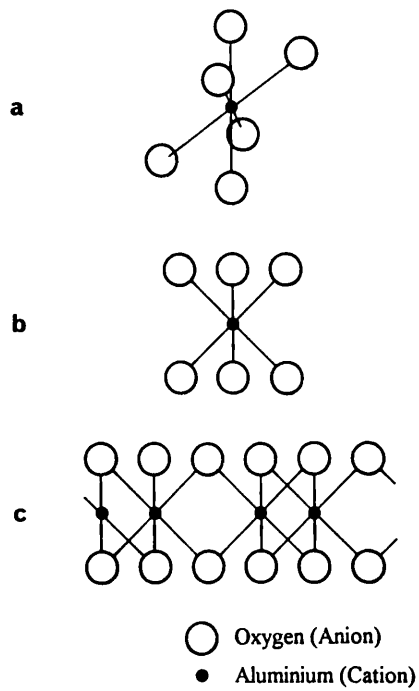


Figure 2.3.2 The cation-oxygen octahedron and the octahedral sheet
(after Deer *et al.*, 1966)

2.4 Weathering profile

A weathering profile may be defined as the vertical extent of a rock sequence from the land surface, which suffers the most severe weathering, down to the unweathered parent rock (Senior & Mabbutt, 1979). The zonation may be formed by either physical or chemical alteration and can vary considerably from place to place because of the variation in climate, rock type and structures (Gerrard, 1988, Thomas, 1994).

In general, the upper layers of the weathering mantle suffer the most intense weathering (Carroll, 1970b), because here the availabilities of water, air and organic life are greatest. Consequently, all kinds of chemical and physical weathering processes are intensely active. For most sedimentary rocks, water movement is mainly downward with considerable leaching at lower levels (Ollier, 1984). This may introduce appreciable amount of stress into the rocks and mineral grains. Towards the base of the weathering mantle is the transition zone where oxidation and reduction are common (Gerrard, 1988), especially in the zone of capillary water just above water table. The transition zone is particularly important in limestone and may even control the level of cave formation (Ollier, 1984) for it is here that fresher unsaturated water is most likely to be available. A model for the weathering zonation sequence is given in Table 2.4.1

Table 2.4.1 Classification of weathered mudrocks. (after Cripps & Taylor, 1981)

Term	Grade	Description
Fresh	IA	No visible sign of weathering
Faintly weathered	IB	Discoloration on major discontinuity surfaces
Slightly weathered	II	Discoloration
Moderately weathered	III	Less than half of rock material decomposed
Highly weathered	IV	More than half of rock material decomposed
Completely weathered	V	All rock material decomposed; original structure still largely intact
Residual soil	VI	All rock material converted to soil; rock structure and fabric destroyed

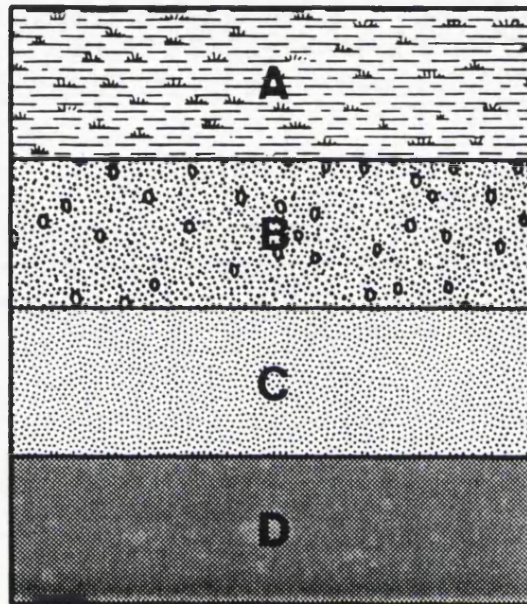
The weathering grades defined by Cripps & Taylor (1981) can not be expected to be found in all rock types and in all climatic conditions. It is more likely that any sequence will be only partly developed. A four layered classification (Chandler, 1969) is often used (Figure 2.4.1) in which the "A" horizon is defined as the zone of complete disintegration, the material in this zone being plastic and exhibiting little or no trace of original structure. The "B" horizon is the zone of advanced disintegration (Gerrard, 1988) and

where the accumulation of the material derived from the "A" zone takes place. The "C" horizon is a transitional zone of partly altered rock overlying the unaltered bedrock and the "D" zone is the unweathered bedrock. In the "A" zone organic matter gradually accumulates, and chemical weathering is most active (Birkeland, 1974). The "B" zone depends largely on the drainage condition of the area. There are cases where the "B" zone is absent because of the high rate of erosion and low permeability. The simple idea of the "C" zone is being a mixture of "A"/"B" zone(s) and unweathered "D" zone. In the early stage of weathering, the parent rock will influence the type of soil and clay minerals that form (Birkeland, 1984). With increasing maturity¹, climate and drainage conditions become increasingly important and the same clay minerals can form from a wide variety of rock types (Ollier, 1984; Macias & Chesworth, 1992).

Topography plays an important role in weathering profile development (Jenny, 1941; Gerrard, 1988). The four layered classification described above is a general idea of weathering zonation. At places which have steep slopes the "A" and "B" zones may not exist or may only appear in very thin layers. This is reasonable because on steep slopes downslope movement does not allow these two layers to be well developed.

Weathering profiles for mudrocks are highly variable from place to place (Gerrard, 1988). The classification described above can not be expected to apply in every case. It only provides a general trend of how the material changes with weathering. The classification schemes can therefore only be used as a reference standard.

¹The term maturity is used in the sense of a measure of chemical and physical progress along some predetermined evolutionary path (Lindsay, 1992).



- A: the zone of complete disintegration and the material in this zone being plastic and exhibiting little or no trace of original structure.
- B: the zone of advanced disintegration and where the accumulation of the material derived from the "A" zone takes place.
- C: is a transitional zone of partly altered rock overlying the unaltered bedrock. The simple idea of the "C" zone is being a mixture of "A"/"B" zone(s) and unweathered "D" zone.
- D: is the unweathered bedrock.

Figure 2.4.1 Four layered model (after Chandler, 1969)

2.5 Weathering in tropical humid environment

In humid tropical environments, weathering is intense (Thomas, 1974, 1994; Ollier, 1984; Macias & Chesworth, 1992). As described previously, weathering processes are essentially dependent on the prevailing climatic conditions. As a consequence, different climates promote different types of weathering. The climatic controls associated with weathering are mainly related to water and temperature. Water is the most important factor affecting many respects of physical and chemical weathering in tropical environments (Thomas, 1994). It is related to the hydrological cycle, that is the total amount of precipitation, intensity of rainfall, proportion of precipitation that forms run-off and precipitation-evaporation ratio. Temperature is also an essential control (Ollier, 1984) which involves mean temperature and temperature range. Many other factors such as relative humidity, drying wind and climatic changeability may also be important locally.

The characteristics of climatic conditions in tropical humid environments include high humidity, high annual rainfall which is often seasonal and long periods of high temperature. There is no doubt that the weathering processes associated with water and high temperature are intensely active. Severe chemical weathering is expected because sufficient water supply and high temperatures, which characterise tropical areas, are the two most important controls promoting chemical reactions (Thomas, 1974). Figure 2.5.1 shows the intensity of chemical weathering in relation to rainfall and temperature. Figure 2.5.2 demonstrates the relative importance of various types of weathering under different temperature and rainfall conditions (Peltier, 1950; Ollier, 1984). Although Peltier and Ollier imply from their diagrams that physical weathering is not strong in high temperature and high rainfall regions, adequate water supply can still be an important control (Chesworth, 1992) and although not directly, maybe indirectly related to physical weathering causing erosion, for example.

In addition to the warm and wet conditions, tectonic activity, in the two cases studied, can contribute to weathering processes (Ollier, 1984). The uplift of the ground surface resulting from lithospheric plate convergence disturbs the environmental system and therefore the system is no longer in equilibrium. As a consequence, rates of erosion increase leading to an acceleration of physical processes, and hence chemical weathering.

Knowing the environmental conditions that characterise the study areas selected in this research, it is possible to describe the prevailing weathering regime. The combination of abundant water and rapid uplift makes the rate of surface erosion specifically high

leading to a quick change in the stress state of underlying rocks. The change in stress state will contribute partly to the enlargement of the pore space due to the elasticity of the material which results in a change in the physical properties of the material and thus its mechanical behaviour. Warm temperature and availability of water and air enable chemical reactions to occur very severely and quickly. For instance, oxidation will occur within a very short period of time once rocks are exposed to water and air. In the upper most layer, rocks suffering from heavy evaporation due to high temperatures and long exposure to sunshine will experience frequent alternate wetting and drying which may result in establishment of stresses in the rocks (Brunsden, 1979; Birkeland, 1984) or introduction of suction pressure to draw fine particles together at a micro-scale (Pandian *et al.*, 1993a) and may subsequently accelerate other chemical reactions (Ollier, 1984). Leaching may be severe because of massive water availability, but it depends very much on the material properties such as permeability and structure. If a material is highly permeable, leaching may result in a weathering profile of great vertical extent.

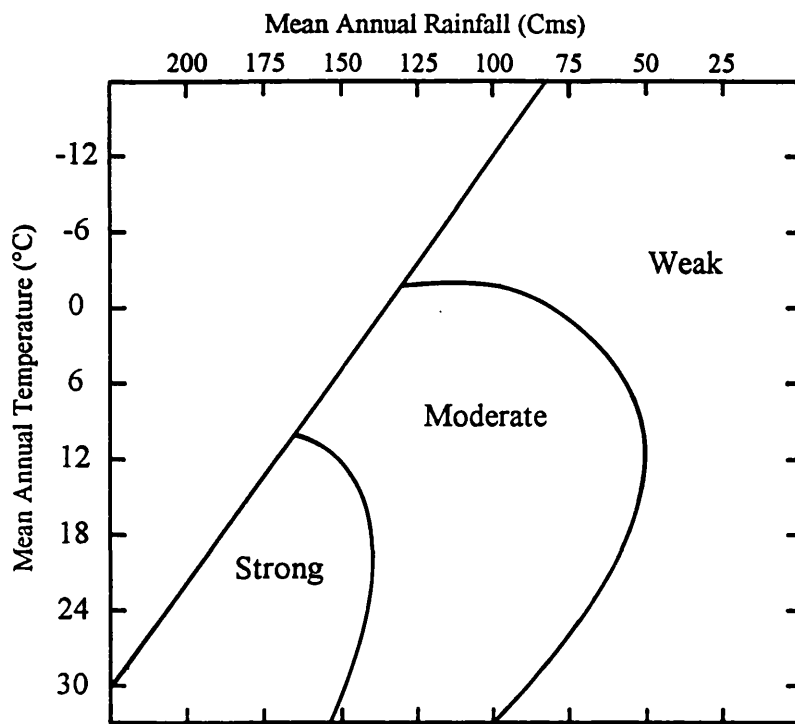


Figure 2.5.1 Intensity of chemical weathering in relation to rainfall and temperature (after Peltier, 1950)

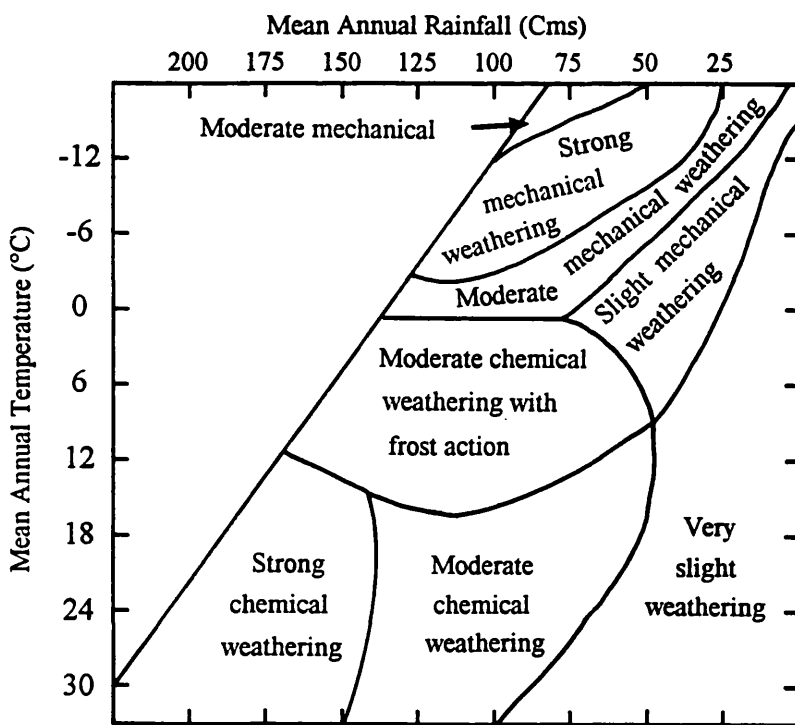


Figure 2.5.2 Diagram suggesting the relative importance of various types of weathering under various temperature and rainfall conditions (after Peltier, 1950)

2.6 Mechanical behaviour and weathering of clays

As far as the aims of the study are concerned, the effect of weathering on clay materials, specifically their geotechnical characteristics, is of most interest. To step into this, it is important to have a broad concept about the physical properties and mechanical behaviour of the material. Clay is one of the natural materials most studied by civil engineers for it is of great importance as a foundation material and causes many problems in engineering works. Much attention has been paid to the mechanical properties of clays. The behaviour is described in the major works providing a description of the deformation behaviour of soil, including Roscoe *et al.* (1958), Schofield & Wroth (1968), Atkinson & Bransby (1978) and Wood (1990). All these works try to establish a common framework to describe the deformation behaviour of all soils.

Before the 1960s almost all the theories of clay behaviour concerning the physical and chemical characteristics were based on the interaction of single particles (Barden, 1972a). These theories stand on the principle that the engineering behaviour of clay is dominantly controlled by individual particles and the relationship with their surroundings. However, in the last two or three decades it has become recognised that both artificial and natural clay soils are made up of clay plates and plate aggregations including peds, crumbs or clusters (Frost, 1967; Barden, 1972a; Pandian, 1993a). It is these particles and aggregations as well as the structures they form which heavily influence the overall behaviour of the clay.

Micro-structural studies have been made on a large number of natural clays by Barden (1972a) using the scanning electron microscope technique. Barden (1972a) revealed that almost no clay soils exhibited single plate "card-house" structure (Figure 2.6.1), but a general occurrence of plates aggregated face to face (Figure 2.6.2). The results of Barden's study conclude that in dispersed conditions the plates aggregation leads to a "turbostratic" structure and in flocculated conditions to a "book-house" structure. Yong (1971) also had a similar suggestion that single plate theory is relevant only to dilute colloidal suspensions, and that natural consolidated clays require consideration as multiple plate units.

It is not an unusual case that a number of tropical residual soils contain holloysite and/or similar clay minerals, and often these clay particles aggregate together to form a larger sized cluster which results in a higher shear strength and many characteristics of a granular soil (Dixon & Robertson, 1970). The increasing evidence for aggregation in clay

particles suggests that the basic deformation mechanisms of clay soil may depend not only on the characteristics of the clay but also on the granular clay aggregates (Canestrari & Scarpelli, 1993).

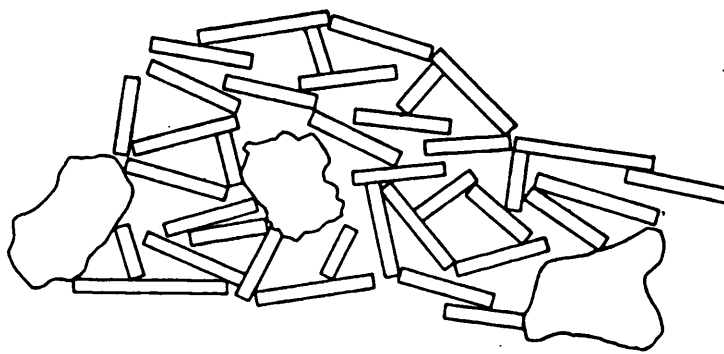


Figure 2.6.1 Diagram showing single plate "card-house" structure

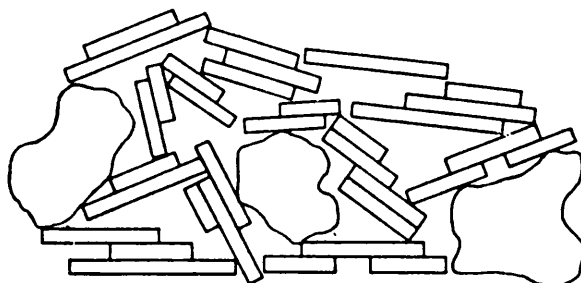


Figure 2.6.2 Diagram showing plates aggregated face to face

Continuous wetting and drying events are thought to be responsible for the aggregation of clay particles, particularly in tropical regions (Lambe & Whitman, 1979; Pandian *et al.*, 1993a). This is because the wetting and drying result in large suction pressure development and small particles are drawn together to become larger grains. Frost (1967) demonstrated the results of the study of a loamy soil in which the strength increased from 352 kPa for in situ conditions to 1620 kPa when the soil was air-dried, re-wetted and compacted to field water content and density. The material also exhibited characteristics of sand after drying and re-wetting. The change in material characteristics is believed to be due to the aggregation of the fine particles. Wallace (1973) also observed similar phenomenon in a residual soil from Papua New Guinea. The permeability increased 100 times when the natural residual soil was dried, re-wetted and compacted to meet the conditions in the field. The increase in permeability was due, partly, to changes both in the nature of particles and voids and in the structure which caused the original clayey soil to become sand-like in its physical characteristics.

Many natural soils are structured (Vaughan, 1985) and the mechanical behaviour of the structured materials cannot be simply described using void ratio-effective stress relationships (Aversa *et al.*, 1993; also see Appendix I). In fact, the presence of micro-structures and cohesive bonds are perhaps more important factors in terms of influencing deformation characteristics such as stiffness and strength, of soil materials in most cases (Petley *et al.*, 1993; Rampello & Silvestri, 1993). Therefore, the mechanical behaviour of natural soils are generally more complicated than published idealised models of soil behaviour because of their micro-structures and bonding effects.

Stiffness and shear strength, for instance, are essentially dependent on the micro-structure and bonding present in the soil material (Burland, 1990). Undisturbed samples with original structures and diagenetic bonding exhibit much higher strength and stiffness than those remoulded and subsequently re-consolidated samples, which without structure and cement, at any given consolidation state (Rampello & Silvestri, 1993).

A preferred orientation of particles in a clay material will result in an overall weakening of the material during deformation (Goldstein *et al.*, 1961). If a material contains a mixture of sand, silt and clay particles, then the clay particle orientation will produce an anisotropy in the rock during deformation, even if the fabric within the material was isotropic to begin with (Viggiani *et al.*, 1993). The anisotropy is normally in the form of a band with low shear resistance which tends to act as a yield locus as it is the weakest area in the rock and will facilitate further shear surfaces to be produced. As soon as any shear displacement occurs, the shear strength along the plane will reduce to the residual

value. Skempton (1964) suggested that this may induce progressive failure around the plane of weakness.

The importance of particle orientation in a soil material on its mechanical characteristics is best demonstrated by the fact that the shear strength of a clay sample with randomly oriented, platy particles is much greater than that of a mass with highly oriented platy particles (Skempton & Petley, 1967). Skempton (1964) conducted a series of direct shear tests on overconsolidated clays under drained conditions. The results, in general, showed that all samples exhibited an initial peak shear strength which rapidly declined as the sample failed. If the displacement continued, then further minor peaks occurred (Figure 2.6.3). The small peaks represented the increased shear resistance of clay particles whose orientation opposed the shearing movement. The shear resistance decreased as the particles gradually became re-aligned (Petley *et al.*, 1993). Skempton (1964) suggested that the reduction of shear strength from the peak value down to the residual in overconsolidated clay materials during shear was a result of a weakening of the sample through an increase in water content of the sample (dilation) and the reorientation of the clay particles within the sample.

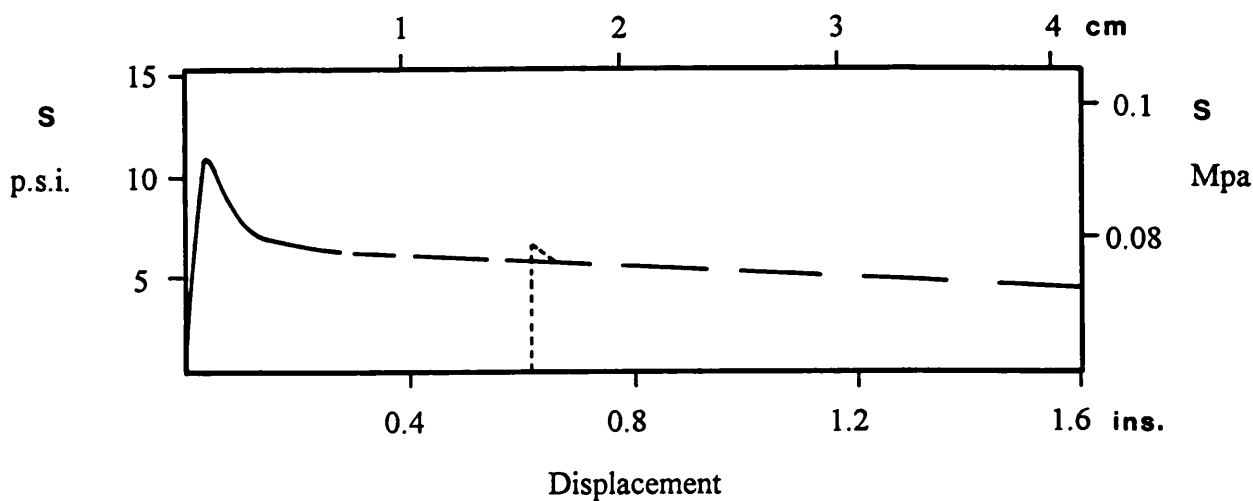


Figure 2.6.3 Results of shear tests conducted on samples from Walton's Wood (after Skempton, 1964)

The true residual strength of a clay material is reached when all the clay particles in the shear zone became oriented parallel to the shear surface at which point, the resistance to the shear displacement of the particles is at a minimum value. It is the continuous displacement that causes the polished shear surfaces which weaken the material (Skempton & Petley, 1967) and it is the friction between the oriented clay particles which determines the magnitude of the residual strength.

The existence of fabrics within weak rocks, such as clay and chalk, also exerts significant influence on their mechanical behaviour during laboratory deformation (Leddra, 1989; Kågeson-Loe *et al.*, 1993; Petley *et al.*, 1993). The most common phenomenon during consolidation of these weak rocks is a reduction in the stiffness. This is due to the failure of the original diagenetic fabric, structure and intergranular bonding in the material. This change in state should not be regarded as simply the achievement of the pre-consolidation pressure, but a consequence of the destruction of natural stiffness due to bonding (Petley *et al.*, 1993; Jones *et al.*, 1994; Kågeson-Loe, 1994).

The peak strength magnitude and failure behaviour of clays are strongly influenced by the structure of the grain fabric with the mineralogical composition exerting only minor influence (Bertuccioli & Lanzo 1993). The number and arrangement of the fractures within stiff clays and shales play an essential role in controlling their mechanical behaviour (Bedian & Khera, 1993; Vallejo *et al.*, 1993). The most important controls are the frequency and the orientation of the fissures. A reduction of 20% in the shear strength is attributed to the presence of frequent micro-fissures and an even larger reduction of 50% can be achieved if the fissures are parallel to the direction of shear displacement (Bedian & Khera, 1993).

The bonding effect has more pronounced influence on the behaviour of soils in the low stress regime than at high stresses (Coop & Atkinson, 1993; Toll & Malandraki, 1993). Investigation made by Toll and Malandraki (1993) indicates that at low confining pressures a bonded soil can sustain higher stress (with higher stress ratio q/p') due to the bonding effect than the unbonded sample, whereas under a high stress regime, both bonded and unbonded samples exhibit very similar stress ratio characteristics. This suggests that during laboratory deformation, the magnitude of the applied confining stress should be taken into account during phenomenological interpretation of the data. The implication is that bonding may be destroyed by increasing confining pressure, causing a reduction in the stiffness of the sample. the reduction is not due to the achievement of the preconsolidation pressure which agrees with the investigations made

by Coop & Atkinson (1993), Petley *et al.* (1993), Jones *et al.* (1994) and Kågeson-Loe (1994).

Dilation is a commonly observed phenomenon while conducting soil triaxial compression tests. It is the means through which a dense or overconsolidated soil can reach its ultimate failure state or the critical state² (Atkinson & Bransby, 1978). For dense and overconsolidated materials, in order to achieve the critical state the volume of the specimen will tend to expand (because majority of overconsolidated soils are on the *dry side of critical*³) which, under undrained circumstance, will result in a negative pore water pressure generation. Dilation has a significant effect on the angle of internal friction of a soil sample and appears to be a function of the specific volume (v) of the sample and mean effective stress (p') (Canestrari & Scarpelli, 1993). It is suggested that dilation is responsible for many soils exhibiting extra friction above the critical state.

The residual strength of a clay soil is controlled by its mineralogy (Kenney, 1967) and is independent of its compaction history (Skempton, 1961). In contrast, the peak strength is controlled by the compaction history and diagenesis of the material (Russell & Parker, 1979). During the compaction and diagenesis, anisotropic textures caused by specific arrangement of the platy clay particles and inter-particle bonds due to cementing agent are formed (Bjerrum, 1967a; 1967b). The role of weathering is to reverse these processes. The original texture will be modified and the diagenetic bonds will be destroyed by weathering.

As described previously in the introduction section of this chapter, many rocks were originally formed at high temperature and pressure and the main part of the weathering process consists of changes in rock or rock fragments to equilibrate to a new environment at lower temperatures and pressures in the presence of air and water. Several kinds of alteration are possible and a material which is an end product of weathering under one set of conditions may become an unstable material for renewed weathering if conditions are different.

The final structure of a soil is often formed through weathering (Barden, 1972b). This is to say that weathering is essentially a disruptive process tending to modify the micro-structure of the materials through breakdown and homogenisation. Many of the soil properties resulting from overconsolidation and compaction are modified by weathering.

²The definition of the critical state is given in appendix I.

³Dry and wet side of critical are introduced in appendix I. The simple explanation of dry side of critical is that the water content of a sample is less than that of the sample at critical state.

Many civil engineers and engineering geologists have been trying to establish a unique scheme to classify different degrees of weathering. However, due to the different characteristics of weathering regimes at different parts of the world and the different nature of different rocks it is extremely difficult, if not impossible, to achieve this aim. Though it is difficult, there are many weathering classifications. Tables 2.6.1, 2.6.2 and 2.6.3 are some examples. Nevertheless, it is important to note that all the classifications are similar in a broad sense, such as increasing oxidation and losing original structures. The individual characteristics, have to be taken into account. Workers' personal opinions and interpretations also have some influence on the recognition of weathering classification.

Table 2.6.1 Weathering scheme for Keuper Marl (after Chandler, 1969)

	<i>Zone</i>	<i>Description</i>	<i>Notes</i>
Fully weathered	IVb	Matrix only	Can be confused with solifluction or drift deposits, but contains no pebbles. Plastic, slightly silty clay. may be fissured.
Partially weathered	IVa	Matrix with occasional clay-stone pellets, less than 1/8 in. dia. but more usually coarse sand size.	Little or no trace of original (I) structure, although clay may be fissured. Lower permeability than underlying layers
	III	Matrix with frequent lithorelicts up to 1 in. As weathering progresses lithorelicts become less angular.	Water content of matrix greater than that of lithorelicts.
	II	Angular blocks of unweathered marl with virtually no matrix	Spheroidal weathering. Matrix starting to encroach along joints; first indication of chemical weathering.
Unweathered	I	Mudstone (often fissured)	Water content varies due to depositional variations.

Table 2.6.2 Engineering grade classification of weathered mudrocks
(after Fookes *et al.*, 1971)

<i>Grade</i>	<i>Degree of decomposition</i>	<i>Field recognition</i>
VI	Residual soil	The original soil is completely changed to one of new structure and composition in harmony with existing ground surface conditions.
V	Completely weathered	The soil is discoloured and altered with no trace of original structures.
IV	Highly weathered	The soil is mainly altered with occasional small lithorelicts of original soil. Little or no trace of original structures.
III	Moderately weathered	The soil is composed of large discoloured lithorelicts of original soil separated by altered material. Alteration penetrates inwards from the surfaces of discontinuities.
II	Slightly weathered	The material is composed of angular blocks of fresh soil, which may or may not be discoloured. Some altered material starting to penetrate inwards from discontinuities separating blocks.
I	Fresh rock, unweathered	The parent soil shows no discoloration, loss of strength or other effects due to weathering.

Table 2.6.3 Weathering scheme for the London Clay at South Ockendon
(after Chandler & Apted, 1988)

<i>Zone</i>	<i>Classification</i>	<i>Description</i>
IV	Fully weathered	Completely remoulded clay, or a few lithorelicts (up to 10mm max. dimension) occupying < 30% of whole, in a matrix of soft to firm remoulded clay; brown or light grey, mottled brown.
IIIb	Partially weathered	Lithorelicts (10 mm to 30 mm average dimension; brown internally) completely separated by remoulded matrix and occupying 30% to 70% of whole; fissure surfaces and matrix often light grey (greyed); selenite crystals common.
IIIa		Dominantly brown (oxidised), with clay fragments showing original clay structure (lithorelicts) with 30 to 70mm average dimension occupying >70% of whole; remoulded matrix developing in fissures and joints; some selenite crystals.
IIb	Partially weathered	Clay fragments bonded by heavily iron stained joints and fissures, the brown coloration penetrating up to 20 mm; centre of fragments the colour of zone IIa clay; fissure spacing typically 70 mm to 120 mm.
IIa		Weathering on surfaces of discontinuities only, with rusty yellow staining on joint, fissure and bedding planes; bulk of clay grey-brown; fissure spacing typically >100 mm.
I	Unweathered	Uniformly grey-brown or grey-blue; discontinuity spacing typically >100 mm

Studies of the effect of weathering on clays can roughly be divided into two classes in an engineering sense. One group comprises of studies which examine the parameters associated with strength characteristics, such as cohesion and angle of internal friction, and the other group concerns modifications made to the structures, such as particle and void characteristics, and fabrics. Mineralogical alteration is very important as far as studies of weathering are concerned but it is relatively insignificant for clay materials within the depth range that many civil engineers are interested (Chandler, 1969, Fan & Jones, 1994).

It is well recognised that in overconsolidated clays the water content, which reflects the void ratio, increases in the material with increasing proximity to the ground surface (Terzaghi, 1936). The easiest and most convenient index of identifying the consequence of weathering in most stiff, overconsolidated clays is the increasing water content resulting from the various weathering processes (Chandler & Apter, 1988). Other than the increase in natural water content, weathering may also lead to changes in particle and void characteristics. Consequently, the mechanical properties of the clays will be modified by the weathering processes.

Reduction in shear strength is a common consequence of weathering (Chandler, 1969; Russell & Parker, 1979). Investigations of the effect of weathering on Keuper Marl (Chandler, 1969) and Oxford Clay (Russell & Parker, 1979) reveal that as the degree of weathering increases the strength of the material decreases. The decrease in strength is the consequence of the decreased effective cohesion and effective internal angle of friction resulting from destructuring induced by weathering. The deformation behaviour is also changed because of the destructuring (Chandler, 1969). The overconsolidation characteristics resulting from the previous compaction history becomes less pronounced as weathering proceeds leading to a decrease in overconsolidation ratio.

Although weathering induced reduction of strength is common, it does not apply in all cases. An opposite effect, increasing strength, has been observed in quite a few investigations (Chandler, 1972; Balasubramaniam *et al.*, 1978; Fan *et al.*, 1994). The weathered samples exhibit higher shear resistance than the unweathered ones at a given specific volume (v) and a given mean effective stress (p'). Chandler (1972) attributed this increased strength to both the restructuring of the originally anisotropic fabric, and an increase in plasticity by weathering. Similar change in characteristics can be expected in other heavily overconsolidated clays and clay shale.

An example of strengthening is demonstrated by Balasubramaniam *et al.* (1978) who studied the strength parameters of some Bangkok clays. Balasubramaniam *et al.* (1978) classified the test clays into three layers: Weathered Clay, which was formed from the overlain Soft Clay by various processes of weathering, approximately 4.5 m in thickness; Soft Clay, extending to a depth of 10m below the weathered Clay, and is highly compressible and lightly overconsolidated; Stiff Clay, often fissured, extending to a depth of approximately 10m below the Soft Clay horizon. The c' (effective cohesion) and ϕ' (effective angle of friction) data obtained from their undrained compression loading tests are given in Table 2.6.4.

Table 2.6.4 Strength parameters of the Bangkok Clays
(data compiled from Balasubramaniam *et al.*, 1978)

Sample	Depth in the profile (m)	c' (kN/m ²)	ϕ (°)
Weathered Clay	0-4	0	22.2
Soft Clay	4-14	0	26
Stiff Clay	14-24	38	24

The results demonstrate that weathering significantly alters the strength properties of the materials. The Stiff Clay is supposed to be an unweathered sample which preserves the original diagenetic structure and overconsolidation characteristics and exhibits a cohesion of 38 kNm⁻². Neither the Soft Clay, which lies above the Stiff Clay, nor the Weathered Clay, which is the top weathered crust, exhibited any cohesion at all, suggesting that cohesion, strongly controlled by bonding, is destroyed by the weathering processes. The change in the angles of internal friction do not follow the sequence of the sample depths but exhibit an initial increase in ϕ from 24° to 26° as the clay changes state from "Stiff" to "Soft". Subsequently, continuous and more severe weathering caused the decrease in the ϕ value to 22.2° as the clay turned into "Weathered". The initial increase in ϕ is believed to be a result of restructuring of the clay induced by weathering leading to the absence of the pre-existing fissures as suggested by Chandler (1972).

Weathering progressively destroys the structures previously formed either during diagenesis or during compaction (Barden & Sides, 1971; Barden, 1972b; Grainger & Harris, 1986; Coulthard & Bell, 1993). Usually, in unweathered overconsolidated clays, samples have good alignment of clay particle assemblages around more poorly aligned larger particles. The partially weathered samples have lost most of their diagenetic bonding and original fabric but still retained some of the pre-existing structures and the

highly weathered samples have a totally different type of fabric. The gradual change in the micro-structure indicates that one of the most important effects of weathering is to modify the original fabric by altering the arrangement of the clay particles.

Chapter Three: Scaly clay and its Natural Occurrence

3.1 Introduction

The aim of this study is to investigate the influence of tropical weathering on the geotechnical characteristics of scaly clays. It is important to have a general knowledge of the back ground information on issues such as the material itself and study areas. In this chapter, the theories on the origin of scaly clays and the general geology of the study areas will be provided.

3.2 Scaly clay

Scaly clay is a fine grained argillaceous sediment. It has a pervasive fabric of lenticular, highly polished, curved, slickensided surfaces. Scaly clays have been discovered and identified both on and off shore in many tectonically active areas including Barbados (Joe's River Formation) (Enriquez-Reyes *et al.*, 1990), Taiwan (Lichi Mélange) (Liou, *et al.*, 1977), the island of Timor (Bobonaro scaly clay) (Barber, 1981), Cyprus (Moni Mélange) (Hsu, 1971) and Italy (Yassir, 1989). The areas are, or have in the recent past, experienced tectonism associated with subduction. In each case scaly clay is associated with major mélange deposits.

Other than in subduction zones, scaly clays have also been reported in Deep Sea Drilling Project (DSDP) core samples. The origin of the DSDP core scaly clays is thought to be related to fault structure (Moore *et al.*, 1986; Schoonmaker, 1986). Most of the scaly clays found within DSDP cores occur adjacent to faults. Cowan (1984) described scaly clays found in association with thrust faults and the decollement zone of the Barbados Ridge. In Cowan's description the texture of the material is very similar to the texture of the Joe's River Formation mélange from Barbados. The difference is that the texture Cowan described appears to be very limited within a narrow band, whereas the Joe's River Formation has a pervasive distribution of scaly textures and forms an extensive body.

3.2.1 Origin of the scaly fabric

The occurrence of the very distinctive scaly texture is believed to be a product of the diagenetic and tectonic histories experienced by these clays (Barber *et al.*, 1986). The

high degree of preferred orientation is widely regarded to be a consequence of shear deformation. Skempton (1966) conducted a series of experiments on remoulded clay samples using direct shear box and triaxial apparatus and discovered that at the onset of shearing, the samples developed a group of micro-shear planes with orientation of 10° to 30° to the principle displacement direction (Figure 3.2.1a). Because the micro-shear planes are not parallel to the direction of the principle displacement, the movement along them will eventually stop as they become locked. Further displacement would lead to the development of new shear surfaces which are parallel to the direction of displacement. Rhombohedral blocks would then be defined by the interaction of the two sets of planes (Figure 3.2.1b), and the blocks would move independently of each other. With further movement, however, the shear planes would join up to form a long, undulating principle surface of shear displacement (Figure 3.2.1c). If movement continued, the entire shear zone would gradually become flattened (Figure 3.2.1d) and any subsequent deformation would result in distortions of the shear zone. A blocky, sheared clay composed of numerous shear lenses is the result. The size and shape of the lenses may vary significantly. Their surfaces could be curved, slickensided and polished producing a fabric similar to that commonly observed in scaly clays (Figure 3.2.2).

Observations made by Skempton (1966), Morgenstern & Tchalenko (1967) and Clark (1970) on the micro-structure of shear zones reveal that the scaly fabrics are produced in areas where the clay particles become strongly aligned parallel to the shear surfaces. Within a very thin layer the platy particles develop a strong preferred orientation. A polished (scaly) surface is the result. The preferred alignment of particles is absent away from the surfaces. Similar characteristics have also been observed by Page & Suppe (1981), Cowan (1984), Moore *et al.* (1986) and Petley *et al.* (1993). Moore *et al.* (1986) attributed the occurrence of the scaly texture that exists in DSDP cores to the shear deformation induced by faulting.

In the scaly clays found adjacent to thrust faults, the scaly texture mostly develops in areas rich in smectite. Moore *et al.* (1986) also reported that no mineralogical alteration occurred during the formation of the scaly fabric. The scaly texture is interpreted as a result of particle reorientation due to the state of shear stress adjacent to fault zones. Moore *et al.* (1986) proposed a model for the development of scaly textures, in which both shear failure and de-watering occur concurrently with faulting of the clay. This would lead to a decrease in the pore fluid pressure within the fault zone mobilising increased normal effective stresses. Consequently, the shear strength of the clay increases during deformation because of the increased shear resistance on the shear surfaces. Further shear failure would then be likely to occur in the weaker adjacent areas.

Propagation of the strain hardening bifurcation due to the deformation will promote the development of the scaly texture throughout the entire mass. A pervasive scaly fabric is the result.

Page & Suppe (1981) suggested that the scaly fabrics of the Lich Mélange in Taiwan may have developed whilst the mélange sediment was deformed during tectonic emplacement. Barber *et al.* (1986) attributed the origin of scaly clays and the occurrence of the scaly texture to the movement of underconsolidated materials within active diapirs. It was suggested in their investigation that when an underconsolidated clay is overlain by normally consolidated material, the difference in the densities of the two materials would generate a metastable condition, leading to an upward movement of the underconsolidated sediment. If the normally consolidated material is faulted, the highly plastic, underconsolidated clay would become mobilised and squeeze into the fault to form a diapir. The high pore fluid pressure of the underconsolidated sediment would then be able to dissipate during upward movement converting the sediment to a denser, normally consolidated material. If the movement of the now densified clay mass continued it would necessitate the development of internal shear failures and polished shear surfaces with random orientation. The characteristic nature of the scaly clay would be a result of the diapiric movement and the expulsion of pore fluids.

Field observations in Barbados (Jones pers. comm.; Allison pers. comm.) and Taiwan (Jones pers. comm. and this study) have revealed that not only is the scaly texture of mélange clays preserved with the weathering zone, but that the texture in various ways interacts with and influences the weathering process. It is the investigation of how weathering affects the characteristically textured clays which forms the major part of the present study.

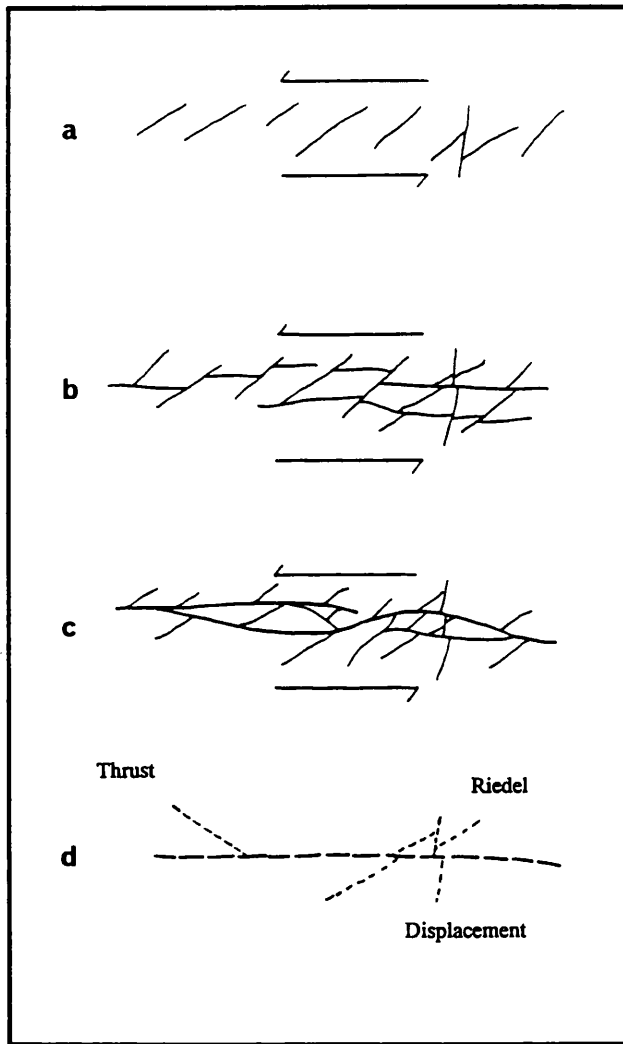


Figure 3.2.1 A schematic representation of the fracture pattern in a shear zone (after Skempton, 1966)

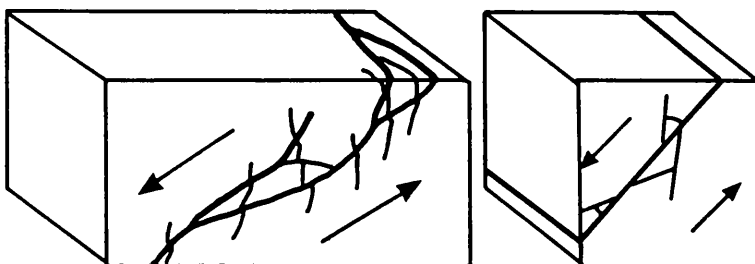


Figure 3.2.2 Block diagrams showing fracture pattern described by Skempton (1966)

3.3 Field areas

The materials examined in this research are the Joe's River Formation scaly clay from Barbados and the Lichi Mélange scaly clay from Taiwan. Both Barbados and Taiwan experience tectonic activity and tropical weathering. The general environmental conditions of the study areas are summarised in this section. In addition, the sample collection is also described.

3.3.1 Barbados

3.3.1.1 Climate

The island of Barbados is located in the Caribbean, on the Barbados Ridge and is the only emergent part of the Caribbean Forearc complex associated with the 2,700 m deep Tobago Trench (Figure 3.3.1). A large proportion (85%) of the surface of the island is Pleistocene coral limestone (Figure 3.3.2), which has been heavily eroded (Speed, 1983). The Scotland District lies in the north-east of the island (Figure 3.3.2) and possesses folded Tertiary sedimentary rocks which, at present, are undergoing strong headward erosion. Extensive mudslides frequently occur, as large parts of the waterlogged clay at the base of the limestone slide away. Furthermore, strong spring erosion is adding to the effects of headward erosion leading to a pronounced loss of agricultural land (Blume, 1968).

The average temperature at sea-level is over 25°C throughout the year, and the difference between the coldest and hottest months is approximately 3°C. Seasonal differences in weathering regime are therefore hardly, if at all, determined by temperature.

Relative humidity is very high in the whole Caribbean area. The recorded climatic data show that the daily variation in humidity is greater than seasonal variation. Normally the highest relative humidity of more than 90% is reached at about sunrise. Rising temperature causes a decrease in relative humidity but never to less than 50% and usually not below 70%.

Heavy precipitation is one of the climatic characteristics of the Caribbean area, caused by atmospheric instability and generally in the form of short and violent showers. Mean annual precipitation in the Caribbean area varies considerably and depends largely on the topographic conditions. For instance, mean annual precipitation increases from 1,100 mm to 2,100 mm with increasing height of 300 m on the island (Blume, 1968). The

annual rainfall of Barbados is some 1,250 mm, and most of it is concentrated in the rainy season from June to December (Blume, 1968). The general climatic type of Barbados can be summarised as tropical moist climate with seasonal rainfall.

3.3.1.2 Geology

The island of Barbados lies on the Barbados Ridge Complex, which is a broad accretionary complex lying east of the Lesser Antilles magmatic island arc (Figure 3.3.3). The complex contains great thicknesses (10 km) of Tertiary sediments with variable degrees of deformation which accumulated on the Atlantic Ocean floor. They include heavily deformed Paleogene flysch, pelagic strata and possible local shallow-water deposits (Westbrook & Smith, 1983; Case *et al.* 1984). The Barbados Ridge composes the major part of the Forearc region of the Lesser Antilles magmatic arc. The toe of the ridge is almost certainly the locus of modern accretion of sediment from the subducting Atlantic sea floor (Westbrook, 1975). The pre-Pleistocene geology of the island of Barbados, which exposes the crest of the Barbados Ridge, is best explained by accretion implying that the ridge as a whole is an accretionary prism (Speed, 1981). Important elements of the geology of the island in this interpretation are the occurrence of many of the pre-Pleistocene rocks in fault-bounded packets (Speed & Larue, 1982).

Three geologic units exposed on the island of Barbados are recognised (Speed, 1981) (Figure 3.3.2). First, an upper cap of Pleistocene reefs which were deposited in place. Second, an intermediate zone of nappes of mainly calcareous pelagic rocks. Third, a basal complex of steeply fault bounded packets of several sedimentary lithotypes. Such rock types and structural features are thought to be a typical product of a tectonically active area which, in this case, was accreted within an inner trench wall during the late Eocene and which today extends to a depth of greater than 5 km below Barbados (Torrini *et al.*, 1985). The three geologic units are briefly described below.

1. Upper Cap

The cap occupies the majority area of the island and is a south-west trending arch of uplifted reefs that progressively young towards the west. It is a Pleistocene reef-related limestone (Torrini *et al.*, 1985) At present, the cap is still raising at a significant but variable rate throughout the area (Brown & Westbrook, 1987). The fastest rate observed occurs along the south-west trending axis with an approximate value of 0.45 mm yr^{-1} , whereas the uplift rates at some other places only attain about half of this (Speed & Larue, 1982).

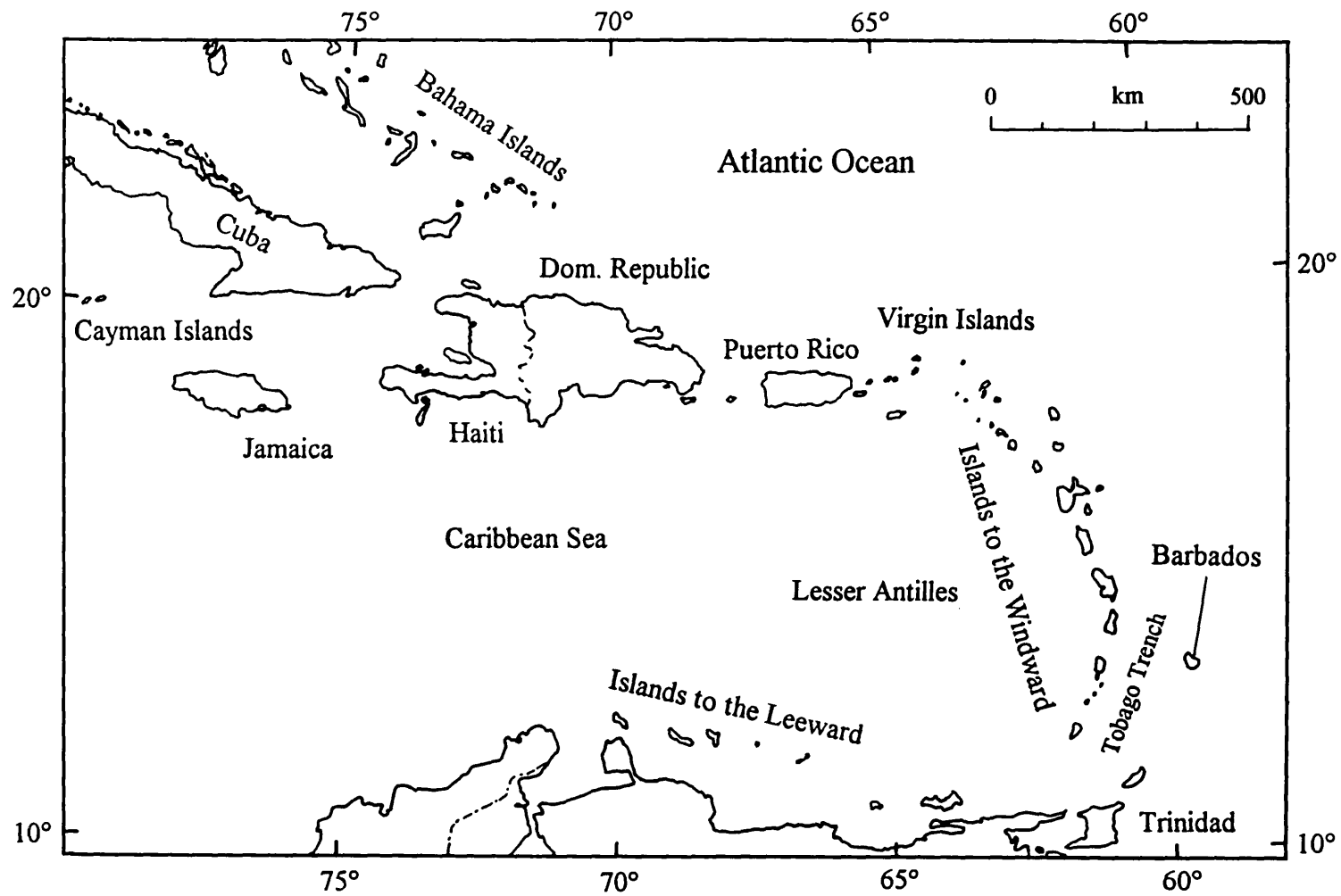


Figure 3.3.1 Map of the Caribbean islands

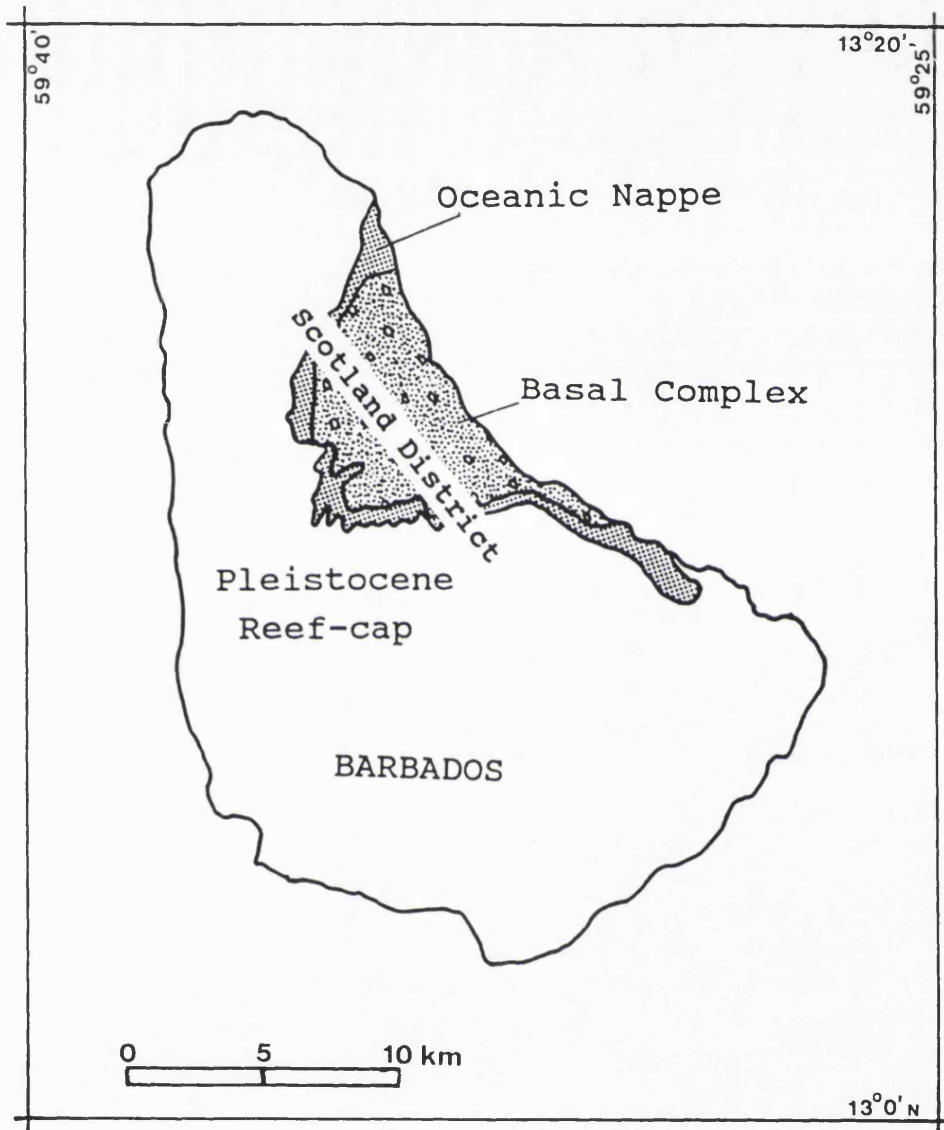


Figure 3.3.2 Geological map of Barbados

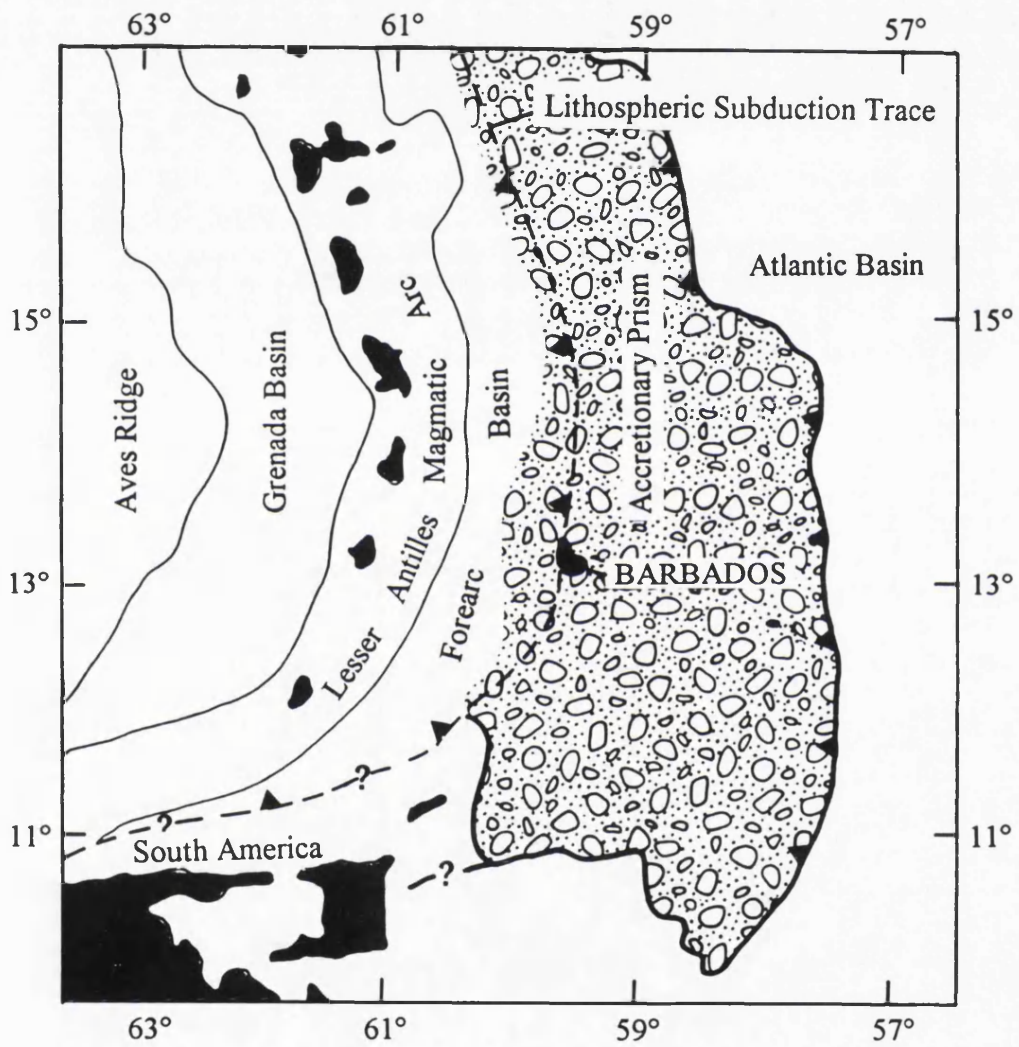


Figure 3.3.3 Regional tectonic unit of the south-eastern Caribbean

2. Oceanic Nappe

The intermediate zone of pelagic rocks comprises two discrete bodies which may not have been originally contiguous. The main belt, the Oceanic Nappe (Figure 3.3.2), lies below the Pleistocene reef cap and crops out in the form of a band rimming the basal complex unit and separating it from the Upper cap. The other body is the Bissex Hill Nappe exposed in the basal complex (Figure 3.3.5). Both bodies contact the rocks of the basal complex with shallow-dipping faults. The age of the rocks of the Oceanic Nappe ranges from middle Eocene to middle Miocene (Speed & Larue, 1982; Larue & Speed, 1984). Strata within the Oceanic Nappe are inclined at shallow angles but are locally tightly folded about east to north-east trending axes, whereas the Bissex Hill Nappe overlies the basement with sub-horizontal contact (Speed & Larue, 1982).

3. Basal Complex

This Basal Complex is the most studied unit in Barbados for it is the key to understanding of the tectonic evolution of the south-east Caribbean. Rocks of the basal complex crop out in north-eastern Barbados (Figure 3.3.2). The basal complex is composed of fault-bounded packets, most of which are sub-vertical and have strikes generally oriented northeast-east (Speed & Larue, 1982). Stratigraphically, each packet is different from adjacent packets and no correlations between any two adjacent packets can be made. Each packet of the basal complex contains rocks of one of three lithic suites, namely, terrigenous, hemipelagic and *mélange*. The terrigenous suite comprises quartzose sandstone and pelitic clastic rocks that accumulated in a trench wedge or sub-sea fan environment. There are no evident correlations among the terrigenous suites. Possible age of this suite is Paleocene to late Eocene (Larue & Speed, 1984). The hemipelagic suite contains radiolarite, mudstone that is occasionally rich in radiolaria with rare interbeds of quartzose turbidite. Radiolaria in the suite indicates that the probable age of the suite ranges from early to middle Eocene (Larue & Speed, 1984). The *mélange* suite, Joe's River Formation, contains massive breccia of mudstones and sandstones, pebbly mudstone and local intervals of bedded mudstone and thin quartzose turbidite (Speed, 1981; Speed & Larue, 1982). Dating based on the matrix indicates that the suite is lower Eocene to upper Paleocene in age (Larue & Speed, 1984). The more detailed geology of the Joe's River Formation will be given later this chapter in section 3.3.1.4.

3.3.1.3 Tectonic setting

Geologically, the island of Barbados lies 160 km east of the Lesser Antilles arc and is the highest point of the Barbados Ridge which is a ridge of sedimentary rock that runs parallel to the arc (Figure 3.3.3). The Lesser Antilles Forearc, a calc-alkaline volcanic island arc, forms the eastern margin of the Caribbean (Westbrook, 1975). This is a tectonically active area where the Atlantic plate is being subducted beneath the Caribbean plate (Figure 3.3.4), at an average rate of 20 mm yr⁻¹ (Pudsey & Reading, 1981). West of the arc is the Grenada Trough, which is a flat-bottomed basin containing a 4 km thick sequence of sediments and the Aves Ridge, which is a submarine ridge with a number of features suggesting that it is an old island arc (Figure 3.3.3) (Westbrook, 1975).

The basal complex unit on the island of Barbados may be representative of rocks and structures of the upper parts of the accretionary prism of the Lesser Antilles arc (Speed, 1983). Seismic surveys and sonar images of the sea floor to the east of Barbados indicate the presence of mud diapirs associated with underconsolidated sediments at depth. It is these sediments that are thought to form the diapiric mélange of which the Joe's River Formation is a part (Biju-Duval *et al.*, 1982; Stride *et al.*, 1982; Brown & Westbrook, 1987).

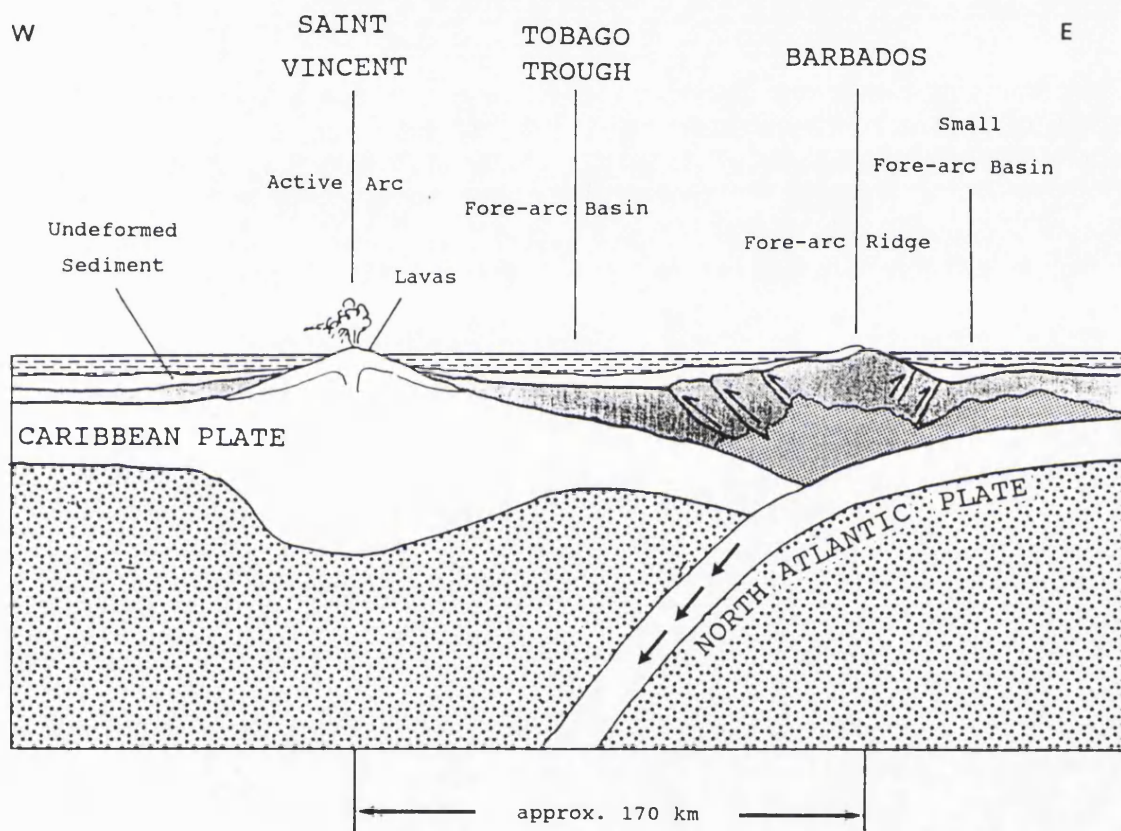


Figure 3.3.4 Tectonic setting of Barbados

3.3.1.4 Joe's River Formation

The Joe's River Formation outcrops in the Scotland District of Barbados (Figure 3.3.5) and is thought to represent a diapiric *mélange* deposit, as opposed to an olistostrome *mélange* (Senn, 1940; Pudsey & Reading, 1981; Barber *et al.*, 1986). The Joe's River Formation has three components. First, a massive breccia of mudstone and sandstone clasts, with a foliated mudstone matrix. Second, a layered breccia of scattered, poorly to well oriented blocks of quartzose turbidite, radiolarite and calcareous pelagic rocks in foliated, sandy, mud-pebbly mudstone. Third, turbidite beds, one of which includes calcareous micro-fossils (Larue & Speed, 1984). The Formation includes a number of large olistoliths embedded in a dark green to brown, silty clay matrix, which appears to be highly inhomogeneous, containing clay rich and silt rich areas. It also contains wisps of uncemented, fine grained sand and streaks of solid hydrocarbon (Enriquez-Reyes & Jones, 1991). In addition to the inhomogeneity, there are nodules of highly plastic, light green clay, which are of variable diameter.

The most distinctive feature of the *mélange* clay is its pervasive fracture pattern (Yassir, 1989; Enriquez-Reyes & Jones, 1991). The material possesses numerous, anastomosing cleavage planes which vary in spacing between 2 mm and 15 mm (Enriquez-Reyes & Jones, 1991). The cleavage surfaces are usually smooth, frequently curved and when exposed in outcrop, display a polished slickensided surface. Only a small shear stress is needed for blocks of unweathered material to break up. The scaly fabric acts as lines of weakness along which disintegration occurs (Plate 3.3.1).

Rapid rates of erosion characterise the surface exposures of the Joe's River Formation. Materials exposed on hill sides are susceptible to erosion by water during torrential rainstorms. If rainstorm events are of long duration, the exposed surface materials become over saturated and liquefied, and then surface flow occurs. The process is particularly noticeable on areas of bare ground exposed by the removal of overlying material.

Landslides are prevalent on many scaly clay outcrops. Geomorphologic mapping completed by Enriquez-Reyes *et al.* (1990) (Figure 3.3.6) provides an example of the spatial distribution of landslides on these terrains. Most of the landslides are of the shallow seated translational type characteristic of mudflows (Brunsden, 1984). Although mudflows are most common in terms of spatial distribution in the Joe's River Formation, there are other shallow transitional slips along streams due to toe erosion. The latter type is pronounced following torrential rain events when stream discharges are at high level.

It has been noted by Enriquez-Reyes *et al.* (1990) that following a recent landslide event the slope may remain stable for a period of time while slides occur at other places. With the progression of time, the slope gradually becomes unstable and failure again occurs. This mechanism repeats continuously, forming a cycle of slope instability throughout the areas where scaly clays are exposed. Deep seated rotational slides are rare. This is unusual because clay rich sediments are often characterised by deep seated failure (Bromhead, 1986). The rapid change in the mechanical properties of the scaly clay at shallow depth and the high frequency of shallow mass movement may be responsible for the absence of rotational failure.

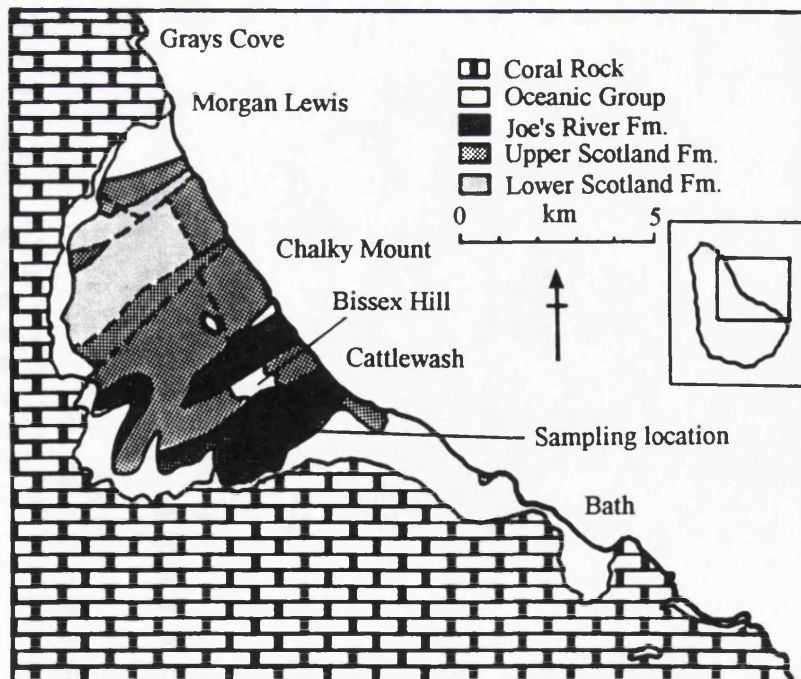


Figure 3.3.5 Geological map of the study area in Barbados

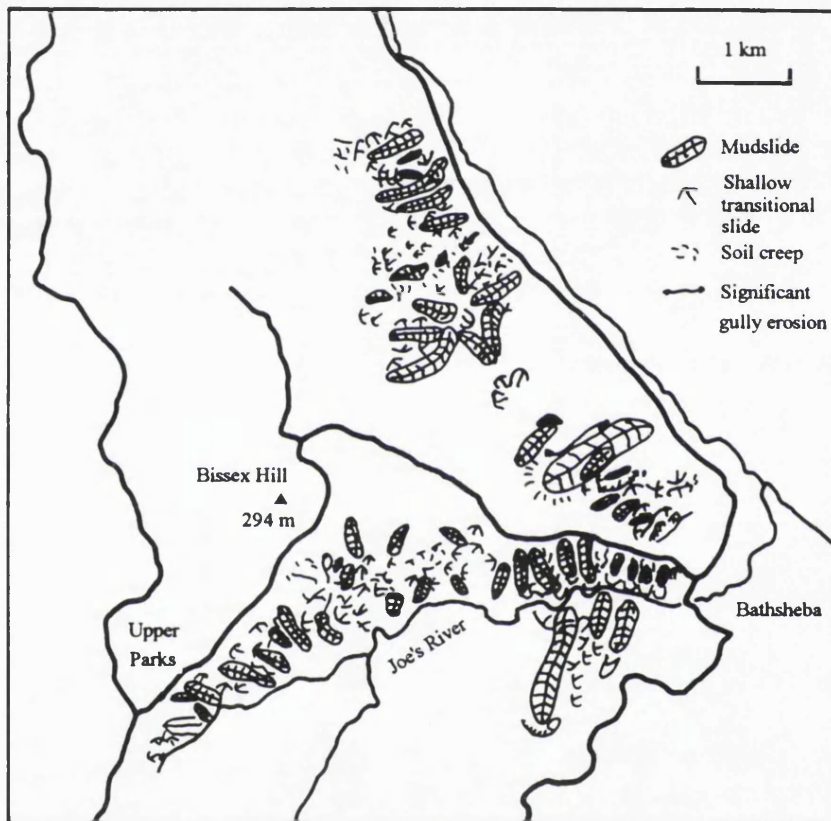


Figure 3.3.6 Geomorphologic map of the study area in Barbados (after Enriquez-Reyes *et al.*, 1990)



Plate 3.3.1 Joe's River Formation scaly clay

3.3.2 Taiwan

3.3.2.1 Climate

Taiwan is located some 150 km off the south-east coast of mainland China (Figure 3.3.7). The Taiwan Strait which has an average depth of 100 m, separates the two. The geographical position of Taiwan is at about 121° East longitude and 23.5° North latitude. The southern part of the island is therefore in the tropical region and the north is in the subtropics. East of the island is the Pacific Ocean, where submarine slopes plunge down with a gradient of 1:10 and the ocean floor reaches a depth of more than 4,000 m about 50 km from the coast (Ho, 1975).

Due to the topographic complexity of the island the climatic conditions, such as temperature, precipitation and humidity, vary significantly from place to place. The data given here are those for the study area, Taitung. The mean temperature is 24°C where the highest temperature ranges from 28° to 31°C and the lowest from 18° to 19°C. The relative humidity is generally high, around 80%. Fluctuation of the relative humidity is fairly small ranging from 70% to 90% throughout the year. Annual precipitation varies significantly from year to year. It seems to be strongly controlled by the number of tropical cyclones that across the island each year. Generally speaking, the annual rainfall of the Taitung area is about 1,800 mm yr⁻¹. Table 3.3.1 gives the climatic data of the study area in Taiwan.

Table 3.3.1. The climatic data of Taitung from 1981 to 1990
(data source: Central Weather Bureau of Taiwan)

Year	Temperatures (°C)	Annual rainfall (mm)	Mean relative humidity (%)
1981	H:29.2; L:18.0; M:23.7	1461.6	83
1982	H:28.0; L:18.4; M:24.1	1353.4	78
1983	H:30.9; L:19.0; M:24.3	1021.3	78
1984	H:28.9; L:18.1; M:24.1	1971.5	78
1985	H:28.5; L:18.9; M:24.2	2063.1	79
1986	H:29.0; L:17.7; M:23.8	1822.2	81
1987	H:28.3; L:17.8; M:23.6	1502.7	82
1988	H:29.7; L:18.3; M:24.2	2035.9	80
1989	H:29.8; L:18.6; M:23.9	1427.8	80
1990	H:30.3; L:18.8; M:24.0	2294.8	84

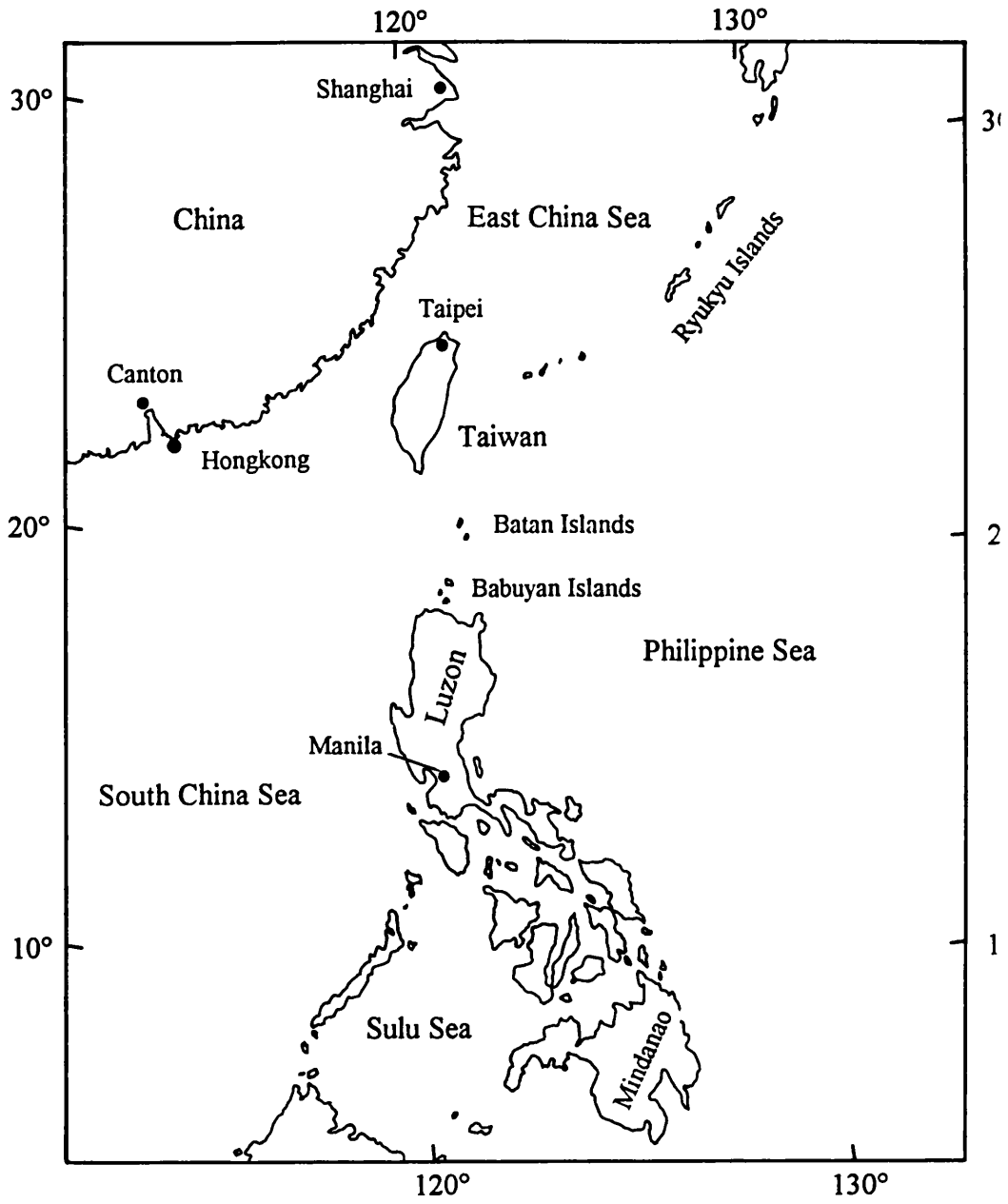


Figure 3.3.7 Map of south-east Asia

3.3.2.2 Geology

Taiwan is a young, recently uplifted island with a longitudinal axis running roughly north-south for a length of 385 km. Approximately two thirds of the land surface is occupied by steep mountains with a highly complex landscape. A major mountain belt, the Central Mountain Range, runs from north to south coinciding with the long axis of the island (Figure 3.3.8, Plate 3.3.2). Most of the island to the west of the range comprises flat, low altitude coastal plains. East of the range lies the Eastern Coastal Range. The two mountain chains are separated by a longitudinal valley which has recently been assumed to be the convergent boundary of the Eurasian continental plate and Philippine oceanic plate. As a consequence, earthquakes and neo-tectonic activity are frequent (Figure 3.3.9).

It was suggested by Ho (1975) that the island of Taiwan was originally a geosynclinal⁴ trough on a metamorphic basement filled with Tertiary sediments to a thickness of more than 10,000 m. The trough had a trend generally north-south and its axis has been shifting progressively westward with successive orogenies. During the present orogeny most of the Tertiary sediment in the geosyncline has been subject to different grades of metamorphism (Ho, 1975). Large igneous intrusions are rare, but there are important areas of volcanic rocks in northern and eastern Taiwan, and the Taiwan strait.

All the major rock formations and structure features in Taiwan occur in long narrow belts, roughly parallel to the axis of the island (Figure 3.3.8). The rocks become progressively younger westwards from the central range to the western foothills. The prevailing structural pattern of all the rocks is that of an elongated arc with its convexity facing westward to the Asian continent.

Geologically, Taiwan can be divided into three provinces (Figure 3.3.10). It is the different nature of the provinces which results in the very different geomorphologic characteristics of different parts of the island. Brief descriptions of the three provinces are as follows.

1. The Central Range

The Central Range runs through almost the whole island, and is the main water ridge between east and west coasts of Taiwan. The range bisects the island into two unequal parts with a ratio of approximately 1:2 for the east and the west sides respectively. The

⁴Geosyncline is an old geological term which has not been widely used in recent literatures. The term in the context actually means a continental margin sedimentary basin.

province contains all the Tertiary sub-metamorphic rocks and the pre-Tertiary metamorphic complex. This geological province may be further subdivided into the backbone range on the eastern flank, made of Palaeozoic rocks, which include schists and gneisses and the Hsuehshan range on the western flank, which is predominantly Paleogene slate.

2. The Western Foothills and Coastal Plain

Non-metamorphosed Neogene rocks are exposed on the Western Foothills extending westwards underneath the western coastal plain. The Western Foothills contain shallow-deposited sediments with a maximum thickness of approximately 8,000 m or more decreasing westwards (Ho, 1975). The age of the Western Foothills is late Oligocene or Miocene to early Pleistocene (Ho, 1979). The rock formations on the Western Foothills are strongly folded and steeply dipping. The thrusting and folding in the Western Foothills are relatively shallow and are thought to result from gravitational gliding which is commonly observed in orogenic regions. Southwest of the foothills region is a wide extent of coastal plain containing most recent alluvial sediments and well-bedded but poorly consolidated clastic deposits (Ho, 1987). The coastal plain has a north-south length of 240 km and a maximum width of 45 km.

3. The Coastal Range

The Coastal Range in eastern Taiwan consists of a now obducted and extinct island arc, and lies east of the Central Range. The two Ranges are separated by a valley, which is fault-bounded on both sides and represents an important tectonic boundary (Ernst, 1983). Associated with the Neogene volcanic rocks of the Coastal Range is a chaotic, sequence of non-stratified, muddy to clayey sediment, known as the Lichi Mélange. The Lichi contains numerous exotic blocks of different sizes, ages and lithologies including ophiolitic materials and was emplaced in late Pliocene to early Pleistocene times beneath the south-western part of the Range (Liou *et al.*, 1977). A more detailed description of the Lichi Mélange will be given later in section 3.3.2.4.

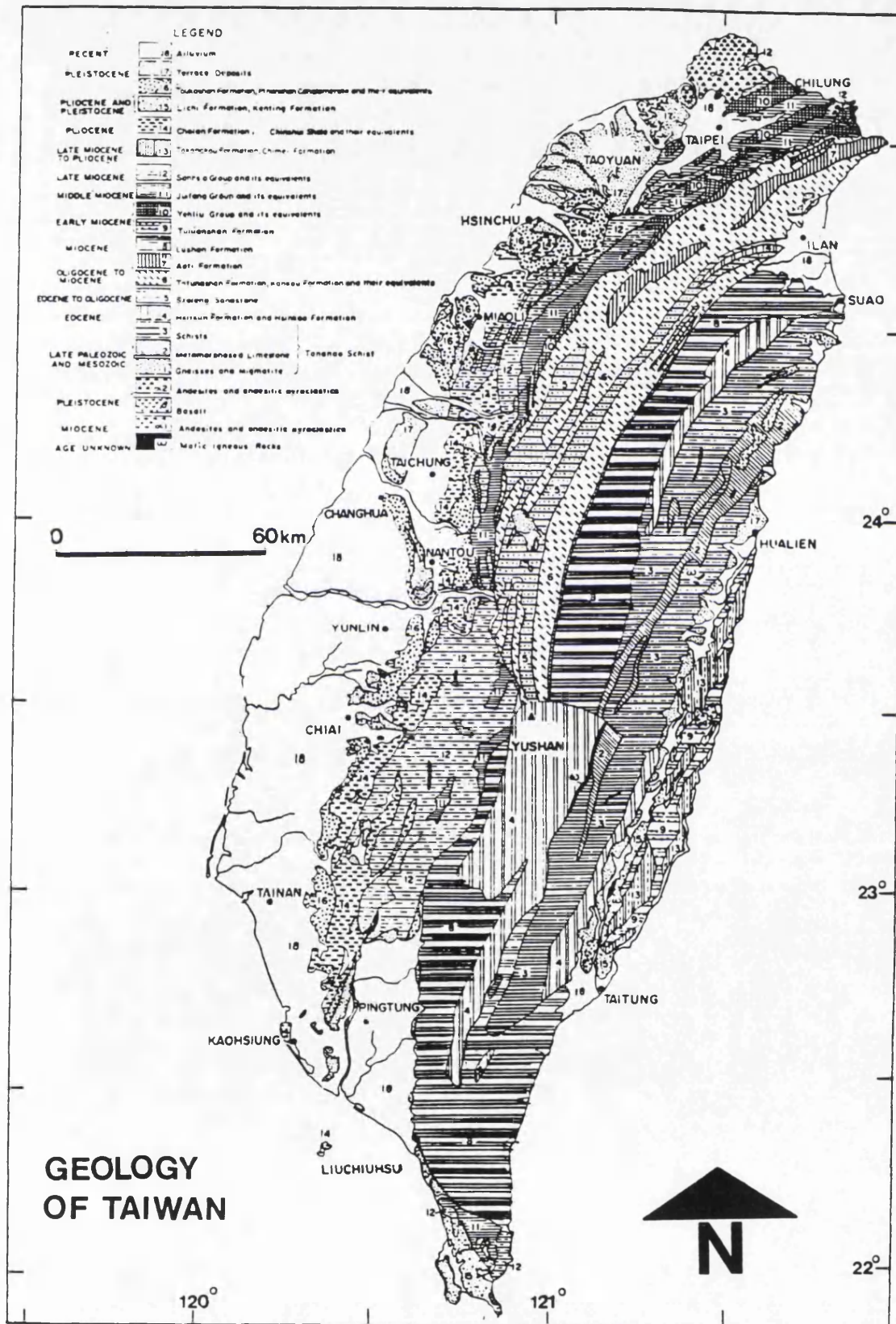


Figure 3.3.8 Geological map of Taiwan (after Ho, 1975)



Plate 3.3.2 Aerial photograph of Taiwan

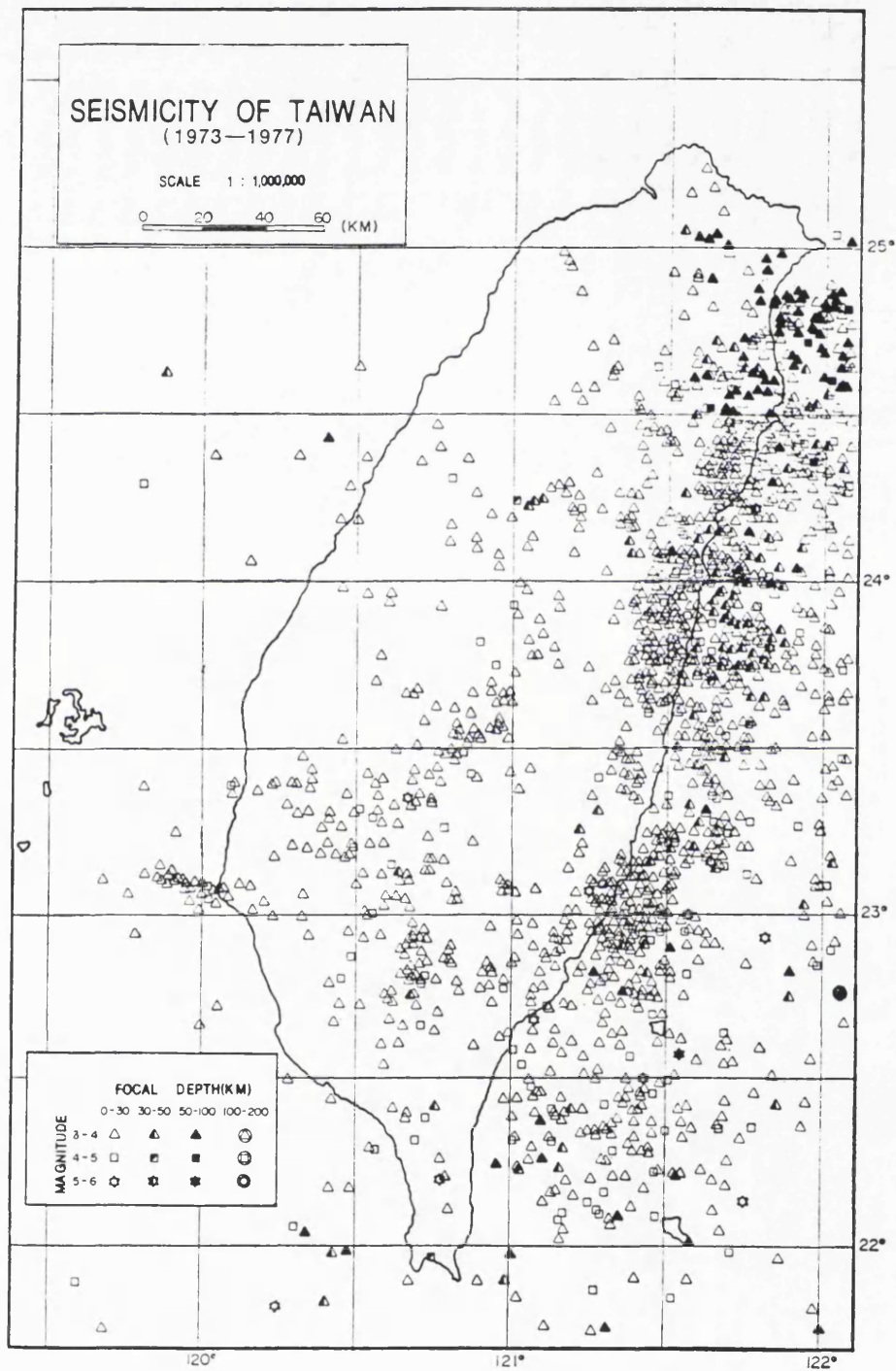


Figure 3.3.9 Seismicity of Taiwan
(source: Institute of Earth Sciences, Taiwan, 1978)

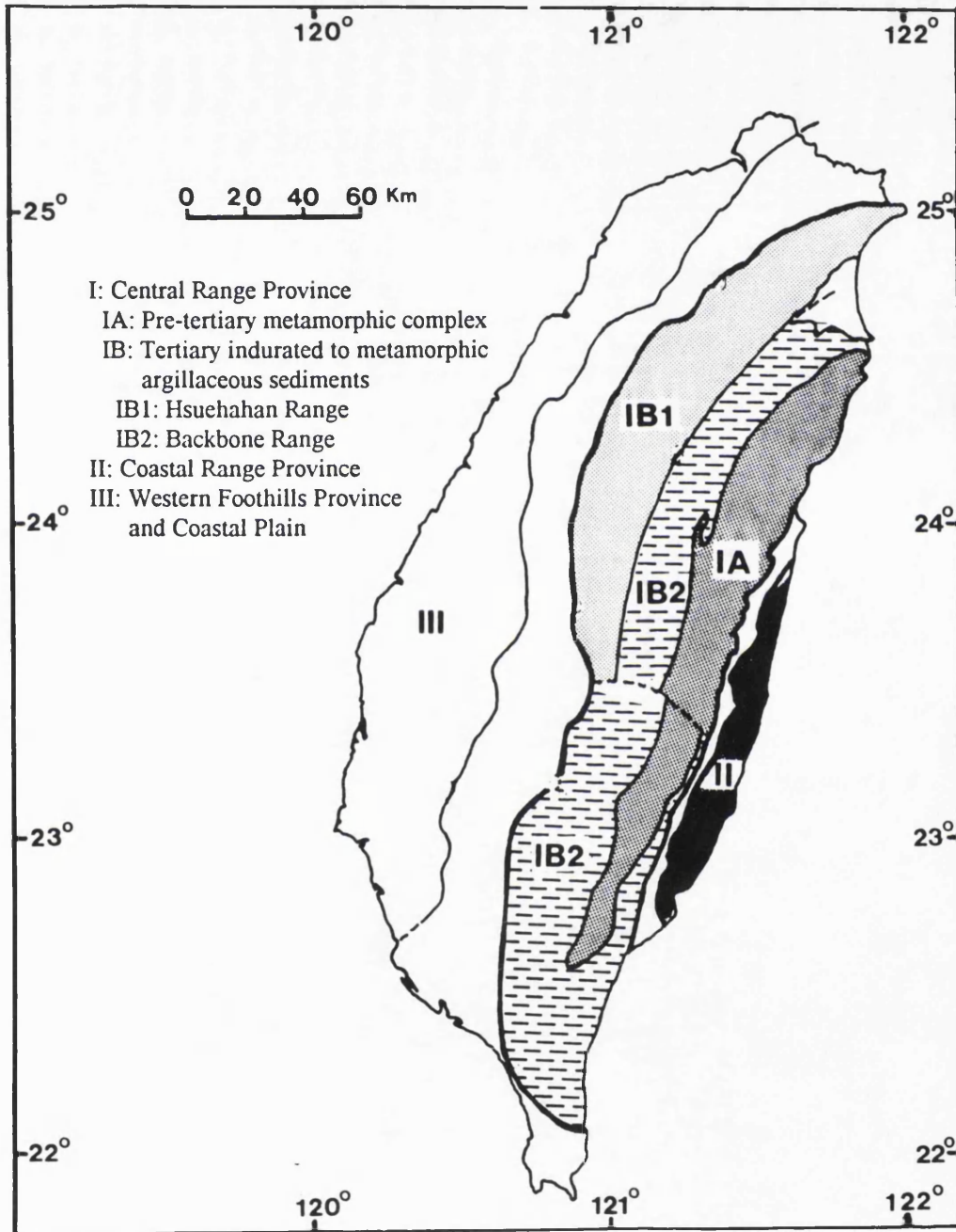


Figure 3.3.10 Geological units of Taiwan (after Ho, 1975)

3.3.2.3 Tectonic setting

Taiwan is a part of the Ryukyu-Taiwan-Philippine island arc chain, rimming the western border of the Pacific ocean (Figure 3.3.11). Tectonically, Taiwan is situated on a convergent and compressive boundary between the Eurasian continental plate and the Philippine oceanic plate (Figure 3.3.12) (Ernst, 1983). As described previously, the valley between the Central Range and the Coastal Range is thought to be the suture of the two plates, by which the Central Range on the continental plate and the Coastal Range on the oceanic plate are separated (Ho, 1982). Figure 3.3.11 demonstrates an active collision of the Luzon Island Arc with the continental margin of Asia. The arc/continent collision started during the Pliocene period and is probably still continuing today, although motion on the plate margin is now more dominantly strike slip (Biq, 1981; Ho, 1982; Lin, 1991). The collision is a very young tectonic event. At present the rate of plate convergence is about 7 cm yr^{-1} in a northwest-southeast direction (Seno, 1977).

The high mountains and steep slopes of the island are a result of the arc/continental collision and have been demonstrated to be still rising at a significant rate (Biq, 1984). For instance, there are more than 30 peaks in the Central Range that are over 3,000 m in elevation. Other than undergoing a collision with the Luzon Island Arc, the island is also involved in the tectonic and thermal processes of the Ryukyu arc system at its northern end (Lin, 1991). Due to the neo-tectonic activity of Taiwan, including the rapid uplift, frequent earthquake and young weak sedimentary rocks, steep hillsides are highly susceptible to instability (Chen, 1987).

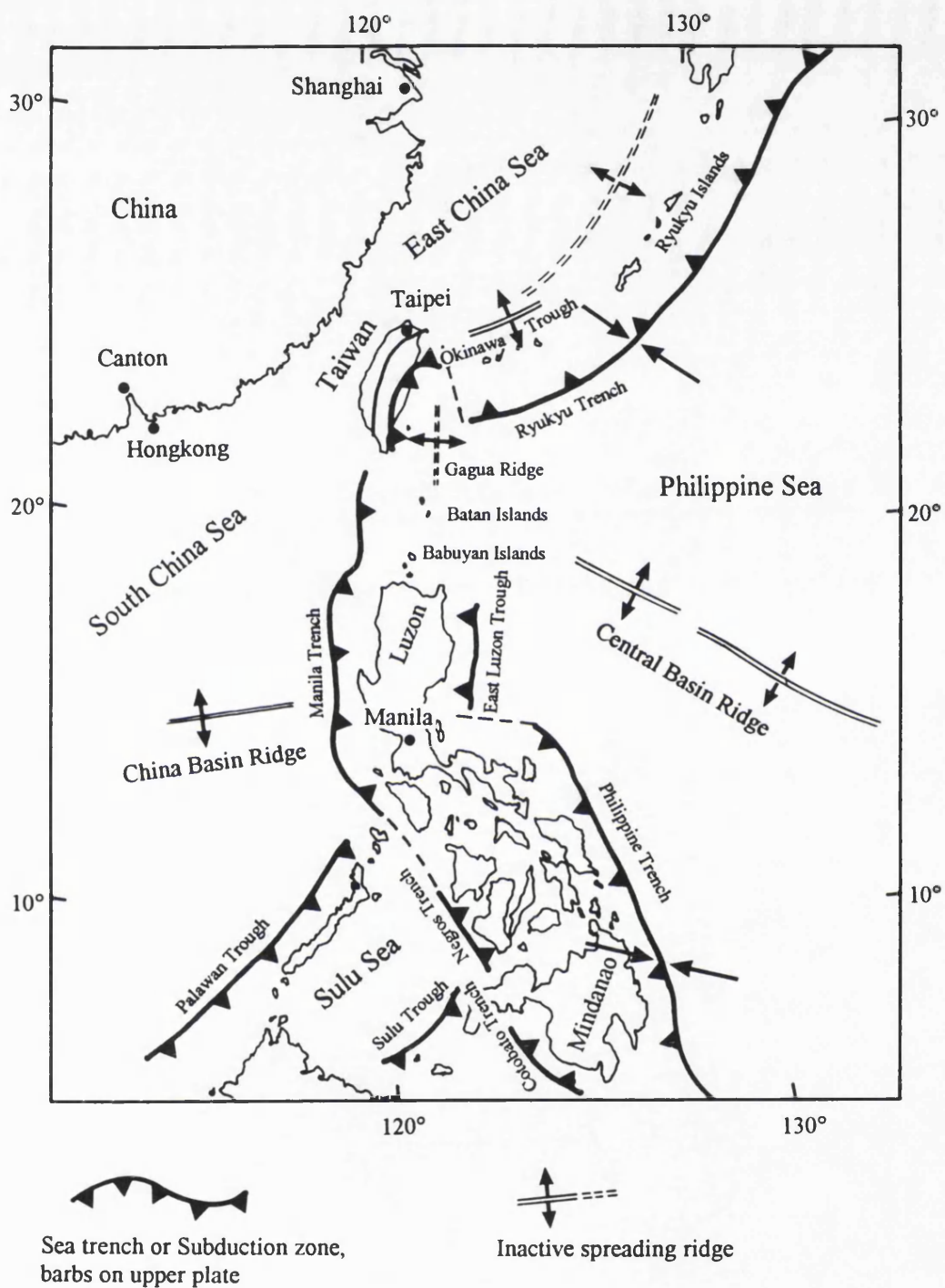


Figure 3.3.11 Principal tectonic features and structural elements in the Ryukyu-Taiwan-Philippine island arc chain. (after Lin & Tsai, 1981)

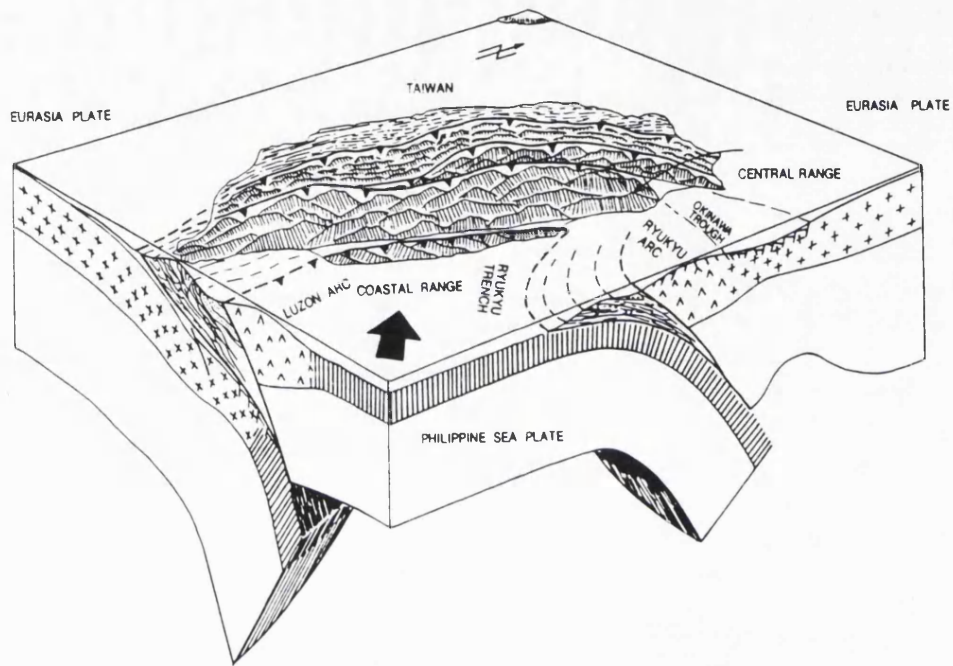


Figure 3.3.12 Tectonic setting of Taiwan (after Ho, 1982)

3.3.2.4 Lichi Mélange

The Lichi Formation (Hsu, 1956) crops out in a long, narrow belt, approximately 3 km to 5 km wide, exhibiting low rolling hill country along the western side of the southern Coastal Range from Taitung to Yuli, a distance of about 65 km (Figure 3.3.13). The type area for the scaly clay is at the vicinity of Lichi near by Taitung, especially close to the Pei-Nan River. The Lichi Formation is a large *mélange*, consisting largely of chaotic, scaly mudstone which encloses abundant exotic fragments ranging in size from silt-sized detrital granules to large blocks up to a kilometre in long dimension (Ernst, 1977; Liou *et al.*, 1977). The landscape of the clayey *mélange* in some cases is marked by smooth, gentle slopes from which protrude resistant exotic blocks, whereas in other places it exhibits a typical badlands topography (Plate 3.3.3). Numerous exotic blocks, cobbles, pebbles and fine-grained water-worn detritus occur within the scaly clay matrix. Microfossil assemblages from the clayey matrix and a few sedimentary blocks indicate mixed Miocene and Pliocene (and possible Pleistocene) ages (Chang, 1967, 1968, 1969; Huang *et al.*, 1979; Chi, 1982; Barrier & Muller, 1984; Chen, 1988). The most remarkable feature of Lichi *Mélange* outcrops is the associated badlands topography (Plate 3.3.3). Vegetation is absent on the slope surface of the badlands area.

The origin of the Lichi Formation has been a major argument since it was first identified. The arguments have centred on whether it is an olistostrome product through gravity sliding or a tectonic *mélange* due to scrapping upon the trench wall (Biq, 1969, 1971, 1973; Hsu, 1976; Wang, 1976; Ernst, 1977; Ho, 1977; Liou *et al.*, 1977; Lo *et al.*, 1978; Page, 1974, 1978; Huang *et al.*, 1979; Teng 1981). It has, however, generally been accepted that the Lichi Formation is directly or indirectly related to the previous subduction of the plates.

As mentioned previously, the Lichi *Mélange* is made of a disturbed scaly mudstone matrix and chaotically disturbed blocks and fragments, of largely sandstones and ophilitic rocks. The presence of the blocks, the weakness of the mudstone, and the lack of normal stratigraphic continuity produce a hummocky topography with hillocks and depressions. The terrain includes many landslides, rapidly growing gullies, and local area of badlands erosion. The *mélange* has an apparent thickness of more than 1km, as determined from an exploratory bore hole (6.5 km south-east of Lichi village) that penetrated 1,061 m without reaching the base of the *mélange* (Meng & Chiang, 1965).

The scaly fabric of the mudstone matrix varies in its degree of development and is not generally randomly oriented. The scaly surfaces are seen to be narrow plastic shear bands

of phyllosilicates with strong preferred orientation, whereas the mudstone between the shear bands exhibits phyllosilicates plates in random orientation (Page & Suppe, 1981).

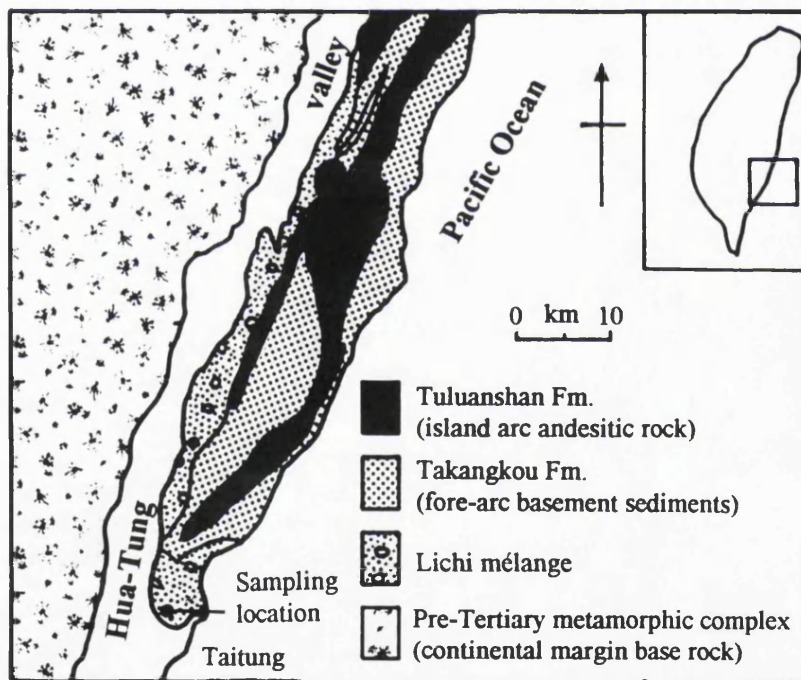


Figure 3.3.13 Geological map of the study area in Taiwan



Plate 3.3.3 Lichi badlands topography

3.4 Sample collection

Samples were extracted from the locations identified in Figures 3.3.5 and 3.3.13. Trial pits were excavated to expose the scaly clays in all stages of weathering from the top to the bottom of the weathering horizon. The visual evidence of weathering on mudrocks is often quite recognisable. Typically the colour is seen to change at shallow depth from grey to brown indicating degrees of oxidation (Chandler & Apted, 1988) and the texture resulting from the diagenesis becomes less evident towards the ground surface (Enriquez-Reyes *et al.*, 1990). The identification of the degrees of weathering for the materials studied is based on the classification scheme established by Chandler & Apted (1988) (Table 2.6.3) and is illustrated in Table 3.4.1. The classification scheme uses field observation in terms of changes in original structure and colour as an indication of degree of weathering (Table 3.4.1).

Undisturbed samples were collected following the standard procedure (Hawkins, 1984). The procedure involved excavating to leave a free standing column of material, which was then carefully shaved down to minimise disturbance to the sample (Plate 3.4.4). The block of material was sectioned into samples of a size suitable for transport to the laboratory. Before removing material, each block was covered in muslin, coated with paraffin wax and sealed within a protective, air-tight tin to prevent moisture loss between extraction and testing and to minimise damage to the fabric in transit.

By using the above technique, a continuous column of material down through the entire weathering profile can be obtained. Three horizons for the Barbados material and four for the Taiwan material were identified by their texture and colour in the field. The extracted samples are temporarily named based on their depths as I, II, III etc. The bottom layer being named as layer I. Therefore, the Barbados samples will be BD-I, BD-II and BD-III, and the Taiwan samples will be TW-I, TW-II, TW-III, TW-IV and a thin top layer for physical and chemical characterisation as TW-V. After a proper classification analysis, the samples were renamed, reflecting their degrees of weathering.

Table 3.4.1 Classification of weathering
(modified from Chandler & Apted, 1988, taken from Table 2.6.3)

<i>Zone</i>	<i>Classification</i>	<i>Description</i>
IV	Fully weathered	Completely naturally remoulded clay, or a few lithorelicts (up to 10mm max. dimension) occupying < 30% of whole, in a matrix of soft to firm remoulded clay; brown or light grey, mottled brown.
III	Partially weathered	Lithorelicts (10 mm to 70 mm average dimension; brown internally) completely separated by remoulded matrix and occupying 30% to 70% or more of whole; fissure surfaces and matrix often light grey (greyed); selenite crystals common. Dominantly brown (oxidised), with clay fragments showing original clay structure; remoulded matrix developing in fissures and joints.
II	slightly weathered	Clay fragments bonded by iron stained joints and fissures, weathering on surfaces of discontinuities only, the brown coloration penetrating up to 20 mm; centre of fragments exhibits the colour of zone I clay; fissure spacing typically 70 mm to 120 mm; bulk of clay grey-brown.
I	Unweathered	Uniformly grey-brown or grey-blue; discontinuity spacing typically >100 mm



Plate 3.3.4 Sampling technique

Chapter Four: Physical and Chemical Characterisation

4.1 Introduction

Physical properties, chemical composition, clay mineralogy and stress history are the dominant factors controlling the mechanical behaviour of soil materials (Skempton, 1961; Kenney, 1967; Lambe & Whitman, 1979; Chandler & Apted, 1988). In order to achieve a better knowledge of the influence of weathering on the deformation characteristics of the materials, it is therefore essential to investigate these properties. This chapter presents the data collected during the first part of the testing programme: the physical, chemical and mineralogical characterisations of the materials to be tested. The data collected include particle size distribution, porosity, natural moisture, bulk density, plasticity index (liquid & plastic limits), clay mineralogy, chemical composition and a qualitative assessment of micro-structure. The same series of examinations were applied to both the Barbados and Taiwan scaly clays: the materials under investigation. The chapter is structured so as to provide a description of each test procedure and the associated sample preparation methodologies. This is then followed by a presentation of the data. The results are then discussed at the end.

4.2 Procedures and sample preparation

Examination of the physical and chemical characteristics of the test materials involves various methods and techniques. The methods are described individually in this section, together with details of the sample preparation techniques.

4.2.1 Particle size distribution

Particle size distribution is one of the most common characteristics determined during investigation of soil materials for engineering purposes (Lambe & Whitman, 1979). This is because the engineering performance of soils is strongly dependent on the grain size present in the soils and grain-size distribution (Liu & Evett, 1984). The grain-size distribution curve gives a basic guide to the classification of the soil and also allows its strength, compressibility and its depositional environment and sedimentary process to be roughly estimated. Grain-size distributions were obtained in this case not only to allow

classification but more importantly to identify whether there is any significant change in particle size caused by weathering processes.

The accuracy of the distribution curve for fined-grained soils is more questionable than those for coarse-grained soils (Lambe & Whitman, 1979). This is because chemical and mechanical treatments applied to natural soils before a particle size analysis, especially before analysis which is based on a sedimentation method such as pipette method, usually result in effective particle sizes that are different from those which truly exist in the natural soil at the fine-grained end of the distribution. However, even if an exact particle size distribution curve were obtained, it would not be much more meaningful in terms of predicting the behaviour of the soil (Lambe & Whitman, 1979). In fact, absolute distribution curves of the materials are not likely to be obtained by means widely used today and are not necessary. It is more essential, in this case, that providing the samples are subject to the same treatment (i.e. same amount of time during crushing and shaking, same concentration of calgon solution etc.), the relative distribution curves obtained will therefore reflect the impact induced by weathering.

The mechanical behaviour of a cohesionless soil can often be related to its particle size distribution, but the behaviour of cohesive soils usually depends more upon their geological history and structure than upon particle size (Vaughan *et al.*, 1988). However, materials like mélange sediments, although cohesive, have a wide particle size distribution which should be investigated as part of any geotechnical study. Such data may also contribute to our understanding of the effects of tropical weathering on soil strength and provide information on the extent to which particle breakage or aggregation processes change the soil structure during weathering.

The methods used to obtain the particle size distribution curves were dry sieving for particles with size greater than 63 μm and a X-ray penetrating technique, namely SediGraph, for the portion that finer than 63 μm . The SediGraph apparatus (see Appendix II) is based on the same theory as the pipette method (i.e. Stoke's law) in that larger grains sink faster than smaller particles but its result is more accurate than that obtained using the pipette technique because manual error is very restricted in the SediGraph apparatus.

In dry sieving, a series of sieves: 4 mm, 2 mm, 1 mm, 500 μm , 250 μm , 125 μm and 63 μm were used. About 500 g of material was taken and oven dried at 90°C for 48 hours. It was thought that the materials from different depths were likely to have different amount of organic matter which may, perhaps, be altered if the drying temperature was

too high, introducing variability in the test result (Osborn pers. comm.). Consequently, a lower temperature, 90°C, and a longer period of time, 48 hrs, were used instead of the standard 105°C for a period of 24 hrs. After each sample had dried it was subject to 30 minutes of hand crushing. The sample was then sieved for 25 minutes and the particles remaining in each sieve were carefully collected and weighed. Measurements were recorded and calculated to percentages, and plotted as a semi-log scale graph describing the coarse part of the distribution.

For the finer portion, 10 g of each sample collected in the < 63 µm tray was taken and mixed with 100 ml of 0.05% calgon solution in a beaker. Calgon was used to help disperse the clay particles. The sample was then stirred using an ultra-sonic probe and poured into the SediGraph 5100 for analysis. The theoretical information of the SediGraph is described in Appendix II. Combining the results from sieving and SediGraph provided the complete particle size distribution curve.

4.2.2 Porosity, moisture content and bulk density

Soil is composed of particles, largely mineral fragments, which form the soil skeleton, and pores which are filled with fluid, largely water and/or air. Pore space constitutes an important part of the whole soil body playing a significant role in terms of influencing the behaviour of the soil and therefore porosity is a fundamental parameter when describing soils (Lambe & Whitman, 1979).

In natural soils water is considered to be part of their structure (Head, 1980). The natural moisture content is therefore one of the most important inherent physical properties affecting engineering performance (Lambe & Whitman, 1979). Water content is dependent on porosity and the ground water condition existing in the field at the time of sample collection (i.e. degree of saturation). The more pore space a soil has the higher its natural moisture content is likely to get (Bell, 1992).

The bulk density of a soil is governed by its mineral grains, pore space and pore fluid for these are the constituents of a soil. The mineralogical composition of a soil may vary significantly from case to case, but the densities of the soil forming minerals do not differ considerably, on average between 2.6 g.cc⁻¹ and 2.7 g.cc⁻¹. As a result, porosity, pore fluid and degree of saturation are the most important factors determining the bulk density.

Porosity (n) is defined as the percentage volume of pore space within the material.

$$n = (v_p/v_s) * 100\% \quad (\text{eq. 4.1})$$

where n = porosity;
 v_p = volume of pore space;
 v_s = volume of sample.

In order to calculate the volume of the specimen, regularly shaped specimens such as cubes, rectangular prisms, or right cylinders are needed. Right cylindrical specimen plugs were produced in this case for both calculating the porosity and conducting triaxial deformation experiments (see sample preparation in Chapter Five). Once the volume of the sample is known, it is weighed after oven drying and its density determined. Having known the volume (v_s) and dry weight (m_d) of the sample and the average density of the mineral grains (d), the volume of the pore space (v_p) can be calculated by equation 4.2.

$$v_p = v_s - (m_d/d) \quad (\text{eq. 4.2})$$

where
 m_d = dry weight of the sample,
d = average density of the mineral grains (2.65 g.cc⁻³)
 m_d/d = volume that solid particles occupy

Once the porosity (n) is obtained, the void ratio (e) can also be determined.

$$e = (n/100)/(1-(n/100)) \quad (\text{eq. 4.3})$$

The moisture content (w) is defined by the amount of water expressed as a proportion by mass of the dry solid particles (BS. 1377, 1990). As a consequence, it can be written as follows:

$$w = ((m_w - m_d)/(m_d - m_c)) * 100\% \quad (\text{eq. 4.4})$$

where w = moisture content;
 m_w = mass of container and wet sample;
 m_d = mass of container and dry sample;
 m_c = mass of container.

At least 30 g of preserved sample was taken, crumbled and weighed in a clean and dry container. The sample was then dried at 90°C for 48 hours and weighed again. The loss of weight is the weight of water originally present in the sample. The moisture content is the percentage ratio of the weight of water to the dry weight of the sample.

Bulk density (ρ) can be defined as the mass per unit volume of the soil material including any pore fluid it contains:

$$\rho = m_s/v_s \quad (\text{eq. 4.5})$$

where ρ = bulk density (g. cc^{-1});
 m_s = mass of sample (g) (in natural undisturbed state)
 v_s = volume of sample (cc)

To determine the bulk density samples need to be regularly shaped. The bulk density was calculated from the cylindrical plug for triaxial testing.

4.2.3 Plasticity index

The most simple expression of the influence of water content on the engineering performance of a fine grained soil is seen in the relative magnitude of the plastic and liquid limits (Casagrande, 1948; Skempton, 1953; Terzaghi & Peck, 1967; Bell, 1992). These are empirical indices determined on samples remoulded to different water contents. These index properties serve to determine the water content at which the soil first behaves as a plastic material (the plastic limit) and at which the soil becomes liquid (the liquid limit) (BS 1377, 1990). The range of water contents over which the soil is plastic is the plasticity index. These index properties reflect the mineralogy of the soil, in particular, the amounts and types of clay mineral present (Skempton, 1953).

A standard method for the determination of liquid limit was proposed by Casagrande (1932) which uses the stability of the walls of a groove inscribed on the sample under repeated dynamic loading to determine the critical water content (Head, 1980). Samples were prepared following BS 1377 (1990) by taking around 200 g of the grain fraction passed by the 425 μm sieve and making a paste by thoroughly mixing this with distilled water. The paste is placed in a standard brass cup and scribed using a standard grooving tool (Figure 4.2.1). The scribed groove is cut normal to the pivot and separates the paste

into two parts. The handle of the Casagrande apparatus is then turned lifting and dropping the cup at two revolutions per second. When the groove in the paste sample closes along a distance of 13 mm (Figure 4.2.2), the number of blows is recorded. The water content of the paste in the vicinity of the groove is then determined. More distilled water is added to the paste and the test procedure is repeated again. Five measurements (number of blows between 12 and 45) are needed. The data are presented as a linear/log plot of water content (linear) against the number of blows needed to close the groove (logarithmic scale). A straight line best fit is then constructed and the water content at 25 blows is defined as the liquid limit of the sample (BS 1377, 1990).

Since the plastic limit is defined as the lowest water content at which the soil still exhibits plasticity (Taylor, 1948; Vickers, 1978; Head, 1980), a definition of the lowest water content needs to be given. It is defined in BS 1377 (1990) as the water content at which the soil can be rolled between fingers and thumb so that clay threads with 6 mm diameter can be reduced to 3 mm diameter without breaking up. Tests are conducted on a clean, flat glass plate. The limiting water content is identified by the presence of longitudinal and transverse cracks on the surface of the 3 mm diameter clay thread (BS 1377, 1990). The action of rolling the thread reduces the water content, so that the action continues until cracks appear while the diameter reaches 3 mm. The water content is then immediately determined at this state. Again, five measurements for each sample are obtained and averaged.

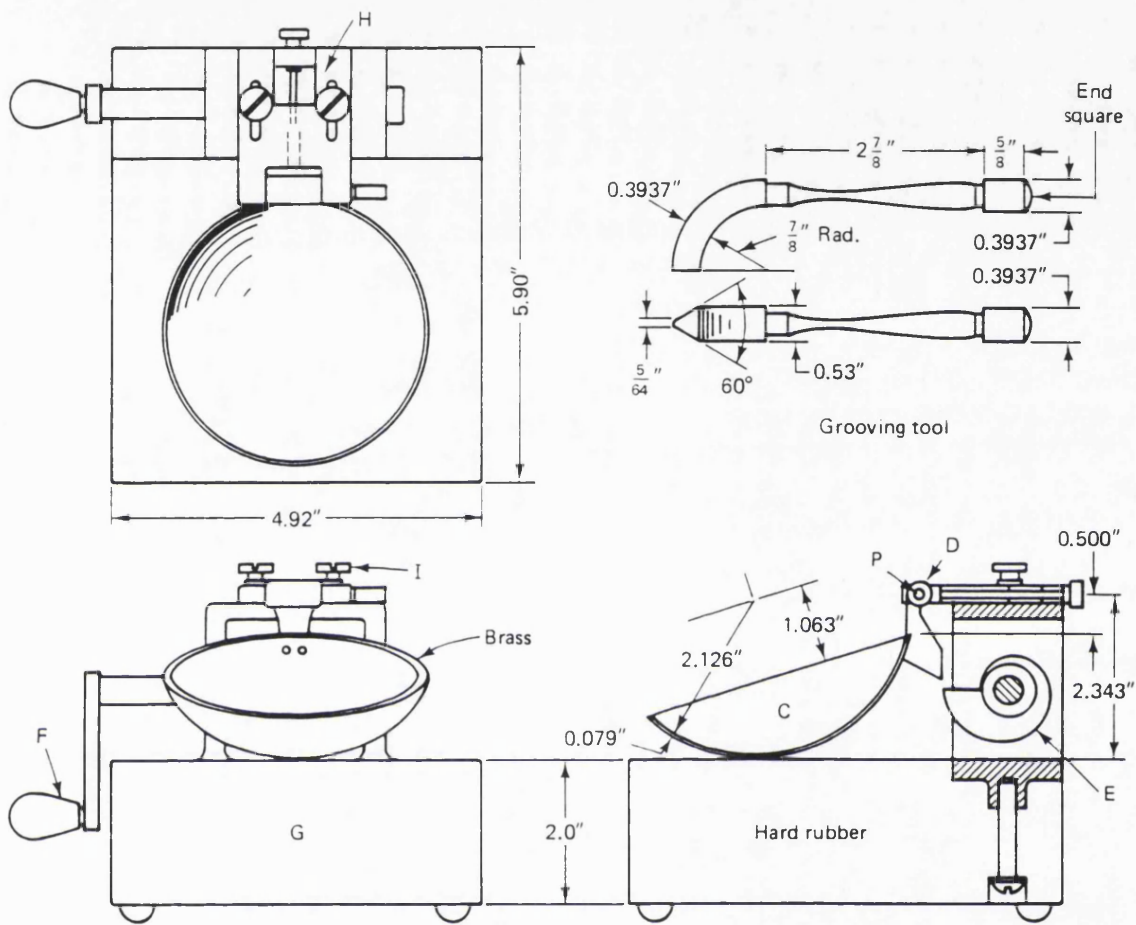


Figure 4.2.1 Casagrande apparatus for Liquid limit determination

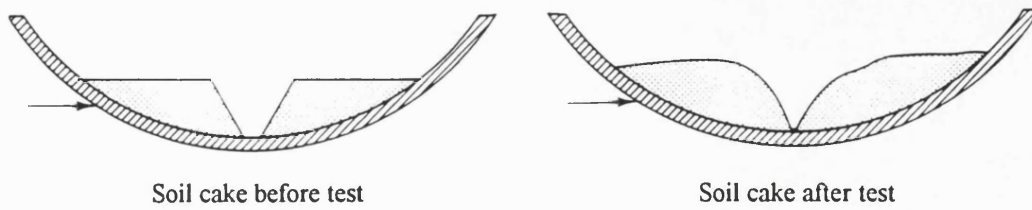


Figure 4.2.2 Diagram illustrating Liquid Limit test

4.2.4 Clay mineralogy

Clay minerals are the most abundant element within argillaceous sediments and different clays influence mechanical behaviour in different ways (Gillott, 1987). The engineering properties of argillaceous sediments are therefore strongly controlled by their clay component and the physical and chemical characteristics of the clay minerals. A well known example is the presence of montmorillonite in a soil. The presence of montmorillonite will result in a dramatic increase in its liquid limit because of the high capacity of water absorption exhibited by montmorillonite (Gillott, 1987).

Although clay is essentially a product of weathering, it is still susceptible to change as its physical/chemical environment changes. When argillaceous sediments are exposed to weathering especially in warm, humid tropical environments, the clay mineralogy may well be changed. It is therefore necessary within the constraints of this study to examine the clay mineralogy of the samples from different depths within the weathering profiles.

The method used to determine the clay mineralogy of samples in this study is X-ray diffraction (XRD). The theory of X-ray diffraction will not be described in detail, but the basic principle is that the different crystal structures of different minerals each diffract X-rays in a characteristic manner. Measurement of the diffraction pattern of a mineral mixture allows, through interpretation, identification of the actual minerals that are present in a mixture. With clay minerals, for instance, although they all have a similar layered structure, the spacing between layers and the crystal unit cell, defined as d spacing, are individually characteristic of each clay type. The d spacing influences the diffraction pattern obtained (Carroll, 1970a; Hardy & Tucker, 1988). When the X-ray beam strikes the crystal layers, each layer produces a reflection of the X-ray beam. It is only when all the reflected beams are in phase that a single diffracted beam is produced. In order to produce this, the distances travelled by the X-ray waves reflected from the layers have to be a whole number times of the wave length. The condition for this is illustrated by equation 4.6 and Figure 4.2.3 (Glasser, 1977). The crystalline structure of the clay minerals is such that the most important X-ray diffractions occur within the 2° to 37° 2θ incident angle (eq. 4.6).

$$2d \sin \theta = n\lambda \quad (\text{eq. 4.6})$$

where d is the interplanar spacing (d spacing) or distance between layers,
 λ is the wave length of the X-rays,
 θ is the angle of the incident beams,
 n is an integer number.

Five slides were prepared for sample from each weathering horizon using the sedimentation pipette technique in order to get clay sized particles ($< 2 \mu\text{m}$). One of them was un-oriented and the other four were identical and oriented by centrifuging. Among the four oriented slides, one was dried at room temperature, two were heated to 300°C and 600°C respectively for an hour and the final one was glycolated in a dessicator for an hour. These differently treated slides are used to help identify the minerals which will be described later. The preparation procedure for all the different horizons was undertaken in as similar manner as possible to ensure that the results are comparable.

The most common way of identifying minerals from the X-ray diffractogram is to compare the d spacings obtained on the diffractogram with the d spacings of standard minerals (Figure 4.2.4 is an example, laboratory working chart produced by Beer, unpublished). Moreover, for clay minerals, in addition to this normally used identification procedure, subsidiary treatments are needed to help the identification. Table 4.2.1 gives an example of the effects of auxiliary glycolating and heating treatments. Those cause distinctive expansion or contraction of the c lattice (unit cell) dimension that are measurable in diffractograms. Those changes are mineral specific and allow more accurate interpretations to be made.

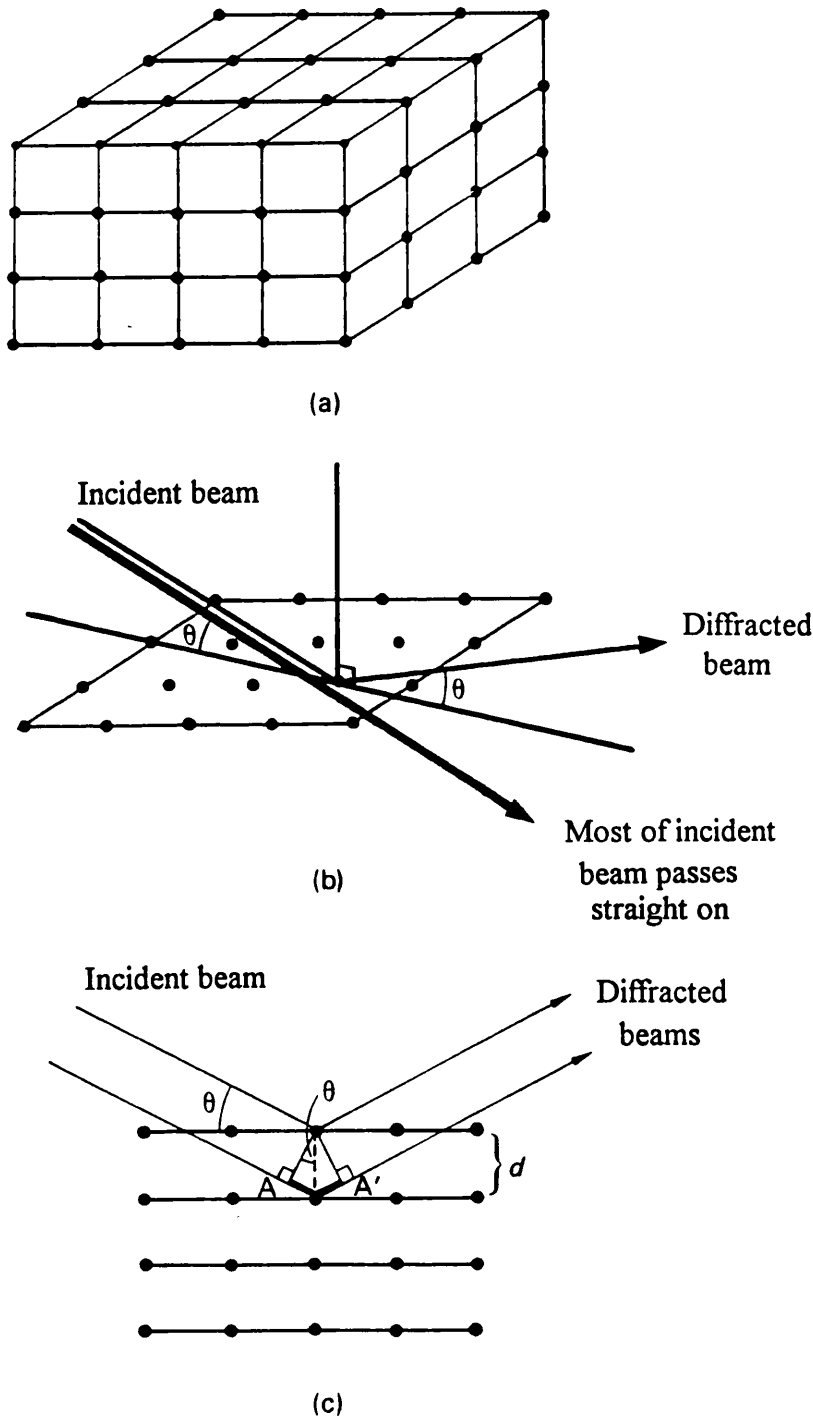


Figure 4.2.3 The diffraction of X-rays. (a) a "single electron lattice". Each dot represents an electron; points behind the surface layers are omitted for clarity. (b) The interaction of an X-ray beam with the top layer of the lattice. (c) The interaction of the beam with subsequent layers in the stack; d is the distance between successive layers. The thickened line AA' represents the path difference between beams reflected from adjacent layers. Reinforcement will occur only when this is a whole number of wave length ($n\lambda$)

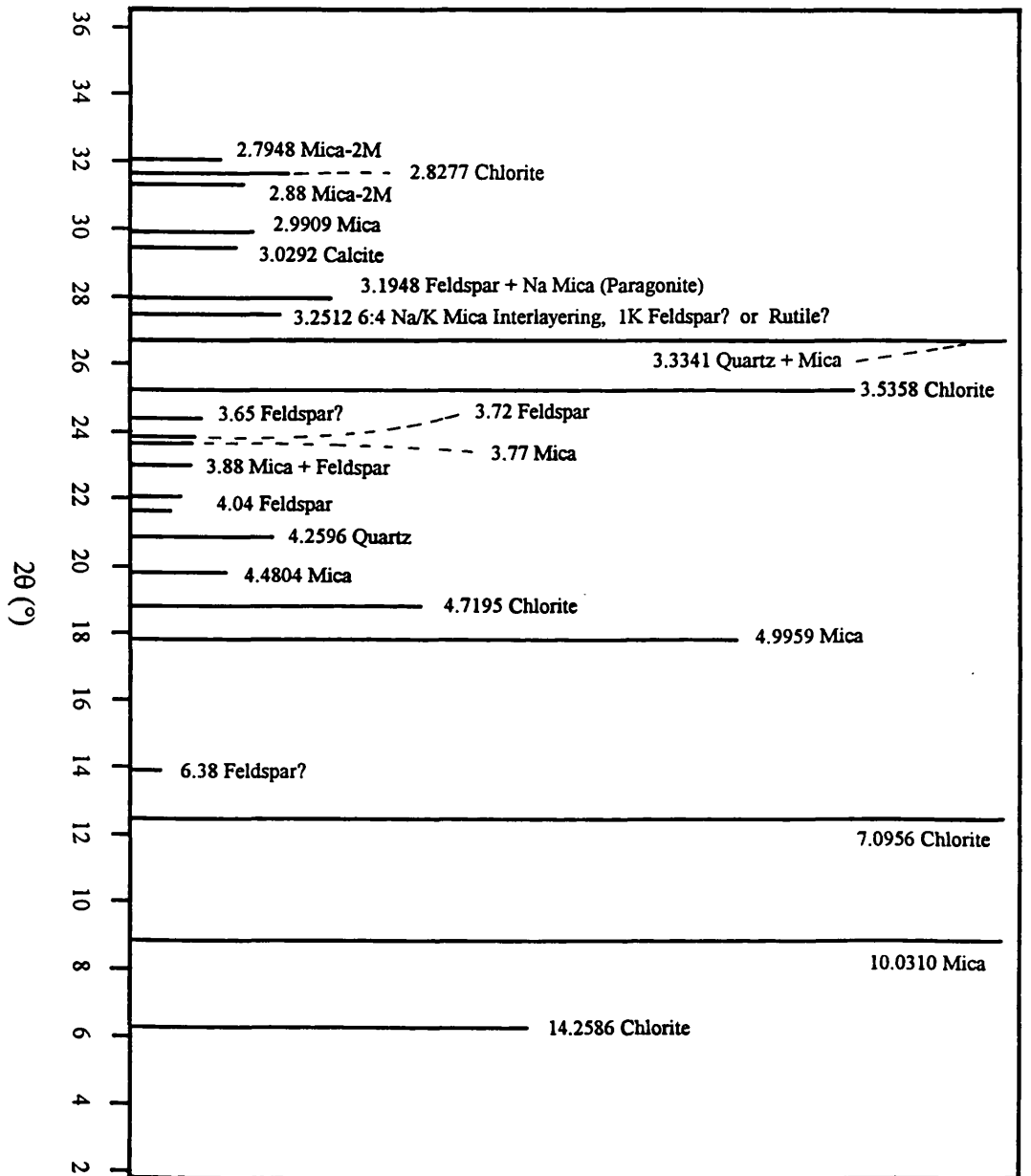


Figure 4.2.4 X-ray diffractogram of oriented mount of clay sediment (laboratory working chart, constructed by Beer, unpublished)

Table 4.2.1 X-ray identification of the principal clay minerals in an oriented mount of a separated clay fraction from sedimentary material (1 Å = 0.1 μm)

Mineral	Basal <i>d</i> spacing (001)	Glycolation effect; 1 hour, 60°C	Heating effect, 1 hour
Kaolinite	7.15Å (001); 3.75Å (002)	No change	Becomes amorphous 550-600°C
Kaolinite, disordered	7.15Å (001) broad; 3.75Å broad	No change	becomes amorphous at lower temperature than kaolinite
Halloysite, 4H ₂ O	10Å (001) broad	No change	Dehydrates to 2H ₂ O at 110°C
Halloysite, 2H ₂ O	7.2Å (001) broad	No change	Dehydrates at 125-150°C; becomes amorphous 560-590°C
Mica, 2M	10Å (001); 5Å (002)	No change	(001) becomes more intense on heating but structure is maintained to 700°
Illite, 1Md	10Å (002) broad	No change	(001) noticeably more intense on heating as water layers are removed; at higher temperature like mica
Montmorillonite Group	15Å (001) and integral series of basal spacing	(001) expands to 17Å with rational sequence of higher orders	At 300°C (001) becomes 9Å
Vermiculite	14Å (001) and integral series of basal spacing	No change	Dehydrates in steps
Chlorite, Mg-form	14Å (001) and integral series of basal spacing	No change	(001) increases in intensity; <800Å shows weight loss but no structural change
Chlorite, Fe-form	14Å (001) less intense than in Mg-form; integral series of basal spacings	No change	(001) scarcely increases; structure collapses below 800°C
Mixed-layered minerals	<i>Regular</i> , one (001) and integral series of basal spacings	No change unless an expandable component is present	Various
	<i>Random</i> , (001) is addition of individual minerals and depends on amount of those present	Expands if montmorillonite is a constituent	Depends on minerals present in inter-layered mineral
Attapulgite	High intensity <i>d</i> reflection at 10.5Å, 4.5Å, 3.23Å, 2.62Å	No change	Dehydration stepwise
Sepiolite	High intensity <i>d</i> reflection at 12.6Å, 4.31Å, 2.61Å	No change	

4.2.5 Micro-structure

As mentioned previously in Chapter Three, scaly clay is a naturally structured soil material. The scaly fabric is the result of locally oriented alignment of platy clay particles. It is now recognised that the micro-structure, such as scaly fabric, is an important control on the mechanical behaviour of argillaceous materials (Leroueil & Vaughan, 1990; Aversa *et al.*, 1993; Bertuccioli & Lanzo, 1993). Since the micro-structure plays an important role in influencing materials mechanical behaviour the natural fabric of the scaly clays investigated during this study have been carefully described.

The study of micro-structure was undertaken using Scanning Electron Microscopy (SEM). The wide range of magnification and the clear 3-D image make the SEM the most simple and effective technique for the study of clay micro-structures. Care must be taken to ensure that the clay fabric is not modified during sample preparation.

Samples were taken from undisturbed blocks of sediment in various orientations including vertical and horizontal sections of the sample columns, and sections parallel to and cross the scaly surface when present. Samples were required to be thoroughly dried and firmly attached to stubs. This gives rise to difficulties because the scaly fabric is very susceptible to any mechanical treatment and may be damaged during dehydration of the sample. To minimise such effects the sample has to be kept in a desiccator at temperature no greater than 60°C for more than 48 hours to ensure that full dehydration occurs without damaging the scaly fabric to a great extent. After dehydration was completed the samples were coated with gold. They were then ready for examination in the SEM.

4.2.6 Chemical composition

Rocks and minerals exposed to environments with warm temperatures and high humidity are expected to undergo chemical alteration. Consequently, an examination of chemical changes through the weathering profile provides both an important understanding of the effects of tropical weathering and a quantitative measure of weathering extent. There are many kinds of chemical analyses to meet different specific purposes. In this study, the bulk composition and degree of oxidation along the weathering profiles are inspected because the chemical investigations were designed as quantitative indices to the state of weathering rather than an investigation of the processes.

A general analysis was completed to gain a picture of the bulk chemical alteration because it is the most widely used way to determine the amount of chemical weathering

that has taken place in a rock (Birkeland, 1974). In addition, the ferrous/ferric iron ratio was of specific interest as oxidation is considered to be an index of chemical weathering (Grainger & Harris, 1986; Coulthard & Bell, 1990).



Three samples of material from each weathering horizon were examined. The examination was carried out in two parts, the general analysis and determination of the ferrous iron content. The data presented in this chapter have been averaged and the raw data can be found in Appendix III. The detailed procedure is also described in steps in Appendix III.

4.3 Results

The results of the tests described above are presented in this section and divided into two sub-sections based on their locations: Barbados and Taiwan.

4.3.1 Barbados

4.3.1.1 Particle size distribution

Figures 4.3.1, 4.3.2 & 4.3.3 illustrate the particle size distribution curves through the depth/weathering profile for the Barbados Joe's River Formation scaly clay. The figures show that in the sand fraction the curves are very similar for all three horizons, but the silt and clay size fraction exhibits some differences. The deepest sample (BD-I) has the highest content of clay (30%), the shallowest one (BD-III) has an intermediate value of 23%, and the sample from the intermediate horizon (BD-II) has the lowest clay content (12%). The order does not vary consistently with depth but seems to be controlled by other factors such as various weathering processes in different horizons.

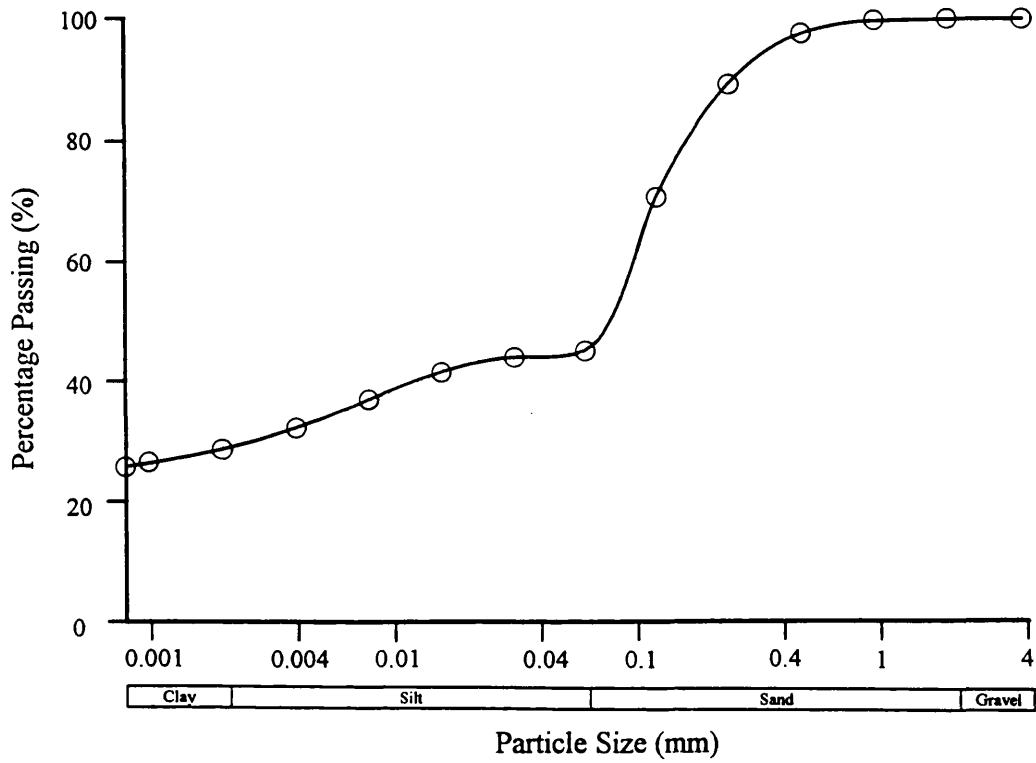


Figure 4.3.1 Particle size distribution curve for least weathered sample, Barbados

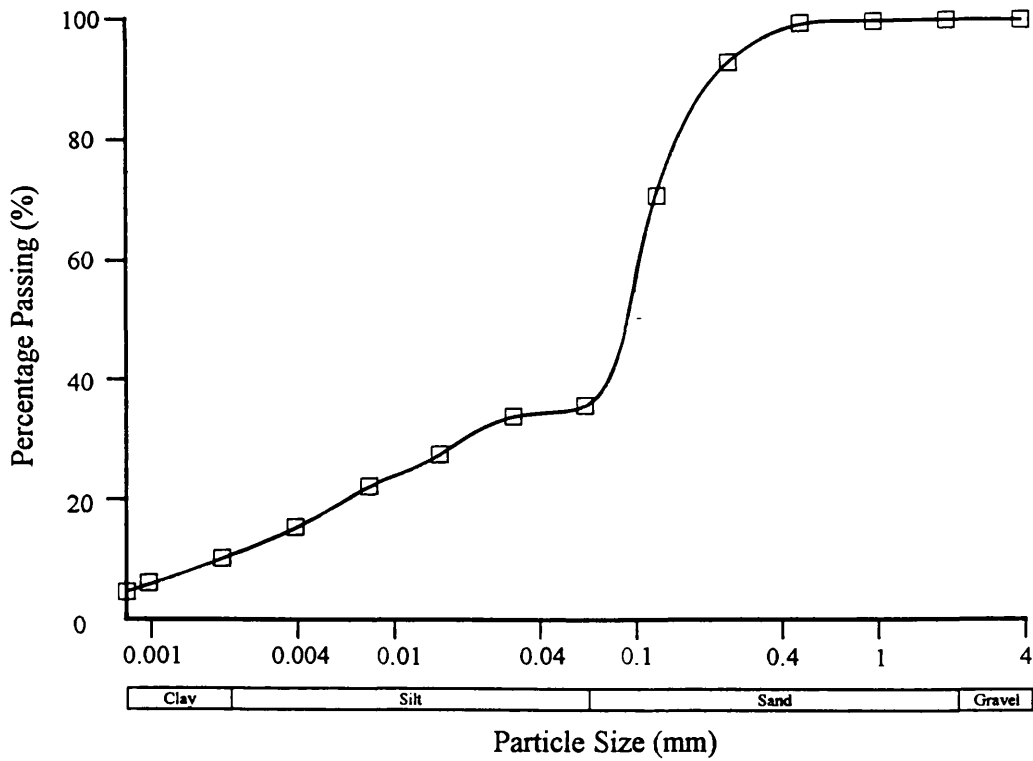


Figure 4.3.2 Particle size distribution curve for partially weathered sample, Barbados

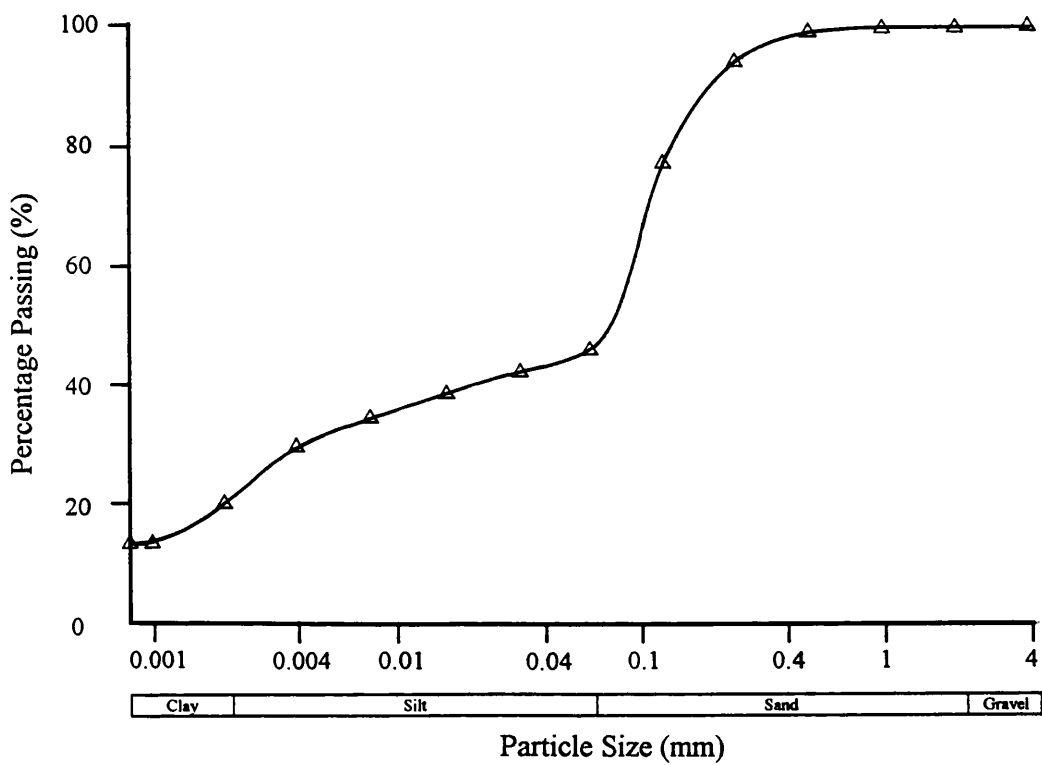


Figure 4.3.3 Particle size distribution curve for most weathered sample, Barbados

4.3.1.2 Porosity, natural water content and bulk density

Table 4.3.1 summarises the porosity, natural water content and bulk density data of the samples. The porosity and moisture content gradually increase from 32.2% to 46.7% and from 22.0% to 32.3% respectively with decreasing sample depth. The bulk density, on the other hand, exhibits a decreasing trend from 2.10 g.cc⁻¹ to 1.91 g.cc⁻¹. These suggest that the pore space is becoming larger in the material closest to the ground surface which results in the increase in natural moisture content and a decrease in the bulk density.

Table 4.3.1 Summary of the porosity, natural water content and bulk density

Sample number	Porosity (%)	Moisture content (%)	Bulk density (g.cc ⁻¹)
BD-I (100-150 cm)	32.2	22.0	2.10
BD-II(50-100 cm)	38.4	29.6	2.04
BD-III(0-50 cm)	47.7	32.3	1.91

4.3.1.3 Plasticity index

Plasticity index data for the Barbados samples are given below in Table 4.3.2. The plasticity index of a soil is largely dependent on its clay mineralogy (Skempton, 1953; Gillott, 1987). Particle size also exerts an influence (Liu & Evett, 1984). The index properties of the Barbados material follow the trend of the particle size distribution. All three samples have plastic limits of around 20%, the deepest and shallowest samples have a very similar liquid limit and plasticity index values of 40% and 20% respectively, and the intermediate depth material has distinctively low values of 30% and 10% respectively.

Table 4.3.2 Summary of the Liquid and Plastic Limits and Plasticity Index of the Barbados samples

Samples	Plastic limits (%)	Liquid limits (%)	Plasticity index (%)
BD-I (100-150 cm)	22.8	42.8	20.0
BD-II (50-100 cm)	19.4	29.3	9.9
BD-III (0-50 cm)	20.3	40.3	20.0

4.3.1.4 Clay mineralogy

The clay mineralogy of samples for the three different horizons are presented in Table 4.3.3, and the X-ray diffraction traces are shown in Figures 4.3.4, 4.3.5 & 4.3.6. The main clay minerals present in all three samples are Chlorite, Kaolinite Mica-2M, Quartz and mixed layer Smectite-Mica. There is no evident change in mineralogy, in terms of formation of new minerals, with depth in the weathering profile suggesting that mineralogical alteration is not pronounced. The profile is however less than two meters in depth which is relatively small from a geological view point.

Table 4.3.3 The clay mineralogy of the Barbados materials

Samples	Chlorite	Quartz	Mica-2M	Kaolinite	Smectite-Mica interlayers
BD-I	***	**	***	***	**
BD-II	***	**	**	***	*
BD-III	***	**	*	***	*

The number of stars do not necessarily represent the relative quantity of each mineral in a sample but simply illustrate the change in X-ray diffraction intensity of minerals between different horizons (also see Figures 4.3.4 to 4.3.6).

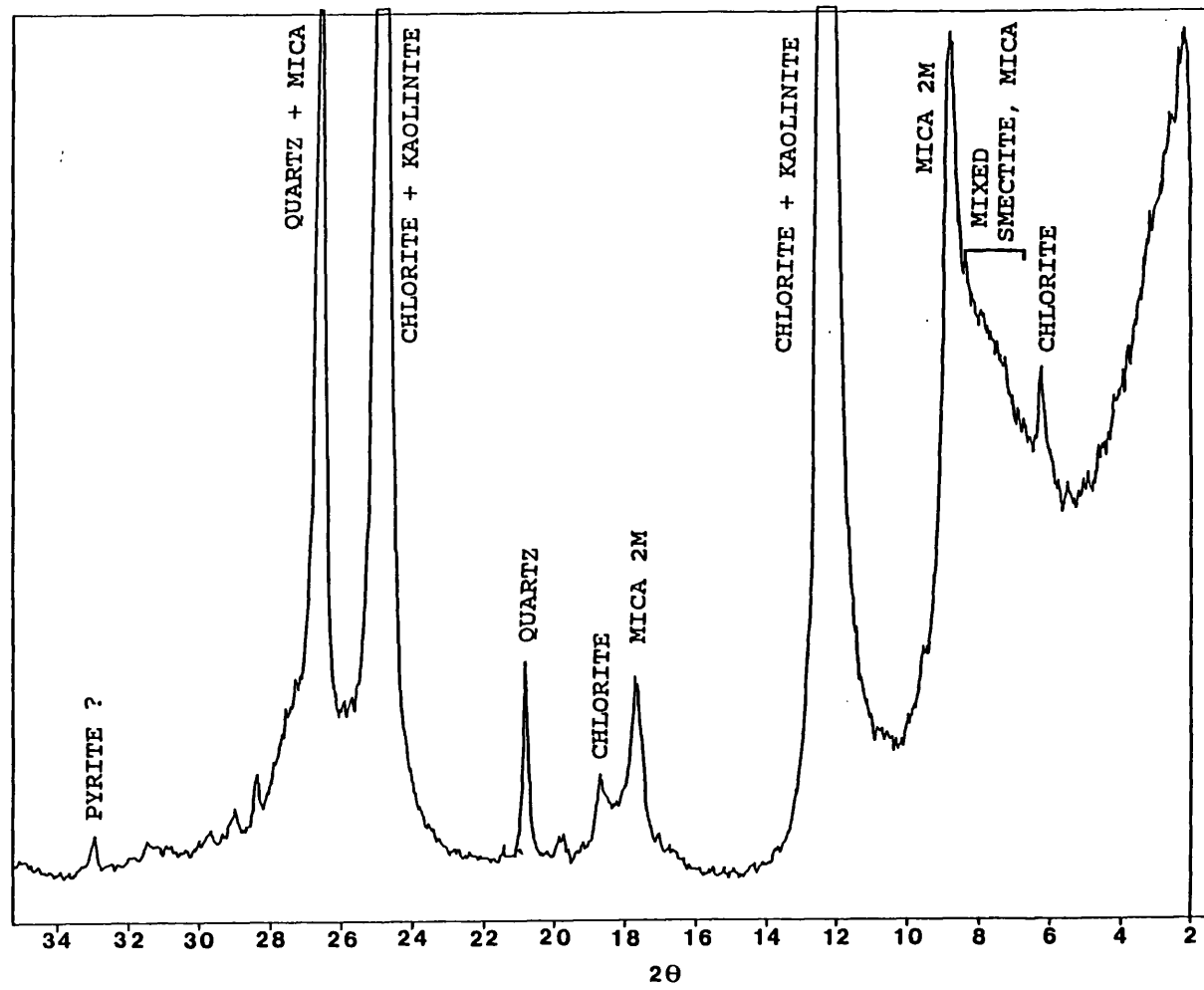


Figure 4.3.4 X-ray diffractogram of the least weathered sample, Barbados (θ is the incidental angle of the X-ray beam)

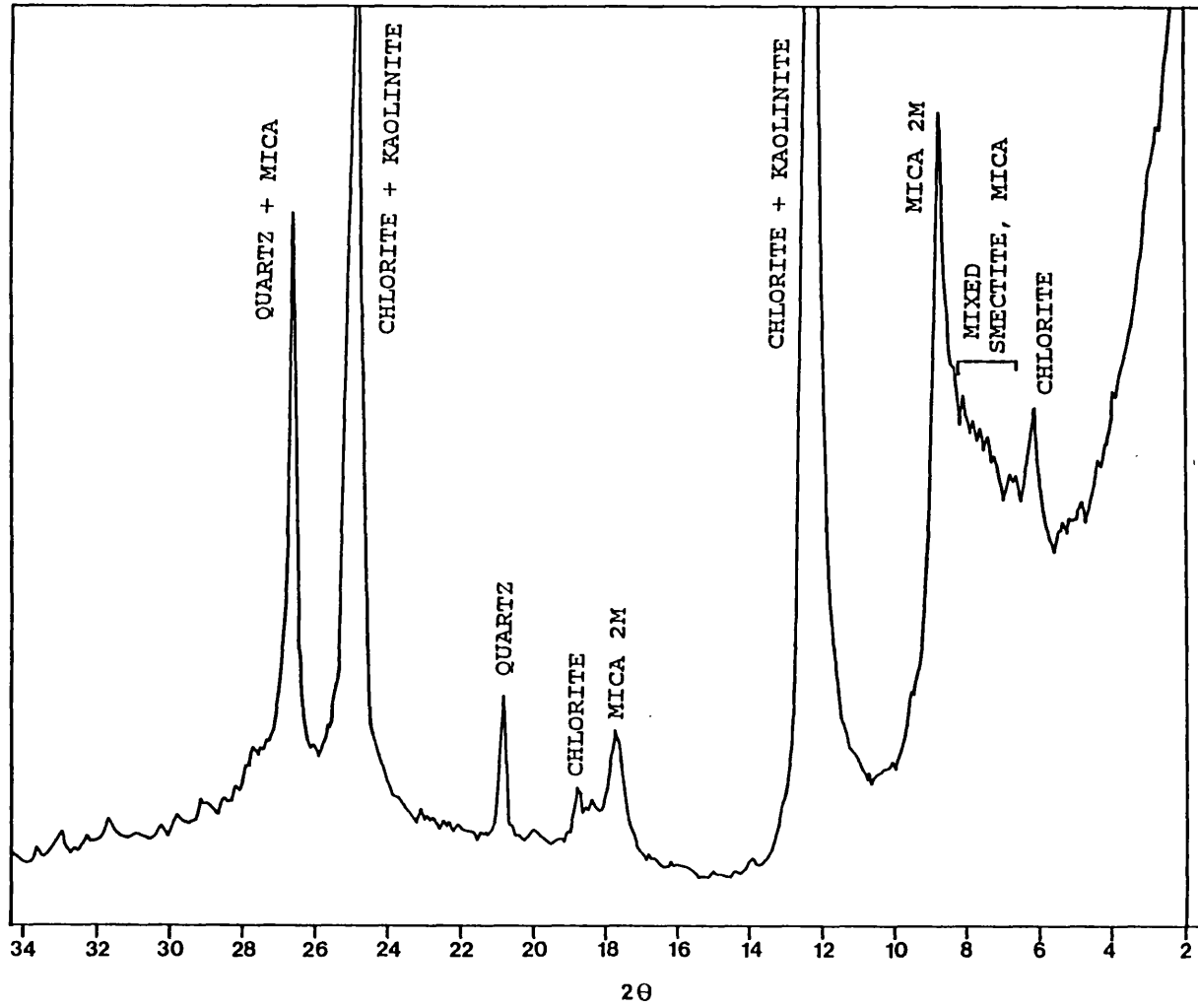


Figure 4.3.5 X-ray diffractogram of the partially weathered sample, Barbados (θ is the incidental angle of the X-ray beam)

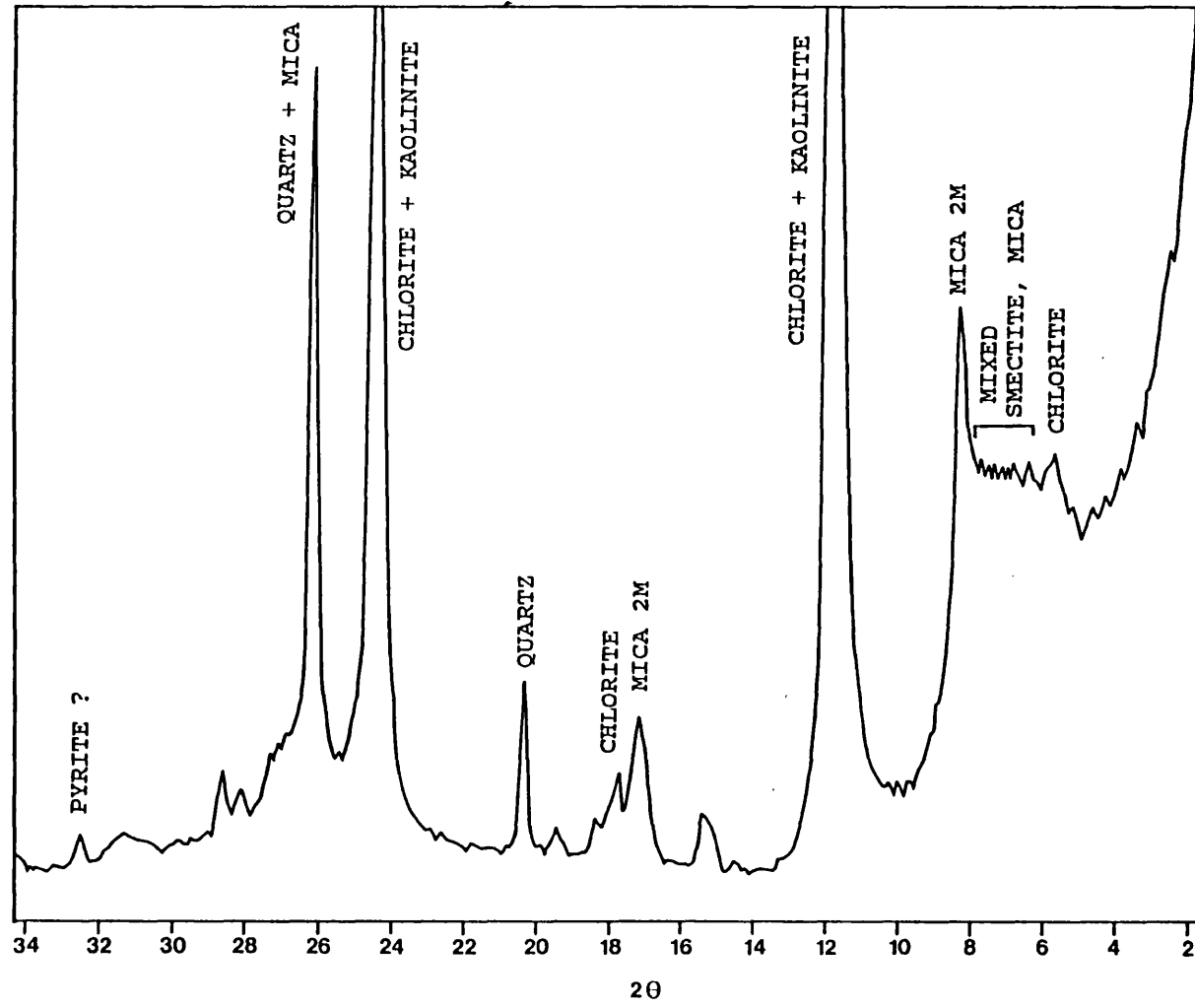


Figure 4.3.6 X-ray diffractogram of the most weathered sample, Barbados (θ is the incidental angle of the X-ray beam)

4.3.1.5 Micro-structure

Study of the micro-structure was completed using SEM photographic technique. Photographs are shown in Plates 4.3.1, 4.3.2 & 4.3.3, in which 4.3.1.(a)-(d) are photographs taken from the deepest sample (BD-I), 4.3.2.(a)-(d) and 4.3.3.(a)-(d) are those of the intermediate depth samples (BD-II), and the shallowest (BD-III) samples, respectively. A preferred alignment of clay particles is seen in Plates 4.3.1.(a) and (b) and the scaly fabric is the result of this alignment. However, preferred orientation is not seen away from the scaly surface. Here, random alignment is observed (Plate 4.3.1.(c) and (d)) even as close as 200 μm from the scaly surface. In other words, the alignment is concentrated along the scaly surfaces but nowhere else. In the intermediate depth horizon sample this preferred orientation is less evident (Plates 4.3.2.(a) and (b)). However, the fabric away from the scaly surface remains more or less the same (4.3.2.(c) and (d)). The preferred orientation is completely absent in the shallowest depth sample (BD-III) and the pore space has been considerably enlarged. This gradual change in micro-fabric was also observed while producing cylindrical specimens for triaxial testing. Pervasive scaly surfaces in the deepest sample caused serious difficulty in trimming specimens to a right-cylindrical shape in the soil lathe.

a



b

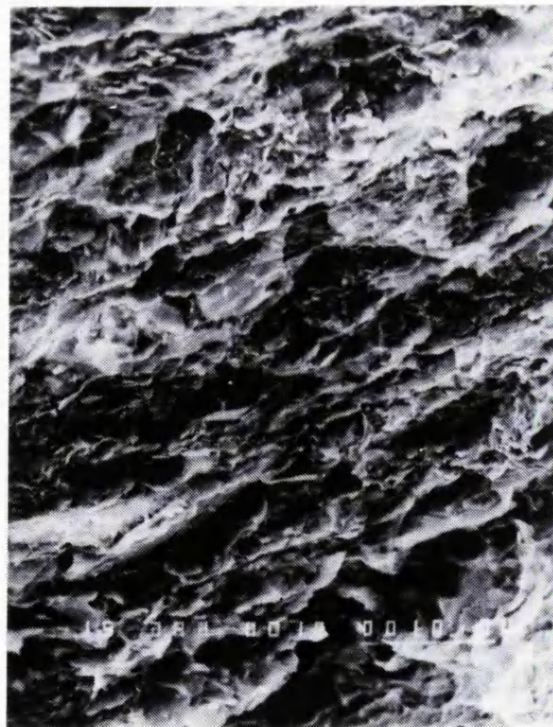
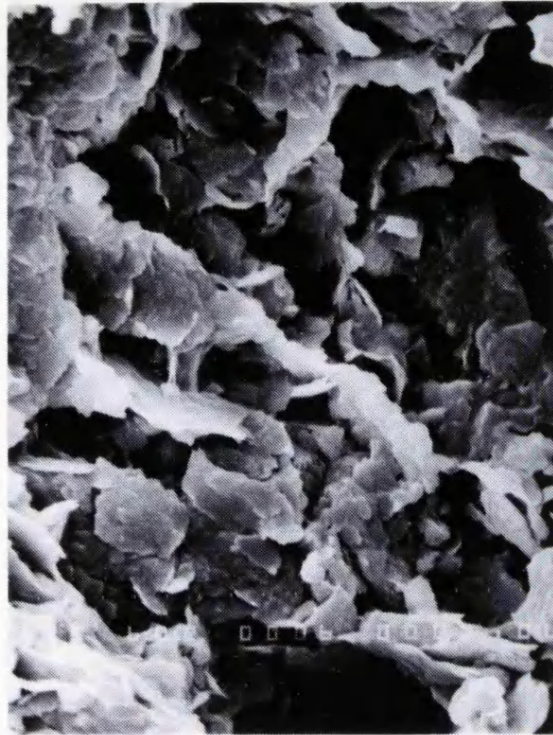


Plate 4.3.1 SEM photographs for the least weathered sample, Barbados. (a), (b): preferred orientation of the clay particles along scaly surface.

c

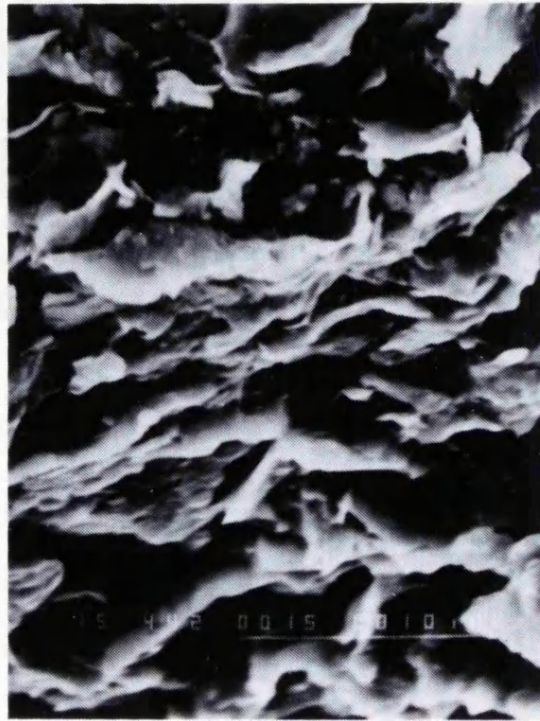


d



Plate 4.3.1 SEM photographs for the least weathered sample, Barbados. (c), (d): random orientation away from scaly surface.

a



b

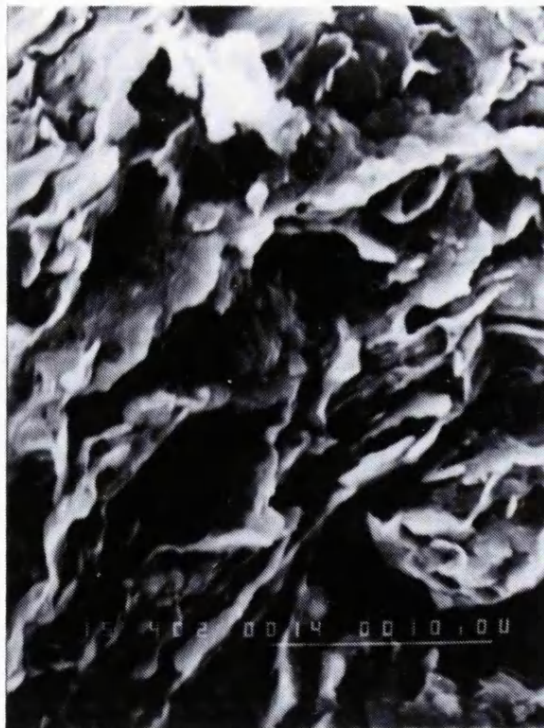
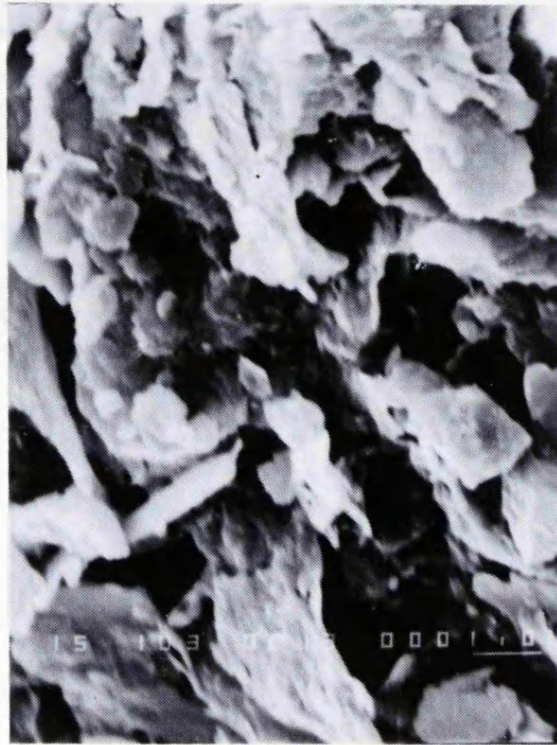


Plate 4.3.2 SEM photographs for the partially weathered sample, Barbados. (a), (b): remnant preferred orientation of the clay particles.

c

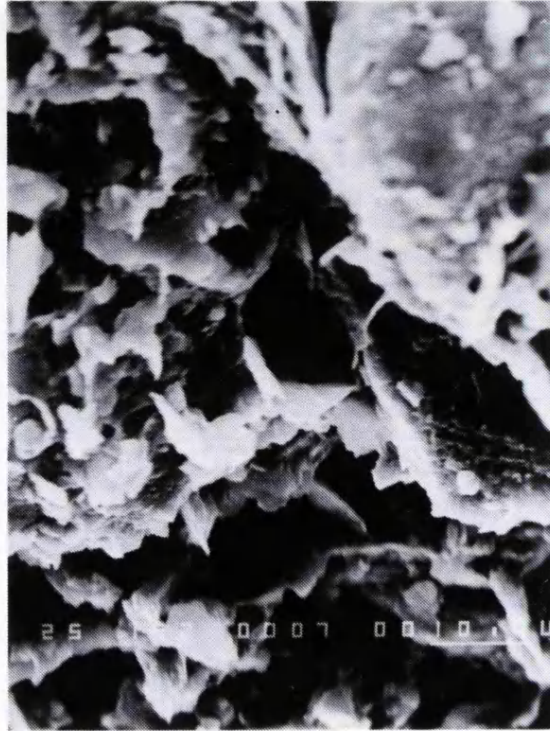


d



Plate 4.3.2 SEM photographs for the partially weathered sample, Barbados. (c), (d): random orientation prevailing the material.

a



b

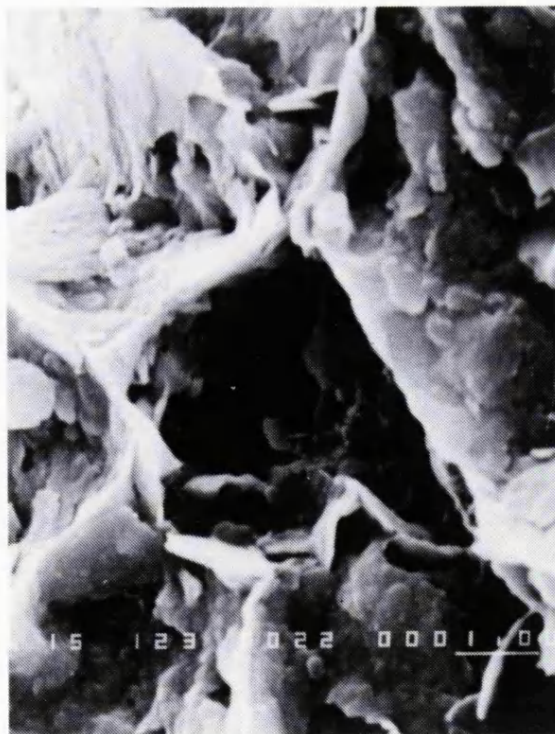


Plate 4.3.3 SEM photographs for the most weathered sample, Barbados. (a), (b): no preferred orientation of the clay particles exist.

c



d

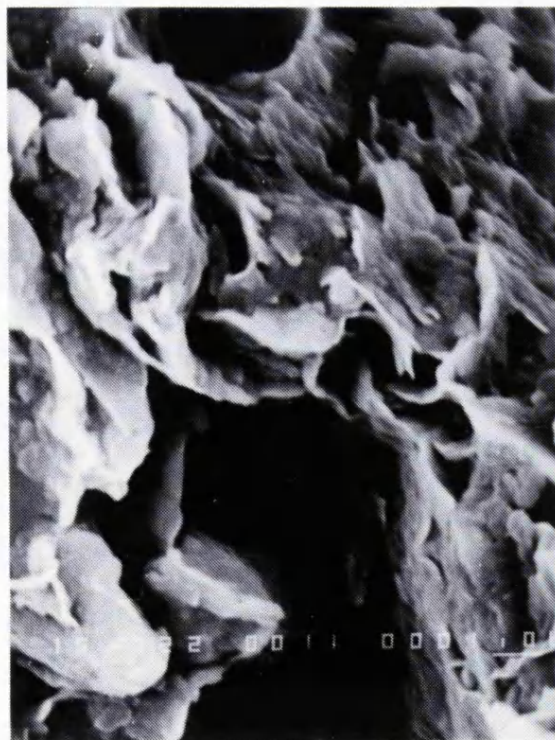


Plate 4.3.3 SEM photographs for the most weathered sample, Barbados. (c), (d): random orientation and pore enlargement can be observed.

4.3.1.6 Chemical analysis

The chemical analysis results are given in Table 4.3.4. The constituents are very similar for all three samples. However, the ferric/ferrous iron ratio decreases with decreasing depth indicating increased oxidation in the materials at shallow depth. This can be taken as a reliable indication that the degree of weathering is changing with depth in the sampled profile in a consistent manner (Chandler, 1972; Grainger & Harris, 1986; Coulthard & Bell, 1990).

Table 4.3.4 The chemical composition of the Barbados samples

Chemical comp.	BD-I	BD-II	BD-III
SiO ₂ (%)	63.69	66.46	67.00
Al ₂ O ₃ (%)	17.21	18.01	15.93
FeO (%)	3.52	1.17	0.93
Fe ₂ O ₃ (%)	1.65	1.02	2.60
MgO (%)	1.11	0.37	0.78
CaO (%)	0.37	0.35	0.33
Na ₂ O (%)	0.18	0.24	0.45
K ₂ O (%)	1.86	0.92	1.23
TiO ₂ (%)	0.93	0.54	0.79
P ₂ O ₅ (%)	0.06	0.03	0.05
MnO (%)	0.04	0.02	0.03
Ignition loss (%)	6.93	8.37	7.35
Total (%)	97.55	97.50	97.47
Fe ⁺² /Fe ⁺³ ratio	2.14	1.18	0.36

4.3.2 Taiwan

As described in Chapter Three, a profile containing four horizons was identified in the Taiwan site, and four layers of material have been sampled. Therefore, the physical and chemical properties examined were determined at four different depths (except the SEM study in which TW-I and TW-II appear to have almost the same characteristics, consequently, only TW-I was photographed). In addition, a thin layer of the top surface material was recovered for examination of its particle size distribution, index properties, clay mineralogy and chemical composition.

4.3.2.1 Particle size distribution

Figures 4.3.7 to 4.3.11 show the particle size distribution curves through the depth/weathering profile for the Lichi Melange scaly clay from Taiwan. They all appear to be very similar in the shape. The wide range of the particle size distribution is because the mélange material is made of a mixture of different sediments and their sizes vary considerably. It is noticeable that all the curves of the Taiwan samples fall in a very narrow band in which the clay content is about 15%-20%, silt is some 20% and, sand and larger portion is about 60%-65%. However, it is also noted that the two bottom samples and the top sample (TW-I, TW-II and TW-V) have a slightly larger portion of fine grains (clay) and less coarse particles (sand) than the other two samples (TW-III and TW-IV).

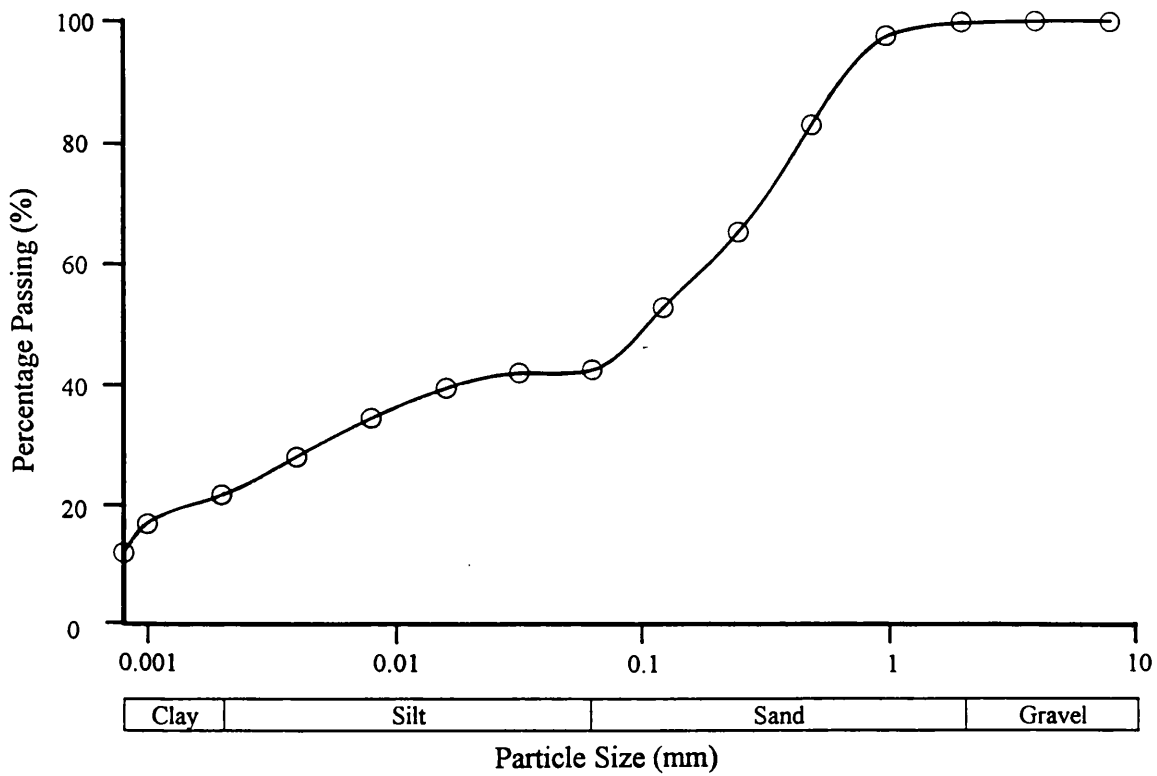


Figure 4.3.7 Particle size distribution curve for least weathered sample, Taiwan

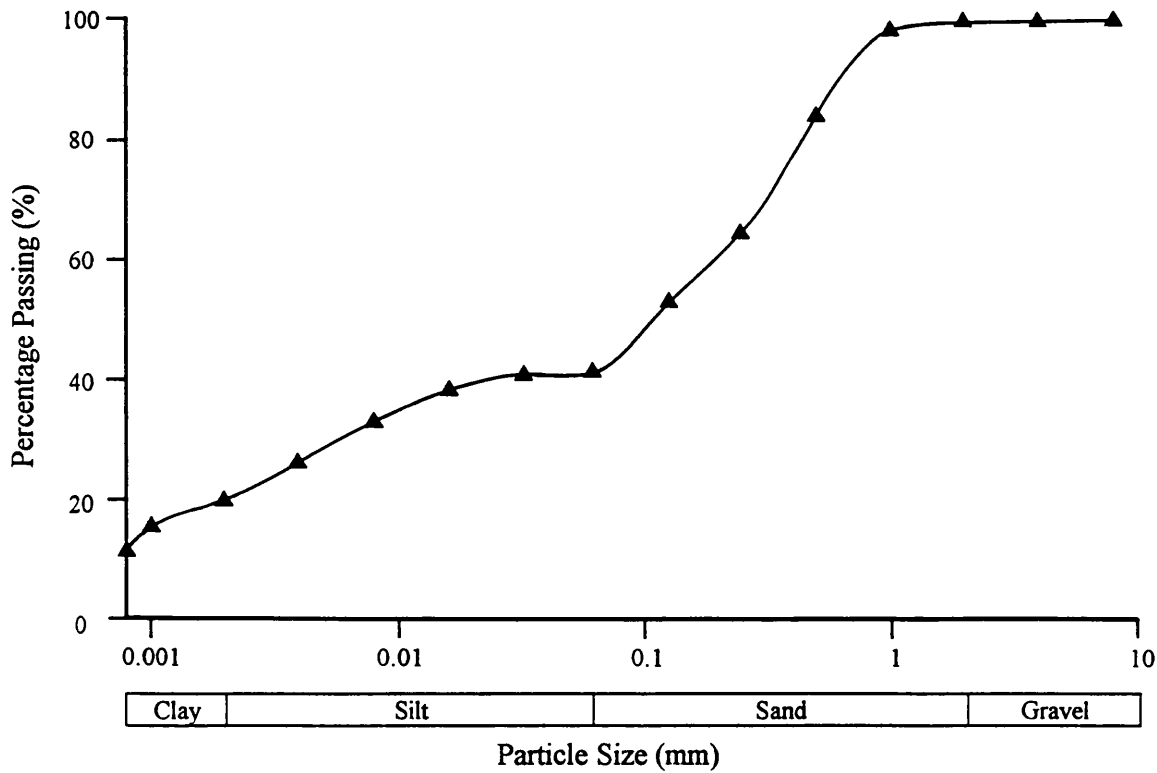


Figure 4.3.8 Particle size distribution curve for slightly weathered sample, Taiwan

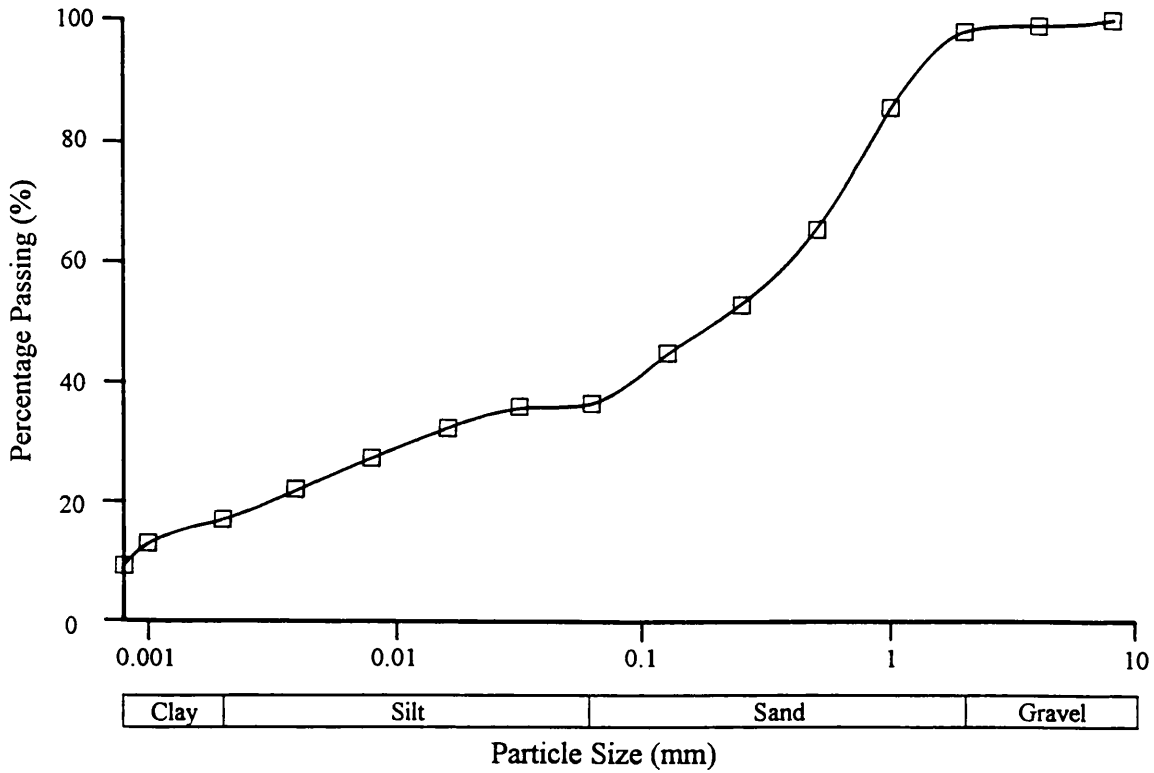


Figure 4.3.9 Particle size distribution curve for partially weathered sample, Taiwan

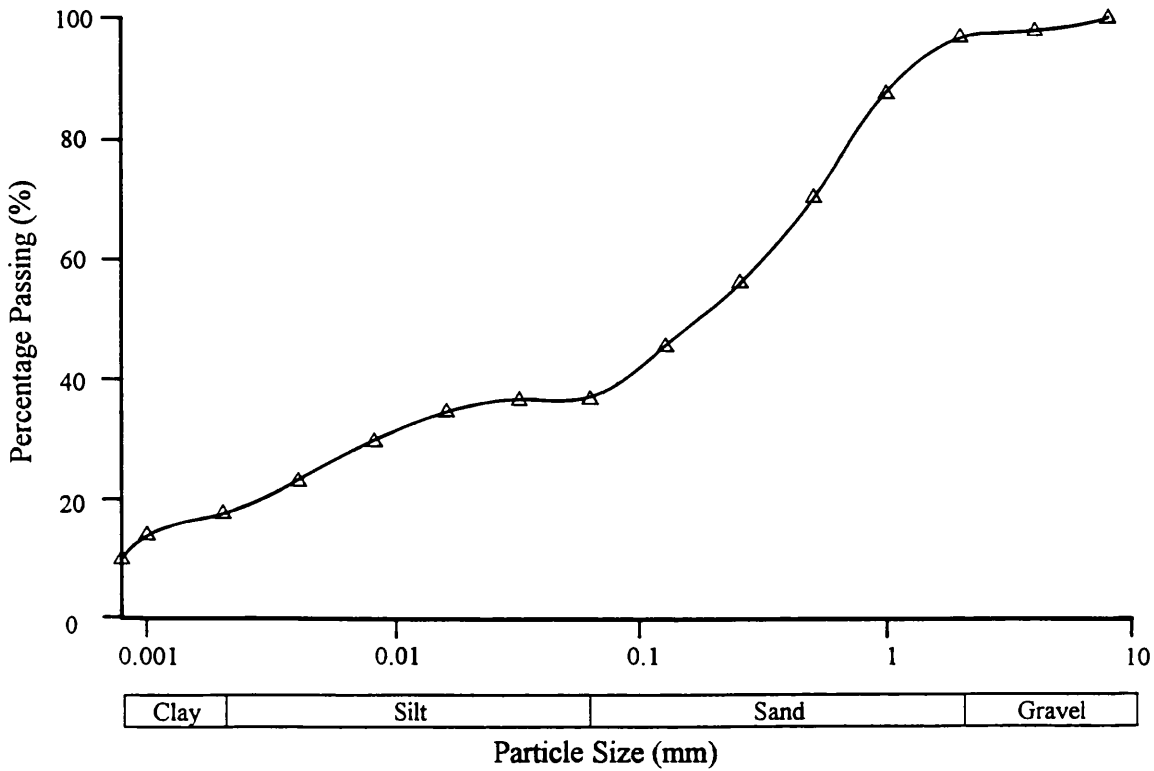


Figure 4.3.10 Particle size distribution curve for most weathered sample, Taiwan

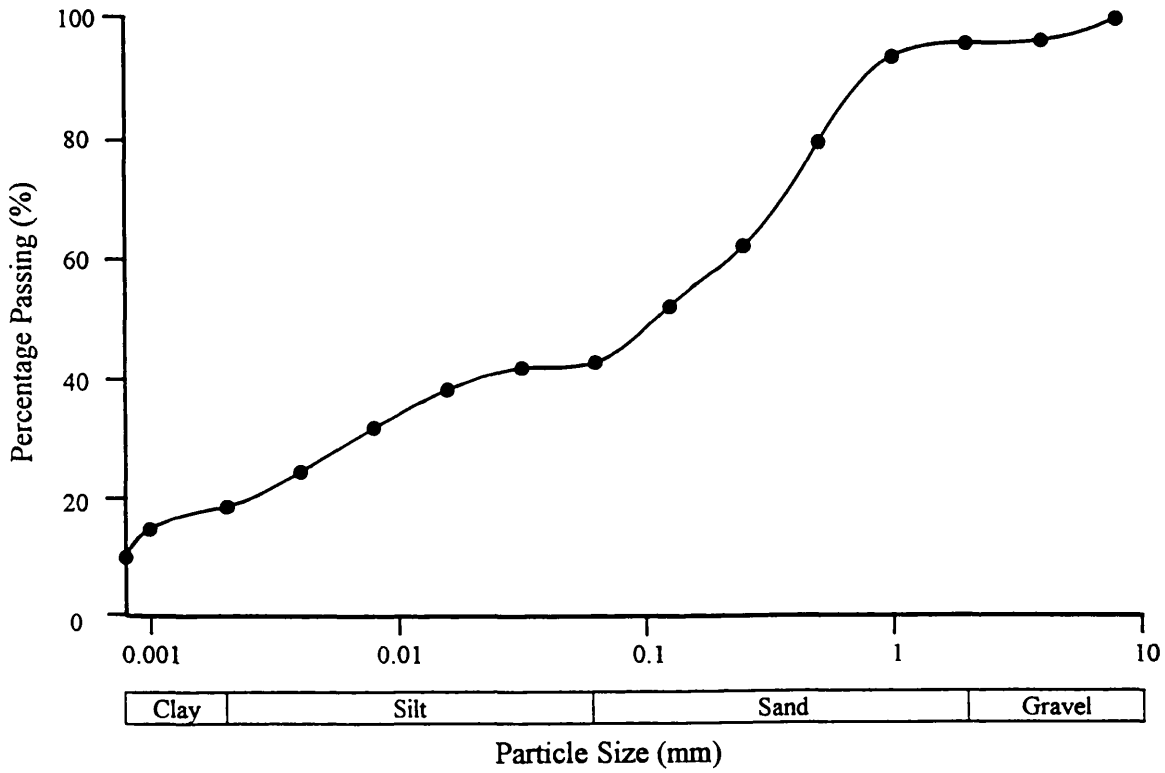


Figure 4.3.11 Particle size distribution curve for top surface sample, Taiwan

4.3.2.2 Porosity, natural water content and bulk density

Table 4.3.5 gives the porosity, natural moisture content and bulk density data for all the samples except sample TW-V because the material from this horizon was very fragile and no regularly shaped specimen could be produced. Porosity and moisture content increase from 20% to 25% and from 9% to 13% respectively, and bulk density decreases from 2.37 g.cc⁻¹ to 2.19 g.cc⁻¹ over the depth range 200 cm to 10 cm. Although the changes are not very large, an increasing trend of increasing pore volume can be seen. Only small differences between the two deepest samples TW-I and TW-II are observed. These are likely to be due to sample variation rather than any significant difference between depth horizons.

Table 4.3.5 Summary of the porosity, natural water content and bulk density of the Taiwan samples

Sample number	Porosity (%)	Moisture content (%)	Bulk density (g.cc ⁻¹)
TW-I(150-200 cm)	20.0	9.0	2.37
TW-II(100-150 cm)	20.0	9.3	2.36
TW-III(50-100 cm)	22.5	10.5	2.28
TW-IV(10-50 cm)	25.5	12.9	2.19

4.3.2.3 Plasticity index

Plastic limit, liquid limit and plasticity index values are given in Table 4.3.6. There is no change in the plastic limit, which is about 20%, and very little change in the liquid limit and plasticity index throughout the profile. The layer TW-III sample appears to have a slightly higher liquid limit of 35% and the surface sample (TW-V) has the lowest at 27.3%. Consequently TW-III has a higher plasticity index of 14.6% and TW-V a low plasticity index of 8.9%.

Table 4.3.6 Summary of the of the Plastic and Liquid Limits and Plasticity Index of the Taiwan samples

Sample number	Plastic limit (%)	Liquid limit (%)	Plasticity index (%)
TW-I(150-200 cm)	19.2	32.2	13.0
TW-II(100-150 cm)	19.3	31.5	12.2
TW-III(50-100 cm)	20.3	34.9	14.6
TW-IV(10-50 cm)	20.1	31.0	10.9
TW-V(0-10 cm)	18.4	27.3	8.9

4.3.2.4 Clay mineralogy

The clay mineralogy of the samples is presented in Table 4.3.7 and their X-ray diffraction traces are shown in Figures 4.3.12 to 4.3.16. Kaolinite is only present in the upper most two samples (TW-IV and TW-V), especially in the surface sample (TW-V) where the chlorite peak appears to be much weaker than in those from greater depth. Although not strictly quantitative, it is possible to estimate the relative change in concentration of a particular mineral using a reference peak. The quartz peak at 2θ of 20.88° is similar for all five samples, and can therefore be used as a reference. It is found that the chlorite and mica-2M peaks, in particular, the ones at low 2θ , are intensely strong in the TW-III sample, but in the TW-IV and TW-V they are relatively weak. This variation is thought to be a consequence of changing concentration of these two minerals.

Table 4.3.7 Summary of the main clay mineralogy of the of the Taiwan samples

Samples	Chlorite	Quartz	Mica-2M	Kaolinite	Smectite-Mica interlayers
TW-I	***	**	***		**
TW-II	***	**	***		**
TW-III	****	**	****		***
TW-IV	**	**	**	*	*
TW-V	*	**	*	**	*

The number of stars do not necessarily reflect the relative quantity of each mineral in a sample but simply illustrate the change in X-ray diffraction intensity of minerals between different horizons. (also see Figures 4.3.12 to 4.3.16)

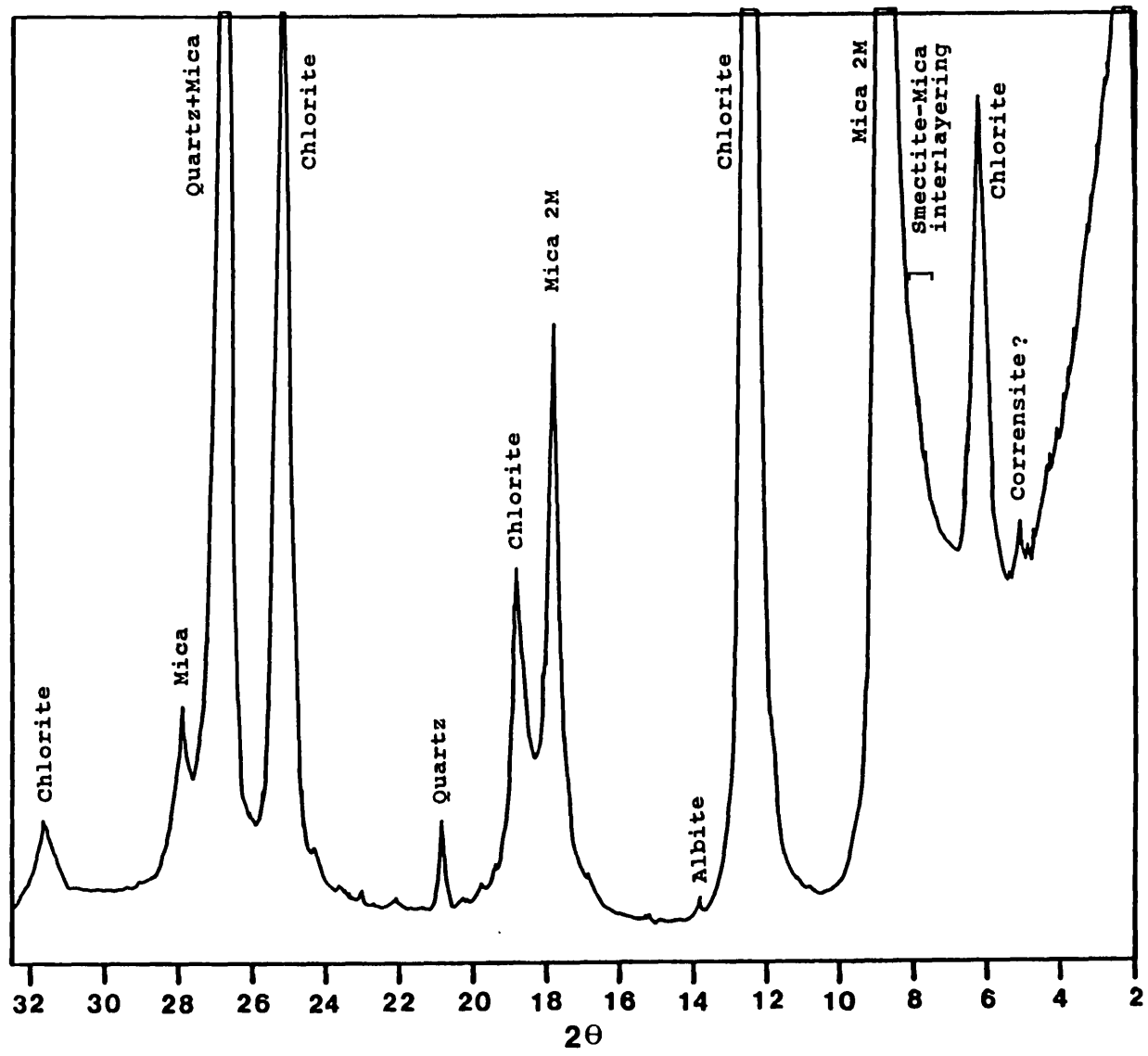


Figure 4.3.12 X-ray diffractogram of the least weathered sample, Taiwan (θ is the incidental angle of the X-ray beam)

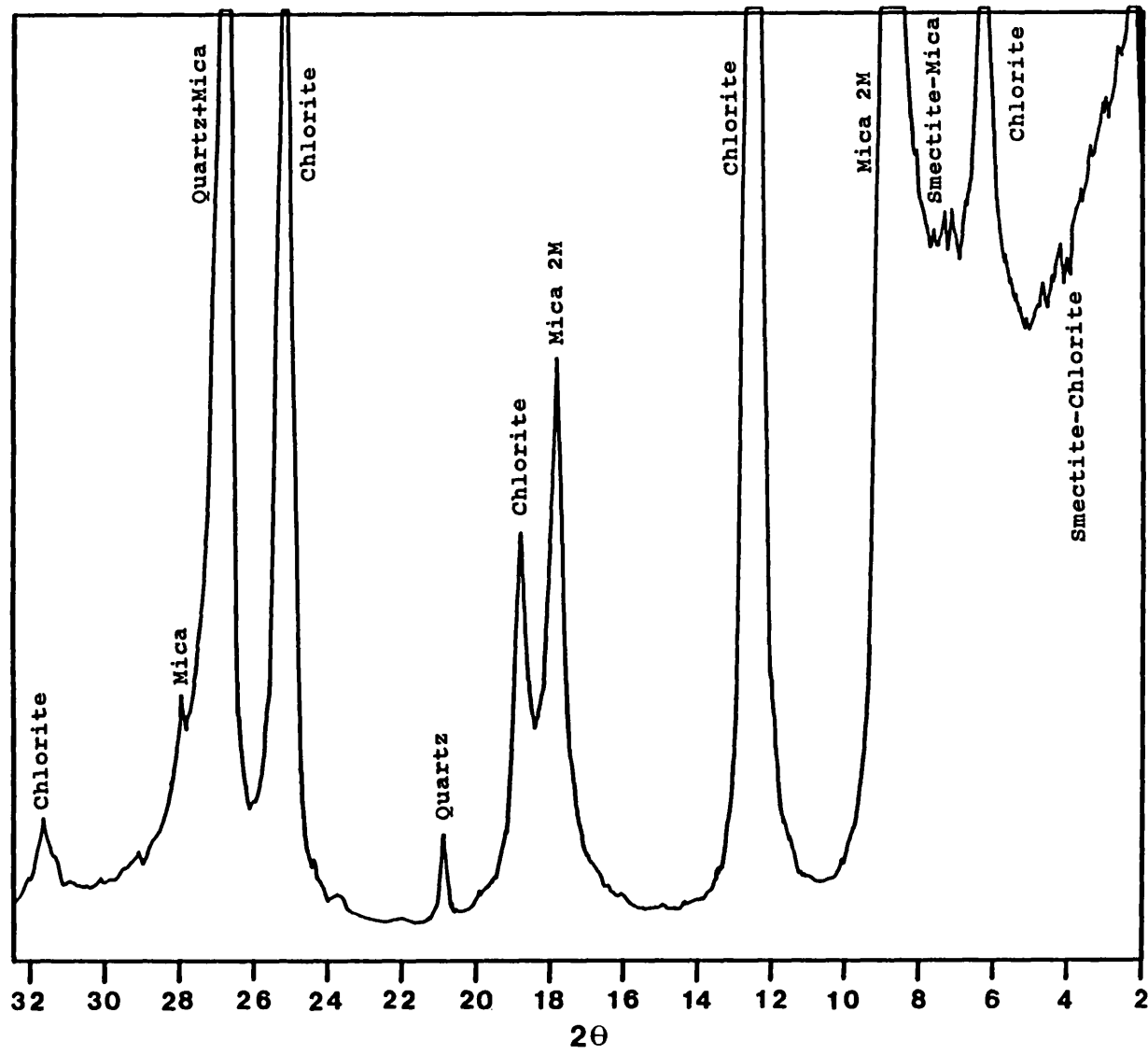


Figure 4.3.13 X-ray diffractogram of the slightly weathered sample, Taiwan (θ is the incidental angle of the X-ray beam)

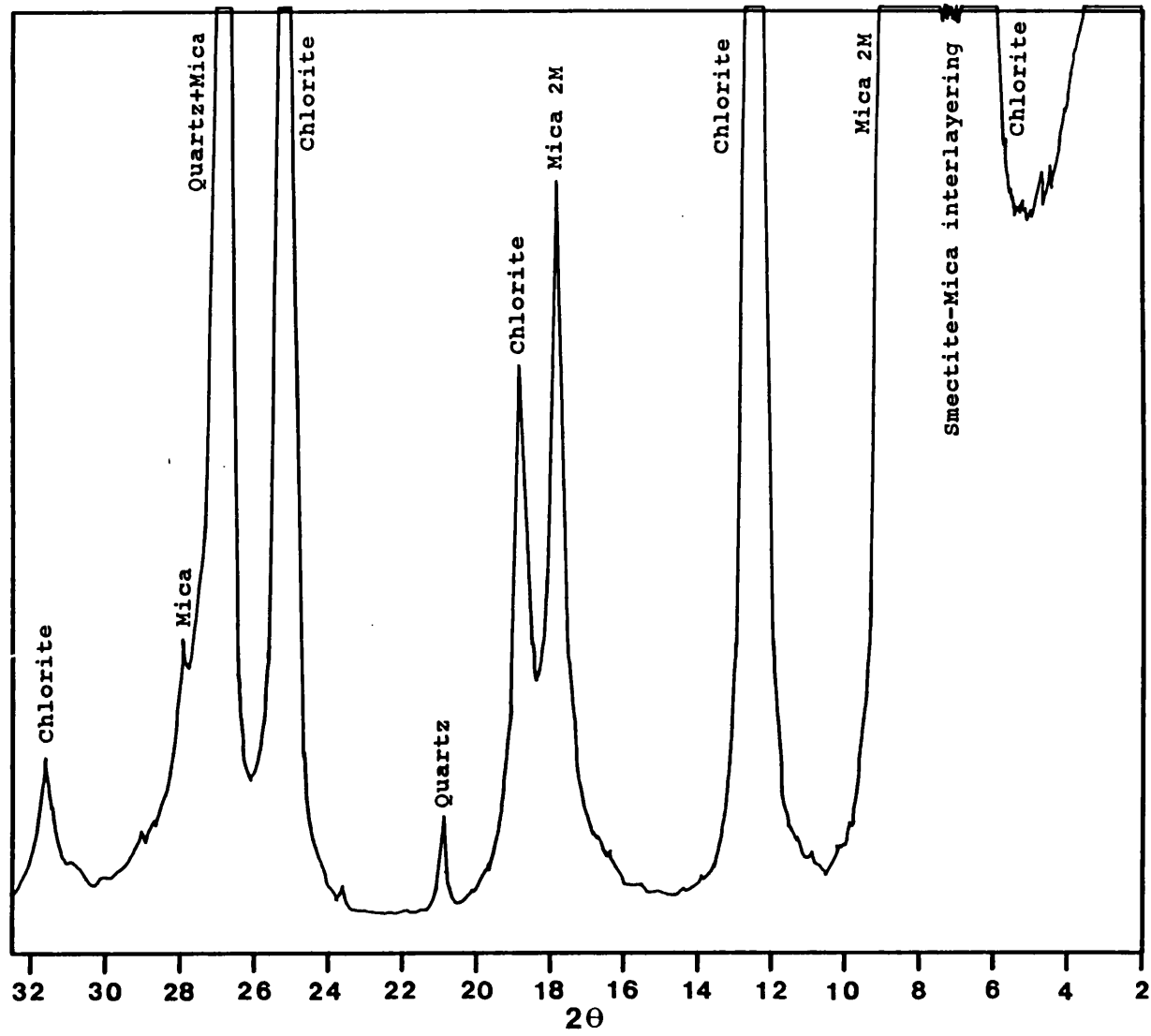


Figure 4.3.14 X-ray diffractogram of the partially weathered sample, Taiwan (θ is the incidental angle of the X-ray beam)

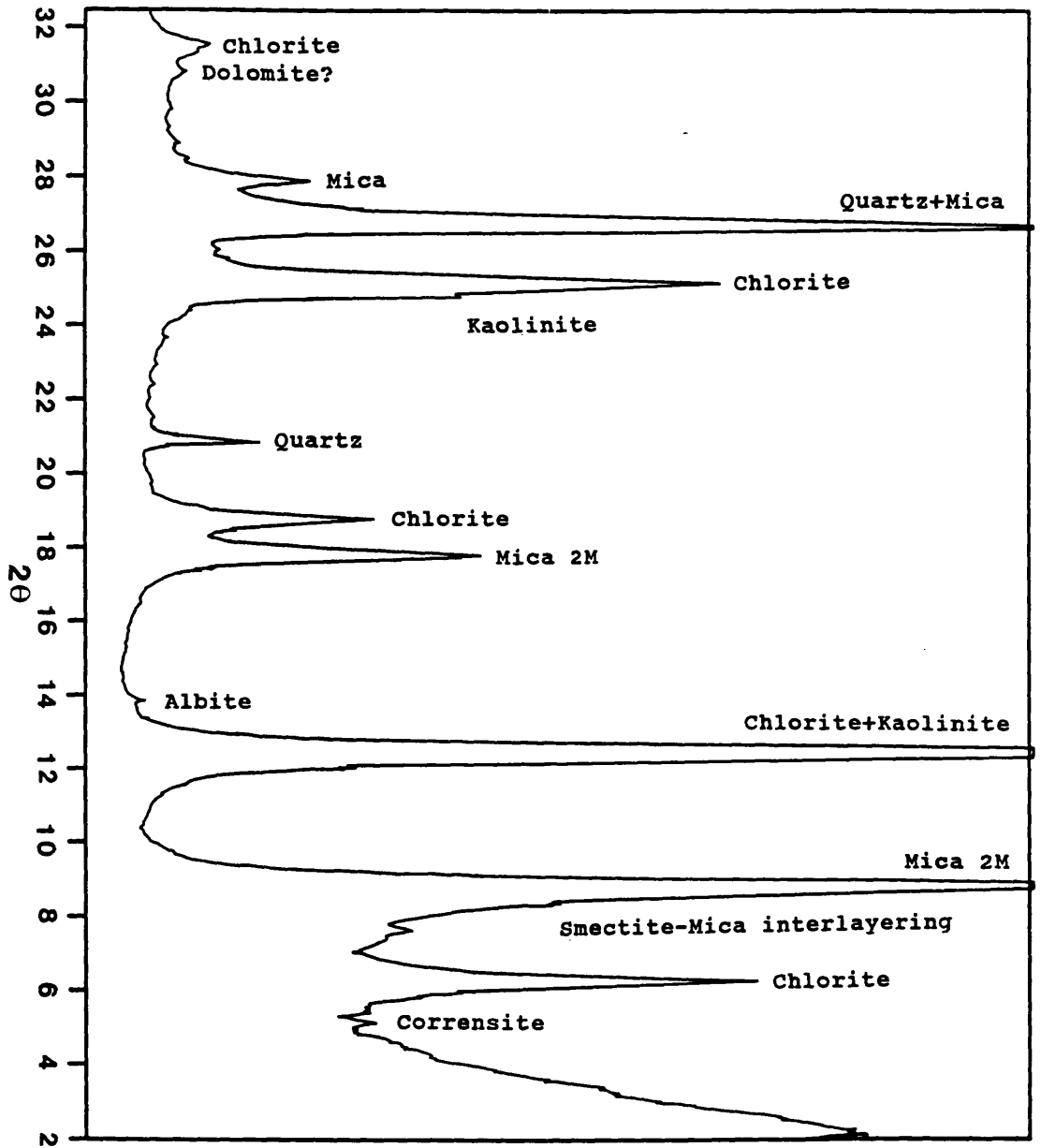


Figure 4.3.15 X-ray diffractogram of the most weathered sample, Taiwan (θ is the incidental angle of the X-ray beam)

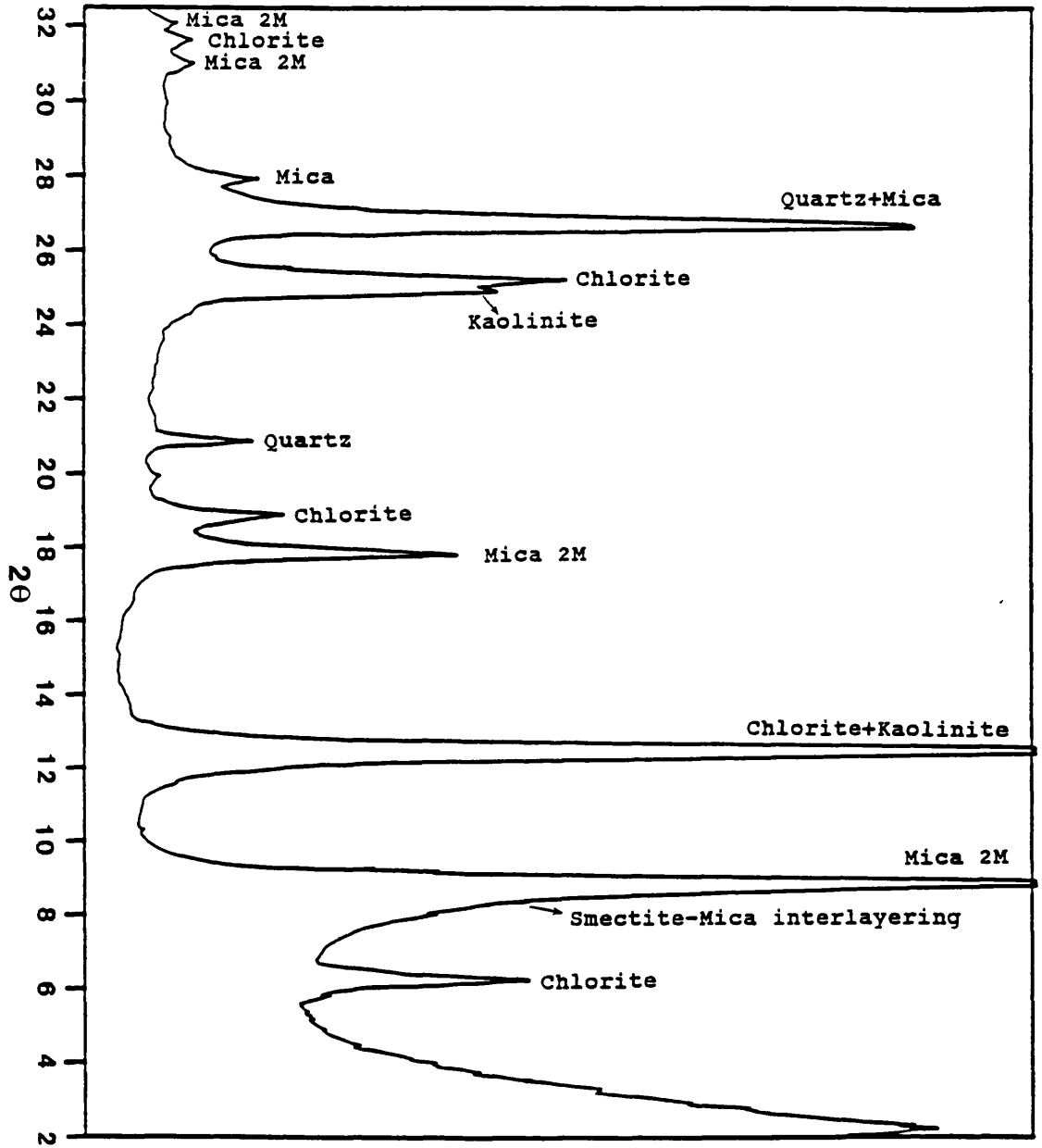


Figure 4.3.16 X-ray diffractogram of the top surface sample, Taiwan (θ is the incidental angle of the X-ray beam)

4.3.2.5 Micro-structure

The SEM photographs taken from the Taiwan samples are presented in Plates 4.3.4, 4.3.5 & 4.3.6 and reveal a gradual change in the extent of particle alignment. The three sample horizons TW-I, TW-III and TW-IV do not exhibit very strong preferred particle orientation or evidence of particle re-orientation. However, there is still some preferred orientation which can be observed in the deepest sample (TW-I) but this is absent in the shallowest sample (TW-IV).

a

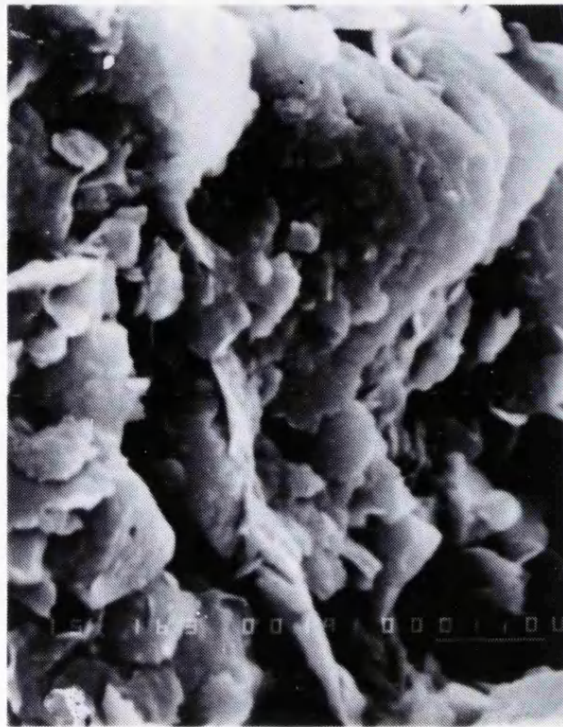


b



Plate 4.3.4 SEM photographs for the least weathered sample, Taiwan. (a), (b): preferred orientation of the clay particles along scaly surface.

c

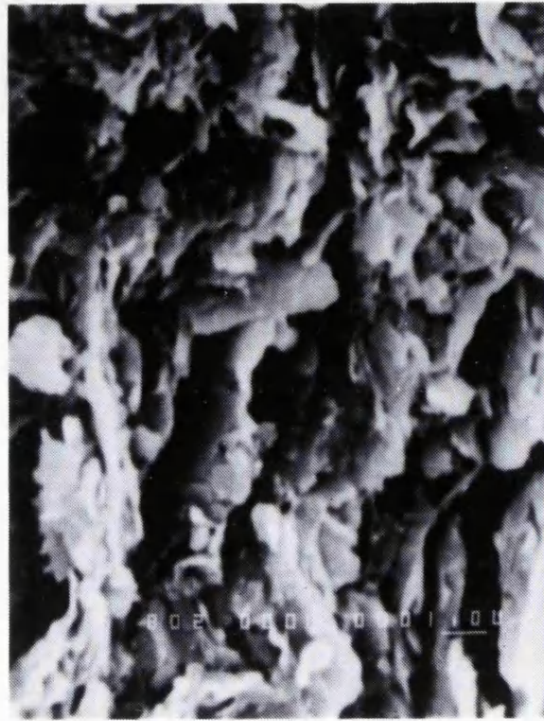


d



Plate 4.3.4 SEM photographs for the least weathered sample, Taiwan. (c), (d): random orientation away from scaly surface.

a



b



Plate 4.3.5 SEM photographs for the partially weathered sample, Taiwan. (a), (b): remnant preferred orientation of the clay particles.

c



d

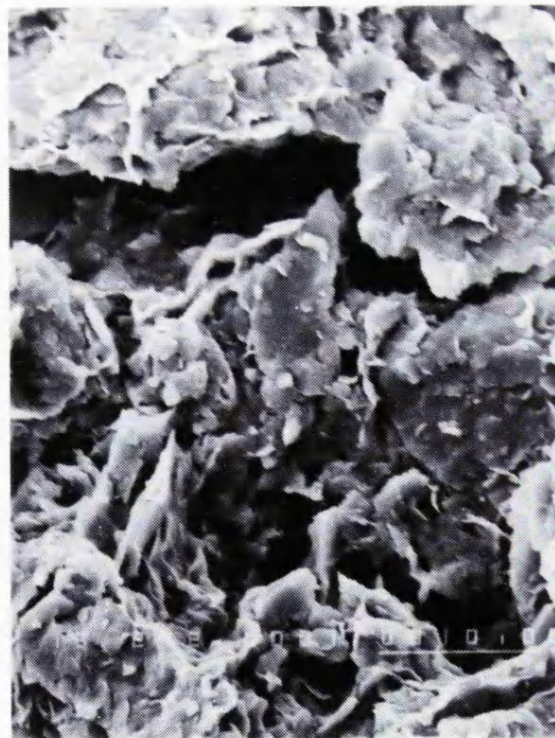
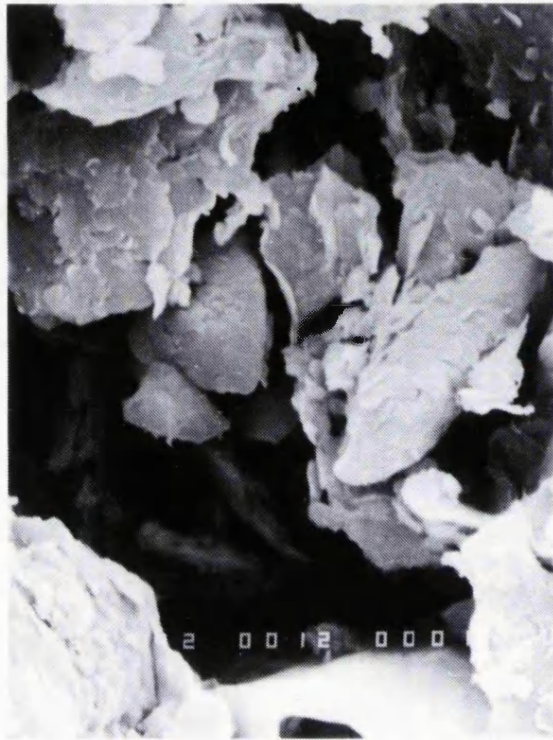


Plate 4.3.5 SEM photographs for the partially weathered sample, Taiwan. (c), (d): random orientation prevailing the material.

a

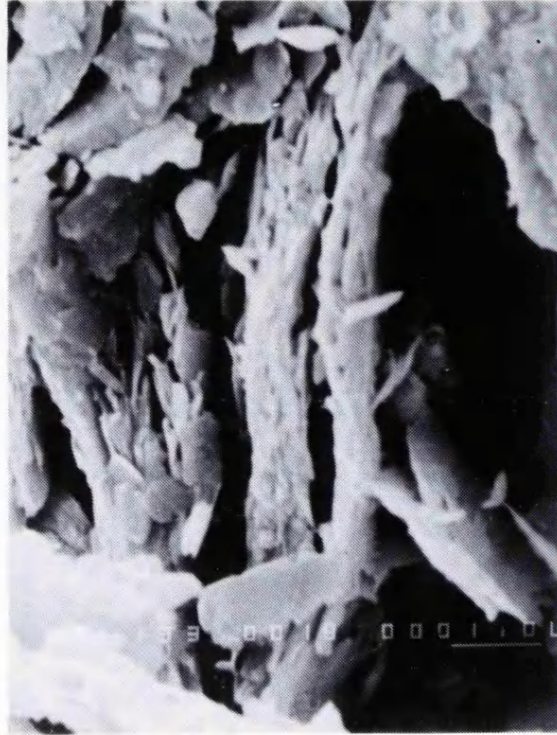


b



Plate 4.3.6 SEM photographs for the most weathered sample, Taiwan. (a), (b): no preferred orientation of the clay particles exist.

c



d



Plate 4.3.6 SEM photographs for the most weathered sample, Taiwan. (c), (d): random orientation and pore enlargement can be observed.

4.3.2.6 Chemical analysis

The chemical analyses for Lichi Mélange scaly clay were completed on the five different horizons. Table 4.3.8 gives the results. The composition data do not show any pronounced changes throughout the profile. However, the ferrous/ferric iron ratio increases from 0.82 to 3.01, as the sample burial depth increases up to about 150 cm. The ratio of TW-II and TW-I are very similar.

Table 4.3.8 The chemical composition of the Taiwan samples

Chemical comp.	TW-I	TW-II	TW-III	TW-IV	TW-V
SiO ₂ (%)	57.94	58.85	58.50	56.56	57.64
Al ₂ O ₃ (%)	18.37	18.19	18.01	19.03	16.71
FeO (%)	4.61	4.49	3.83	4.14	2.72
Fe ₂ O ₃ (%)	1.53	1.53	1.74	2.77	3.33
MgO (%)	2.69	2.74	2.71	2.50	2.43
CaO (%)	0.75	0.82	1.04	0.92	2.38
Na ₂ O (%)	1.36	1.49	1.40	1.09	1.26
K ₂ O (%)	3.43	3.45	2.82	3.73	2.77
TiO ₂ (%)	0.86	0.85	0.83	0.89	0.87
P ₂ O ₅ (%)	0.08	0.08	0.09	0.09	0.10
MnO (%)	0.07	0.08	0.07	0.09	0.08
Ignition loss (%)	6.25	5.97	5.72	6.73	7.41
Total (%)	97.95	98.54	96.76	98.53	97.69
Fe ²⁺ /Fe ³⁺ ratio	3.01	2.94	2.20	1.50	0.82

4.4 Discussion

Attention has been paid to the changes in physical-chemical properties and mineralogical composition induced by weathering processes. From the particle size distribution curves, materials from both locations exhibit characteristics of sedimentary mélange matrix insofar as the distribution curves cover a wide range of particle size from clay to very coarse sand size. Interestingly, the intermediate horizon samples (BD-II and TW-III) in both cases have the lowest content of clay sized particles and the highest content of silt and fine sand sized grains (Figures 4.3.1 to 4.3.3 and Figures 4.3.7 to 4.3.11 respectively) although the difference, particularly in the Taiwan samples, is not very significant. This phenomenon indicates that with the onset of this type of weathering the clay fraction decreases rather than increases, which causes a relative increase in the silt and fine sand fraction. Subsequently, the clay fraction increases again with further weathering. As discussed previously (Chapter Two, section 2.2) it has been generally

agreed that physical weathering is likely to introduce stress causing mineral grains to break down along lines of weakness to smaller particles and this is seen in the upper part of the weathering profiles where the clay content increases with decreasing sample depth. However, for test materials which consist of large amounts of clay minerals, small particles may aggregate to become larger grains, often termed peds, during exposure to wetting and drying conditions (Dixon & Robertson, 1971). The formation of larger sized grains can be observed in the lower part of the profiles (Figures 4.3.1, 4.3.2, 4.3.7, 4.3.8 & 4.3.9). The aggregation of clay sized grains may be aided by specific mineralogy, the presence of cementing agents, appropriate pore fluid characteristics and/or chemical bonding effects (Pandian *et al.*, 1993a). In tropical environments, wetting and drying is an usual process and often occurs within the near surface material due to the warm temperature and high humidity. Particle aggregation to form larger peds is therefore, probably, an important process in terms of the effect of tropical weathering at the early stage. Such a factor should be taken into consideration when studying the mechanical behaviour of such aggregated materials e.g. BD-II and TW-III (see Chapter Five).

The porosity data of the Barbados and Taiwan clays show a correlation with depth. The deeper samples have smaller pore volumes. This is also reflected by the natural moisture content and bulk density data (Tables 4.3.1 & 4.3.5). The increase in pore volume is thought to be largely attributed to destructuring induced by weathering processes (Barden & Sides, 1971; Barden, 1972b). Particle reorientation often occurs during destructuring leading to the re-arrangement of the original alignment of particles and thus an increase in the void space. It is the reorientation of the particles that primarily contributes to the increase in the pore volume.

In addition to the destructuring by weathering that gives rise to an increase in pore volume, elastic rebound resulting from geologic unloading (decrease in mean effective stress) may also partly contribute to the pore enlargement. The increase in pore space from depth to ground surface may suggest that the effective stress is larger when material is buried at depth than that at near ground surface. According to consolidation theory (see Appendix I), the volume of a material increases (decreases) due essentially to decrease (increase) in mean effective stress. Assuming the mineral grains are not compressible, the change in volume must have taken place in the pore space. The porosity and moisture content are, therefore, increasing as material moves from deep to shallow, and the bulk density, on the other hand, is decreasing in that same order.

Furthermore, it is noticeable that in the Barbados data (Table 4.3.1) the increase in porosity and moisture content with decreasing depth does not correlate very well. In

other words, the increase in porosity from BD-I to BD-II is 6.2% which results in a 7.6% increase in the moisture content, but the increase in porosity from BD-II to BD-III (9.3%) only results in an increase of 2.7% in the moisture content which is much less than the value it should be (11%, calculated from porosity). This indicates that the BD-III sample was not fully saturated in the field and the degree of saturation is controlled by other factors such as climatic conditions and capillary rise.

From examination of the Atterberg limits, it can be noted that in both cases the plastic limit values do not differ greatly between different weathering horizons nor between the two clay types. A more pronounced variation is recorded in the liquid limit values (Tables 4.3.2 & 4.3.6). This is particularly evident in the Barbados samples. As described previously, the Atterberg limits are primarily controlled by the mineralogy and clay content of the sample (Skempton, 1953). Since the mineralogical composition is not appreciably changed, the particle size distribution will instead play an important role in determining the plasticity index (Lambe & Whitman, 1979). A sample with less fine particles has a smaller total surface area, and it is this that results in a lower liquid limit and consequently lower plasticity index.

In the Taiwan samples, the situation is complicated slightly. Although the intermediate depth sample (TW-III) has the lowest content of clay sized particle it exhibits the highest liquid limit. If the variation in liquid limits between different horizons are not due simply to sample variation or to test error (the difference between TW-I and TW-III is less than 3%), then the variation may be a result of the difference in the amount of a particular clay mineral present in the samples. It can be observed that the intensity of the mixed-layered clay (smectite-mica inter-layering) and mica-2M peaks are the strongest in the TW-III sample. Because the high capacity of water absorption of the mixed-layered clay the TW-III sample exhibits a higher liquid limit and thus higher plasticity index.

In the case of the TW-IV and TW-V samples the decrease in liquid limit is thought to correlate with the presence of kaolinite and the decrease in intensities of chlorite, mica-2M and inter-layered smectite-mica peaks (Table 4.3.7 and Figures 4.3.15 & 4.3.16). The decrease in the liquid limit is however, very small. This indicates that the change in index properties caused by mineralogical alteration is limited.

The clay mineralogy shows no significant alteration with depth in the Barbados samples and only very minor changes in the Taiwan material, although there may be some changes in terms of the relative quantities of different mineral species which seem to be reflected in the index properties (Figures 4.3.12 to 4.3.16). In theory, chemical

weathering is expected to be at its most vigorous under humid tropical conditions and results in considerable changes in clay mineralogy very quickly. However, the studied material is clay dominant and is highly impermeable. This characteristic restricts the penetration of surface water into the subsurface which directly reduces the activity of the chemical alteration. Furthermore, clays are essentially products of weathering. Although the present surface environment may not be exactly the same as that in which they were formed, they may be chemically relatively stable. As a result, mineral alteration is not as intense as seen in other rocks, igneous rock for example. Moreover, in both cases the profiles do not exceed more than two meters in depth and both sites are in a highly dynamic environment in which the mass movements are frequent. The time period between exposure of material at the ground surface and it being washed away by a torrential storm event or it being removed by down slope mass movement is very short. Under these circumstances, the limited change in clay mineralogy is, perhaps, understandable.

In the Taiwan samples, a slightly more obvious quantitative change can be seen in clay mineralogy within the profile (Figures 4.3.12 to 4.3.16). The chlorite, mica-2M and mixed-layered smectite-mica peaks show gradual increase from TW-I to TW-III (Figures 4.3.12 to 4.3.14), and then a decrease towards the surface (Figures 4.3.15 & 4.3.16). This is, probably, due to the sample variability. However, a kaolinite peak starts to appear in TW-IV and the intensities of mica-2M, chlorite and mixed-layered smectite-mica peaks are reduced considerably (Figure 4.3.15). The same phenomenon is seen even more clearly in the surface material TW-V (Figure 4.3.16). The indication is that the kaolinite might be the weathering product of mica-2M and/or chlorite and/or mixed-layered smectite-mica for kaolinite is absent in the lower three horizons TW-I, TW-II and TW-III. It is recognised that kaolinitic weathering (Thomas, 1974) is common in tropical regions.

The progressive change in observed micro-structure, especially in the Barbados samples, indicates that weathering affects materials starting from the discontinuity surfaces which will be more susceptible to diffusion and subsequently spread throughout the material (Plates 4.3.1, 4.3.2 & 4.3.3). Because of the movement of water along the scaly fractures, the preferred particle orientation is progressively destroyed as the material becomes more heavily weathered. In the most weathered material the scaly fabrics no longer exist and the materials can then be regarded as effectively and naturally remoulded.

In the previous description (section 3.4), degrees of weathering were simply identified by macro-structural observation (scaly fabric), visual evidence (change in colour) and the sample burial depth (Table 3.4.1). Although most of the weathering classifications (Tables 2.6.2 & 2.6.3 are examples) were based on these factors, chemical alteration has been used to provide a quantitative indication of weathering extent. A decrease in the ferrous/ferric iron ratio is seen in the material sampled close to the ground surface which indicates that oxidation is at its most severe at the surface and decreases downwards. The similarity in the ferrous/ferric iron ratio observed in the TW-I and TW-II samples indicates that these materials have both experienced little oxidation implying that oxidation ceases below a certain depth (about 1.5 meters). It is probable that this depth is strongly controlled by the permeability of the material. The more permeable the material is, the deeper the oxidation can reach

According to the ferrous/ferric iron ratio data (Tables 4.3.4 & 4.3.8), the degrees of weathering experienced by the materials can, therefore, be more accurately defined: For the Joe's River Formation scaly clay (Barbados) the bottom horizon with depth of 100 cm-150 cm (BD-I) has a ferrous/ferric iron ratio of 2.14 indicating that it is relatively speaking Least weathered and is therefore named as **BDL**; the intermediate depth horizon extracted from a depth of 50 cm-100 cm (BD-II) exhibits a ferrous/ferric iron ratio of 1.18 suggesting that the horizon has been more heavily weathered than the BDL layer and has as a result been given the name of **BDP** (Partially weathered); and the upper most horizon recovered from a depth of 0 cm-50 cm (BD-III) shows the most severe oxidation with a ferrous/ferric iron ratio of 0.36 and is named as **BDM** in which the letter "M" means: Most weathered in the entire profile.

A similar principal is applied to the Lichi Mélange scaly clay from Taiwan: The bottom layer, recovered from a depth of 150 cm-200 cm (TW-I) has the highest ferrous/ferric iron ratio of 3.01 and exhibits no obvious sign of weathering, and is therefore named as **TWL** (equivalent to **BDL**); the immediate overlying horizon with a depth of 100 cm-150 cm (TW-II) which displays great similarity to TWL but with a Slightly higher degree of oxidation is given the name of **TWS** (Slightly weathered) the layer above **TWS** is from a depth between 50 cm to 100 cm (TW-III) which has an oxidation ratio of 2.20 and is considered to be Partially weathered is named as **TWP**; the horizon (TW-IV) overlying **TWP** is the layer thought to represent a heavily weathered state exhibiting a oxidation ratio of 1.50. This layer is named as **TWM** (Most weathered) which is equivalent to the upper most horizon of the Barbados sample (**BDM**). The very Top surface sample (TW-V) exhibits the lowest ferrous/ferric ratio and is given a name of **TWT**.

As a summary a few points, in terms of the effect of weathering, can be drawn from the data that are presented so far. These are:

- Pore space increases as weathering proceeds;
- Pre-existing scaly texture (macro-scale) is progressively destroyed by weathering which is a result of reorientation of clay particles (micro-scale);
- Particle aggregation may have occurred during weathering;
- No pronounced mineralogical alteration has occurred during weathering;
- No significant changes occur in the bulk chemical composition, but the degree of oxidation is increasing as materials move towards the surface;

A more thorough discussion will be followed in the main discussion chapter, Chapter Six, after the triaxial deformation data are presented in Chapter Five.

Chapter Five: Mechanical Characteristics of the Two Scaly Clays

5.1 Introduction

Mechanical characteristics govern the responses of a material to changes in the prevailing state of stress. For weak sedimentary rocks and soil materials, two aspects of their mechanical behaviour, consolidation and shear resistance, are the most important and commonly measured parameters in geotechnical surveys (Lambe & Whitman, 1979). These properties of weak rocks, are not entirely inherent but are dependent on factors such as compaction history, particle and pore characteristics, fabric, and mineralogy (Skempton, 1953; Barden, 1972a, 1972b; Atkinson & Bransby, 1978; Vaughan, 1985; Craig, 1992). In other words, the mechanical behaviour of a material will change if any of these characteristics are modified, i.e. it is dependent on the previous deformation history.

The results of experiments to investigate the mechanical behaviour of the materials examined in this research, using triaxial compression apparatus, are reported here. An extensive series of standard consolidated undrained triaxial deformation experiments have been completed on the materials from both Barbados and Taiwan. The structure of this chapter is similar to that of Chapter Four in which the equipment, sample preparation and testing procedure are initially described followed by a presentation of the experimental results in two sub-sections. A discussion specific to the recorded mechanical behaviour is given at the end of the chapter. In order to avoid confusion, the experiments are named on the basis of their locations, degrees of weathering, which were defined in the previous chapter, and the effective consolidation pressure while they were deformed under undrained condition. Table 5.1.1 gives the name list of the triaxial experiments conducted in the present study.

Table 5.1.1 The experiments conducted in the study

Experiment names	Sample location	Degree of weathering	Eff. cons. pressure
BDL-100	Joe's River Formation	Least weathered	100 (kPa)
BDL-200	Joe's River Formation	Least weathered	200 (kPa)
BDL-400	Joe's River Formation	Least weathered	400 (kPa)
BDP-50	Joe's River Formation	Partially weathered	50 (kPa)
BDP-100	Joe's River Formation	Partially weathered	100 (kPa)
BDP-200	Joe's River Formation	Partially weathered	200 (kPa)
BDP-400	Joe's River Formation	Partially weathered	400 (kPa)
BDM-100	Joe's River Formation	Most weathered	100 (kPa)
BDM-200	Joe's River Formation	Most weathered	200 (kPa)
BDM-400	Joe's River Formation	Most weathered	400 (kPa)
BDR-100	Joe's River Formation	Mud flow	100 (kPa)
TWL-100	Lichi Mélange Formation	Least weathered	100 (kPa)
TWL-400	Lichi Mélange Formation	Least weathered	400 (kPa)
TWS-100	Lichi Mélange Formation	Slightly weathered	100 (kPa)
TWS-200	Lichi Mélange Formation	Slightly weathered	200 (kPa)
TWS-400	Lichi Mélange Formation	Slightly weathered	400 (kPa)
TWP-100	Lichi Mélange Formation	Partially weathered	100 (kPa)
TWP-200	Lichi Mélange Formation	Partially weathered	200 (kPa)
TWP-400	Lichi Mélange Formation	Partially weathered	400 (kPa)
TWP-400a	Lichi Mélange Formation	Partially weathered	400 (kPa)
TWM-100	Lichi Mélange Formation	Most weathered	100 (kPa)
TWM-200	Lichi Mélange Formation	Most weathered	200 (kPa)
TWM-400	Lichi Mélange Formation	Most weathered	400 (kPa)

5.2 Methodology

In investigations of the stress and strain characteristics of rock and soil materials the triaxial compression test is, probably, the most widely used method. The methodology employed to measure mechanical behaviour in this research mainly followed the standard procedures such as British Standard 1377 (1990). In addition, there were a few techniques used in the study which did not fully agree with the Standard but seem to be more feasible in this case. For example, some of the triaxial tests were conducted using samples of smaller size than that described in the Standard because of the low permeability characteristics of the studied material. A brief description of the methodology and details of the exceptions are therefore given.

5.2.1 Test equipment

The investigations of the mechanical behaviour were performed using a conventional soil triaxial deformation cell (Figure 5.2.1, Plate 5.2.1). There are several types of standard tests which can be conducted in a triaxial cell, including Consolidated Undrained Triaxial tests, Consolidated Drained Triaxial tests, Pore Fluid Pressure Dissipation tests, and tests without lateral strain, the K_0 -test (Bishop & Henkel, 1962). Different types of experiments need different transducers. The K_0 -test, for instance, needs a device which is able to detect the radial strain during compression (Figure 5.2.2), so that the cell pressure can be adjusted to maintain the radial strain at zero.

In the deformation cell used in the present study, axial load, cell pressure (confining fluid pressure), both top and bottom pore fluid pressures, axial displacement and sample volume change can be measured using different types of transducers and a volume gauge (Table 5.2.1). The calibration data for these different transducers are provided in Appendix IV. Figure 5.2.3 is the schematic diagram of the drainage board⁵ which illustrates how the system operates to control and measure pore fluid pressures and volume changes of the sample. Cell pressure is maintained using a gas-water interface volume gauge driven by a constant air pressure pump, which is capable of generating 2,000 kPa air pressure, controlled through a pressure regulator with a working range of 0 kPa to 750 kPa. Thus the cell pressure is controlled by the air pressure regulator. All data were recorded directly by the integrated laboratory data logging system. The logging time interval was adjustable and therefore able to meet the specific requirements of individual tests.

Table 5.2.1 Types of transducer used in the study

Measurements	Types of transducers	Ranges
Axial load	Load cell	0-4.5 (kN)
Confining cell pressure	Pressure transducer	0-7,000 (kPa)
Top pore fluid pressure	Pressure transducer	0-1,500 (kPa)
Bottom pore fluid pressure	Pressure transducer	0-1,500 (kPa)
Axial displacement	LVDT	0-25 (mm)
Volume of expelled pore fluid	Volume gauge	0-100 (cc)

⁵Drainage board is a board on which all the valves, controlling the fluid flow in and out of the sample, are fixed.

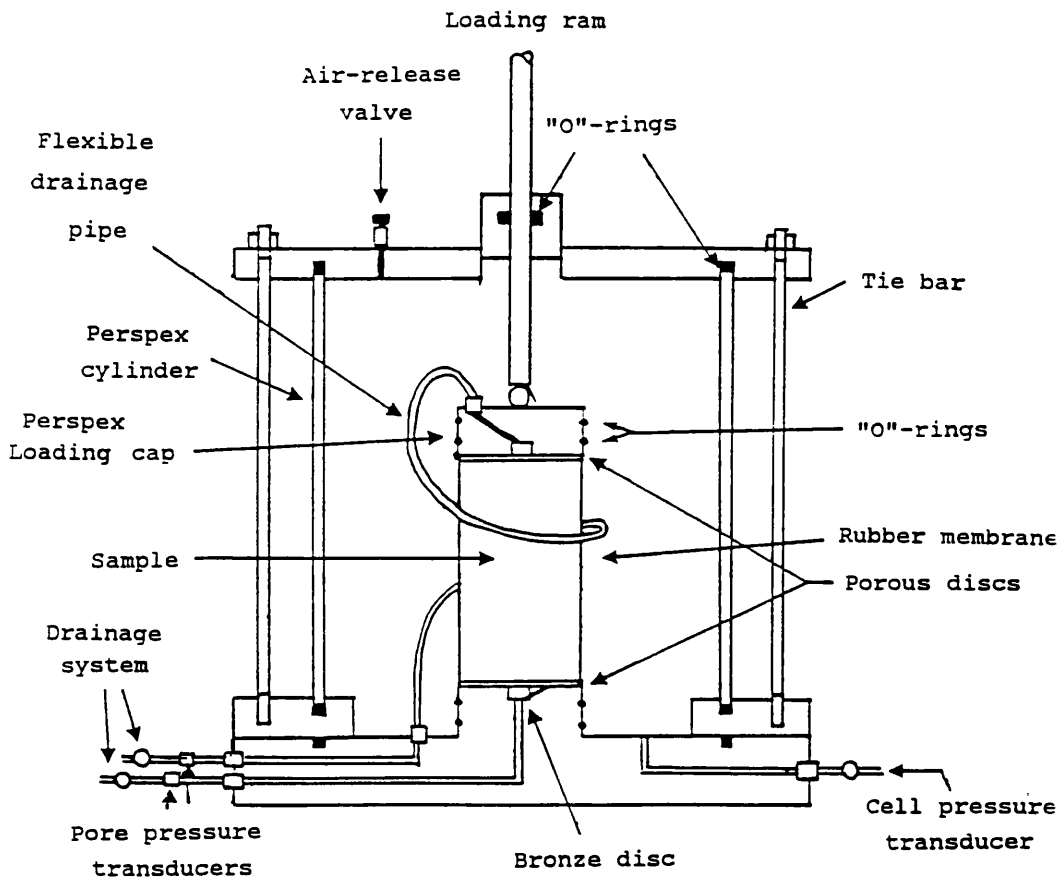


Figure 5.2.1 The triaxial deformation cell used in the study

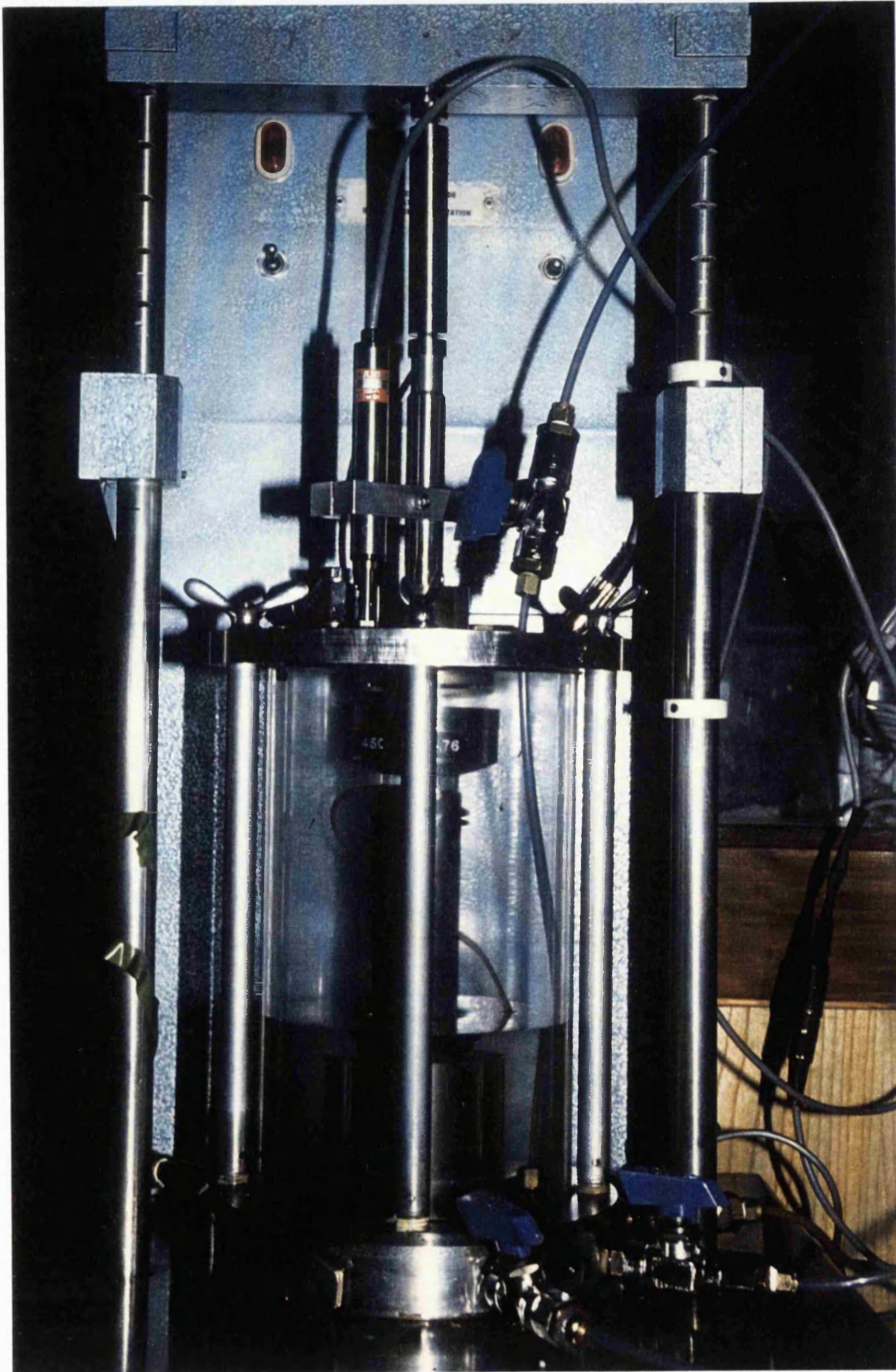


Plate 5.2.1 The triaxial deformation cell used in the present study

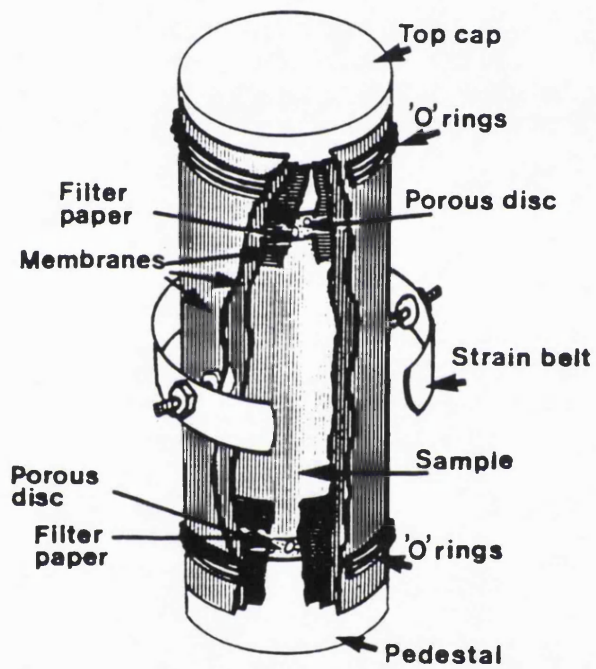


Figure 5.2.2 Sample in the membrane with a strain belt, which enables radial strain to be monitored

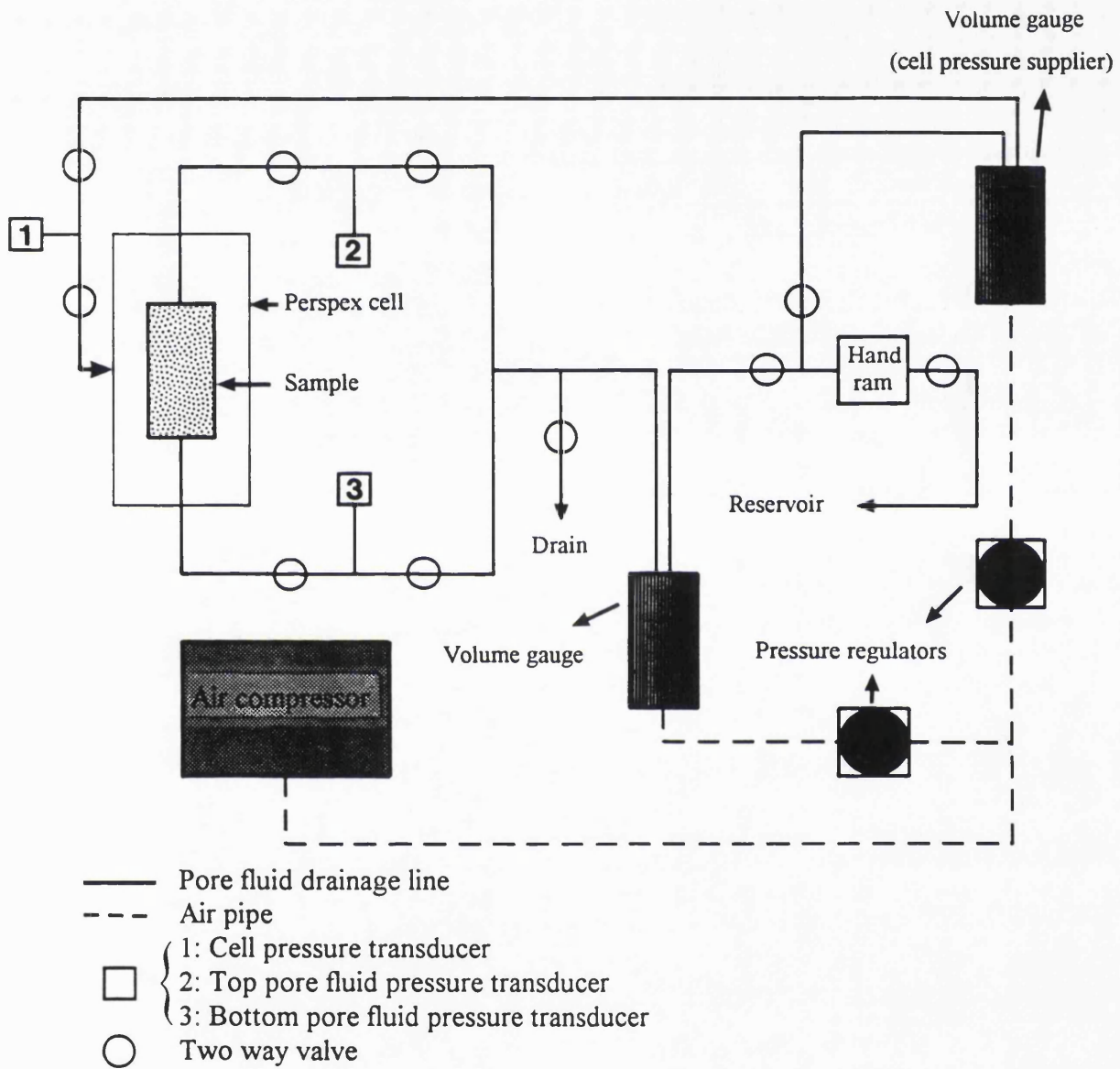


Figure 5.2.3 Schematic diagram of the drainage board

5.2.2 Test specimen preparation

The specimens required for testing in this type of deformation cell are a right cylinder with a diameter/height ratio of 0.5. All the Barbados samples were approximately 38 mm in diameter and about 76 mm in length (BS 1377, 1990). However, for materials with extremely low permeability such as the Lichi Mélange scaly clay from Taiwan, this size was too great to allow full consolidation within the time constraints of the project. A smaller sample size was therefore used. Details of this reduction in size are described later in this chapter.

The 38/76 mm right cylindrical specimens of Barbados samples were produced using a standard soil lathe (Figure 5.2.4). A small block with the long axis parallel to the vertical direction recorded in the field was cut carefully from the undisturbed, preserved sample (Head 1982). To prevent specimen drying out during the preparation, which causes surface cracks to appear, the samples were repeatedly sprayed with distilled water. On removal of the specimen from the soil lathe, it was cut to the required length and the ends made plane and normal to the specimen axis within 0.5 degree (BS 1377, 1990). Due to the pervasive scaly fabric and the inhomogeneity of the material sample specimens broke into pieces easily and therefore extra care had to be paid during sample preparation.

The Lichi Mélange scaly clay contains numerous clasts of varying size and hardness and it was not possible to produce specimens using the soil lathe without damaging the sample and its fabric. An alternative low-vibration coring technique was therefore employed instead of the soil lathe. The Lichi Mélange scaly clay was very stiff when in its natural state but became muddy very quickly when in contact with water. Coring had, therefore, to be slow enough to minimise disturbance to the natural fabric, but fast enough to prevent the sample softening and turning into its remoulded state.

As mentioned previously, a smaller specimen size was needed for the Lichi Mélange scaly clay. In theory, the time required for completion of consolidation of a sample has a root square function relationship to the distance that the pore fluid travels. As a result, reduction in size, both length and diameter, by a factor of two will shorten the time required for consolidation by a factor of four. The sample size was reduced by a factor of 1.5 which gives a specimen approximately 51 mm in length and 25.4 mm in diameter. This follows the work of Petley (1994) who determined that a reduction in the size of the test specimen by a factor of 1.5 does not have a measurable effect on the experimental results. Samples smaller than this are affected by inhomogeneity of the material

properties of the test material which introduces variability in the test results (Petley, 1994).

Once a cylindrical specimen was produced, it was enclosed in a thin latex rubber membrane sealed to both the top cap and bottom platen of the cell using rubber o-ring seals (Figure 5.2.5, Plate 5.2.2). Sometimes two membranes were used because the sand and coarser particles tended to puncture the membrane under pressure. The membrane acts as a seal to separate the specimen from the confining fluid. Between the specimen and both the top cap and bottom platen filters were placed (Figure 5.2.5) to prevent detached particles invading the drainage system. Drainage connections to the top and base of the sample were made through the top cap and pedestal (Figure 5.2.5). Top and bottom pore fluid pressures can therefore be measured independently, and fluids drained from the specimen through these lines.

The Barbados samples received no further treatment before they went into the cell. However, for the Taiwan material, reduction in specimen size did not adequately shorten the consolidation time. To further accelerate consolidation side drainage was employed. A filter paper, trimmed to the right size and shape, was placed around the sample (Head, 1986; Yassir, 1989) allowing pore fluid to drain from the sample, not only vertically but also horizontally. Although side drainage speeds up the consolidation remarkably, there was a disadvantage. In such experiments pore fluid pressure measured at the undrained end of the sample did not represent the pore fluid pressure in the interior of the specimen. This is because the filter paper increases the fluid communication between top and bottom of the specimen, over the surface of the sample cylinder, and the pressure at the surface is reduced compared with that in the interior of the sample. The extent of this depends on how impermeable the test material is. The consolidation path for a low permeability material using side drainage will thus have a form shown in Figure 5.2.6. An apparent rapid increase in mean effective stress without appreciable volume strain is recorded during the first part of the consolidation. This is due to the reduction in measured pore fluid pressures at the boundary of the specimen. Most of the volume strain occurs subsequently when top and bottom pore fluid pressures have equalised. Therefore, real pore fluid pressure and effective stress can only be determined by closing the drainage line for a period to allow the measured pore fluid pressures to equalise with those in the interior of the sample. The consolidation paths of experiments TWL-400 (Figure 5.4.38) and TWS-400 (Figure 5.4.44) show the typical response to closing the drainage line during consolidation. The upper curves in Figures 5.4.38 & 44 are the recorded experimental behaviour using the re-equilibrated pore fluid pressures, and the lower curves, the true consolidation paths.



Figure 5.2.4 Manual soil lathe and trimming saw used to produce cylindrical specimen for triaxial testing

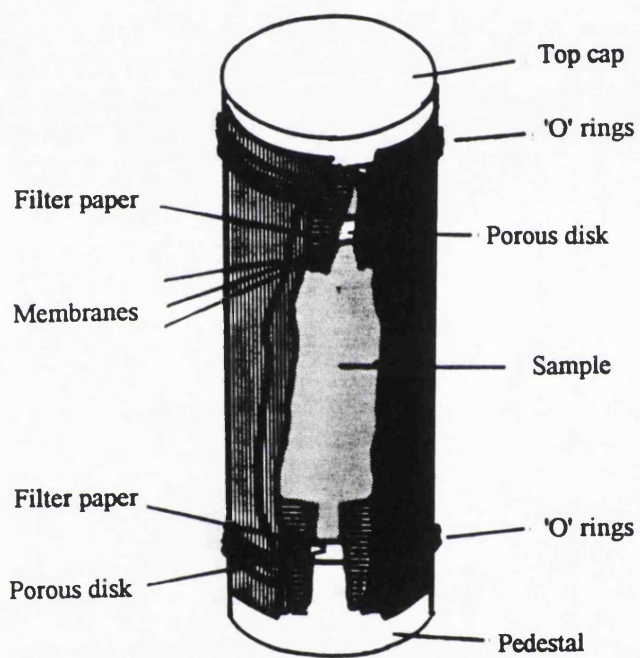


Figure 5.2.5 Sample in the membrane

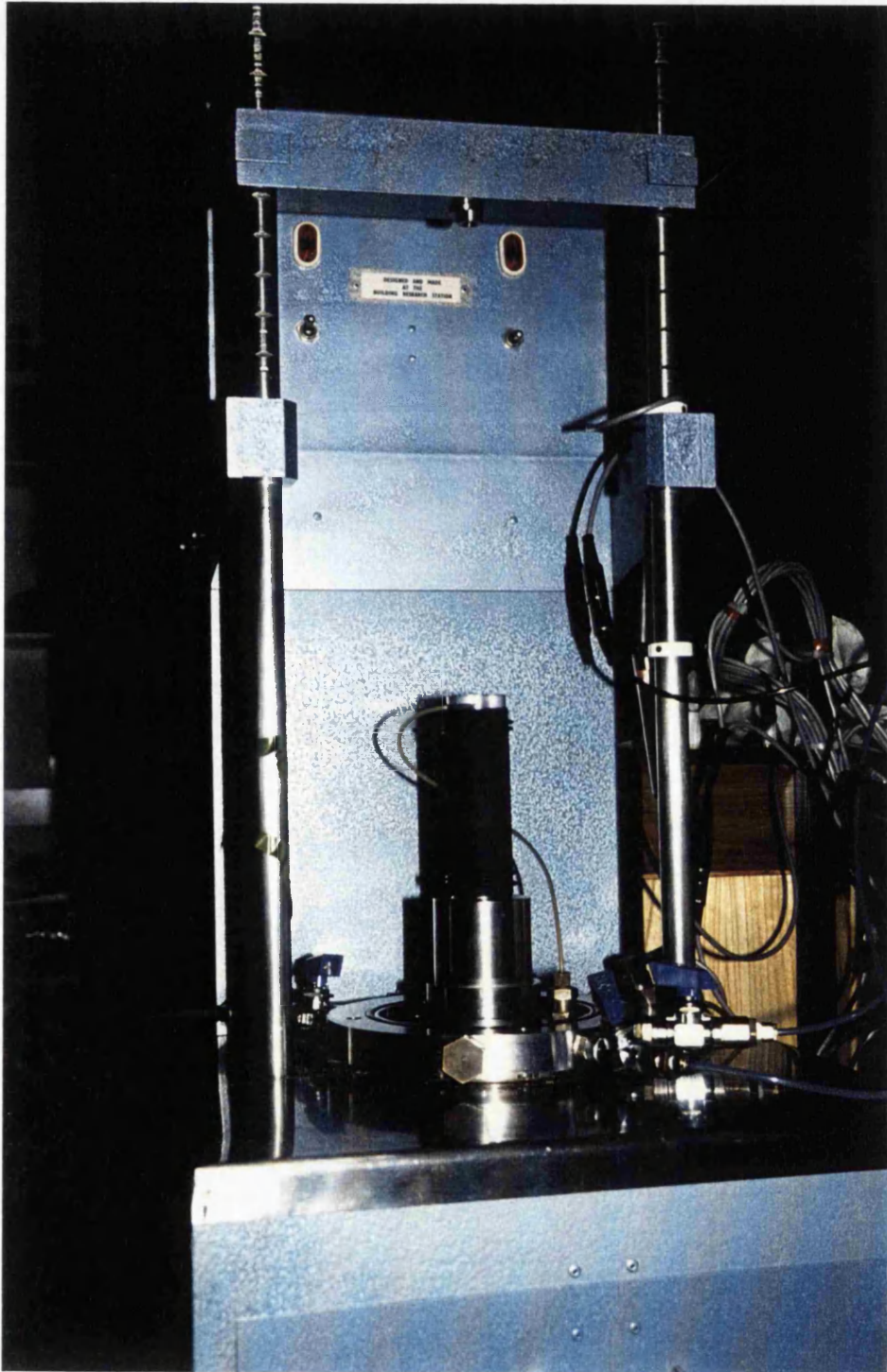


Plate 5.2.2 Experiment setting up

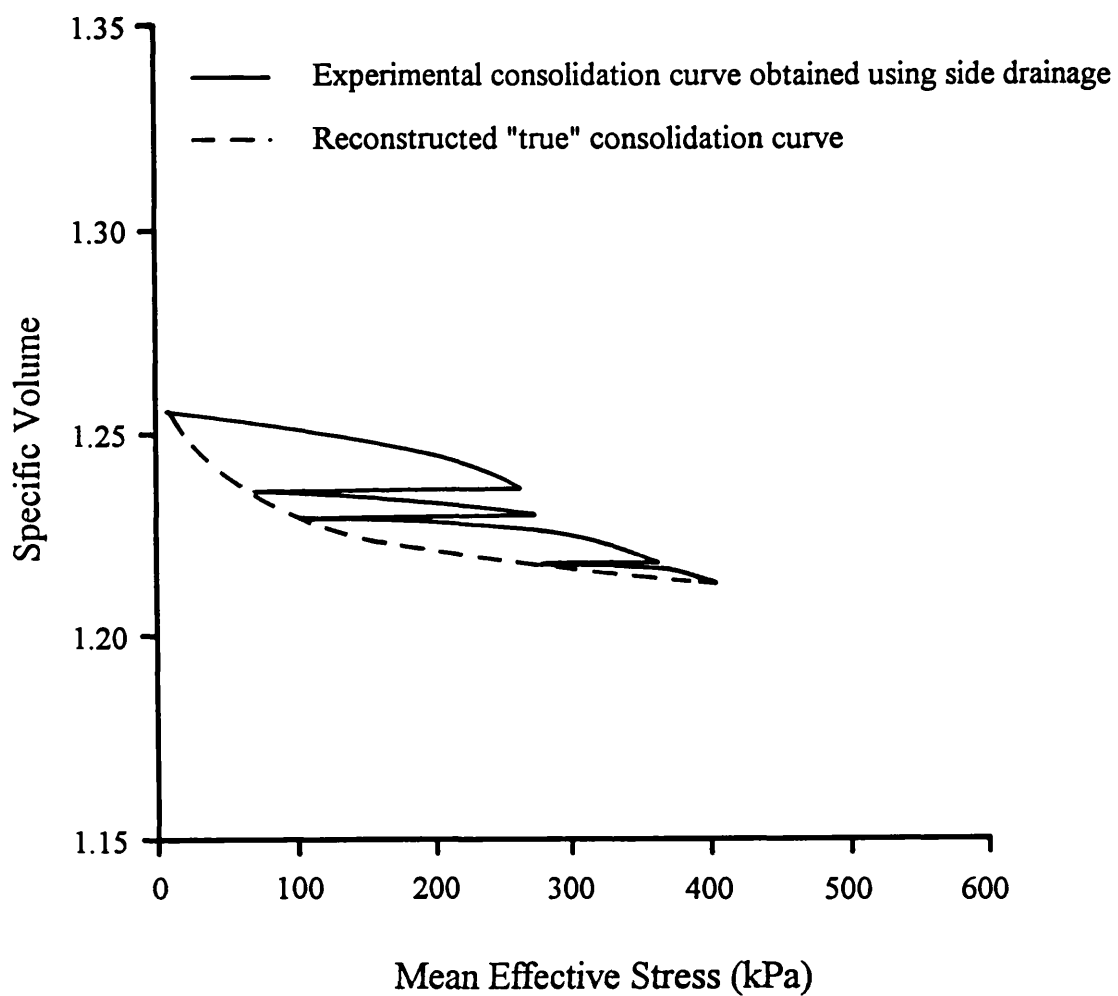


Figure 5.2.6 Typical consolidation curve for using side drainage and reconstructed consolidation path.

5.2.3 Test procedures

Each Isotropic Consolidation Undrained Triaxial Deformation experiment consists of two parts. First, the specimens were saturated and subsequently consolidated under isotropic stress conditions to the desired effective consolidation pressures. They were then deformed axially to failure through axial loading under undrained conditions. In natural, undisturbed soil samples the degree of saturation depends on the field conditions such as the depth from which the sample was collected with respect to the ground water table, capillary saturation, time since the last significant precipitation event, and evaporation. Saturation in the laboratory was therefore necessary to make the test conditions between different samples as similar as possible.

Soils are generally a multiphase system consisting of a mineral phase (the mineral skeleton) and a fluid phase (the pore fluid) which consists of air and/or water (Figure 5.2.7) (Lambe & Whitman, 1979). The nature of the fluid phase will influence the characteristics of the mineral surfaces and affect the process of force transmission at particle contacts. As a consequence, it may be expected that an increment of stress applied to a soil mass would be carried in part by the mineral skeleton as an effective stress, and in part by the pore fluid as a pore fluid pressure (Terzaghi & Peck, 1967; also see Appendix I). In a fully water-saturated soil the compressibility of the soil skeleton is substantially greater than that of the pore fluid at the prevailing stress states (Atkinson & Bransby, 1978). Thus, essentially all of a stress increment applied to a fully saturated soil is carried by the pore fluid during undrained isotropic compression (Skempton, 1954; Bishop, 1976; Lambe & Whitman, 1979). Since both soil grains and the pore water are effectively incompressible, the volume of a fully saturated sample can only change in response to deformation if pore water is displaced from the pore space. Under such conditions pore fluid pressure is reduced and the effective stress increases. The variation of soil volume with time following application of a load will therefore be governed by complex interactions between the total stress, pore fluid pressure, permeability and compressibility. This time-dependent process of volume change as pore water being expelled out from the pores is known as consolidation (Lambe & Whitman, 1979) and is responsible for the increase in effective stress.

For the Barbados samples isotropic consolidation was undertaken by increasing the confining fluid pressure incrementally until the desired pressure was achieved (BS 1377, 1990). Conversely, in all of the tests on the Taiwan samples, cell pressure was not increased incrementally but applied directly at the desired magnitude for consolidation. The change in procedure was due to the low permeability of the Taiwan material. When

a sample is isotropically compressed under undrained conditions the applied stress increment will be taken by the pore fluid and will generate a pore fluid pressure (under fully saturated condition, this is equivalent in magnitude to the increase in the total confining stress). Subsequently, when one end of the sample is opened to the volume gauge a head difference will be established across the sample and flow will be initiated. If the sample has a very low permeability equilibration of pore fluid pressures takes an extremely long time and can result in an asymmetric distribution of compressional strain in the sample. This can be partly overcome using a larger stress interval.

During consolidation, without using side drainage, only one end of the specimen was open to the volume gauge which permitted pore fluid to drain to a constant back pressure in the volume gauge. The pore fluid pressure at the undrained end of the sample was monitored and taken as the true pore fluid pressure within the specimen. The back pressure served to maintain the pore water saturation in the sample by keeping trace amounts of air in solution. The test results are unaffected by the magnitude of the back pressure, because these are dependent solely on the prevailing state of effective stress (Atkinson & Bransby 1978).

During the consolidation process the effective stress gradually increased as pore water was expelled from the specimen, causing a reduction in pore fluid pressure. At the end of consolidation, when the undrained pore fluid pressure was equalised with the applied back pressure, the drainage line was closed and the sample was deformed axially at a constant rate of displacement while the confining fluid pressure was held constant. It was noted in Addis & Jones (1989) that in testing porous sedimentary rock samples the axial displacement rate within a certain range ($4 \times 10^{-4} \text{ m min.}^{-1}$ to $10^{-3} \text{ m min.}^{-1}$) does not have a noticeable effect on the material behaviour for this type of deformation. However, for naturally structured materials with low permeability such as those studied here, the displacement rate has to be slow enough to maintain the pore fluid pressures at both ends in an equilibrium state. If the displacement rate is too fast, this will lead to a non-uniform pore fluid pressure distribution across the sample and thus non-uniform effective stress states, causing inaccurate results. An axial displacement rate of $5 \times 10^{-5} \text{ m min.}^{-1}$ was used for Barbados tests and a rate of $2 \times 10^{-5} \text{ m min.}^{-1}$ for Taiwan experiments.

For all the experiments reported here during undrained triaxial deformation the deviatoric stress increased until the sample failed⁶. The behaviour of natural soils, however, rarely follows the ideal behaviour predicted by published models such as Cam Clay or the

⁶Failure was deemed to have occurred which the sample continued to shorten at constant axial stress and pore pressure.

critical state. Because of this, the tests were each taken to as large an axial strain as possible.

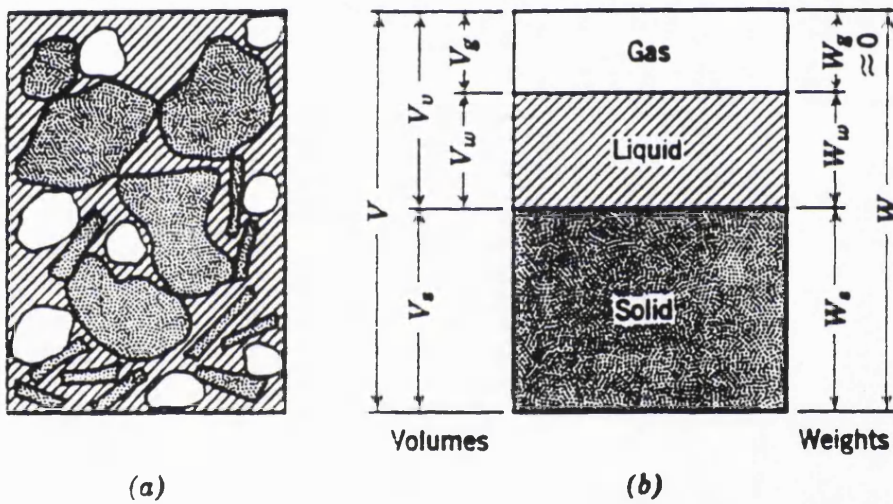


Figure 5.2.7 Relationships among soil phase: (a) element of natural soil; (b) element separated into phases.

5.3 Reference state concept

In recent years, it has become the practice to refer the behaviour of undisturbed samples to a reference state, which is generally the same material in a remoulded condition. The reference state is the state in which the sediment does not have any intergranular bonding, intergranular cement or sedimentary fabric. The mechanical behaviour of the material in this state is then used as a reference to facilitate comparison of behaviour exhibited in the natural state.

The significance of the reference state is understandable. However, there is an increasing awareness that the mechanical behaviour of sedimentary rock and soil materials is dominantly controlled by existing structures and diagenetic fabrics within the materials (e.g. Barden, 1972a, 1972b; Vaughan, 1985; Vaughan *et al.*, 1988; Burland, 1990; Aversa *et al.*, 1993; Petley *et al.*, 1993, Rampello & Silvestri, 1993). It has also been found that fine-grained soils in general appear to have a very similar micro-structure at their remoulded state (Pandian *et al.*, 1993b). Since a material at its remoulded state (reference state) does not possess any intergranular bonding, intergranular cement or sedimentary fabric, which primarily determine the mechanical behaviour of the material, the behavioural pattern at this state will therefore be completely different from that at an undisturbed condition. From this point of view, the usefulness of the reference state seems to be limited.

Although the use of the reference state appears to be limited in cases like the present study, a comparison has been made of the behaviour of the undisturbed and remoulded materials. One of the Barbados experiments was conducted on material recovered from a mud flow, which, although, not artificially remoulded in the laboratory, was believed to have been reworked in its natural environment. The natural moisture content was higher than its liquid limit (i.e. the material was in a liquid state while extracted). The triaxial compression test result for this mud flow material is presented at the end of the Barbados result section, 5.4.1.4.

5.4 Experimental results

5.4.1 Joe's River Formation, Barbados

Ten Isotropic Consolidation Undrained Triaxial Compression experiments were performed on the Joe's River Formation scaly clay. Three on the least weathered, three on the most weathered and four on the partially weathered samples. The effective

consolidation pressures used in each group of experiments were 100 kPa, 200 kPa and 400 kPa, with an additional 50 kPa effective consolidation pressure experiment conducted on one of the partially weathered samples. By repeating the tests under similar conditions on samples with various degrees of weathering, the change in the deformation characteristics can be detected. The experiments are described separately below. The initial dimensions and the porosity data of the Barbados specimens are summarised in Table 5.4.1:

Table 5.4.1 Initial dimensions and porosities of the Barbados specimens

Exp. names	Initial length (mm)	Initial diameter (mm)	Initial porosity (%)
BDL-100	76.66	38.27	31.21
BDL-200	76.32	38.95	32.81
BDL-400	76.34	38.66	32.92
BDP-50	76.32	37.91	36.99
BDP-100	77.16	38.31	38.04
BDP-200	72.72	38.09	36.46
BDP-400	77.72	37.03	37.17
BDM-100	73.72	38.39	42.72
BDM-200	75.32	38.33	41.64
BDM-400	75.04	38.47	42.23
BDR-100	72.58	38.29	55.76

5.4.1.1 Least weathered sample experiments

Three specimens taken from the least weathered horizon were isotropically consolidated to different effective confining pressures (100 kPa, 200 kPa and 400 kPa) and subsequently deformed axially under undrained conditions to shear failure using a displacement rate of 5×10^{-5} m min.⁻¹. The consolidation behaviour is presented in Figures 5.4.1 to 5.4.6, among which Figures 5.4.1, 5.4.3 & 5.4.5 are specific volume against mean effective stress in linear scale and Figures 5.4.2, 5.4.4 & 5.4.6 specific volume against mean effective stress in logarithmic scale. It is seen that the volume strain during isotropic consolidation is limited as the consolidation paths exhibit very low angles. The two lower effective stress experiments have volume strains at the end of consolidation less than 2%, and that of the 400 kPa experiment increases to 7%.

The results of the undrained triaxial deformation phase of these experiments are presented in Figures 5.4.7 to 5.4.10 including the stress-strain curves, stress paths, horizontal-vertical stress relationships and pore fluid pressure development during

undrained loading. None of the three experiments exhibited clear peak and residual strengths (Figure 5.4.7), although in experiment BDL-400 the strength (deviatoric stress) stayed at about 440 kPa for a considerable interval of axial strain (from 5% to 9%) and then the deviatoric stress started to gently increase.

The experiment BDL-200 was terminated at an axial strain of about 7%. This was because the specimen developed a shear failure plane at an early stage so that as axial strain continued to accumulate during the latter stage of the experiment there was a possibility that the membrane might be punctured by the displaced material. The early termination meant that the final shear stress (deviatoric stress) of BDL-200 sample was less than that of BDL-100 sample. The early failure plane development of the BDL-200 sample can also be observed in the stress-strain plot in which the BDL-200 exhibited ductile behaviour earlier than the other two tests at an axial strain of about 1% (Figure 5.4.7).

An abrupt change in direction of the stress path is seen in the experiment BDL-400 (Figure 5.4.8) where the rate of increase of the deviatoric stress was suddenly reduced whilst the mean effective stress was continuously increasing. This is a consequence of a sudden reduction in the pore fluid pressure which caused the deviatoric stress to remain constant (Figures 5.4.7 & 5.4.10) and the mean effective stress to increase giving the abrupt change in the stress path.

The horizontal-vertical stress relationships (Figure 5.4.9) show that the effective horizontal stress continually decreases due to the development of pore fluid pressure until the samples reach the state when deformation becomes localised through the formation of a shear failure plane. After this the horizontal effective stress increases again. The phenomenon can be demonstrated more clearly in Figure 5.4.11 which is Figure 5.4.7 superimposed on to Figure 5.4.10. The form of the stress/axial strain curves and pore fluid pressure/axial strain curves indicates that the samples behaved in a ductile manner when pore fluid pressure maxima developed.

Table 5.4.2 Summary of the deviatoric stress, mean effective stress and pore fluid pressure states at the beginning of dilation and end of the BDL experiments.

Exp. names	p'_i (kPa)	q_d (kPa)	p'_d (kPa)	q_t (kPa)	p'_t (kPa)	u_d (kPa)	u_t (kPa)	Back pressure
BDL-100	100	140	110	310	190	90	65	50
BDL-200	200	180	180	260	220	125	115	50
BDL-400	400	420	410	460	480	180	125	50

where p'_i is the starting mean effective stress (consolidation pressure)

q_d is the deviatoric stress while sample started to dilate

p'_d is the mean effective stress while sample started to dilate

q_t is the deviatoric stress while test was terminated

p'_t is the mean effective stress while test was terminated

u_d is the pore fluid pressure while sample started to dilate

u_t is the pore fluid pressure while test was terminated

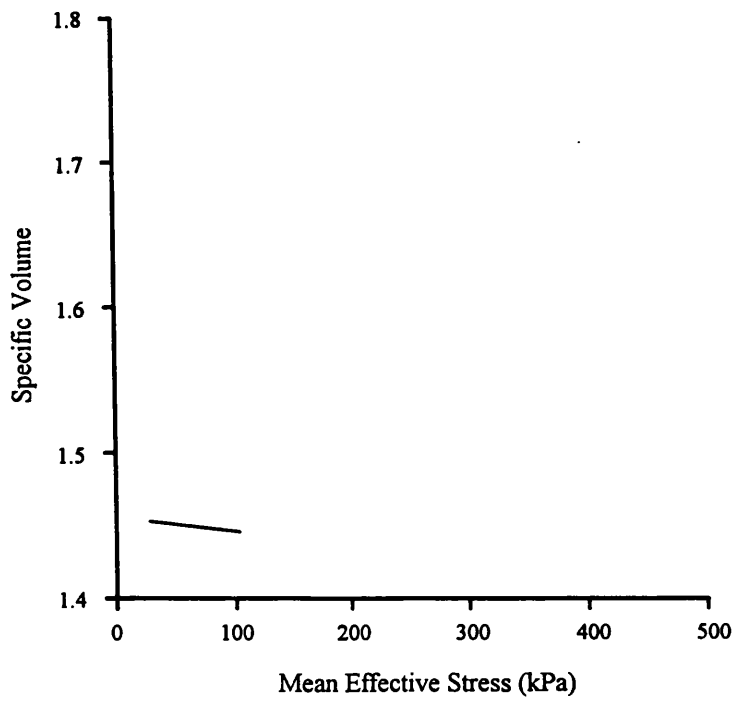


Figure 5.4.1 Consolidation path of experiment BDL-100 (in linear scale)

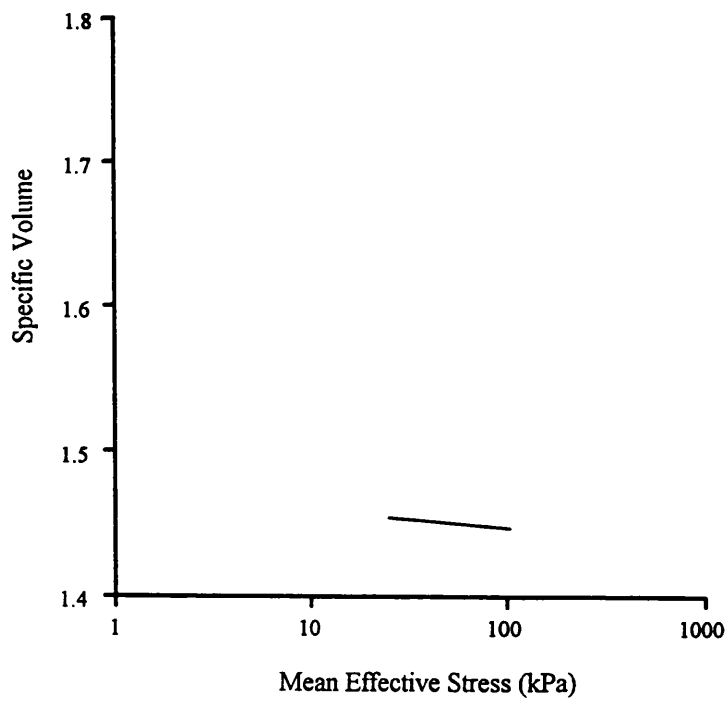


Figure 5.4.2 Consolidation path of experiment BDL-100 (in logarithmic scale)

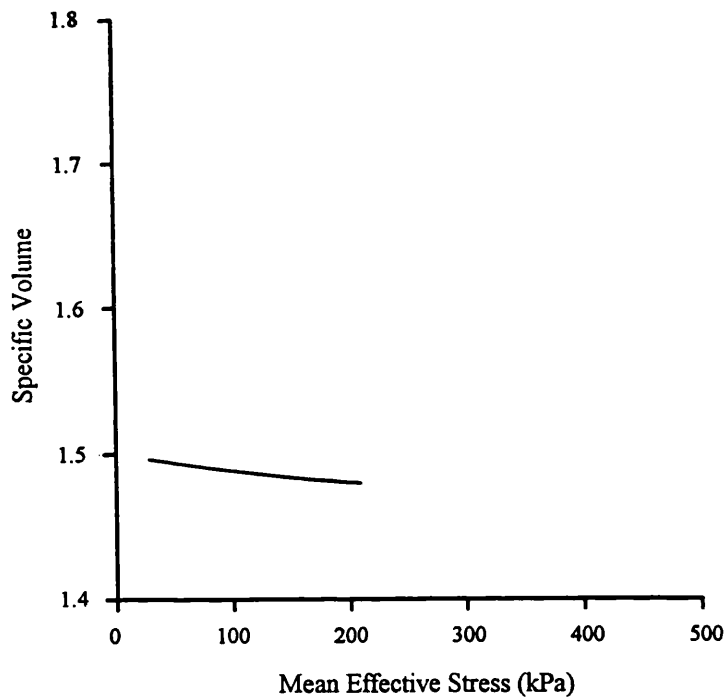


Figure 5.4.3 Consolidation path of experiment BDL-200 (in linear scale)

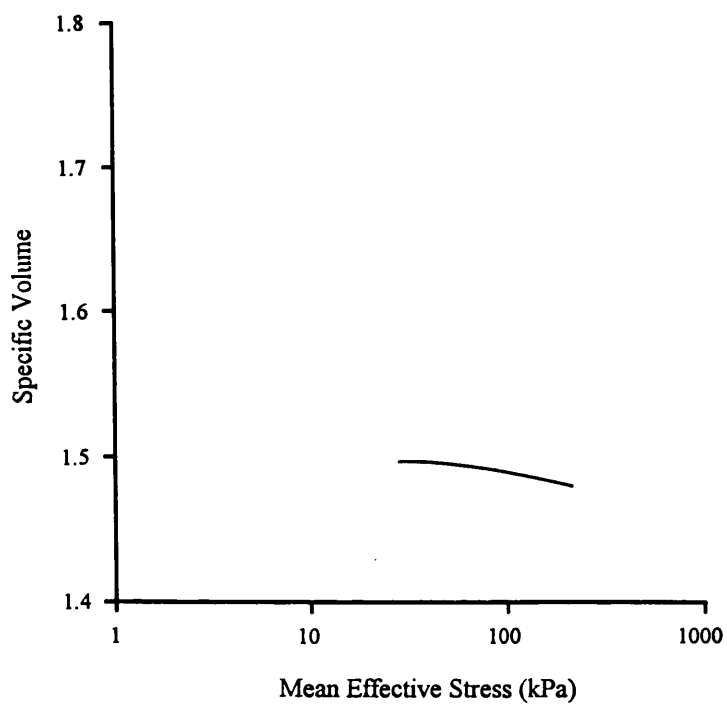


Figure 5.4.4 Consolidation path of experiment BDL-200 (in logarithmic scale)

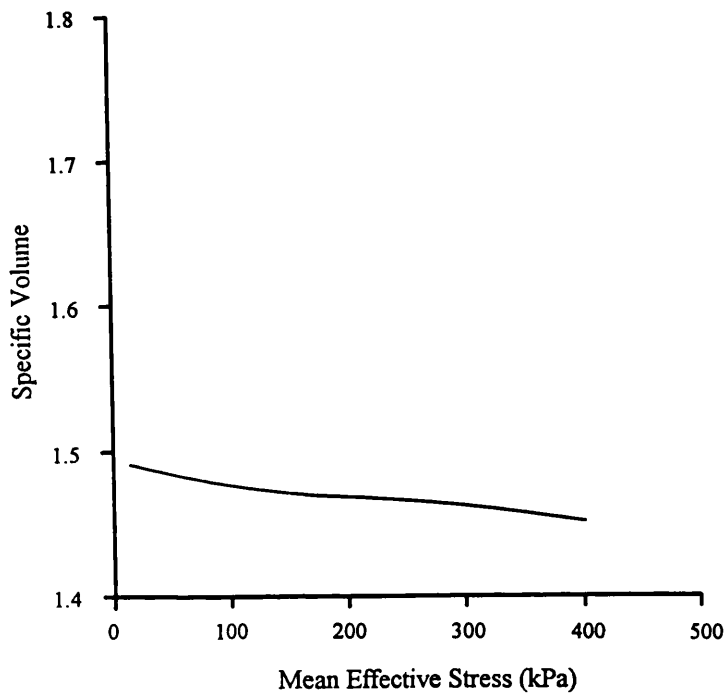


Figure 5.4.5 Consolidation path of experiment BDL-400 (in linear scale)

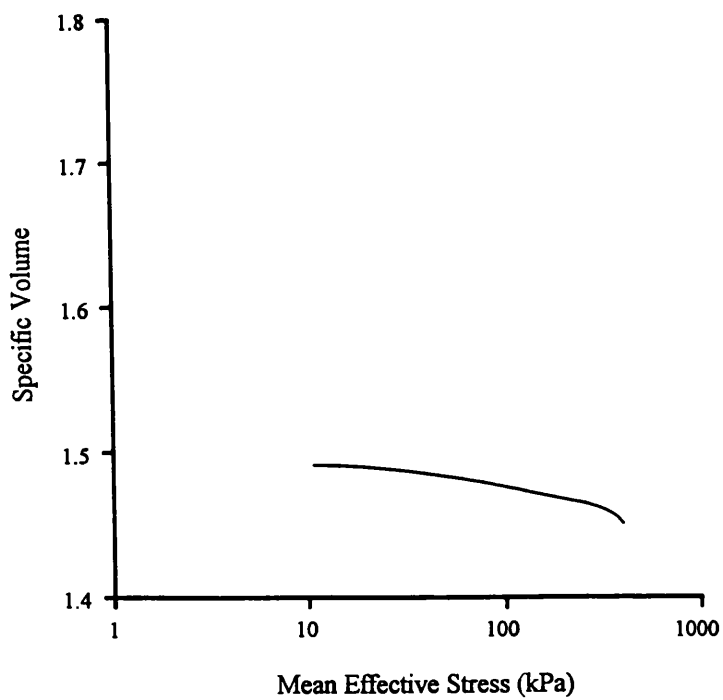


Figure 5.4.6 Consolidation path of experiment BDL-400 (in logarithmic scale)

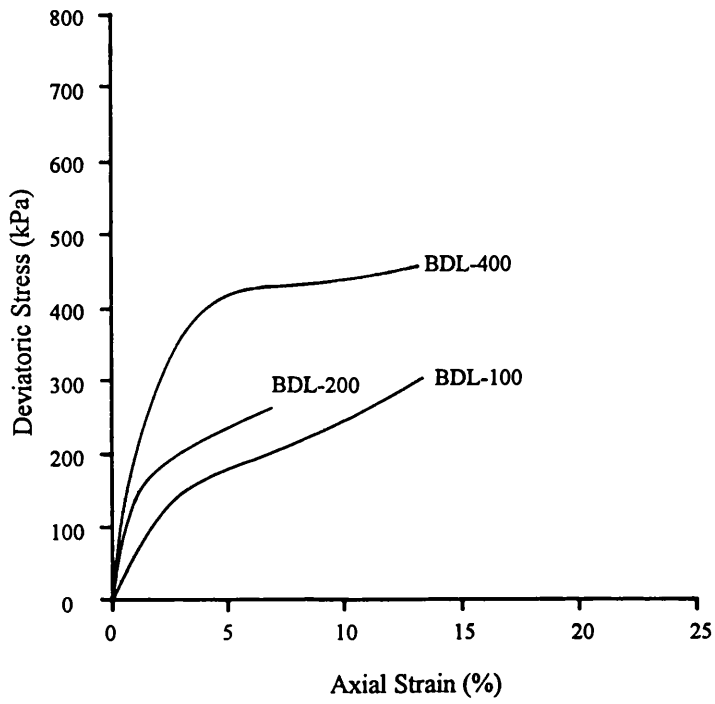


Figure 5.4.7 Stress-strain curves for BDL experiments

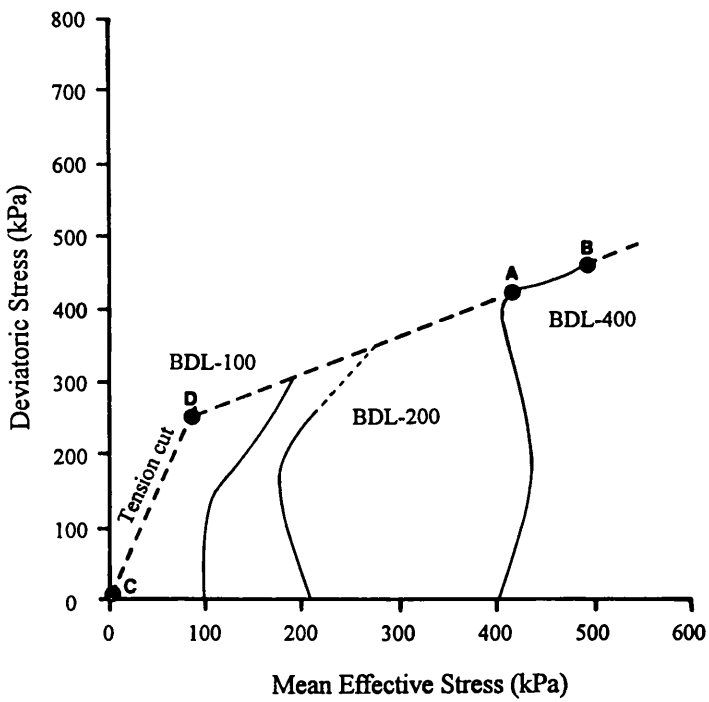


Figure 5.4.8 Stress paths for BDL experiments

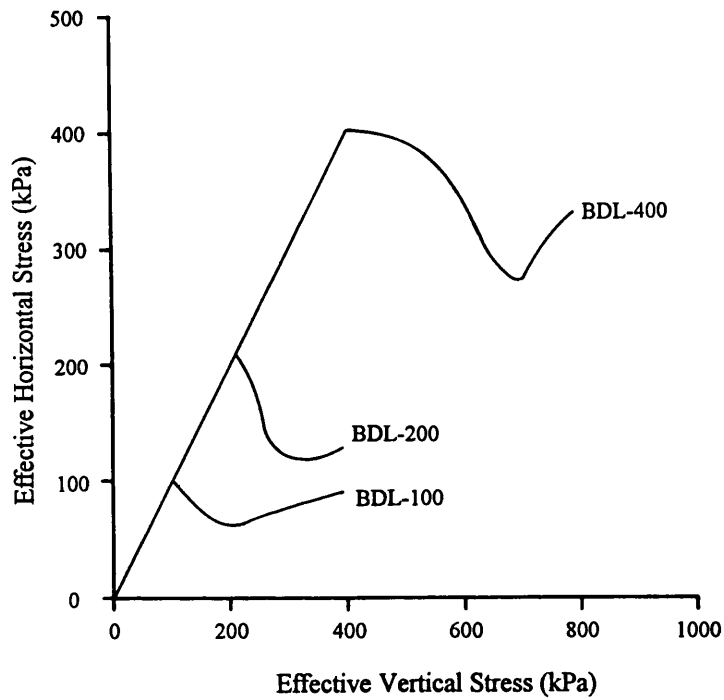


Figure 5.4.9 Effective horizontal-vertical stress relationships for BDL experiments

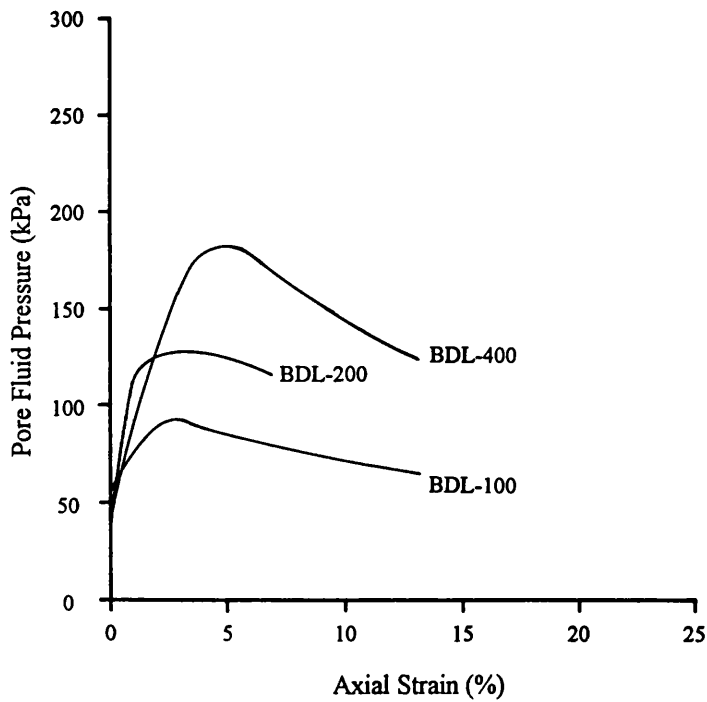


Figure 5.4.10 Pore fluid pressure development during undrained compression for BDL experiments

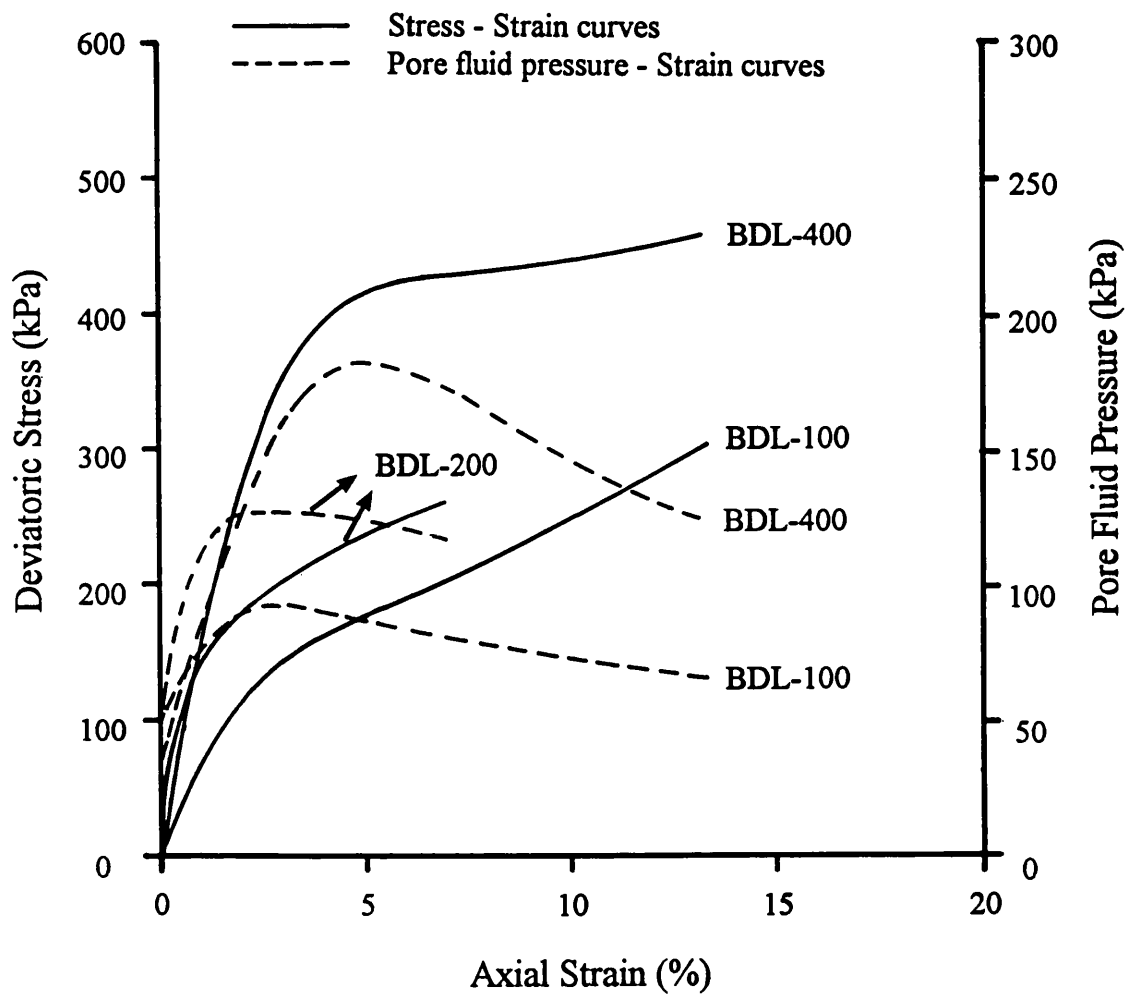


Figure 5.4.11 Diagram showing relationship between deviatoric stress and pore fluid pressure during undrained compression for BDL experiments

5.4.1.2 Partially weathered sample experiments

Four experiments were completed on the partially weathered clay at effective confining pressures of 50 kPa, 100 kPa, 200 kPa and 400 kPa respectively. There were failures of the back pressure system in experiment BDP-50 and of the drainage system in experiment BDP-200 which caused a deflection in the consolidation path and missing data respectively (Figures 5.4.12 to 5.4.17). Somewhat larger volumetric changes were recorded in the experiments on partially weathered materials, compared with those for the least weathered clay. For example, BDP-400 achieves a volumetric strain of about 8.5% during consolidation. The consolidation paths of the experiments were, however, still relatively flat.

During undrained deformation and shear failure, all four experiments were taken to axial strains exceeding 15%. The samples in this group of experiments appeared to have reached an ultimate state at which the shear strength stayed more or less constant except experiment BDP-400, which exhibited strain hardening before the experiment was terminated (Figure 5.4.18). The experimental data indicates a slight increase in strength during the last part of loading but this is attributed to the increase in cross-sectional area of the specimens whilst they were shortening. Figure 5.4.19 shows the stress paths of the four experiments among which the three conducted at lower confining stresses have very similarly shaped paths. Pore fluid pressure development is highly restricted and the stress paths swing to the right as the axial stress is increased. This indicates that dilation started at the beginning of undrained deformation. Experiment BDP-400 started similarly, and the stress path swung to the right. However, in this case dilation soon stopped and increased pore fluid pressure development caused the path to curve back to the left until it reached the point of maximum pore fluid pressure generation. After this the sample again began to dilate which continued until the experiment was terminated.

Figure 5.4.21 gives a better picture of pore fluid pressure development along the undrained deformation phase of the experiments. In experiment BDP-50, there was very little pore fluid pressure build up during the early stage of axial loading. Subsequently, a negative pore fluid pressure (pressure lower than the applied back pressure) was observed. In experiments BDP-100 and BDP-200, small positive pore fluid pressure responses were observed, although they were small when compared to the magnitude of the associated increase in deviatoric stress. Sample BDP-400 which ceased dilation gave a relatively large pore fluid pressure response.

The effective horizontal-vertical stress relationships of this group of experiments are illustrated in Figure 5.4.20 and show that the horizontal effective stresses in the three lower confining pressure experiments remained more or less constant whilst the samples were being deformed to shear failure. Conversely, in the high confining pressure experiment (BDP-400), the horizontal effective stress decreased prior to development of the shear failure plane and then increased. This is because the large confining pressure inhibited dilation resulting in pore fluid pressure development leading to a decrease in the effective confining pressure thereby facilitating the shear failure.

Table 5.4.3 Summary of the deviatoric stress, mean effective stress and pore fluid pressure at the beginning of dilation⁷ and the end of test for BDP experiments.

Exp. names	p'_i (kPa)	q_d (kPa)	p'_d (kPa)	q_t (kPa)	p'_t (kPa)	u_d (kPa)	u_t (kPa)	Back pressure
BDP-50	50	170	90	220	130	30	18	20
BDP-100	100	400	230	440	260	25	5	20
BDP-200	200	460	310	560	360	80	70	35
BDP-400	400	500	360	710	490	260	200	50

⁷All four BDP samples dilate from the beginning of the undrained loading. The beginning of dilation here means the places where the stress path starts to curve towards the right.

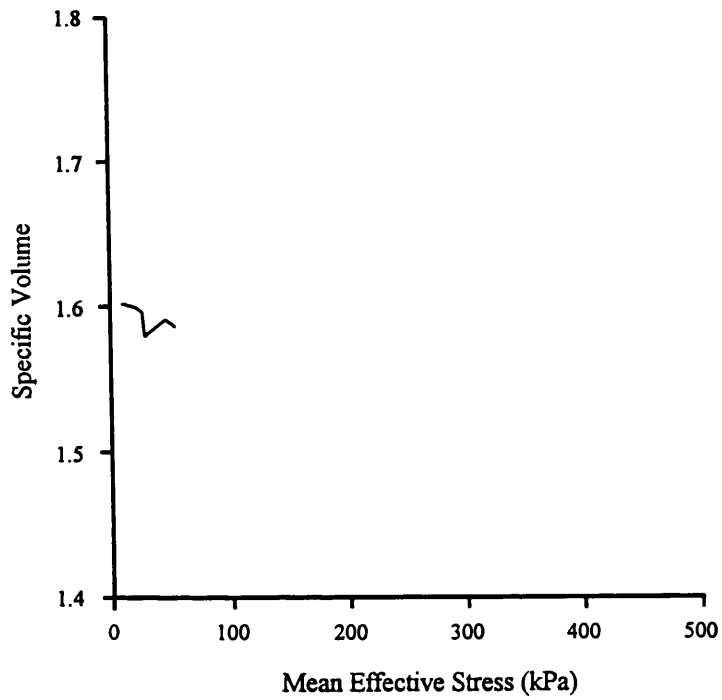


Figure 5.4.12 Consolidation path of experiment BDP-50 (in linear scale)

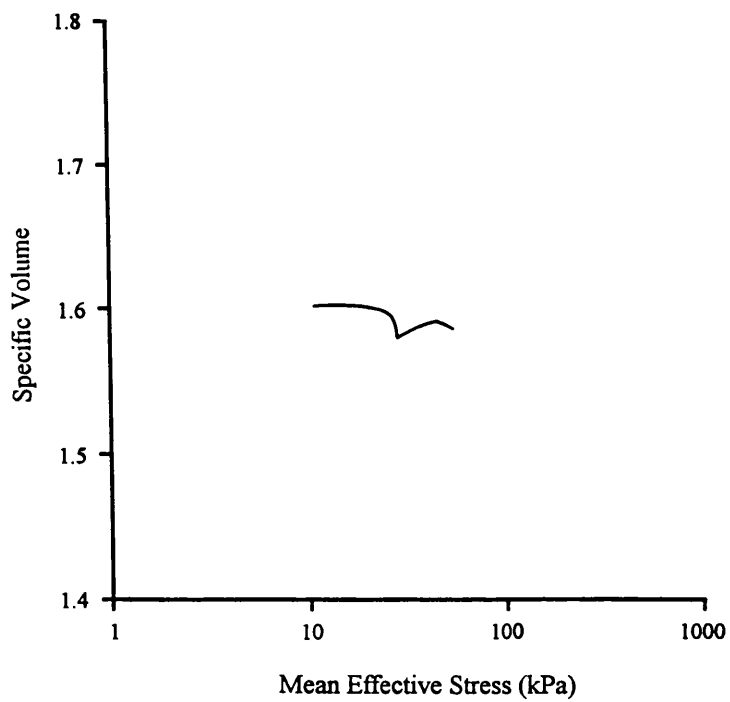


Figure 5.4.13 Consolidation path of experiment BDP-50 (in logarithmic scale)

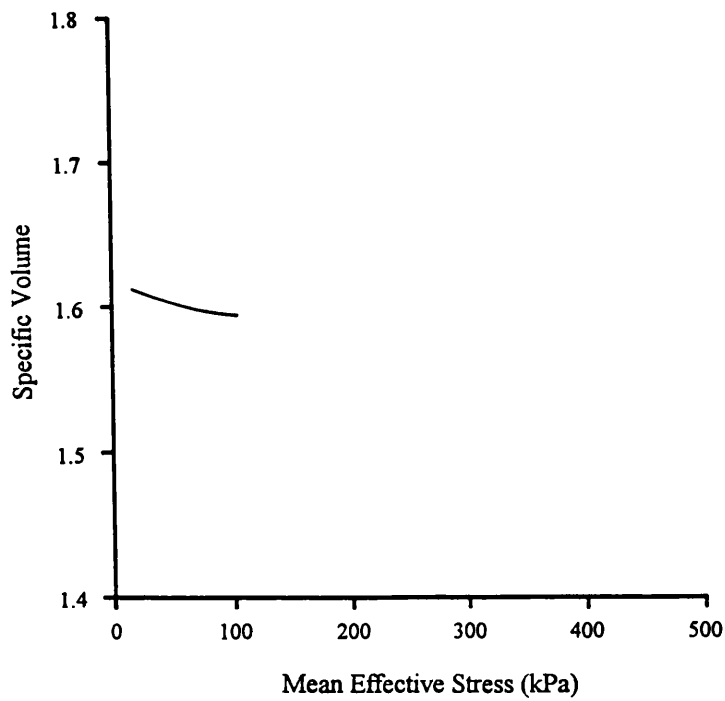


Figure 5.4.14 Consolidation path of experiment BDP-100 (in linear scale)

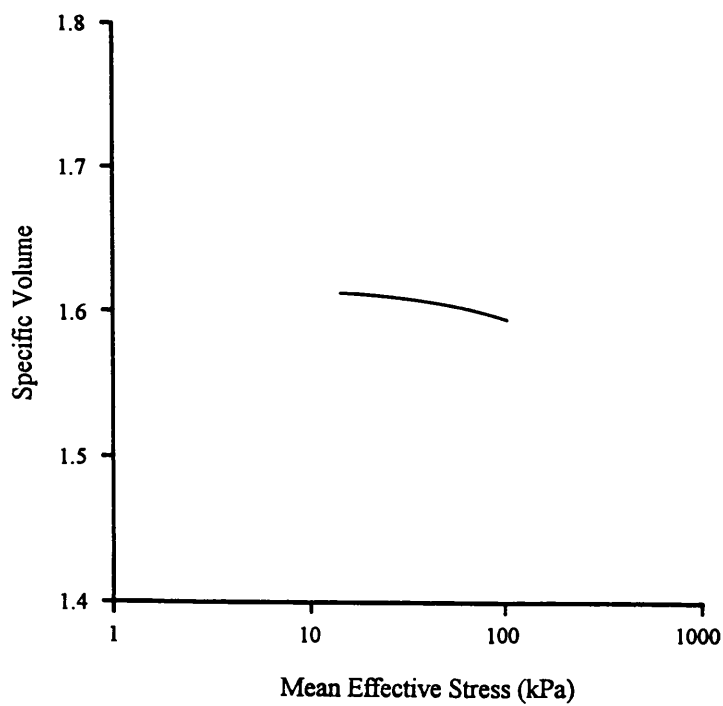


Figure 5.4.15 Consolidation path of experiment BDP-100 (in logarithmic scale)

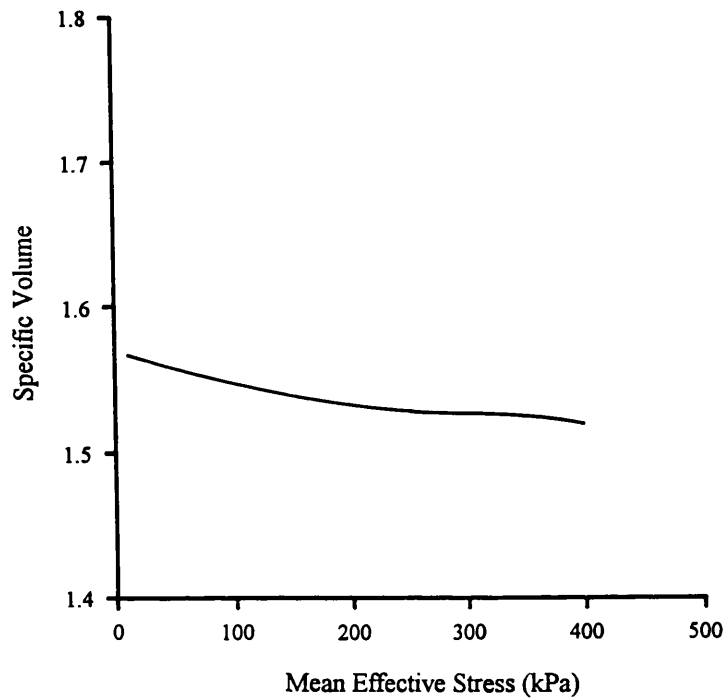


Figure 5.4.16 Consolidation path of experiment BDP-400 (in linear scale)

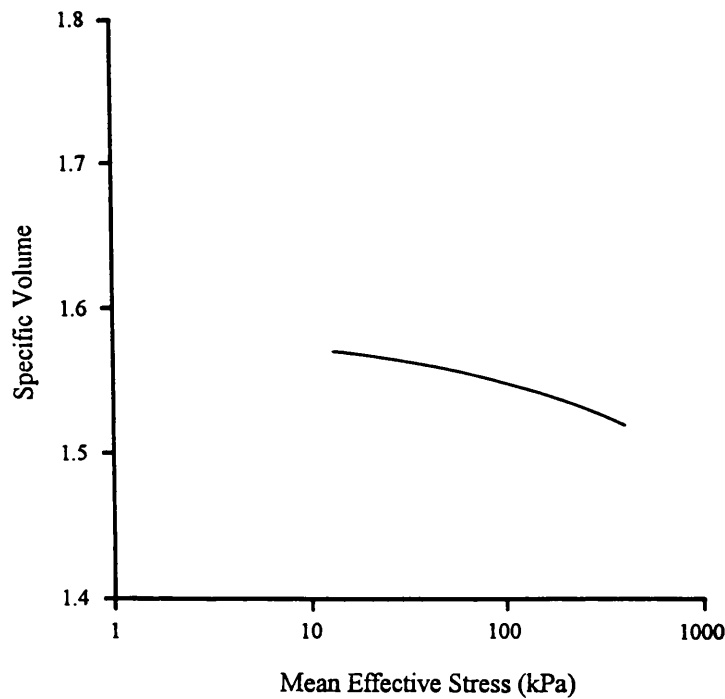


Figure 5.4.17 Consolidation path of experiment BDP-400 (in logarithmic scale)

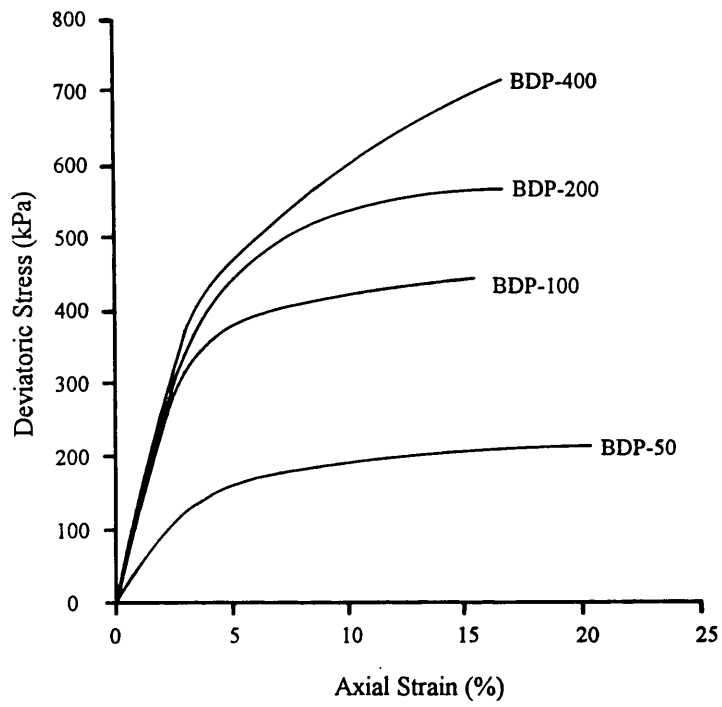


Figure 5.4.18 Stress-strain curves for BDP experiments

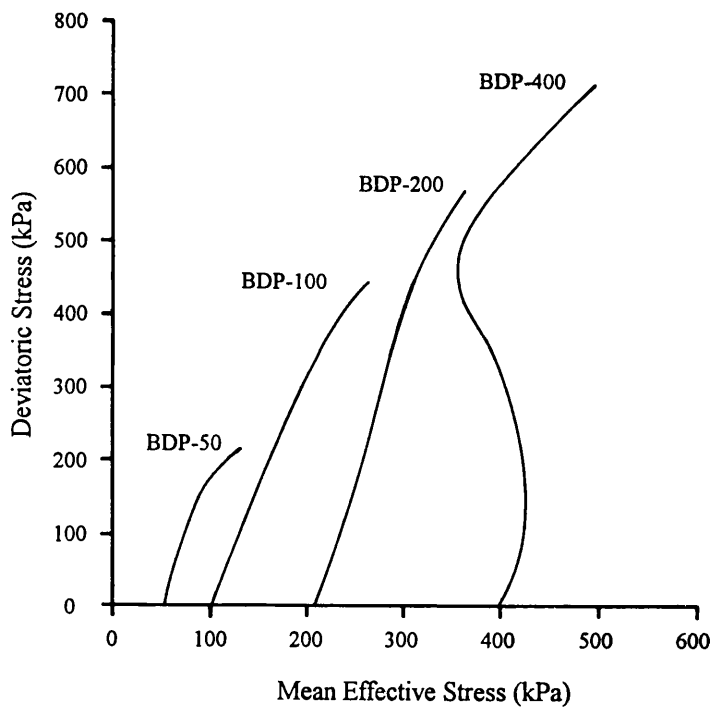


Figure 5.4.19 Stress paths for BDP experiments

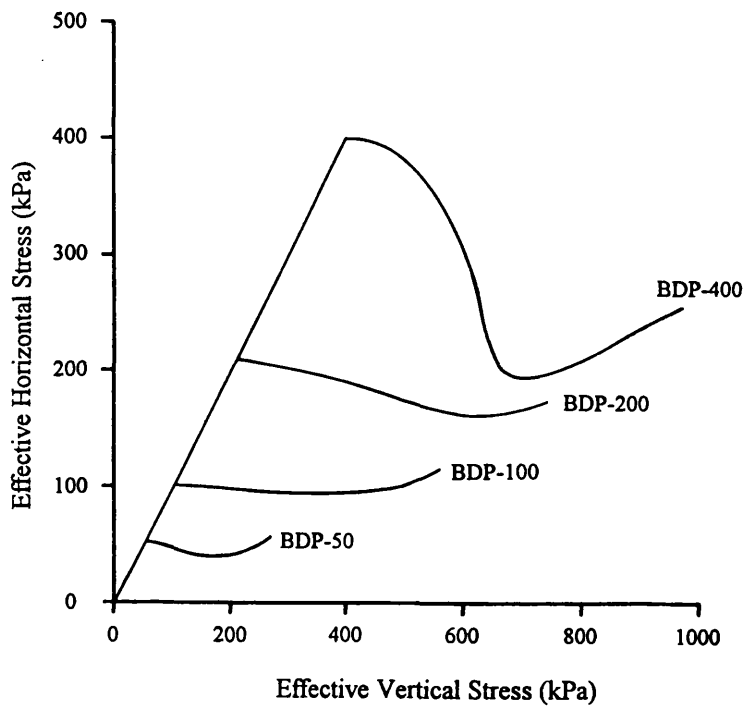


Figure 5.4.20 Effective horizontal-vertical stress relationships for BDP experiments

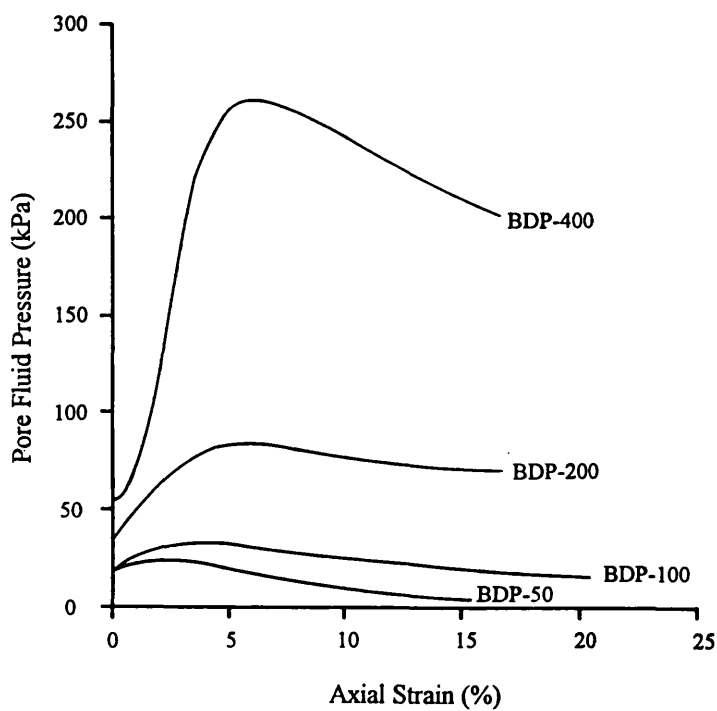


Figure 5.4.21 Pore fluid pressure development during undrained compression for BDP experiments

5.4.1.3 Most weathered sample experiments

The consolidation paths of the three experiments (Figures 5.4.22 to 5.4.27) are more distinctive than those from the other two groups of experiments. The volumetric strains for the three experiments are 6.6% for BDM-100, 5% for BDM-200 and 12% for BDM-400. A failure in the cell pressure supply system occurred while experiment BDM-200 was undergoing the last part of consolidation which caused an unloading and reloading effect seen in Figures 5.4.24 & 5.4.25. As a result of this system failure, the experiment demonstrated an excellent example of normal consolidation and over consolidation behaviour. The slope of the unloading/reloading path is much smaller than that of the original consolidation path.

The stress-strain curves of the three experiments recorded during undrained triaxial deformation (Figure 5.4.28) show that all three samples had reached the ultimate state at which the sample strained at constant deviatoric stress. The stress path and effective horizontal-vertical stress relationship plots (Figures 5.4.29 & 30) are, in each case, very similar. A large proportion of the applied deviatoric stress contributed to the development of the pore fluid pressure causing the horizontal effective stress to decline rapidly whilst the vertical effective stress remained almost constant until the samples started to dilate. This behaviour is completely different from that seen in the BDL and BDP experiments.

Table 5.4.4 Summary of the deviatoric stress, mean effective stress and pore fluid pressure at the beginning of dilation and the end of test for BDM experiments.

Exp. names	p'_i (kPa)	q_d (kPa)	p'_d (kPa)	q_t (kPa)	p'_t (kPa)	u_d (kPa)	u_t (kPa)	Back pressure
BDM-100	100	105	90	120	95	105	105	50
BDM-200	200	170	150	220	185	165	145	50
BDM-400	400	290	275	330	305	280	260	50

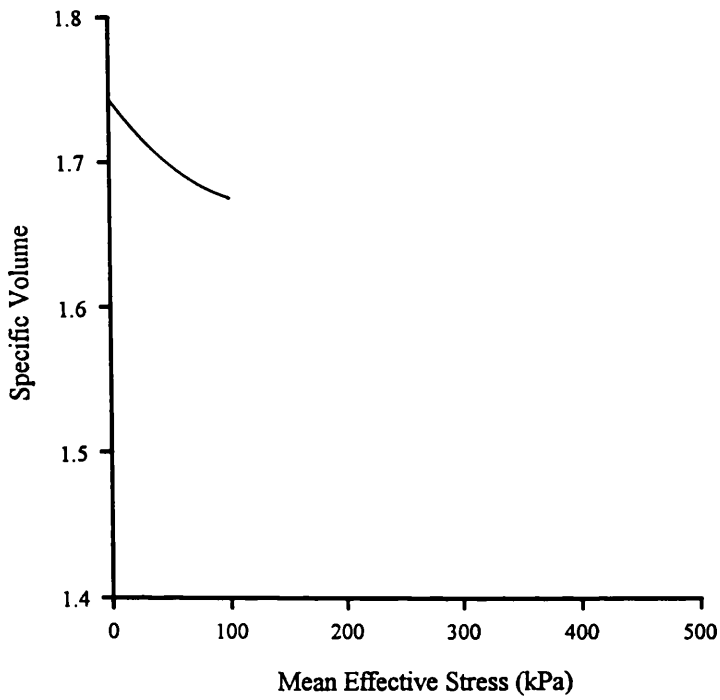


Figure 5.4.22 Consolidation path of experiment BDM-100 (in linear scale)

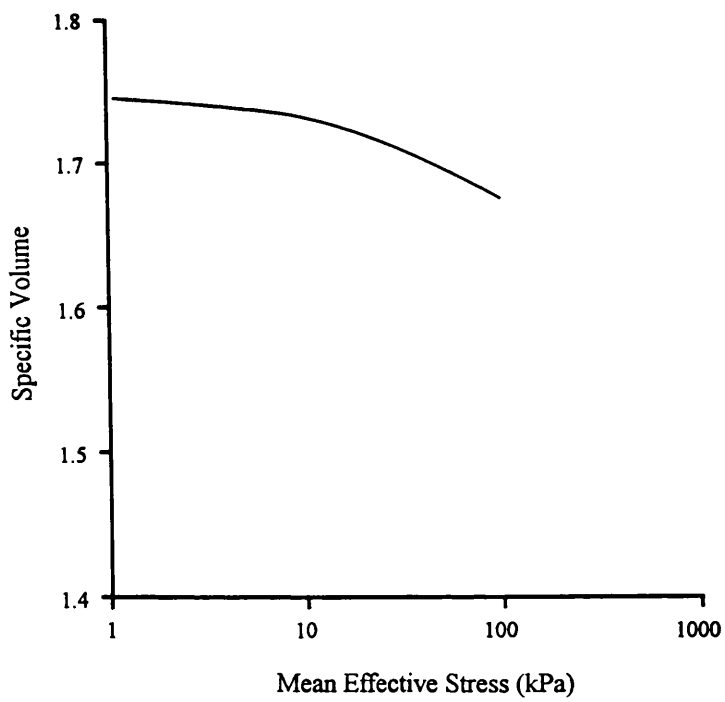


Figure 5.4.23 Consolidation path of experiment BDM-100 (in logarithmic scale)

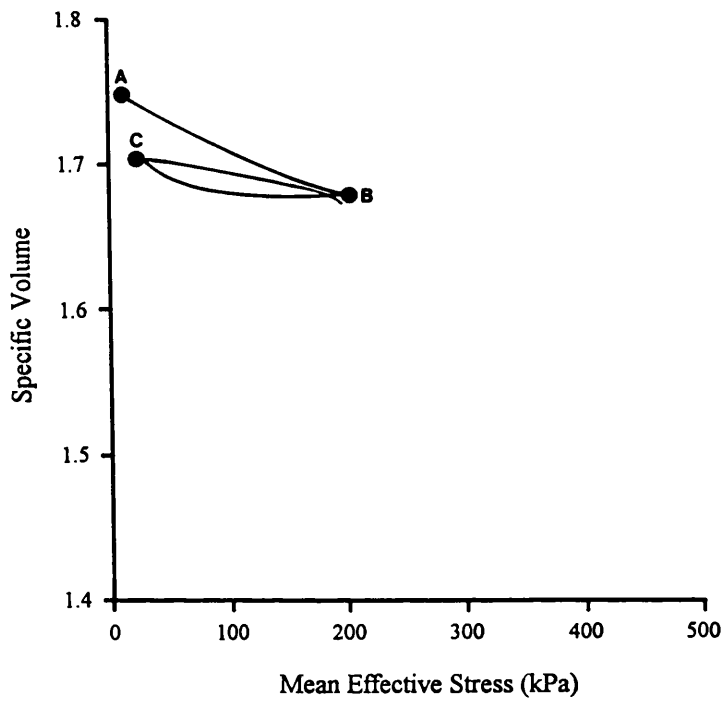


Figure 5.4.24 Consolidation path of experiment BDM-200 (in linear scale)

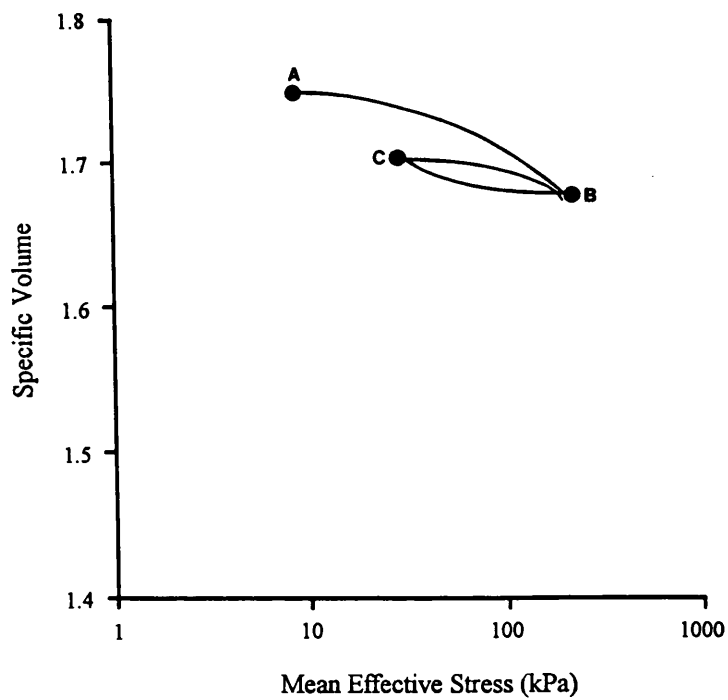


Figure 5.4.25 Consolidation path of experiment BDM-200 (in logarithmic scale)

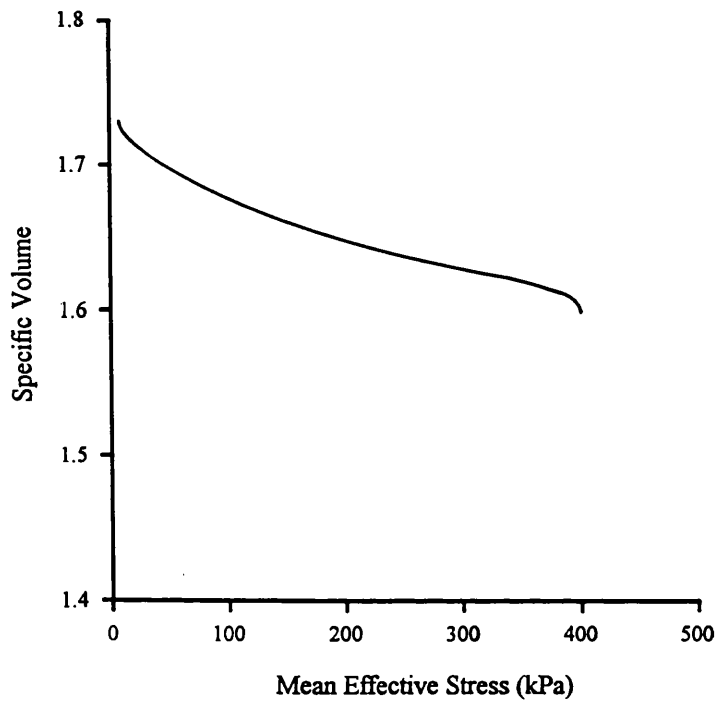


Figure 5.4.26 Consolidation path of experiment BDM-400 (in linear scale)

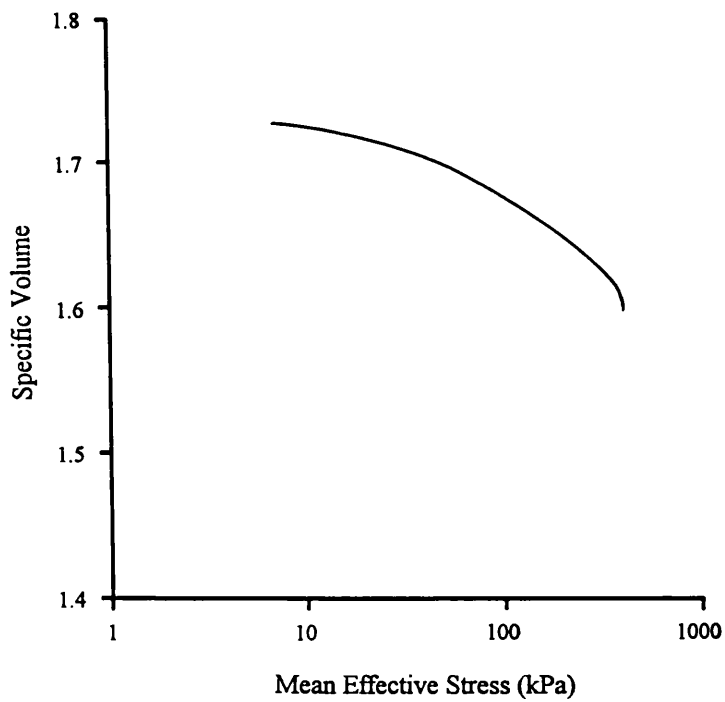


Figure 5.4.27 Consolidation path of experiment BDM-400 (in logarithmic scale)

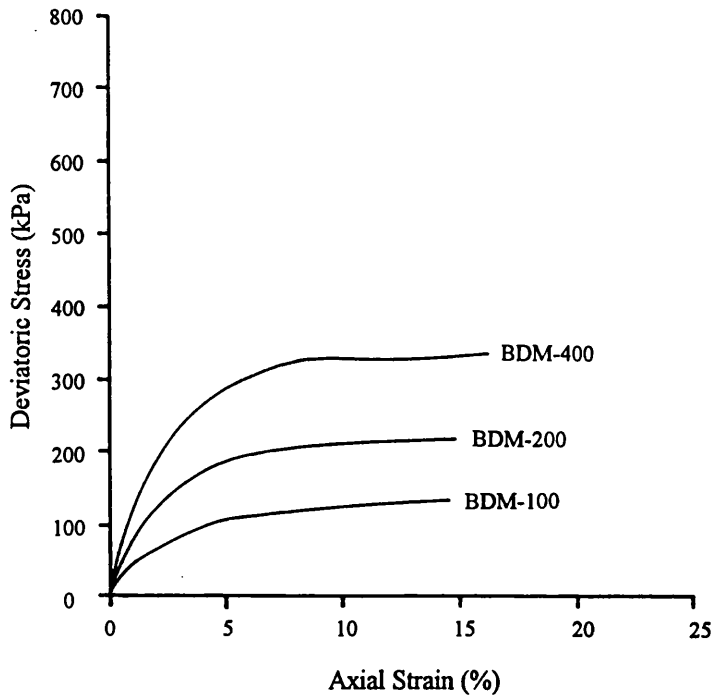


Figure 5.4.28 Stress-strain curves for BDM experiments

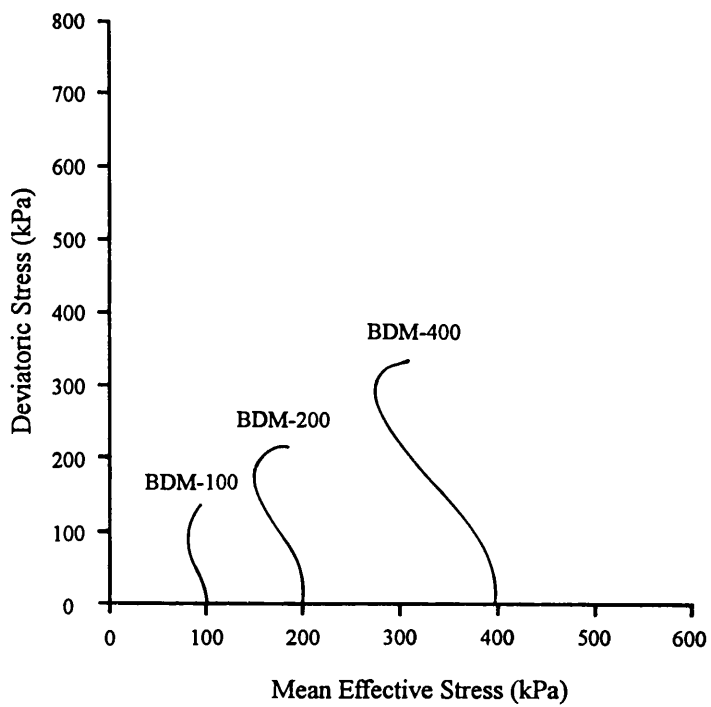


Figure 5.4.29 Stress paths for BDM experiments

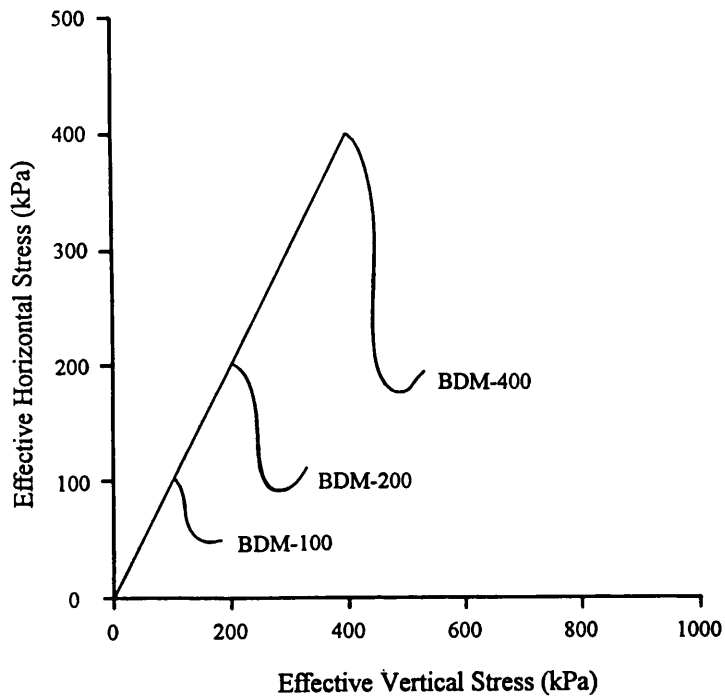


Figure 5.4.30 Effective horizontal-vertical stress relationships for BDM experiments

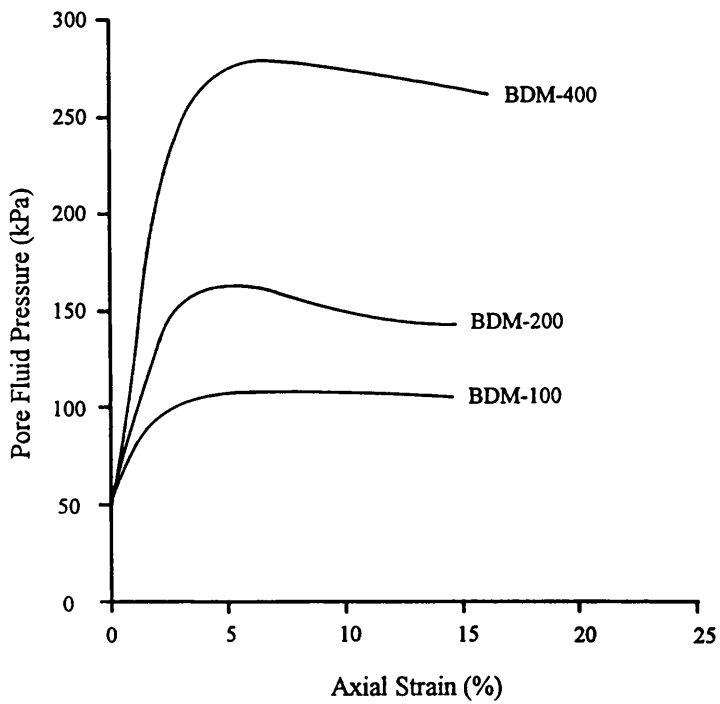


Figure 5.4.31 Pore fluid pressure development during undrained compression for BDM experiments

5.4.1.4 Mud flow material experiment

This experiment was conducted on the material which was thought to have been naturally remoulded. Table 5.4.5 describes some information of the experiment. The effective confining pressure was 100 kPa. The initial specific volume of the specimen was 2.27, much higher than any of the other samples (1.45-1.75) and the gradient of the consolidation path in the v - $\ln p'$ space (Figure 5.4.33) is very much larger than in any of the Barbados experiments. Nearly 11% of volumetric strain had accumulated by the end of the consolidation. When compared with other experiments conducted at the same confining pressure (2%, 3% and 6% volumetric strain), this figure is much larger, exceeding even the volume strains recorded for least and partially weathered materials after consolidation to 400 kPa.

Table 5.4.5 Testing condition of the naturally remoulded sample

Exp. name	Initial length	Initial diameter	Porosity	Remark
BDR-100	72.58 mm	38.28 mm	55.8%	Naturally remoulded

In the undrained loading phase of this experiment the ultimate state of constant deviatoric stress and pore fluid pressure was attained after axial strain reached 5% (Figures 5.4.34 & 5.4.37). Subsequently, deformation continued at constant mean effective stress (Figure 5.4.35) and no changes in stress state, nor sample volume were recorded indicating that the critical state had been achieved.

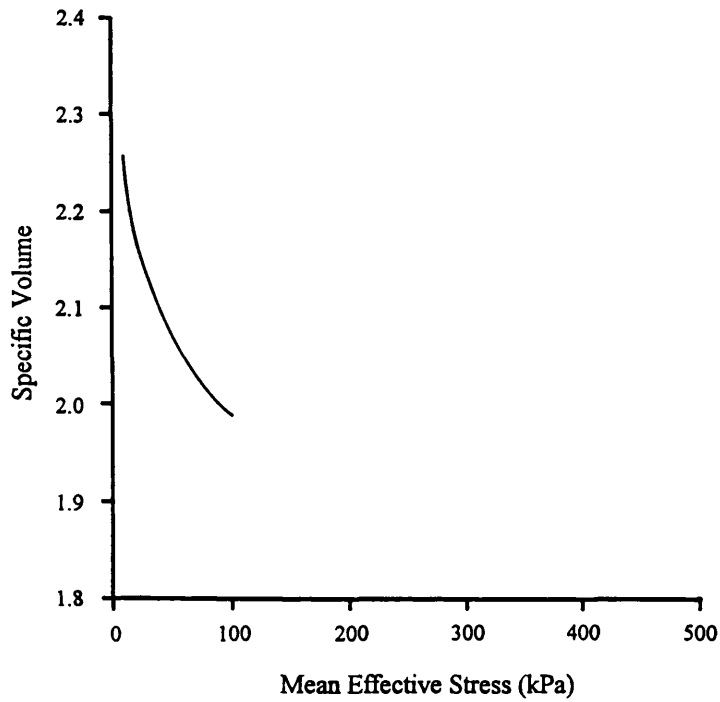


Figure 5.4.32 Consolidation path for experiment BDR-100 (in linear scale)

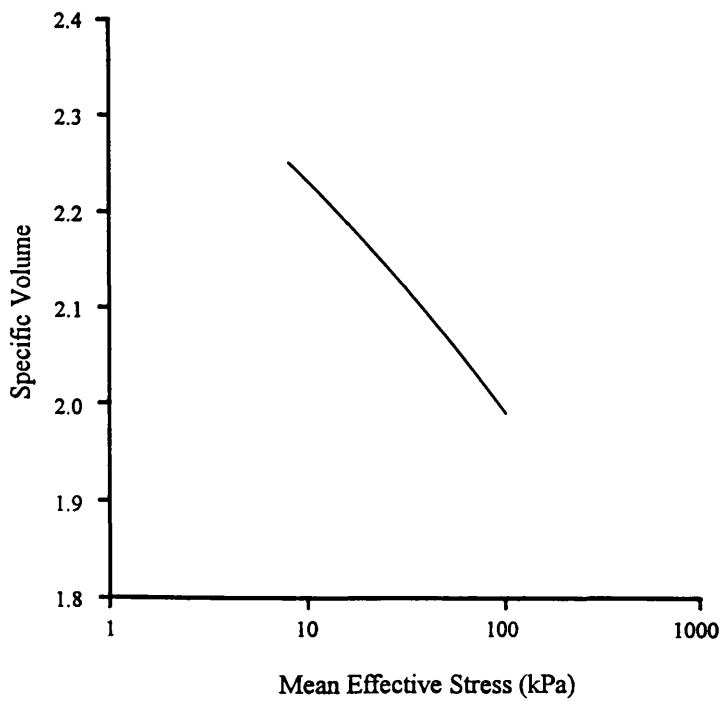


Figure 5.4.33 Consolidation path for experiment BDR-100 (in logarithmic scale)

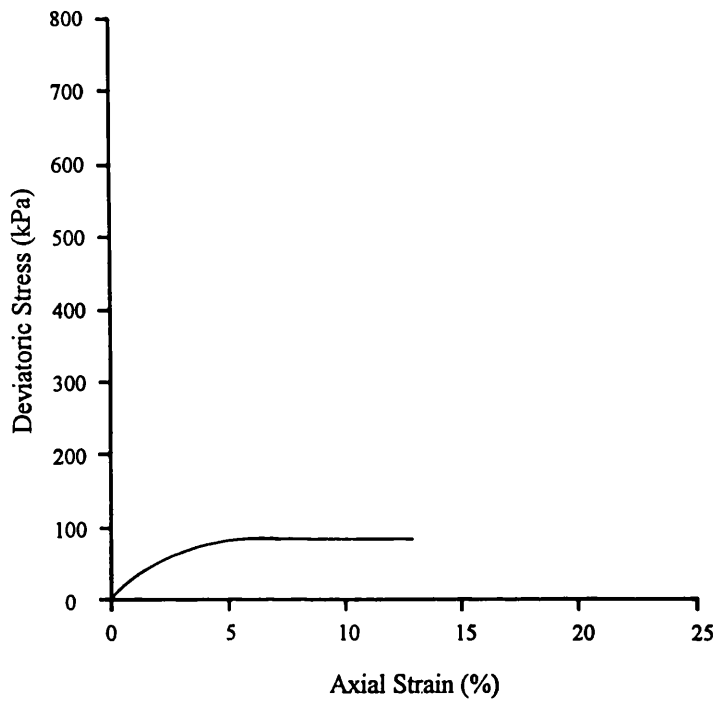


Figure 5.4.34 Stress-strain curve for experiment BDR-100

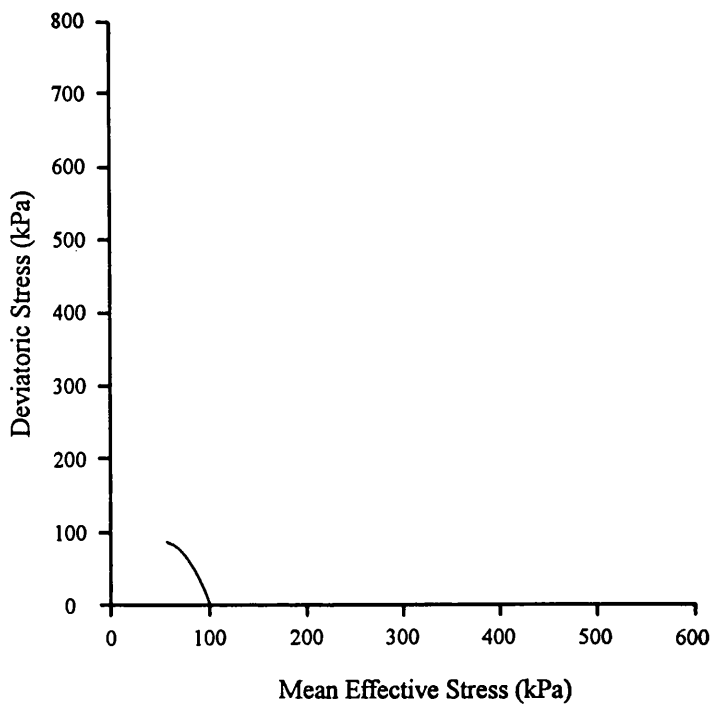


Figure 5.4.35 Stress path for experiment BDR-100

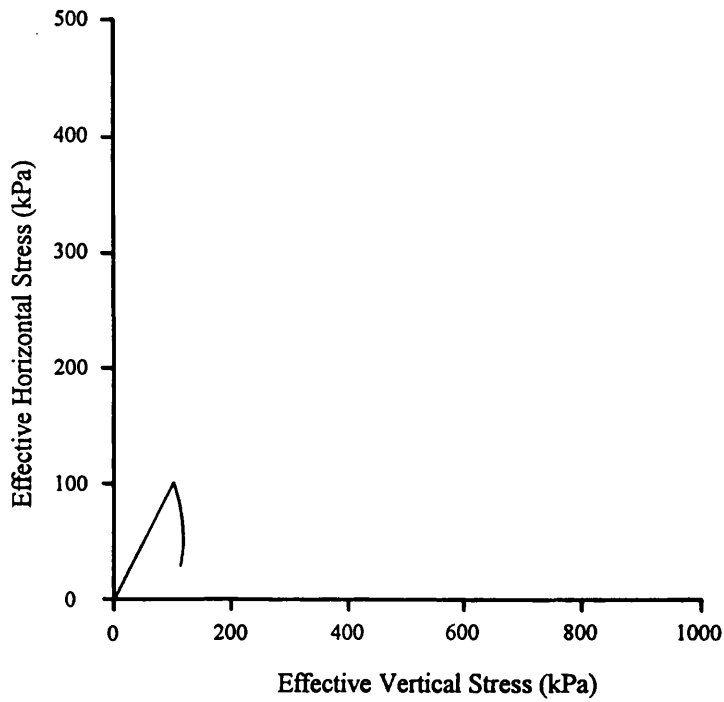


Figure 5.4.36 Effective horizontal-vertical stress relationship for experiment BDM-100

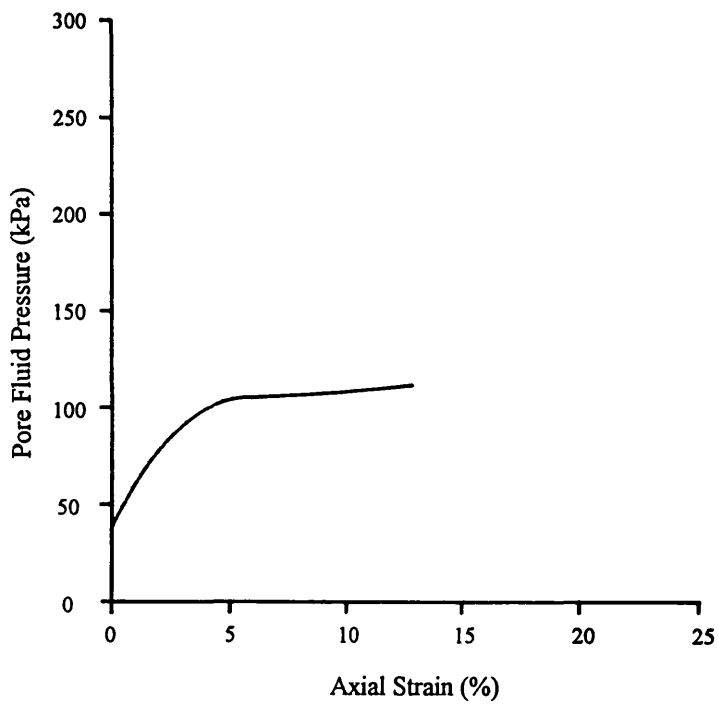


Figure 5.4.37 Pore fluid pressure development during undrained compression for experiment BDR-100

5.4.2 Lichi Mélange, Taiwan

Twelve Isotropic Consolidation Undrained Triaxial Compression experiments were completed on samples of the Lichi Mélange scaly clay from Taiwan. Three experiments were conducted on samples from each weathering horizon, except the one from the deepest horizon (TWL) for which only two experiments, at 100 kPa and 400 kPa effective confining pressure, were completed. This was due to the fact that the TWL sample and TWS sample were materially very similar (also see Chapter four) and the limited testing time available. The twelfth test, TWP-400a, was a repeat of experiment TWP-400 but used a smaller sized sample. The consolidation path for experiment TWP-400 could not be accurately drawn because the sample, which had a very low permeability, was allowed to dissipate the pore fluid pressure from both ends to facilitate completion of the experiment in a reasonable time. Therefore, the undrained pore fluid pressure could not be measured and nor could the evolution of effective stress state through time be determined. Repeating the experiment on a smaller sized specimen facilitated monitoring undrained pore fluid pressures thereby allowing proper description of consolidation as well as providing some information on the influence that sample size exerts on the deformation behaviour. Consolidation data are presented only for the experiments conducted at the highest confining pressures, that is 400 kPa. This is because the consolidation paths recorded for the other lower pressure experiments are not the true ones due either to the use of side drainage or to draining from both ends of the sample thus preventing the undrained pore fluid pressure from being determined.

Table 5.4.6 Initial dimensions and porosities of the Taiwan specimens

Exp. names	Initial length (mm)	Initial diameter (mm)	Initial porosity (%)
TWL-100*	74.36	37.72	20.1
TWL-400*	51.96	25.31	19.3
TWS-100	74.92	37.91	20.3
TWS-200*	52.76	24.93	20.8
TWS-400*	51.08	24.93	19.7
TWP-100	75.44	37.60	21.9
TWP-200	77.64	37.89	23.1
TWP-400	75.14	37.93	22.3
TWP-400a	52.06	25.42	22.9
TWM-100*	76.40	38.85	25.4
TWM-200*	49.56	25.17	25.1
TWM-400*	77.92	38.29	26.3

*: Employ side drainage

5.4.2.1 Least weathered sample experiments

As previously explained, only 100 kPa and 400 kPa effective consolidation pressure experiments were completed in this group of tests. Unlike the Barbados tests, the cell pressure was increased to the desired total confining pressure directly in one increment and pore fluid pressures were then allowed to dissipate. The results of the consolidation phase of TWL-400 are presented in Figures 5.4.38 & 5.4.39. The volume change of the sample during the laboratory consolidation was about 13%. As described previously in section 5.2 the upper curve is the recorded experimental data using side drainage, which does not give real pore fluid pressure and thus mean effective stress state of the specimen, and the lower curve was reconstructed from the data where both top and bottom drainage lines were closed, which is thought to be the true consolidation path.

Figures 5.4.40 to 5.4.43 present the results of the undrained triaxial deformation phase of the two experiments including stress-strain curves, stress paths, effective horizontal-vertical stress relationships and pore fluid pressure-axial strain plots. No clear peak or residual strength can be observed (Figure 5.4.40). Both samples had stress paths which rose almost vertically (Figure 5.4.41) but begin to curve to the right, indicating the onset of dilation at an axial strain of around 3.5%. This coincides with when the generation of pore fluid pressure was at a maximum (Figure 5.4.43). Subsequently, the deviatoric stress continually increased until the experiments were terminated. The effective horizontal-vertical stress relationship plot shows that, in both cases, the effective horizontal stress initially decreased until the pore fluid pressure development reached a maximum. This was followed by a recovery of stress during sample dilation whilst the effective vertical stress continually increased (Figure 5.4.42).

Table 5.4.7 Summary of the deviatoric stress, mean effective stress and pore fluid pressure at the beginning of dilation and the end of test for TWL experiments.

Exp. names	p'_i (kPa)	q_d (kPa)	p'_d (kPa)	q_t (kPa)	p'_t (kPa)	u_d (kPa)	u_t (kPa)	Back pressure
TWL-100	100	70	90	110	130	130	110	100
TWL-400	400	250	400	440	550	190	105	100

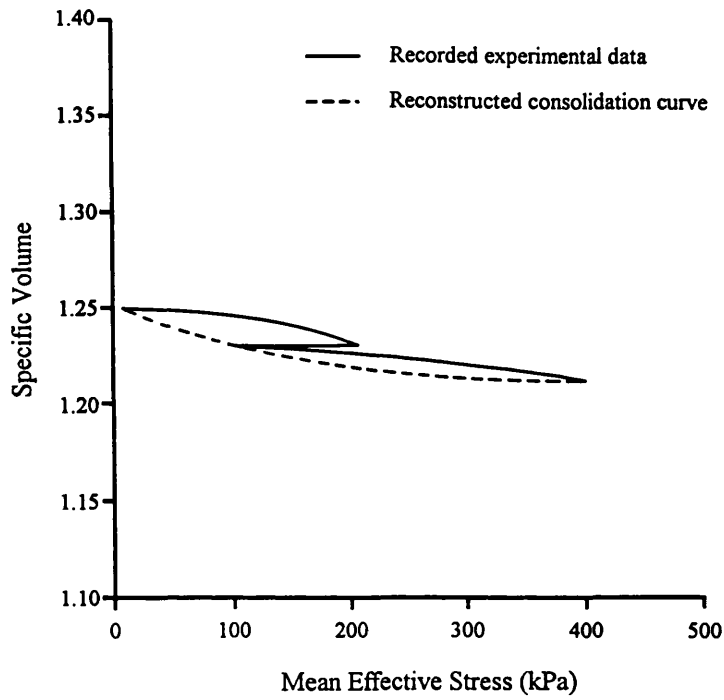


Figure 5.4.38 Consolidation path of experiment TWL-400 (in linear scale)

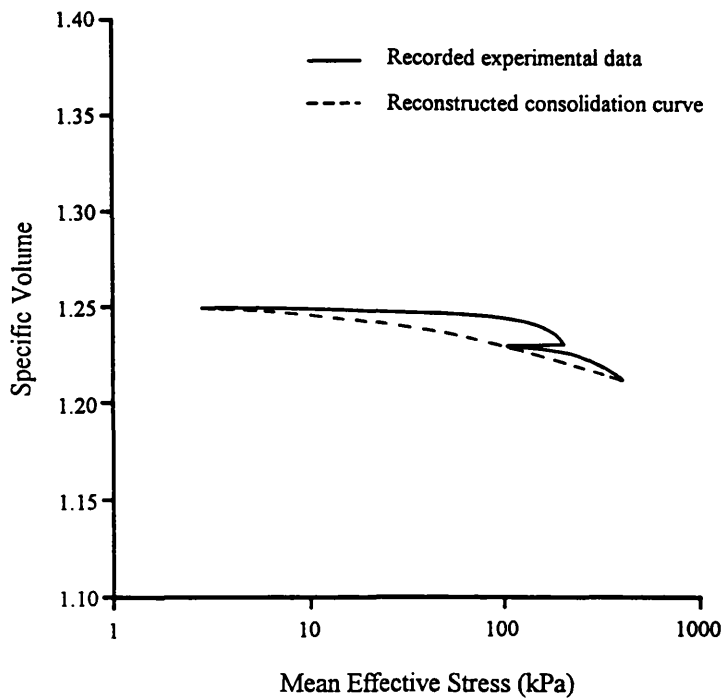


Figure 5.4.39 Consolidation path of experiment TWL-400 (in logarithmic scale)

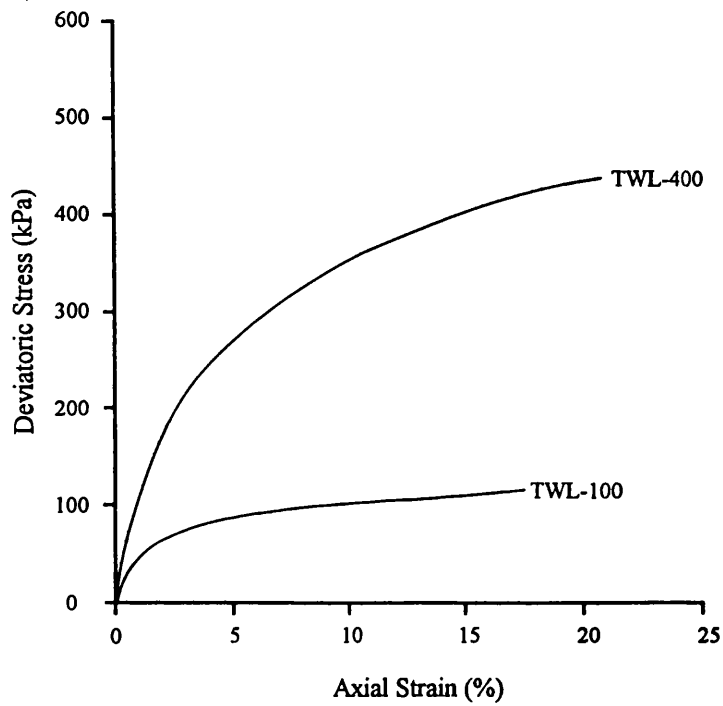


Figure 5.4.40 Stress-strain curves for TWL experiments

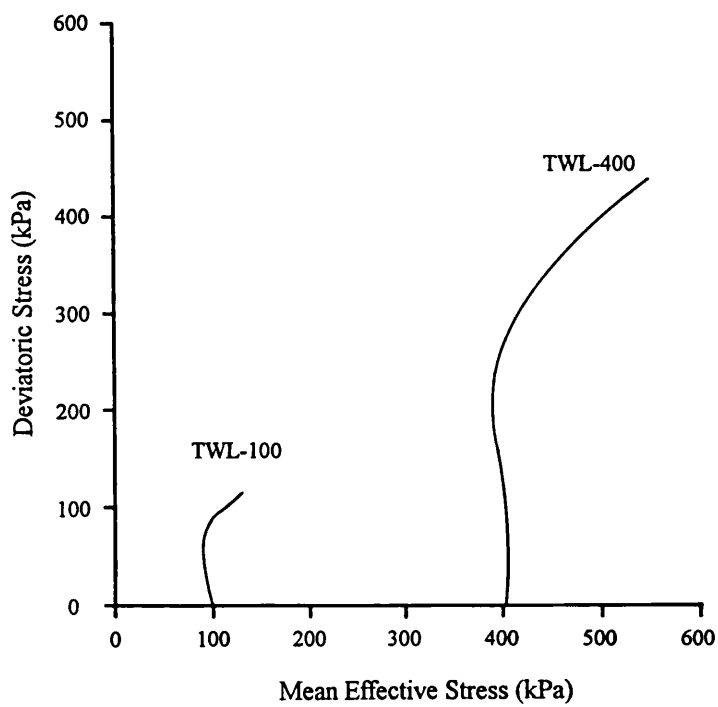


Figure 5.4.41 Stress paths for TWL experiments

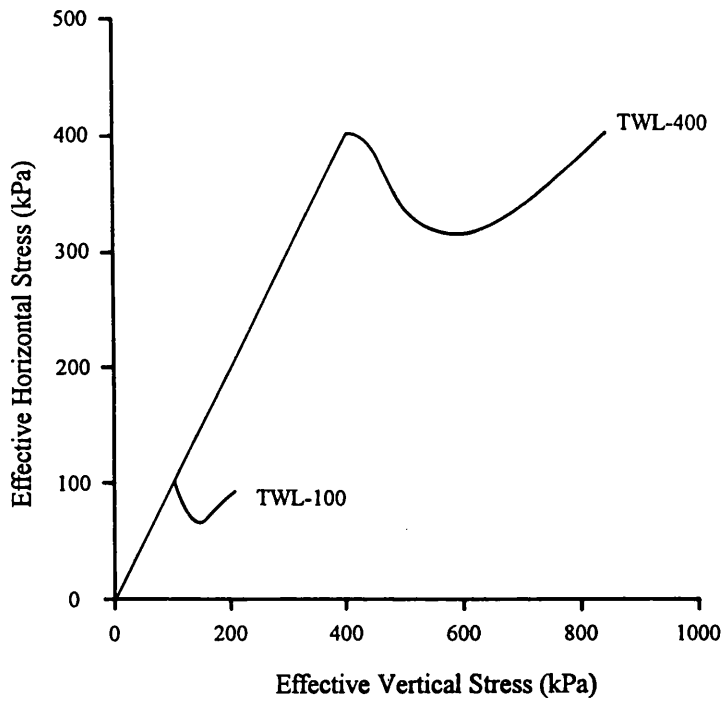


Figure 5.4.42 Effective horizontal-vertical stress relationships for TWL experiments

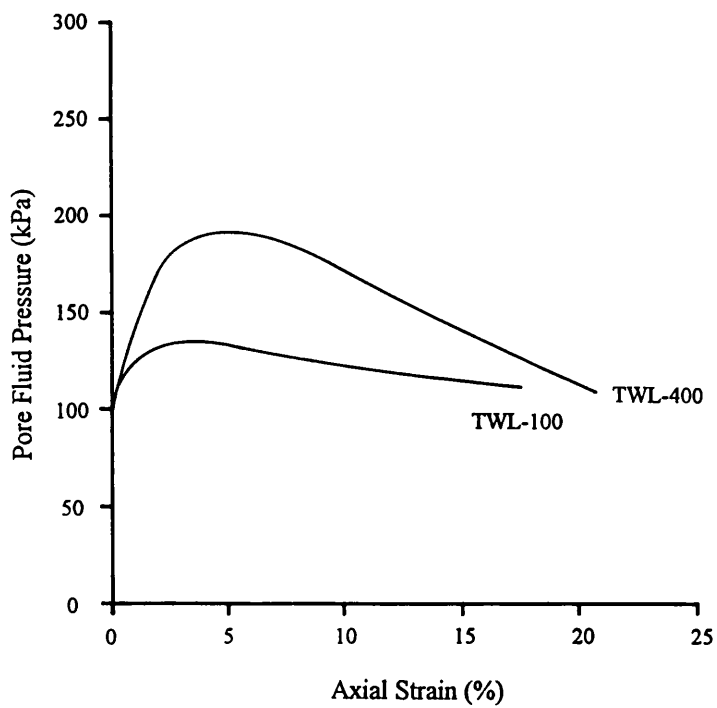


Figure 5.4.43 Pore fluid pressure development during undrained compression for TWL experiments

5.4.2.2 Slightly weathered sample experiments

The data of the consolidation phase of experiment TWS-400 are presented in Figures 5.4.44 & 5.4.45. A 14% volume strain was recorded at the end of consolidation. In terms of the shape of the curve, this is very similar to that of experiment TWL-400.

The undrained triaxial deformation behaviour of the TWS material is also very similar to that of the TWL material. No clear peak and residual strengths were observed, but a strength drop can be seen in experiment TWS-400 at about 2.5% axial strain (Figure 5.4.46). Following the drop in strength, the deviatoric stress continued to increase until the end of the experiment. Interestingly, both TWS-400 and TWL-400 followed almost exactly the same stress-strain curve until the strength drop but subsequently TWS-400 (Figure 5.4.46) remained weaker than TWL-400 (Figure 5.4.40).

All three TWS experiments generated considerable pore fluid pressure during the early stage of undrained deformation resulting in a decrease in the effective horizontal stress (Figure 5.4.48). However, as deformation continued this generated pore fluid pressure started decreasing because the sample began to dilate which caused the effective horizontal stress to increase again. The dilation of all three samples started at some 4% axial strain. This figure is also very similar to that observed for the TWL samples. The magnitude of the generated pore fluid pressure seems to be irrelevant to the effective confining pressure in this case (Figure 5.4.49) for TWS-100 and TWS-200 had similar magnitudes of pore fluid pressure development during undrained deformation.

Table 5.4.8 Summary of the deviatoric stress, mean effective stress and pore fluid pressure at the beginning of dilation and the end of test for TWS experiments.

Exp. names	p'_i (kPa)	q_d (kPa)	p'_d (kPa)	q_t (kPa)	p'_t (kPa)	u_d (kPa)	u_t (kPa)	Back pressure
TWS-100	100	70	80	110	120	145	120	100
TWS-200	200	140	200	220	265	155	120	100
TWS-400	400	230	400	350	500	185	125	100

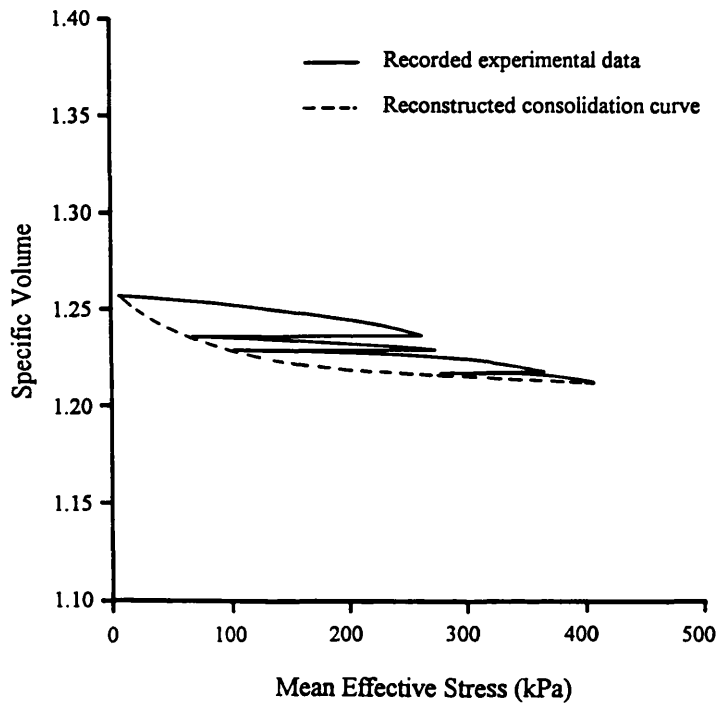


Figure 5.4.44 Consolidation path of experiment TWS-400 (in linear scale)

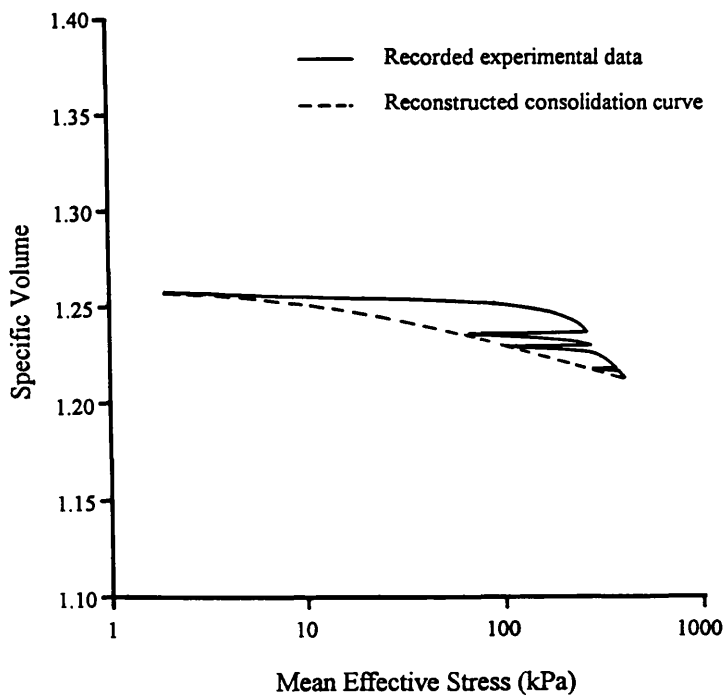


Figure 5.4.45 Consolidation path of experiment TWS-400 (in logarithmic scale)

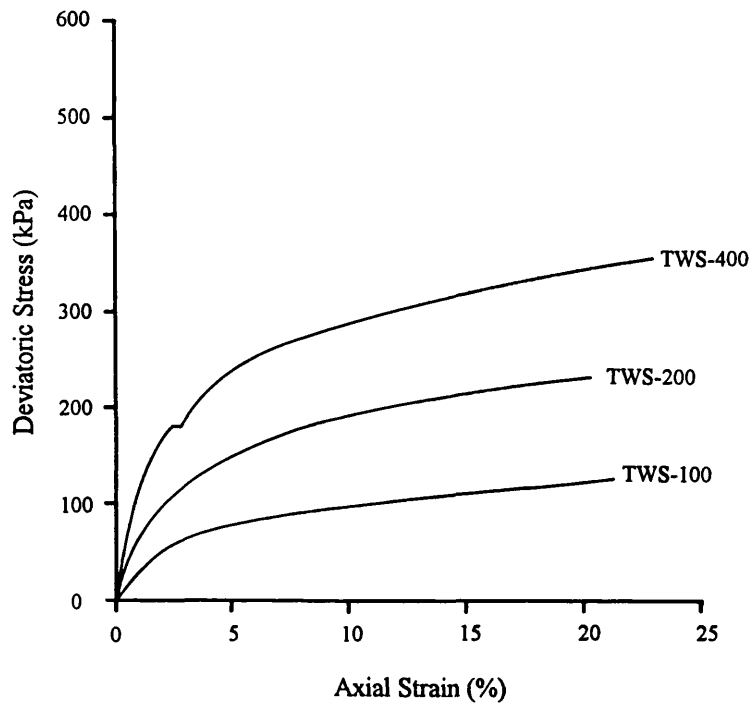


Figure 5.4.46 Stress-strain curves for TWS experiments

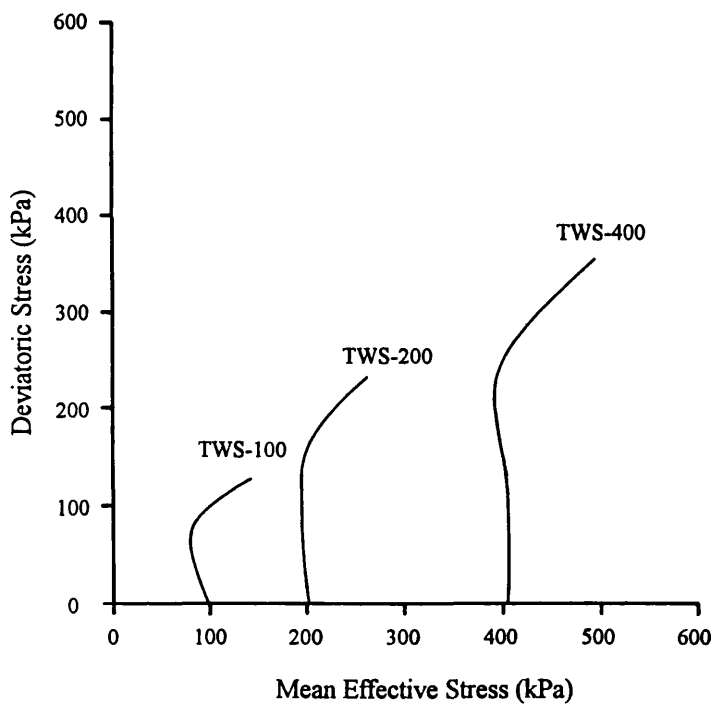


Figure 5.4.47 Stress paths for TWS experiments

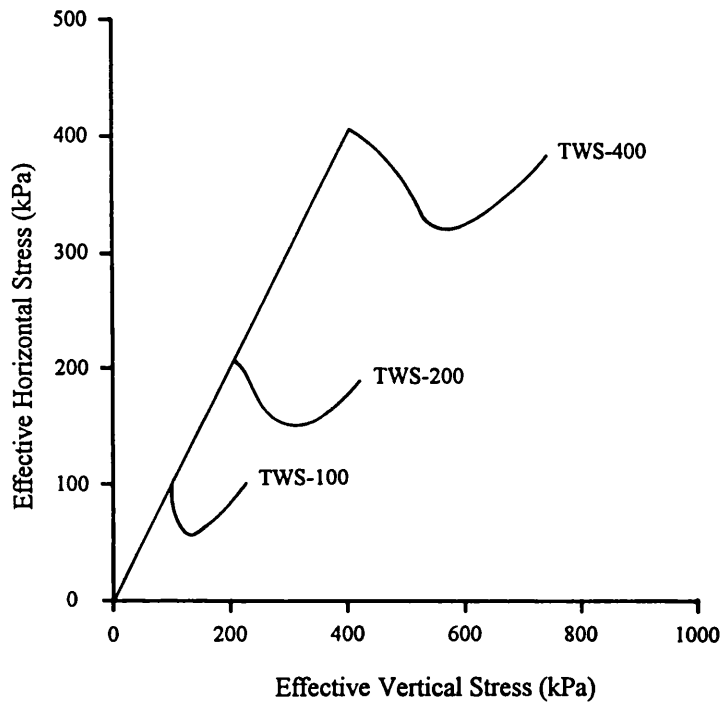


Figure 5.4.48 Effective horizontal-vertical stress relationships for TWS experiments

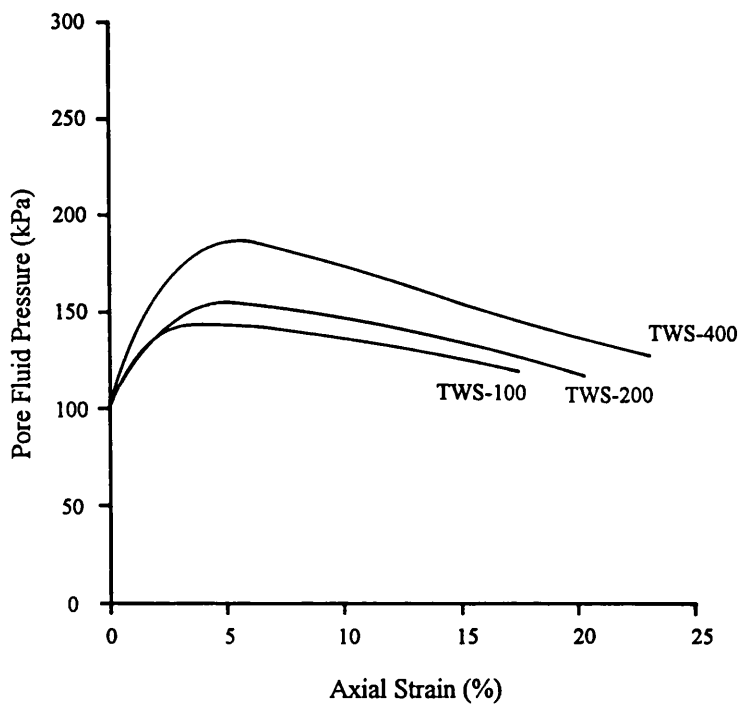


Figure 5.4.49 Pore fluid pressure development during undrained compression for TWS experiments

5.4.2.3 Partially weathered sample experiments

The consolidation path illustrated in Figures 5.4.50, 5.4.51 was obtained from experiment TWP-400a. Good consolidation data could not be obtained from experiment TWP-400 because in order to complete the consolidation with the standard sized sample, both top and bottom drainage lines were open and undrained pore fluid pressure could not be monitored. As explained earlier, the experiment TWP-400a was a repeat of experiment TWP-400 but using a smaller specimen size, without side drainage. In this experiment the consolidation behaviour could be monitored and showed that the major volume change occurred at the very start of the test, which was not accompanied by an increase in the mean effective stress as the sample volume decreased. After the rate of volume change slowed down, the mean effective stress started to increase. Nearly 11% volume strain was recorded at the end of the consolidation process.

Figures 5.4.52 to 5.4.55 present the undrained triaxial deformation results of the four TWP experiments. Strain hardening is seen in all four tests. None of the experiments seemed to have reached an ultimate failure state (Figure 5.4.52). A drop in strength occurred at 3% axial strain in the experiment TWP-400a. The deviatoric stress stayed at 260 kPa for a period of approximately 0.75% axial strain and subsequently increased again. The development of pore fluid pressure in all four TWP experiments during undrained deformation was more restricted than those seen in the TWL and TWS experiments and as a result, the stress paths are inclined to the right (Figure 5.4.53), and the slope of the effective horizontal-vertical stress relationship during undrained loading is much less steep (Figure 5.4.54). Similar to that observed in the TWS experiments there is no obvious relationship between pore fluid pressure development and the magnitude of the applied confining pressure. The pore fluid pressures that develop in each test are of similar magnitude except TWP-400a (Figure 5.4.55), and seem to be independent of the confining pressure.

Table 5.4.9 Summary of the deviatoric stress, mean effective stress and pore fluid pressure at the beginning of dilation⁸ and the end of test for TWP experiments.

Exp. names	p'_i (kPa)	q_d (kPa)	p'_d (kPa)	q_t (kPa)	p'_t (kPa)	u_d (kPa)	u_t (kPa)	Back pressure
TWP-100	100	110	110	150	130	75	70	50
TWP-200	200	200	240	320	300	90	65	50
TWP-400	400	470	510	565	570	90	95	50
TWP-400a	400	465	420	510	480	205	190	100

⁸All four TWP samples dilate from the beginning of the undrained loading. The beginning of dilation denoted here means the places where the stress path starts to curve towards the right.

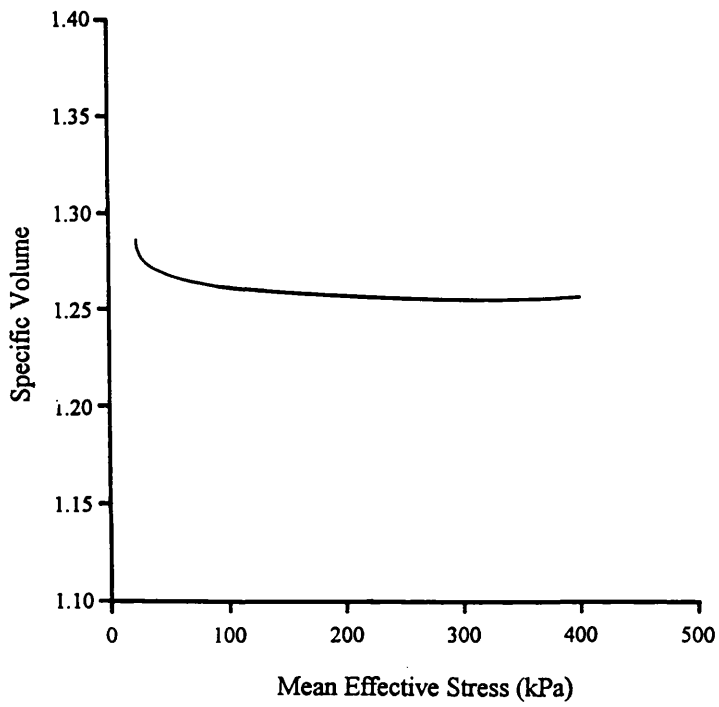


Figure 5.4.50 Consolidation path of experiment TWP-400 (in linear scale)

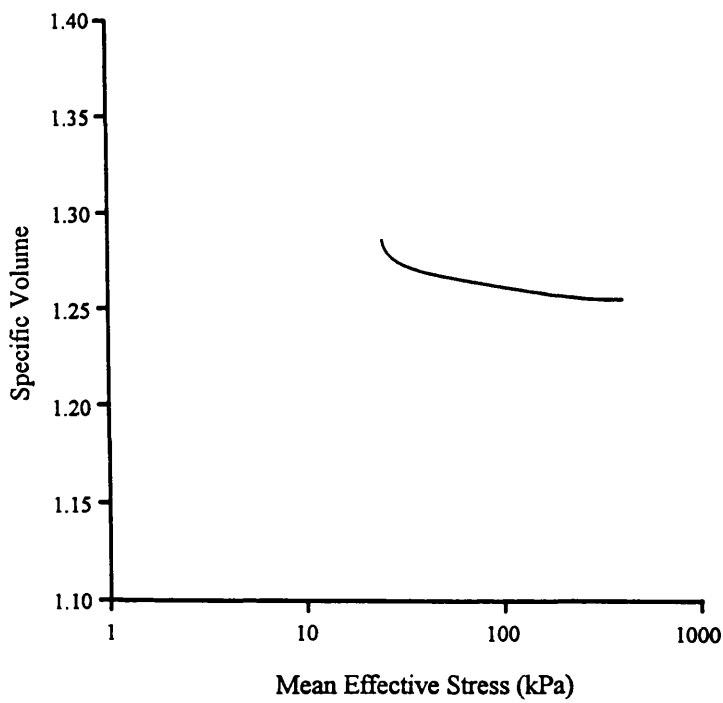


Figure 5.4.51 Consolidation path of experiment TWP-400 (in logarithmic scale)

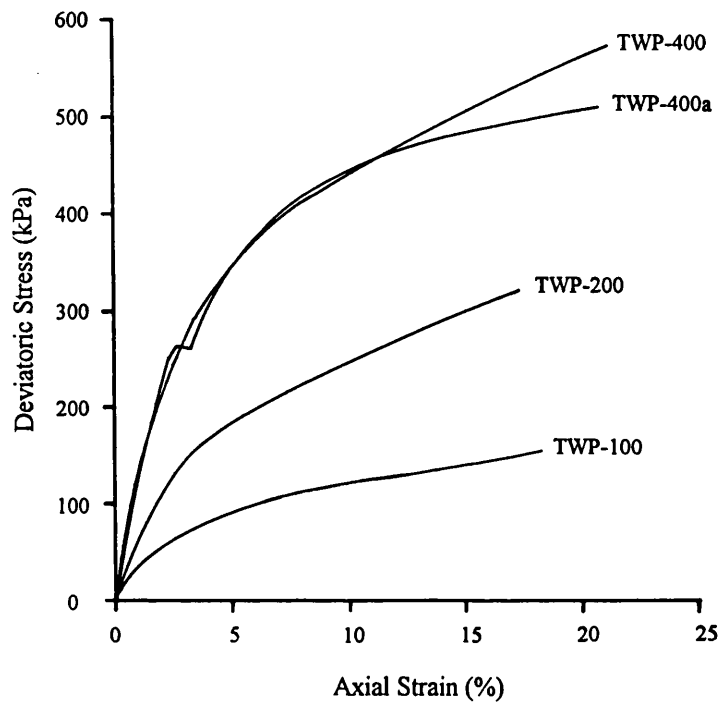


Figure 5.4.52 Stress-strain curves for TWP experiments

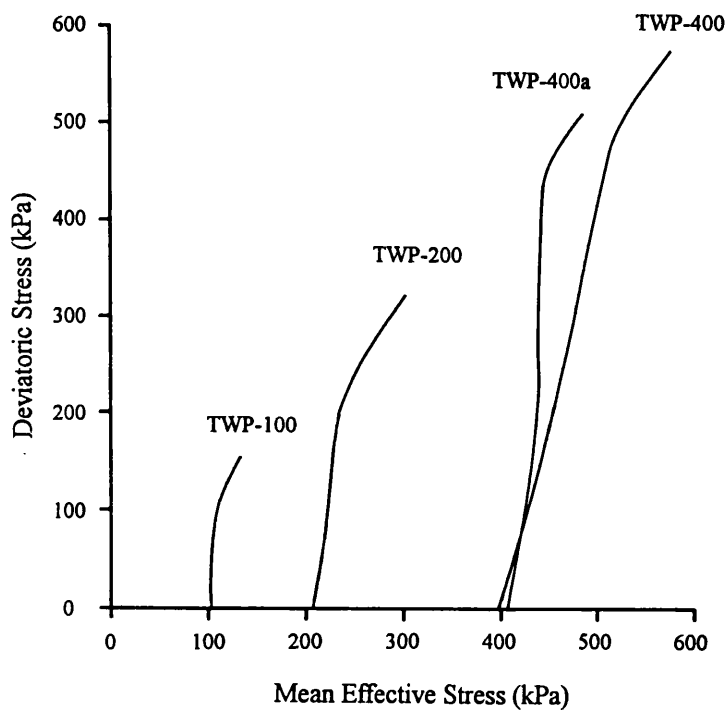


Figure 5.4.53 Stress paths for TWP experiments

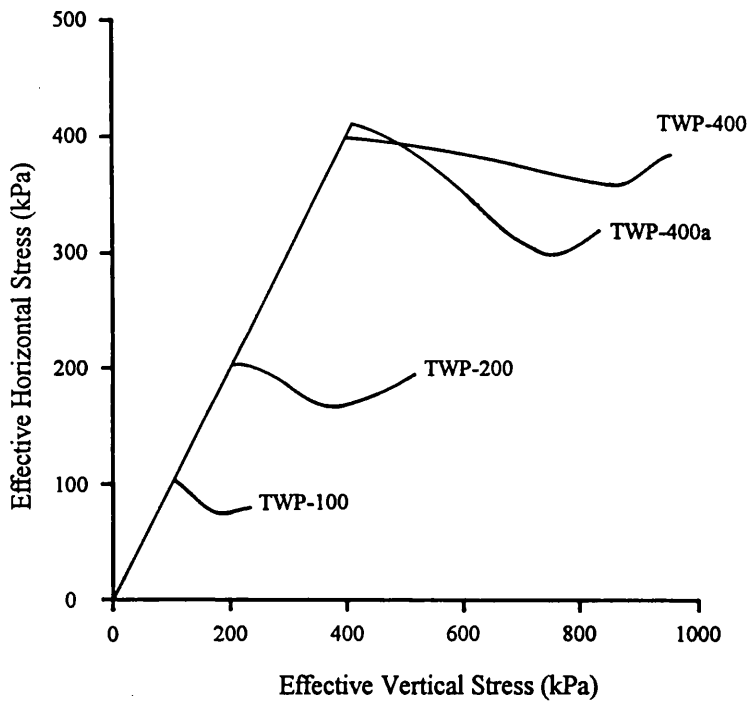


Figure 5.4.54 Effective horizontal-vertical stress relationships for TWP experiments

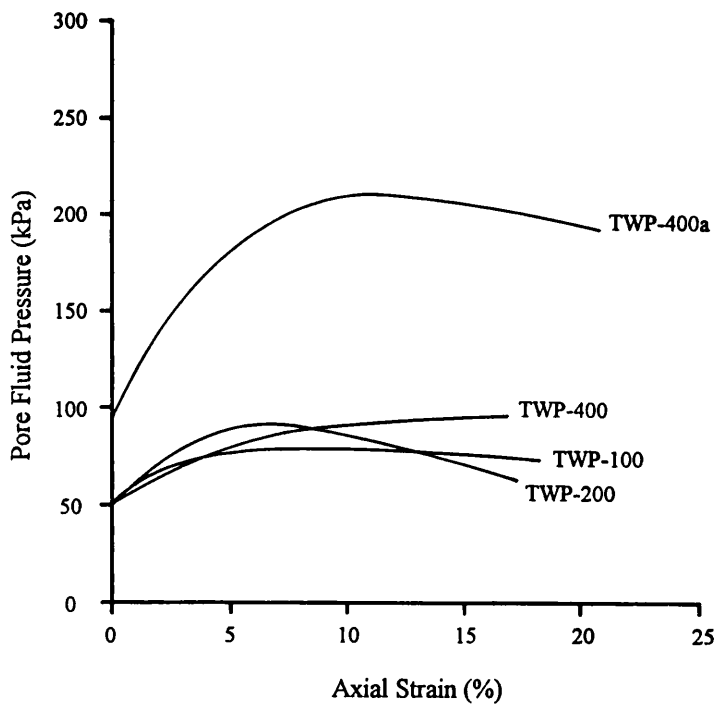


Figure 5.4.55 Pore fluid pressure development during undrained compression for TWP experiments

5.4.2.4 Most weathered sample experiments

The consolidation record of experiment TWM-400 was subject to a disaster. A fault occurred on the computer logging system and as a result, all data files were lost and could not be recovered. Thus the consolidation recorded for this test was lost. The consolidation path reported here was reconstructed from back-up readings in a laboratory note book.

Unlike the other three 400 kPa confining pressure Taiwan tests, this experiment, TWM-400, was conducted using a standard specimen size of 76 mm in length and 38 mm in diameter. A change in slope is seen in the specific volume-mean effective stress log scale plot (Figure 5.4.57). According to soil mechanics this change in slope represents the condition when the material changes from an overconsolidated to a normally consolidated state. The stress prevailing at this turning point is described as the pre-consolidation pressure of the material. In this case, the pre-consolidation pressure is about 40 kPa. At the end of consolidation the recorded volumetric strain had a value of 10.56%.

The undrained triaxial deformation results of the three TWM experiments are presented in Figures 5.4.58 to 5.4.61. Both TWM-100 and TWM-200 exhibited a reduction in strength during undrained deformation (Figure 5.4.58). In TWM-100 this occurred at 4.5% axial strain and in TWM-200 at about 5.5% axial shortening. In both cases strain hardening followed leading to a recovery of strength. Strain hardening continued until the end of each test (Figure 5.4.58). Experiment TWM-400 did not exhibit an abrupt reduction in strength as seen in the other two lower pressure experiments, instead it reached a peak strength at about 6.5% axial strain and then started to gradually decrease to a residual value at about 10% axial strain (Figure 5.4.58). A series of photographs were taken whilst sample TWM-400 was being deformed and these are displayed in Appendix V. These provide a good visual record of how the shear deformation of the sample developed. A visible shear failure plane develops as the strength approaches the peak at 6.5% shortening. Subsequently deformation becomes localised on the plane and the strength of the sample progressively decreases to the residual value.

In the stress paths diagram (Figure 5.4.59), all three experiments show steep, almost vertical, paths. Both TWM-100 and TWM-200 reached a point beyond which dilation occurred (i.e. the stress path turns to the right), whereas TWM-400 did not exhibit dilation but appeared to attain an ultimate state where the deviatoric stress, mean effective stress and pore fluid pressure stayed more or less constant.

The pore fluid pressure development during undrained deformation in the three experiments are given in Figure 5.4.61. The pore fluid pressure reached its maximum value whilst TWM-100 and TWM-200 were experiencing their reduction in strength, and whilst TWM-400 was at its peak strength where the shear deformation started to localise. Peak pore fluid pressure development corresponds with a change in direction of the stress paths in these experiments. This is due to the sensitivity of the mean effective stress to the change in pore fluid pressure.

Table 5.4.10 Summary of the deviatoric stress, mean effective stress and pore fluid pressure at the beginning of dilation and the end of test for TWM experiments.

Exp. names	p'_i (kPa)	q_d (kPa)	p'_d (kPa)	q_t (kPa)	p'_t (kPa)	u_d (kPa)	u_t (kPa)	Back pressure
TWM-100	100	90	100	120	130	130	115	100
TWM-200	200	140	190	180	235	160	135	100
TWM-400	400	290 ⁹	370	260	385	230	200	100

⁹In experiment TWM-400 there was no dilation behaviour observed. The values of q_d and p'_d here are those at peak strength condition.

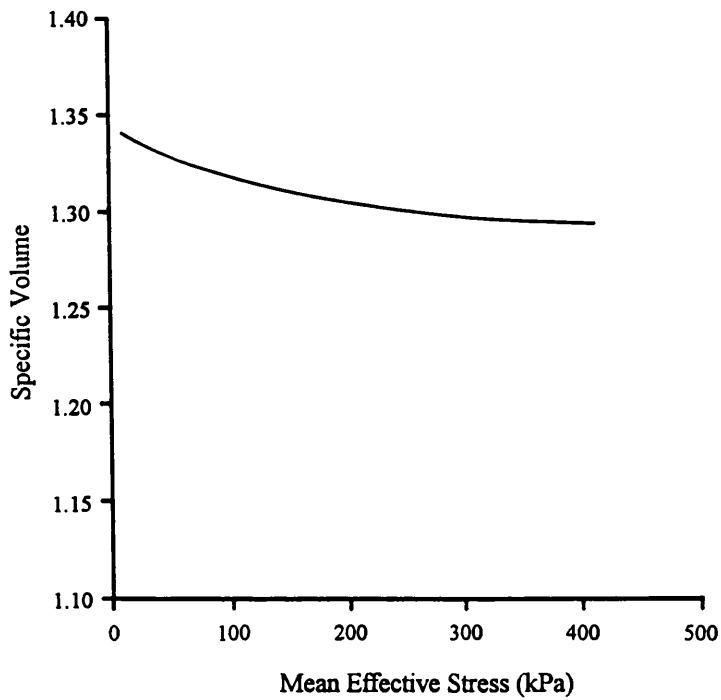


Figure 5.4.56 Consolidation path of experiment TWM-400 (in linear scale)

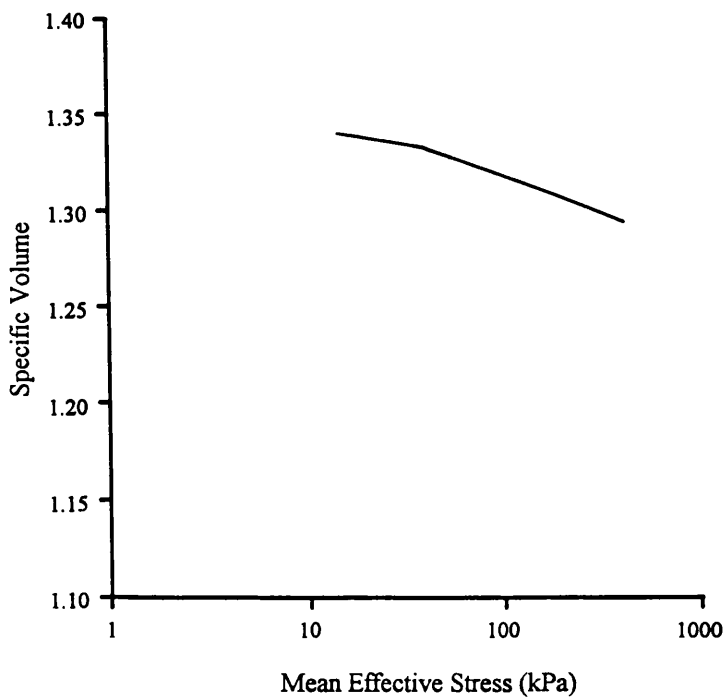


Figure 5.4.57 Consolidation path of experiment TWM-400 (in logarithmic scale)

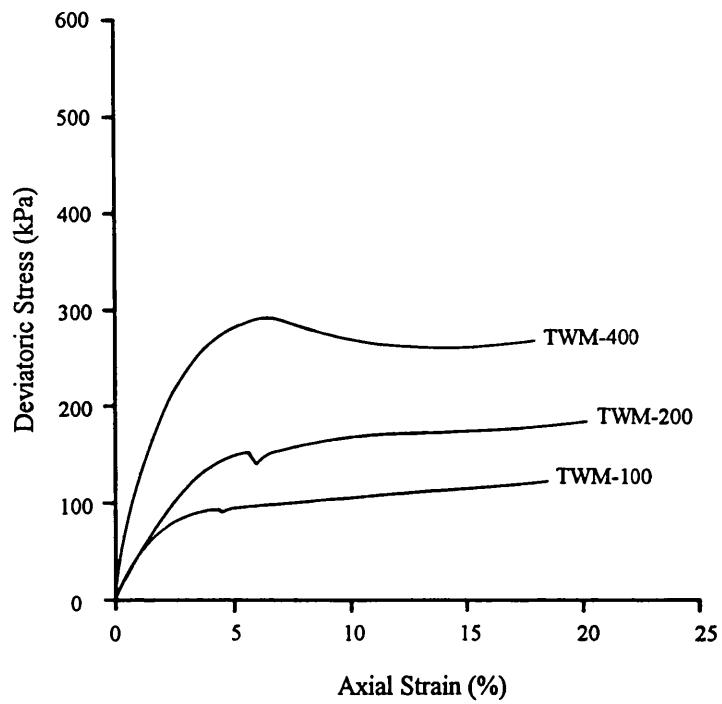


Figure 5.4.58 Stress-strain curves for TWM experiments

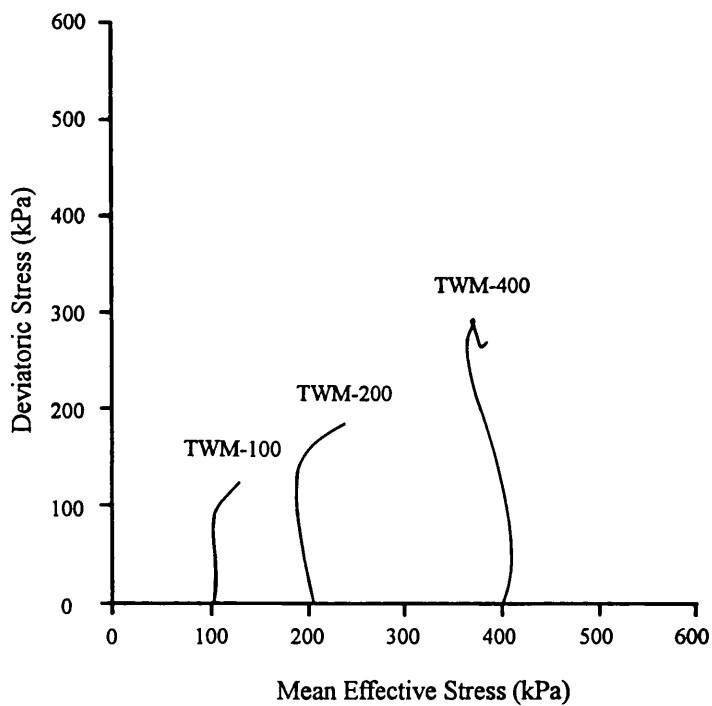


Figure 5.4.59 Stress paths for TWM experiments

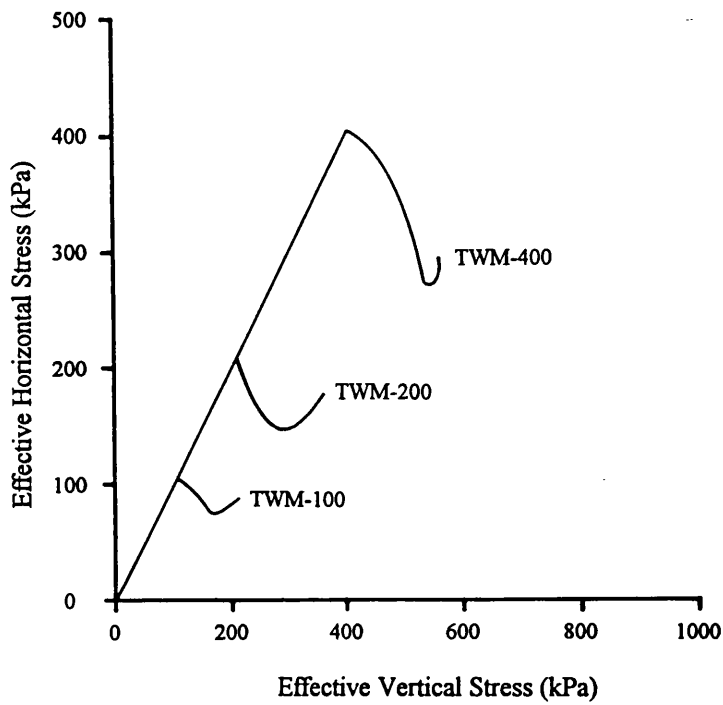


Figure 5.4.60 Effective horizontal-vertical stress relationships for TWM experiments

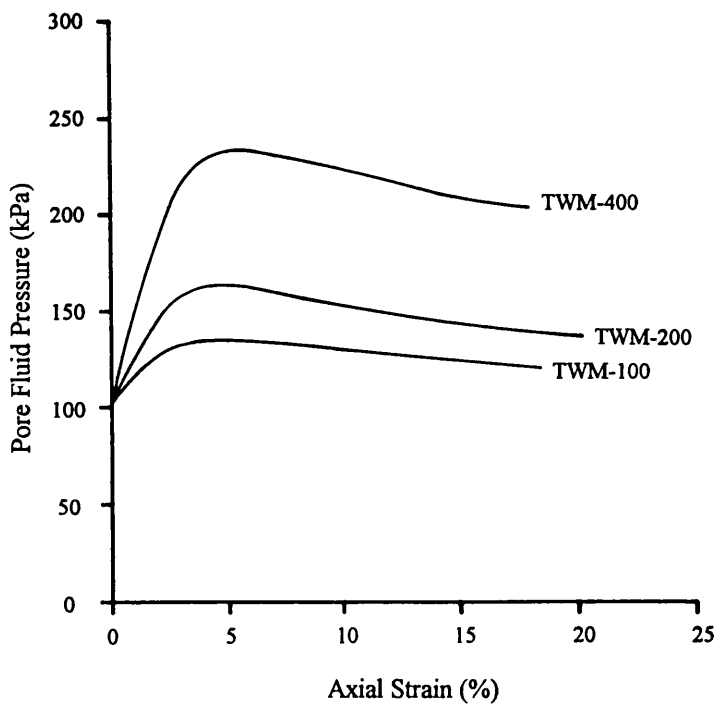


Figure 5.4.61 Pore fluid pressure development during undrained compression for TWM experiments

5.5 Discussion

Both Barbados and Taiwan materials exhibit noticeable variations in their mechanical behaviour between different horizons. These variations in behaviour appear to be a result of physical and chemical changes brought about by variations in the extent of weathering. This section will focus on the changes in mechanical characteristics of each material. A general discussion in which the mechanical behaviour and physical characterisation are combined will be deferred until the main discussion in Chapter Six.

5.5.1 Barbados

5.5.1.1 Consolidation

The consolidation paths of the samples from the three different horizons show an obvious change in their slopes (Figures 5.5.1 & 5.5.2). The BDL paths appear to be very flat, only very small volumetric changes occur during laboratory consolidation. This is the typical consolidation behaviour of a material which has been previously consolidated to a much greater effective stress than the consolidation pressures used during the laboratory testing. Thus the BDL sample is overconsolidated and in the laboratory study has been subject to stresses far below the magnitude of its pre-consolidation pressure. In BDP experiments, the slopes of the paths are slightly greater than those recorded for the BDL experiments although the difference is small. This might be explained as an apparent reduction in overconsolidation ratio between the BDL and BDP samples due to the increased weathering. Although the overconsolidation ratio of the BDP material had been decreased, the material was still overconsolidated, the state of the material was still on the swelling line (Figure 5.5.3) and therefore, the consolidation path retains a gentle gradient in the v - $\ln p'$ space. The three BDM samples all exhibited a much greater gradient to their consolidation paths, suggesting that the material was behaving in a normally consolidated manner. Thus, the successive changes that accompany weathering appear to result in a progressive reduction in the degree of overconsolidation.

It is noted that there is a common feature for all three different weathering class materials in the v - $\ln p'$ diagram, Figure 5.5.2, for example: the consolidation paths are not straight lines but appear to be slightly concave downward, especially towards the end of each test. It is believed that this is due to secondary compression of the samples, occurring as they were being consolidated (primary compression). Secondary compression is a process by which the sample volume changes slowly with time. It is largely independent of the effective stress. Commonly, the rate of secondary compression is so small (almost negligible) that it can only be observed after the end of consolidation. However, in this

study the materials were highly impermeable and always took very long time to complete primary consolidation, consequently, the effects of this time dependent secondary compression were able to accumulate giving rise to the increased compression.

The unloading and reloading cycle in experiment BDM-200 (Figures 5.4.23 & 5.4.26) illustrates the normal- and over-consolidation behaviour of the material. Comparison is made between Figures 5.4.23 & 5.4.26 and Figure 5.5.3, and it is found that line AB in Figures 5.4.23, 5.4.26 is equivalent to the normal consolidation line AB in Figure 5.5.3a, b and lines BC (unloading) and CB (reloading) are the swelling line and correspond to lines BD and DB in Figure 5.5.3. It is seen that the slope of the reloading curve (CB) of experiment BDM-200 is very similar to those of the isotropic compression curves of the BDL and BDP experiments. This supports the suggestion that both BDL and BDP are overconsolidated and BDM behaves more like a normally consolidated soil.

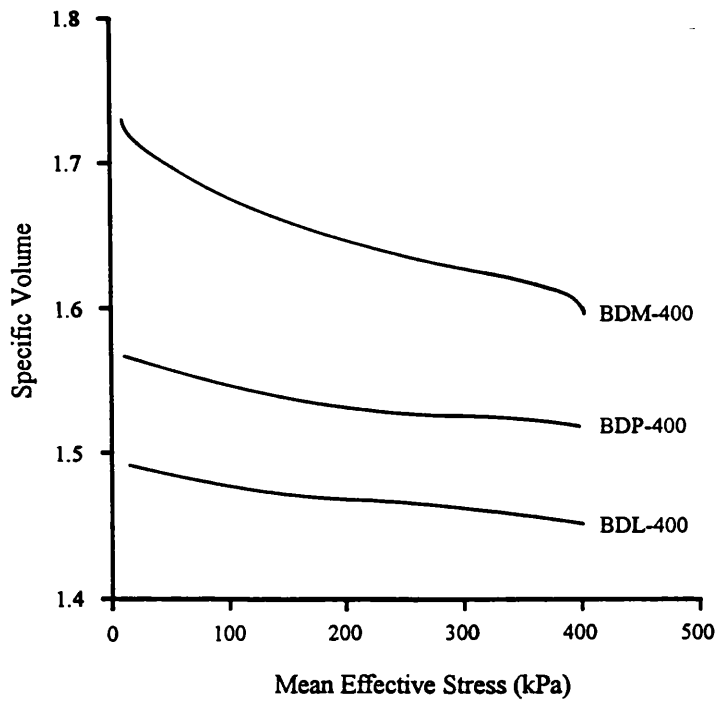


Figure 5.5.1 Consolidation path for experiments BDL-400, BDP-400 and BDM-400 (in linear scale)

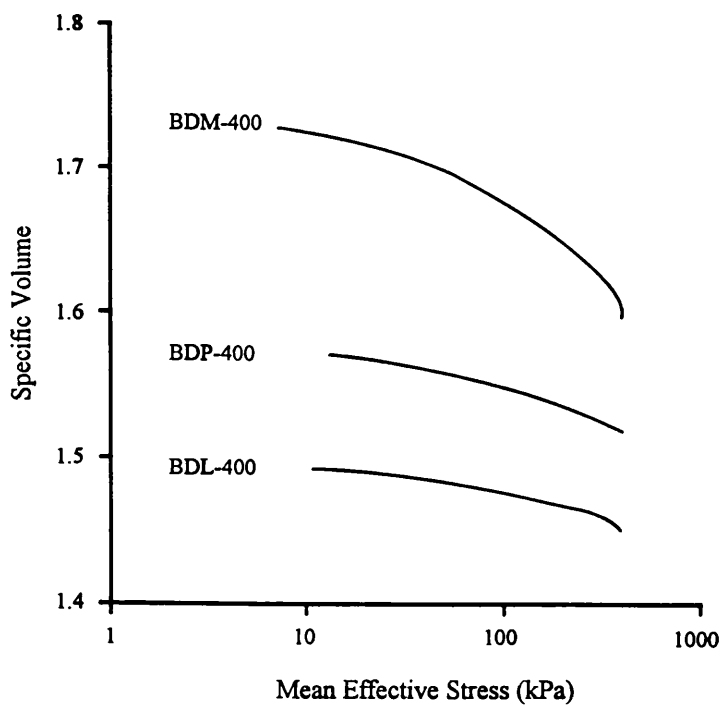


Figure 5.5.2 Consolidation path for experiments BDL-400, BDP-400 and BDM-400 (in logarithmic scale)

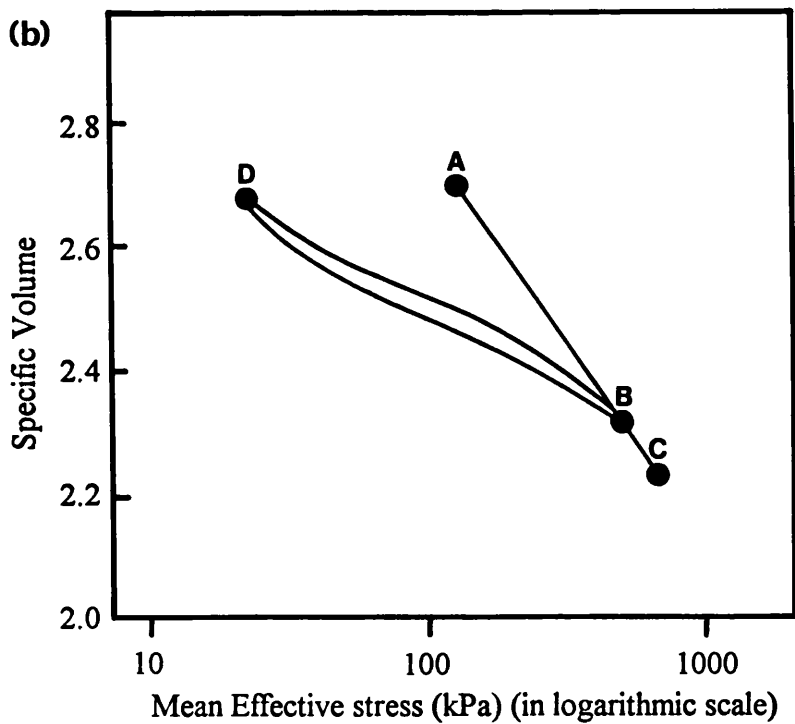
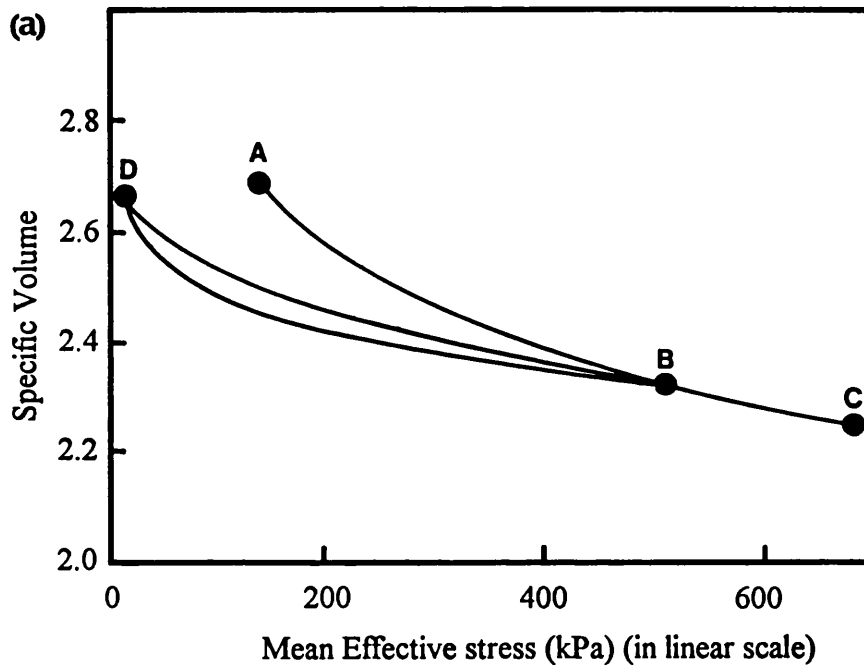


Figure 5.5.3 Isotropic compression of kaolin clay: (a) loading-unloading-reloading path in linear scale. The unloading-reloading section (DB) is generally termed swelling line; (b) same data plotted in logarithmic scale (taken from Atkinson & Bransby, 1978)

5.5.1.2 Undrained triaxial deformation

Experiments on least weathered samples

During undrained deformation the three BDL samples behaved in a manner very similar to a heavily overconsolidated clay (Atkinson & Bransby, 1978). The idealised stress paths for samples with different overconsolidation ratios deformed undrained to failure start from the $q = 0$ plane and rise almost vertically to the state boundary surface (Figure 5.5.4). The paths then traverse the surface until failure occurred at the critical state line (providing that the conditions within the sample are uniform). In natural soil samples, however, failure of overconsolidated samples may occur prematurely, probably soon after the sample reaches the Hvorslev state boundary surface because of natural heterogeneity (Farmer, 1983). Loudon (1967) normalised stress paths for undrained tests on overconsolidated samples of kaolin clay (Figure 5.5.5). The pattern of the stress paths for BDL samples (Figure 5.4.8) is very similar to those of more heavily overconsolidated samples in Loudon's experiments (1967) which rose steeply towards the Hvorslev surface. The three BDL experiments may not have reached the critical state line because the sample each failed whilst they were on the Hvorslev surface (BDL-100 & BDL-400), or even below the Hvorslev surface (BDL-200).

The stress path for sample BDL-400 (Figure 5.4.8) rose more or less vertically until the deviatoric stress (q) reached 420 kPa, at which condition the pore fluid pressure started to decrease relatively quickly whilst the deviatoric stress continued to gently increase. The decrease in pore fluid pressure resulted in an increase in the mean effective stress (p'). It seemed that the sample has reached the Hvorslev surface at point A, and the line AB could represent the projection of the Hvorslev surface on the q - p' space for a particular specific volume (Figure 5.4.8). An extension of line AB is drawn across the q - p' space intercept with the tension surface (CD), it is seen that the stress path of BDL-100 sample just achieved the Hvorslev surface (line DAB) when the experiment was terminated, and that sample BDL-200 was still beneath the Hvorslev surface at the end of the experiment. As mentioned in the results section 5.4.1.1, BDL-200 was terminated at about 7% axial strain. It is believed that sample BDL-200 had reached neither the critical state line nor the Hvorslev surface, but a shear failure plane developed and is clearly seen (Plate 5.5.1). The indication is that a heavily overconsolidated, structured material could develop a shear failure plane before it reaches the state boundary surface.

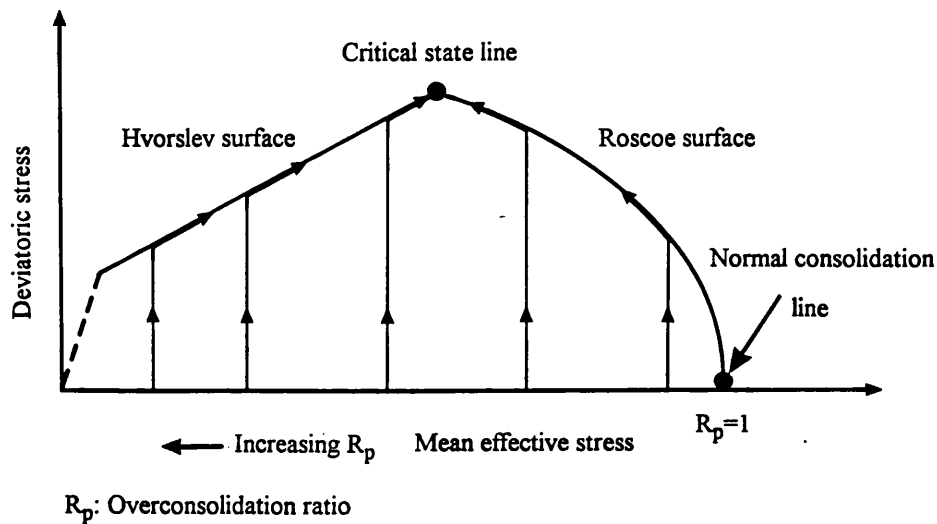


Figure 5.5.4 Expected undrained test paths for samples at different degrees of overconsolidation (overconsolidation ratio), (after Atkinson & Bransby, 1978)

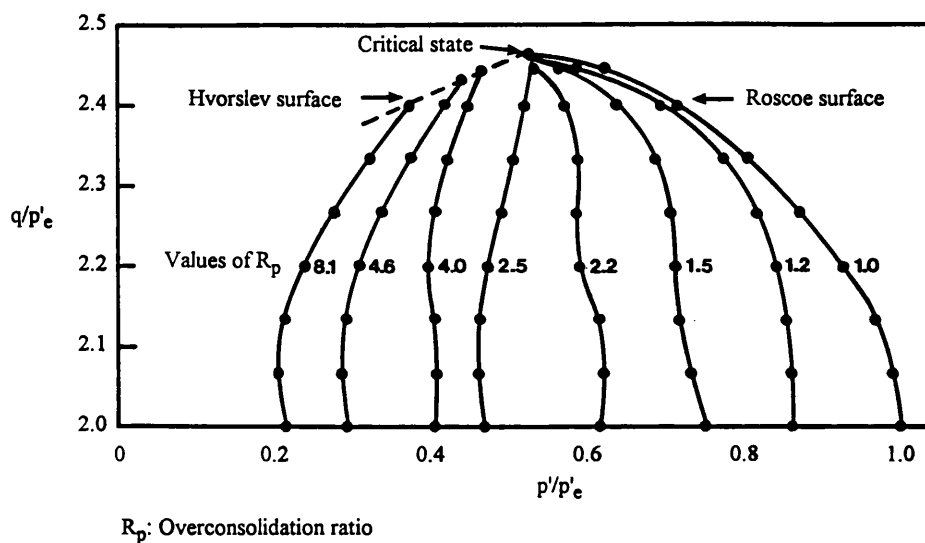


Figure 5.5.5 Normalised stress paths for undrained tests on overconsolidated samples of kaolin clay (Loudon, 1967, diagram taken from Atkinson & Bransby, 1978)

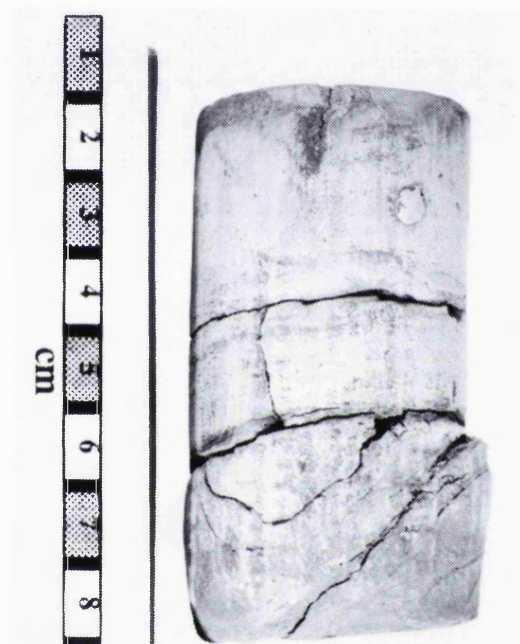


Plate 5.5.1 Sample BDL-200, the experiment was terminated early. Photograph showing the clearly defined shear failure plane

Since pore fluid pressure development during undrained deformation exerts a controlling influence on the stress path, it is worthwhile examining the Skempton pore pressure parameters throughout the experiments. Skempton (1954) introduced the pore pressure parameters A and B, in which B is an index of sample saturation and is unity when the sample is fully saturated, and A can be used to understand the consolidation state of a material (a description of the Skempton pore pressure parameters is given in Appendix I). Figure 5.5.6 reveals the relationship of the deviatoric stress and the pore pressure parameter A for BDL experiments during undrained deformation. In Skempton's description, the value of A at failure is dependent on sample's consolidation history (overconsolidation ratio). Typical A values for different materials are summarised in Table 5.5.1. The more heavily overconsolidated the material, the lower the A value will be. According to Table 5.5.1, BDL-100 and BDL-400 both have A values at the termination of the experiments which fall into the heavily overconsolidated category, which confirms the interpretation of the stress paths. The deviatoric stress in experiment BDL-200 was increasing and its pore fluid pressure was decreasing when the experiment was terminated at 7% axial strain (Figures 5.4.7 & 5.4.10). It therefore seems reasonable to presume that if experiment BDL-200 had not been terminated, its final A value would have been continuously decreasing until it reached a similar value to those of BDL-100 and BDL-400 samples.

Table 5.5.1 Typical A values at failure for materials with different consolidation states.
(After Lambe & Whitman, 1979)

Material (saturation = 100%)	A (at failure)	Reference
Very loose fine sand	2 to 3	Typical values given by Bjerrum (1954)
Sensitive clay	1.5 to 2.5	
Normally consolidated clay	0.7 to 1.3	
Lightly overconsolidated clay	0.3 to 0.7	
Heavily overconsolidated clay	-0.5 to 0	
Very sensitive soft clays	>1	From Skempton and Bjerrum (1957)
Normally consolidated clays	0.5 to 1	
Overconsolidated clays	0.25 to 0.5	
Heavily overconsolidated clays	0 to 0.25	

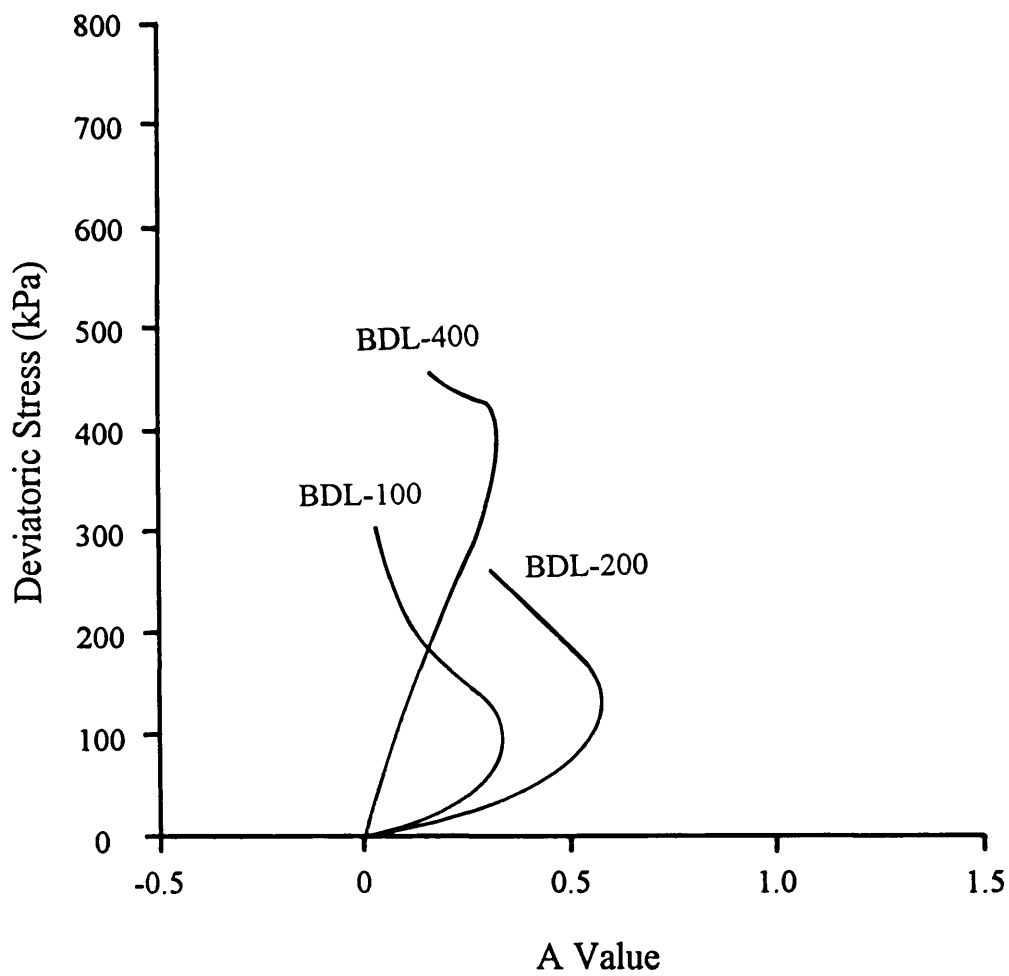


Figure 5.5.6 Deviatoric stress-Skempton pore pressure parameter A relationships for BDL experiments

Experiments on partially weathered samples

The three lower confining pressure experiments in this group of four exhibit a very similar pattern when their stress paths are compared (Figure 5.4.19). They all slope to the right as they rise towards the ultimate failure state, showing strong dilation from the very beginning of undrained deformation. Experiment BDP-400, also exhibits dilation at the beginning of undrained compression but on reaching a higher mean effective stress, which inhibited further dilation of the sample, positive pore fluid pressure generation started which resulted in the stress path curving towards the left until it approached the failure envelop where dilation was resumed. Although at this greater effective confining pressure the stress path differed from those of the other three tests, it nonetheless ended up on the same failure envelop indicating a consistency in overall failure behaviour.

The results of the BDP experiments indicate that the BDP samples were behaving in a manner closely akin to a moderately overconsolidated material (compare Figures 5.4.19 with 5.5.5). Thus the stress paths fit the same framework as for the BDL experiments (Figure 5.5.4). The difference between BDL and BDP is that the BDP experiments did not show the same undisturbed soil structure effect as exhibited by the BDL experiments (i.e. vertical stress paths and early failure of samples) but instead displayed strong dilation from the start of undrained loading (stress paths curves to the right, Figure 5.4.19).

To explain the strong dilation behaviour exhibited by the BDP samples, another point of view may have to be considered in the interpretation of the data. Atkinson & Bransby (1978) illustrated that although the behaviour of sand is very different to clays, it is possible to use a framework which serves for clays to understand the behaviour of sand. Instead of using normally consolidated and heavily overconsolidated as two extremes for describing the influence of soil fabric on deformation behaviour, loose and dense packing are used to replace these two states.

Typical isotropic compression curves for loose and dense specimens of quartz sand are shown in Figure 5.5.7 which indicate that for the stress levels used in the laboratory testing, both loose and dense samples of the sand may be regarded as overconsolidated, as they both lie to the left of the estimated normal consolidation line AC. The undrained deformation behaviour of both the loose and dense sand is illustrated in Figure 5.5.8 where, at the stress level used in the laboratory testing (< 500 kPa), samples attain the critical state line in an extremely loose condition. This is often looser than the loosest state that can be set up by pouring sand in the laboratory and can only be reached

through dilation, during deformation in which particles roll around each other (Atkinson & Bransby, 1978). Figure 5.5.9 gives normalised stress paths for both loose and dense samples under both drained and undrained conditions.

The stress paths for the three lower pressure BDP experiments are similar to those of the dense sand described by Atkinson & Bransby. The strongly dilatant behaviour of the BDP samples is one of the characteristics typical of a sand. In order to achieve the critical state, at which the packing density is extremely loose, the samples tend to expand and start to dilate from the beginning of undrained deformation and therefore, generation of pore fluid pressure is restricted. As a result, the effective stress path is inclined to the right.

Inspection of the Skempton pore pressure parameter A was also made for the BDP experiments (Figure 5.5.10). The final A values for the four experiments fall in-between -0.1 to 0.3, which is equivalent to the range for heavily to moderately overconsolidated clays (Table 5.5.1). Comparison of the A values for the BDP and BDL experiments shows that, the former have a slightly lower value. However, this should not be interpreted as BDP material being more heavily overconsolidated than BDL, it may be a reflection of the BDP samples developing characteristics similar to a sand.

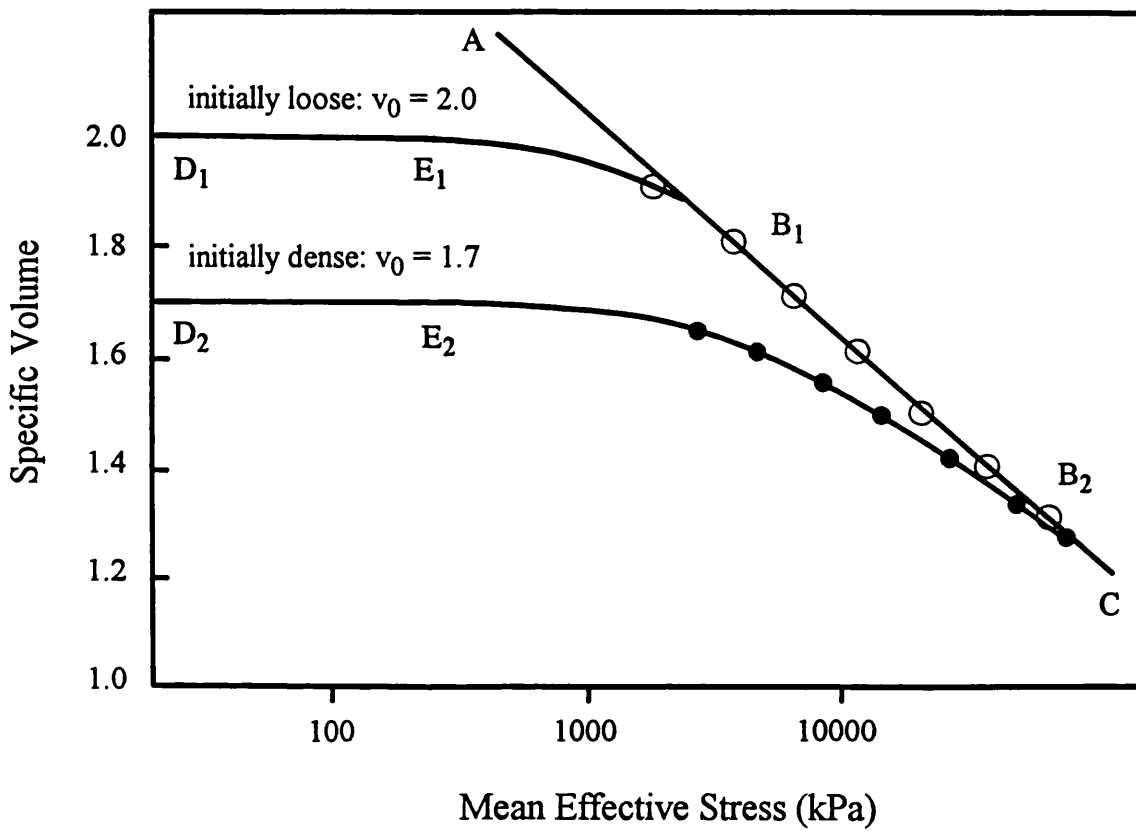


Figure 5.5.7 Isotropic compression of quartz sand (after Vesic & Clough, 1968, diagram taken from Atkinson & Bransby, 1978)

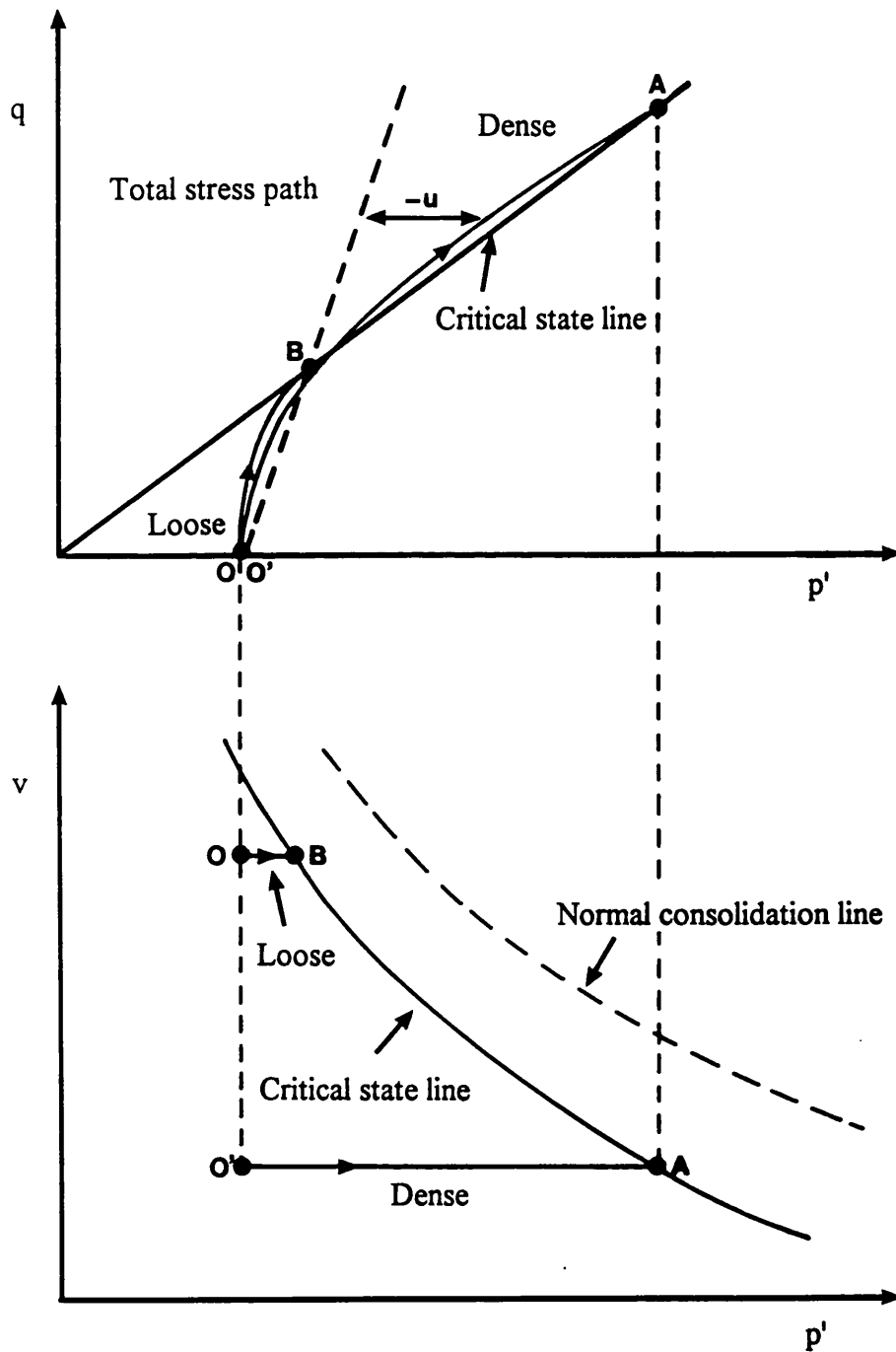


Figure 5.5.8 Stress paths in $q : p'$ and $v : p'$ space for undrained tests on dense and loose specimens of sand (after Atkinson & Bransby, 1978)

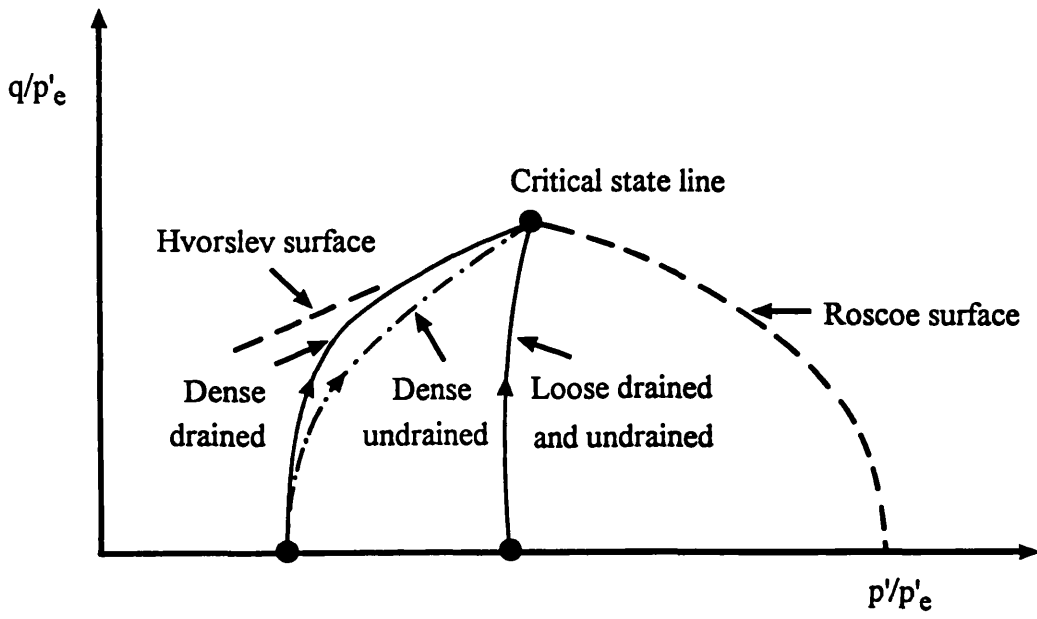


Figure 5.5.9 Normalised stress paths in $q/p'_e : p'/p'_e$ space for drained and undrained tests on loose and dense samples of sand

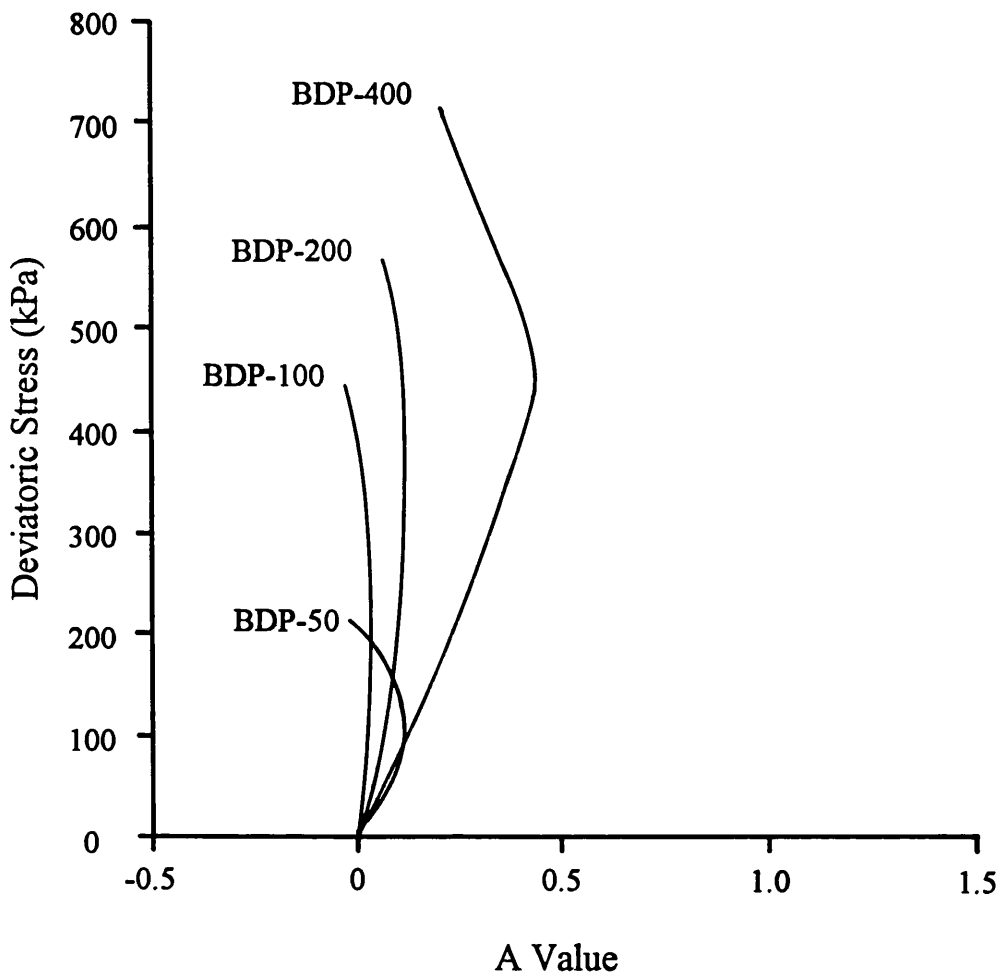


Figure 5.5.10 Deviatoric stress-Skempton pore pressure parameter A relationships for BDP experiments

Experiments on most weathered samples

The three BDM experiments all exhibited similar characteristics during undrained deformation. Each sample reached an ultimate failure state at which shear strength remained constant whilst the sample continued to strain. The three stress paths also exhibit very similar forms.

The stress paths (Figure 5.5.11a) and stress-strain curves (Figure 5.5.11b) of the three BDM experiments are compared with the expected stress paths (Figure 5.5.11c) and stress-strain curves (Figure 5.5.11d) of a normally consolidated sample presented by Atkinson & Bransby (1978) respectively. The two sets of diagrams exhibit great similarities indicating that BDM is very similar to the ideal normally consolidated material that Atkinson & Bransby (1978) described. The difference is that the BDM paths did not stay at their lowest mean effective stress state (p'), but exhibited some dilation at the end of the experiments resulting in that the paths curving back towards the higher mean effective stress.

As with the BDL and BDP experiments the response of the Skempton pore pressure parameters during undrained deformation has been determined. Figure 5.5.12 illustrates the relationship between the deviatoric stress and the A parameter for the BDM test results. The values of the A parameter for the BDM experiments are generally greater than recorded in the other two groups (BDL & BDP experiments) and fall into the normally consolidated and/or lightly overconsolidated category (Table 5.5.1).

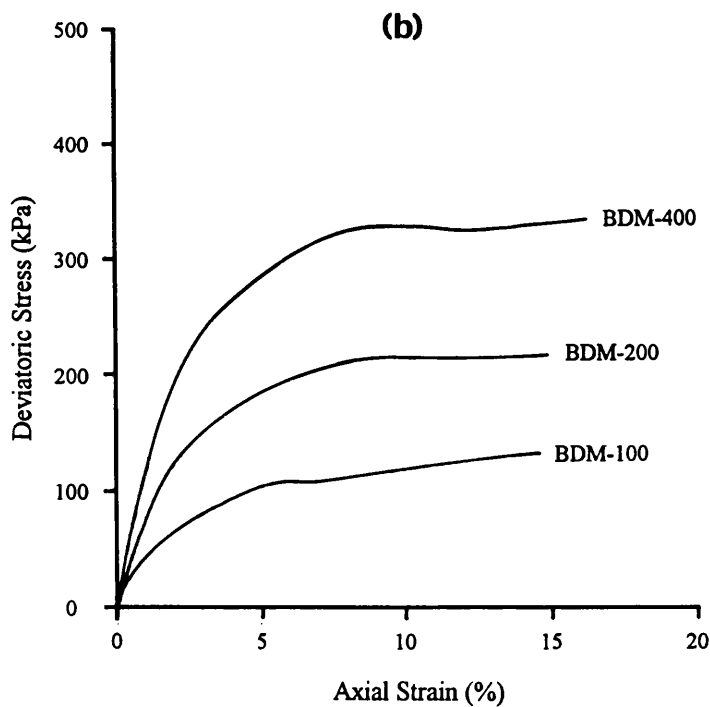
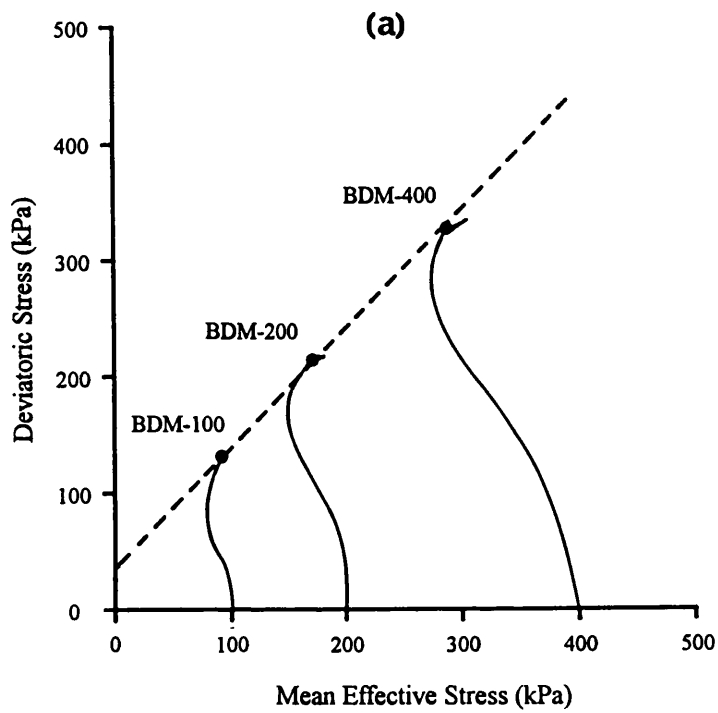


Figure 5.5.11 Comparison between BDM experiments and expected normally consolidated material tests. (a) Stress paths for BDM experiments. (b) Stress-strain curves for BDM experiments.

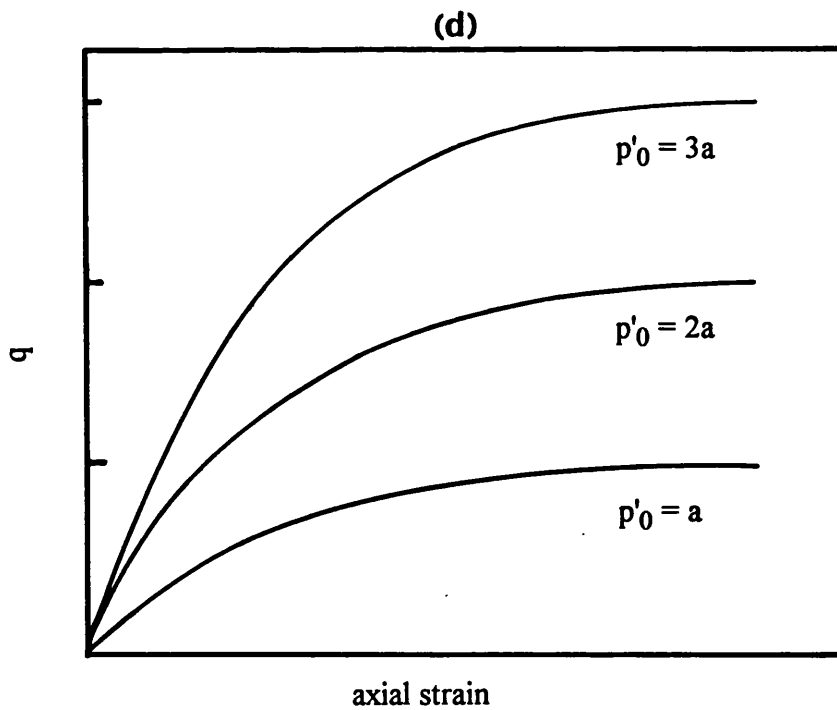
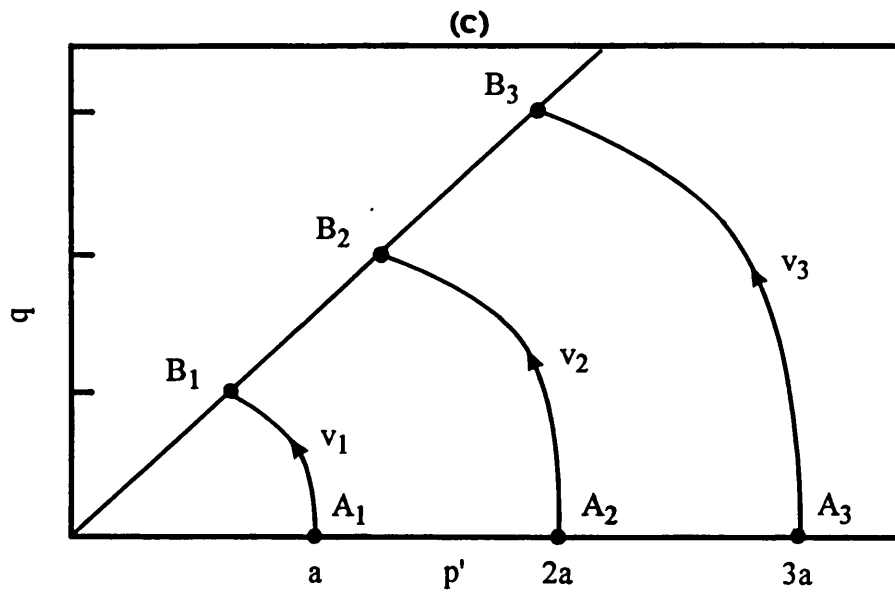


Figure 5.5.11 Comparison between BDM experiments and expected normally consolidated material tests. (c) Stress paths for normally consolidated material at different effective confining pressures. (d) Stress-strain curves for normally consolidated material at different effective confining pressure.

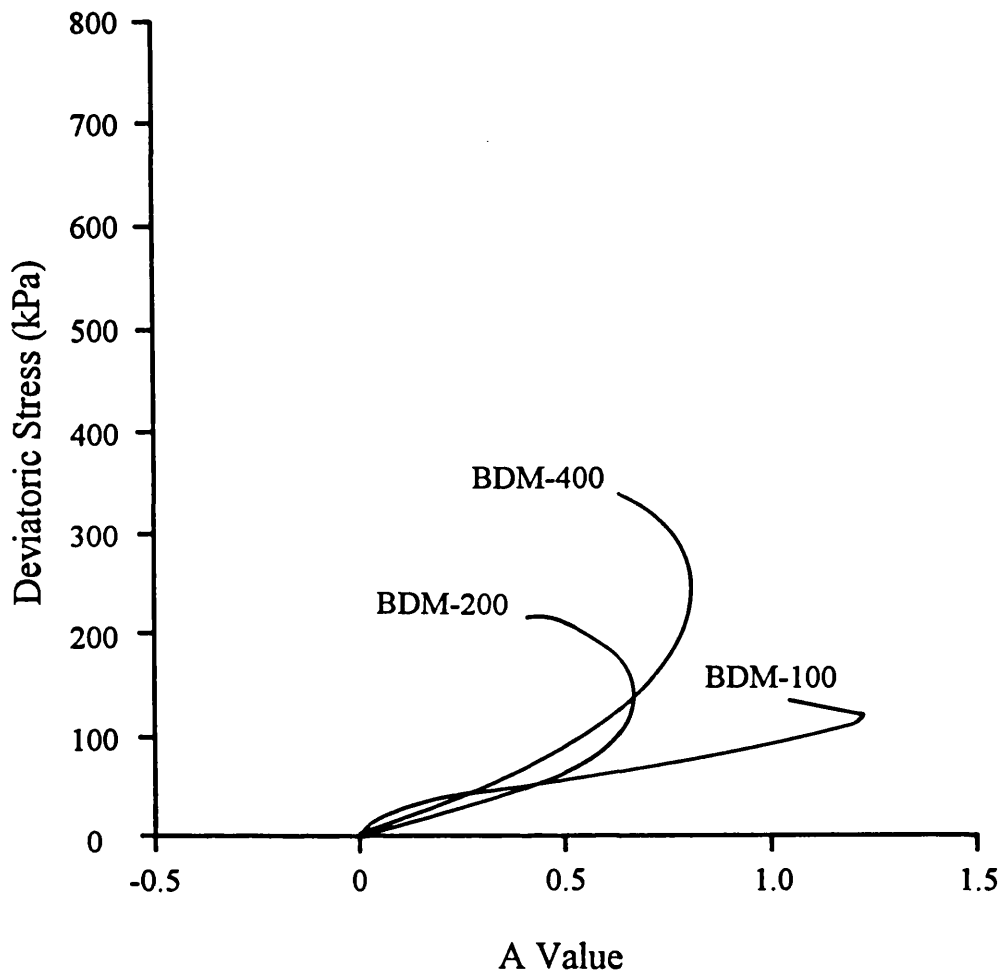


Figure 5.5.12 Deviatoric stress-Skempton pore pressure parameter A relationships for BDM experiments

5.5.1.3 Summary of the mechanical behaviour of the Joe's River Formation scaly clay

Examination of the isotropic consolidation and undrained deformation results suggests that the three groups of experiments appear to reveal a change in the overconsolidation ratio. Results of the BDL experiments indicate heavy overconsolidation, those of the BDP experiments heavy to moderate overconsolidation (although the deformation behaviour exhibits characteristics of both clay and sand), whilst those of the BDM experiments conform to the behaviour of a lightly overconsolidated/normally consolidated material. When the Joe's River Formation scaly clay is converted from an unweathered to a partially weathered state the original structured soil fabric resulting from diagenesis and overconsolidation is gradually lost causing a change in the mechanical characteristics exhibited by the material. Consequently, as the scaly clay becomes partially weathered it exhibits intense dilation during undrained deformation unlike the more rigid, less dilatant response of the least weathered, structured soil. However, the structure resulting from the previous consolidation history still exists causing the sample to behave in a manner closely akin to that of a heavily to moderately overconsolidated material. As weathering continues, the remnant structure from overconsolidation is largely destroyed and the material becomes structurally remoulded. The normal consolidation behaviour exhibited by the most weathered samples is the result.

Regardless of the change observed in the apparent overconsolidation ratio, the shear resistance does not change with depth into the weathering profile in a simple manner. The partially weathered material BDP exhibits the highest shear resistance whilst the most weathered material is the weakest. This observation is in direct contradiction of the widely held view that as weathering takes place the material becomes weaker. Thus, although weathering of the clays reported here leads to destruction of the original structure and increase in pore volume, these changes are accompanied by a strengthening during the early stage of the weathering process. Only at shallow depth does weathering serve to reduce the shear strength of scaly clay. This unusual phenomenon is considered in more detail in the following discussion chapter.

5.5.2 Taiwan

5.5.2.1 Consolidation

Due to the use of side drainage in the experiments TWL-400, TWS-400 and TWM-400, it is difficult to accurately identify their consolidation paths. The approximate paths can however be estimated. In terms of the total volume change during laboratory consolidation the TWL and TWS samples expelled more pore fluid (13% and 14%) than the TWP and TWM samples (some 11%). This behaviour differed from the Barbados samples and was unexpected.

There are a few possibilities which may explain this. First, both TWL-400 and TWS-400 experiments employed side drainage which effectively changed the flow direction and enabled the pore fluid to flow out of the sample specimens more easily. As a consequence, pore fluid pressure was able to dissipate much more easily and completely. In TWP-400, in contrast, pore fluid could only flow vertically from the specimen. This would not cause any problem if the material was reasonably permeable, but the studied materials are practically impermeable (without sufficient pressure head across the specimen) and contain various soil fabrics which may influence direction of fluid flow. Thus consolidation behaviour may be drainage path dependent which would result in the volume change in experiments TWL-400 and TWS-400 being larger than in experiments TWP-400. Although experiment TWM-400 also employed side drainage it was conducted using a standard specimen size, which is three times greater in volume than that of a smaller sized sample. This is, perhaps, the reason for the measured volume change in experiment TWM-400 being smaller than those recorded in the TWL-400 and TWS-400 experiments.

The second possible explanation concerns the structure of the material. As presented in Chapter Four, the SEM results indicate that both TWL and TWS samples contain high concentrations of scaly fractures formed by locally oriented platy clay particles. Considerably fewer scaly fractures were observed in the TWP and TWM samples. When the TWL and TWS specimens were subject to an isotropic consolidation, the confining pressure may have caused preferential closures of the scaly fractures and consequently increased volume change.

In the TWP-400 experiment the majority of the volume change occurred at the beginning of consolidation with little dissipation of the pore fluid pressure. The mean effective stress did not increase as the pore fluid drained out of the specimen. As described in section 5.2.3, in those experiments without using side drainage, only one end of the specimens was open for fluid drainage and the undrained pore fluid pressure at the

opposite end was taken as the pore fluid pressure prevailing in the specimen. Because the material is highly impermeable the soil fabric may have acted as a discontinuity to the fluid flow, so that the two ends of the specimen could not communicate and the pore fluid pressure at the undrained end remained unchanged as pore fluid was expelled from the drained end. Only when the head difference between two ends of the specimen became sufficient would pore fluid pressures at the undrained end show a response to fluid drainage.

A change in gradient, at a mean effective stress of 40 kPa, is seen in the consolidation path of experiment TWM-400 in the $v\text{-ln}p'$ plot (Figure 5.4.57). This is usually an indication of the pre-consolidation pressure. However, given the geological history of the scaly clay and its highly weathered state, it is more likely that the pre-consolidation pressure indicated is not real but a result of the change in soil structure induced by weathering. If it were real, a similar pre-consolidation pressure should have been detected in the other three horizons because they represent less than 1.5 m difference in burial depth.

The consolidation data of the Taiwan experiments fail to provide adequate information of how weathering affects materials because the use of side drainage and the effect of very low permeabilities cause unavoidable inconsistencies in the experiment data set. In order to gain a better understanding of the effect of weathering on material behaviour, the undrained deformation characteristics have also to be taken into account.

5.5.2.2 Undrained triaxial deformation

Experiments on least and slightly weathered samples

In spite of small differences caused by sample variability, the two groups of experiments exhibit remarkably similar stress path patterns, both being a typical heavily overconsolidated, structured soil (Figure 5.5.5). The paths rise vertically showing that pore fluid pressure generation is restricted during the onset of undrained deformation and then swing to the right as the rate of dilation increases. In Figure 5.5.13 the stress paths for the five experiments are plotted together. The stress path for experiment TWL-400 matches those of TWS-100 and TWS-200, and the stress paths for TWL-400 and TWS-400 follow almost exactly the same track until the sample dilation rates increase. Subsequently the TWL-400 path lies slightly above the TWS-400 path.

The same comparison was done with the stress-strain curves (Figure 5.5.14). Again, the TWL-400 and TWS-400 curves are almost identical until a strength drop occurred in TWS-400 sample at about 2.5% axial strain. This indicates that both TWL and TWS samples are representative of virtually identical materials. Sample TWS-400 happened to have a local weakness which causes the subsequent difference.

In the analysis of the Barbados clay results the Skempton pore pressure parameter A was used as an indicator of the state of consolidation. To facilitate comparison of the results the Taiwan data were treated in a similar manner. Both the TWL and TWS experiments all ended up with A values in the range 0 to 0.1 (Figures 5.5.15 & 5.5.16), which according to Table 5.5.1 (Lambe & Whitman, 1979) are values typical of heavily overconsolidated materials. There is a slight difference between TWL-100 and TWS-100 in that experiment TWS-100 appears to generate more pore fluid pressure at the beginning of the undrained shear. This may be simply due to sample variability.

None of the five experiments attained the constant stress condition characteristics of the ultimate failure state. At the end of each experiment deviatoric stresses were still increasing as the samples were straining indicating that the critical state was not achieved.

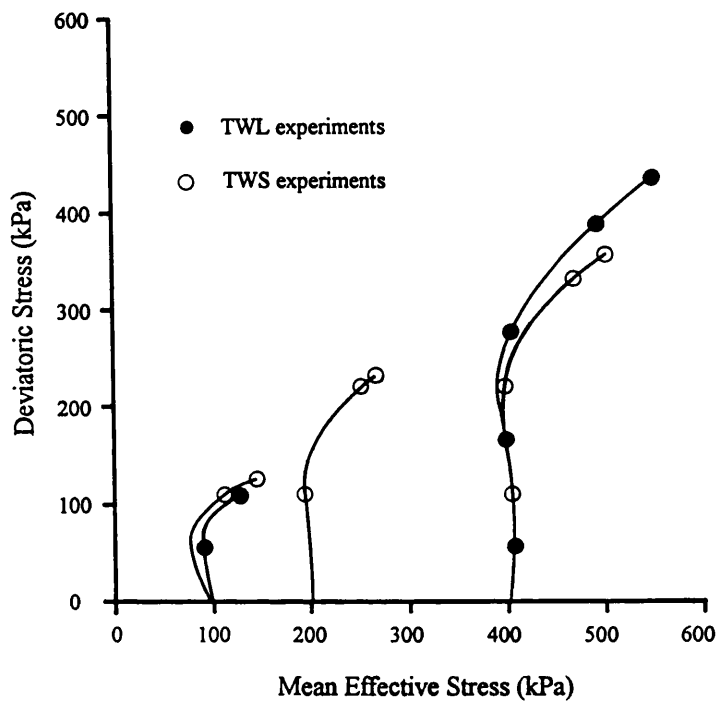


Figure 5.5.13 Stress paths for both TWL and TWS experiments

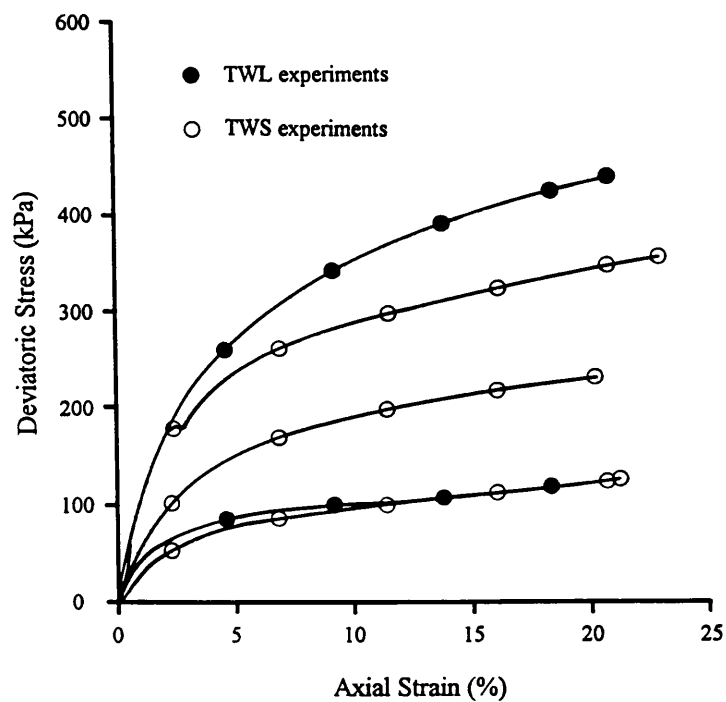


Figure 5.5.14 Stress-strain curves for both TWL and TWS experiments

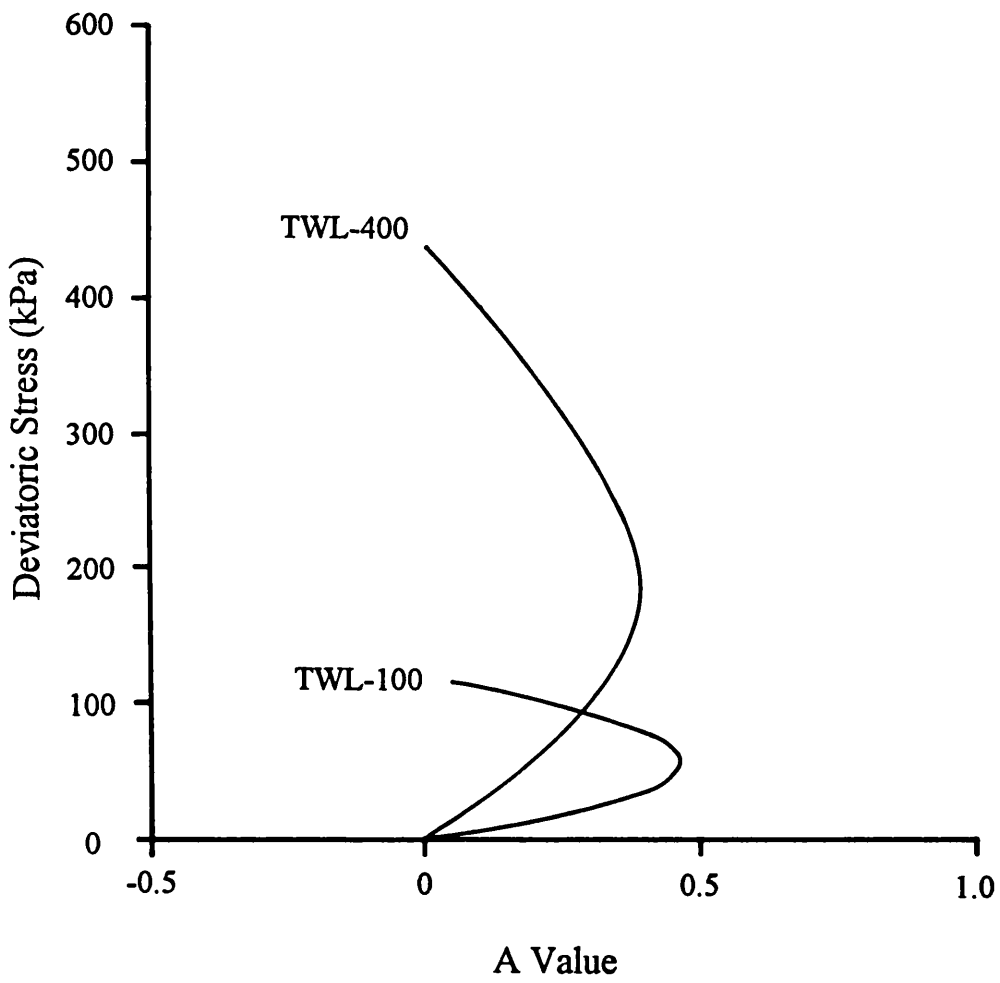


Figure 5.5.15 Deviatoric stress-Skempton pore pressure parameter A relationships for TWL experiments

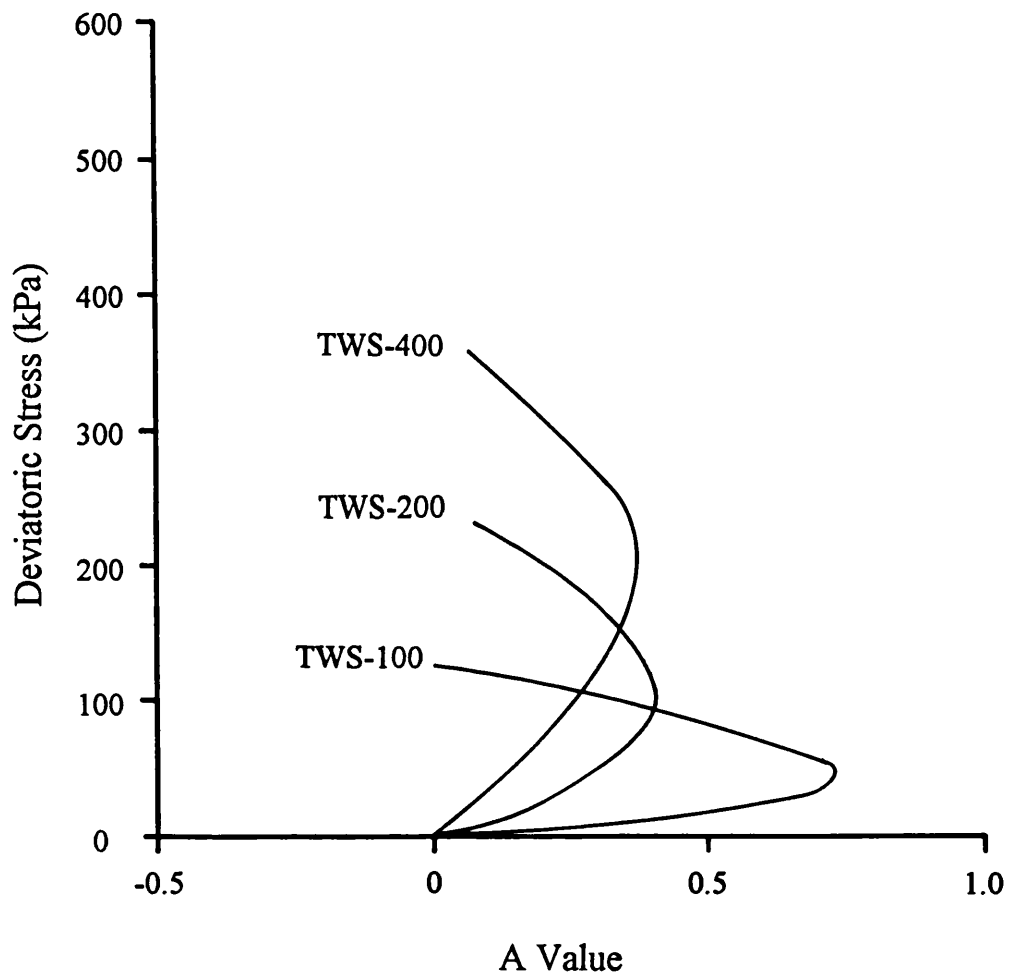


Figure 5.5.16 Deviatoric stress-Skempton pore pressure parameter A relationships for TWS experiments

Experiments on partially weathered samples

Less pore fluid pressure generation during undrained triaxial deformation was recorded in the four TWP experiments which caused the stress paths to be inclined towards larger mean effective stresses indicating that the samples started to dilate from the outset of undrained deformation. This is similar to the behaviour observed in the BDP experiments discussed earlier (section 5.5.1.2). The two highest pressure experiments, TWP-400 and TWP-400a, exhibited a slight difference in their stress paths (Figure 5.4.53). A larger pore fluid pressure response to undrained deformation was recorded in the TWP-400a experiment (Figure 5.4.55) causing its stress path to lie to the left to the stress path of the TWP-400 experiment (Figure 5.4.53). However, the two stress paths ended up at more or less the same failure envelop suggesting that the difference in pore fluid pressure generation in the two experiments may be due simply to sample variability. The stress-strain curves show that the samples were still strain hardening when the experiments were terminated indicating that neither sample had reached the critical state/ultimate failure state.

The values of the Skempton pore pressure parameter A for the TWP experiments (Figure 5.5.17) are of similar magnitude to those recorded during the TWL and TWS experiments. This suggests that the TWP material is also heavily overconsolidated under the pressure range used for the laboratory testing.

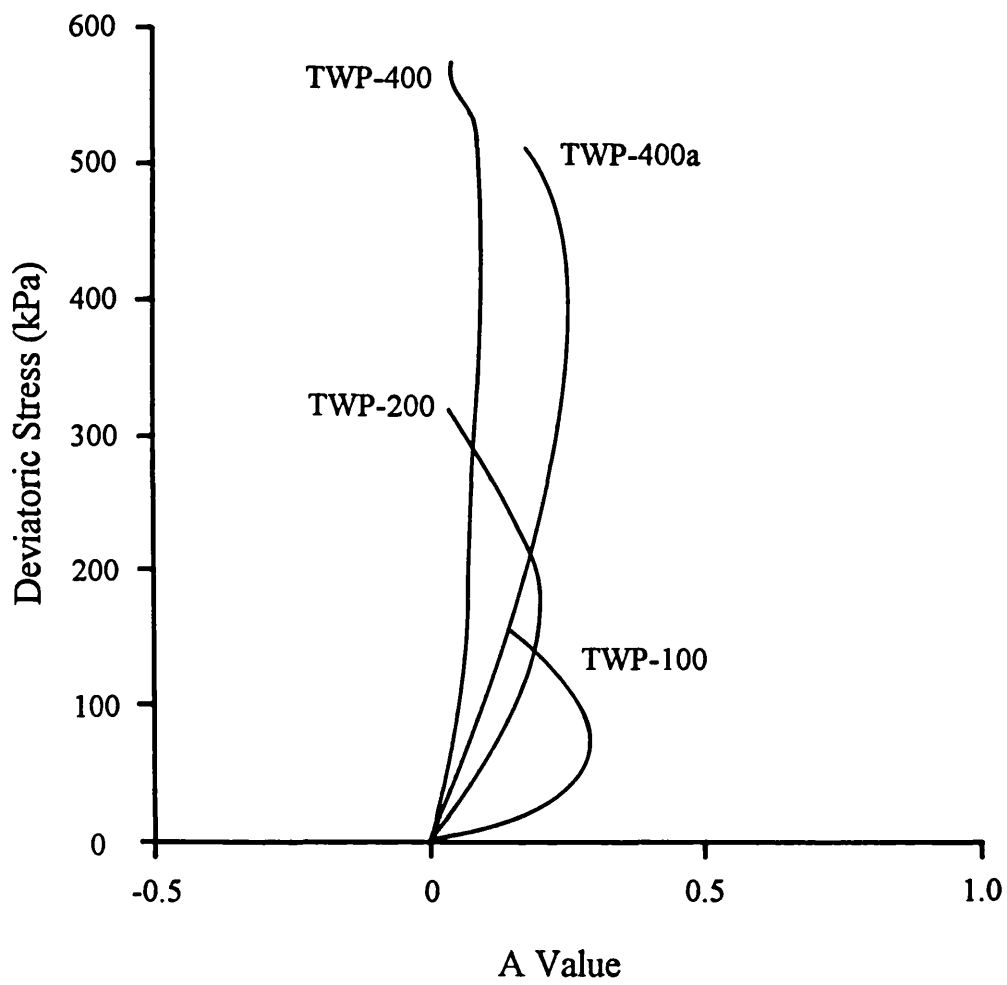


Figure 5.5.17 Deviatoric stress-Skempton pore pressure parameter A relationships for TWP experiments

Experiments on most weathered samples

The stress paths for the TWM-100 and TWM-200 experiments were very similar to those for TWP-100 and TWS-200 experiments respectively. The paths rise vertically towards the failure envelop until a certain point beyond which the samples started to dilate (Figure 5.4.59) suggesting that the TWM-100 and TWM-200 samples were overconsolidated. Unlike the two lower pressure experiments, the TWM-400 sample did not exhibit any dilation behaviour but showed clear peak and residual strengths during the undrained loading (Figure 5.4.58, 59). This suggests that the TWM-400 sample was not as heavily overconsolidated as the TWP and TWS materials.

Inspection of the deviatoric stress/A value plot of the TWM experiments (Figure 5.5.18) also reveals that both TWM-100 and TWM-200 samples are overconsolidated because their A values at failure are between 0.1 and 0.2 whereas TWM-400 sample has an A value at failure of 0.4 indicating that it is moderately overconsolidated.

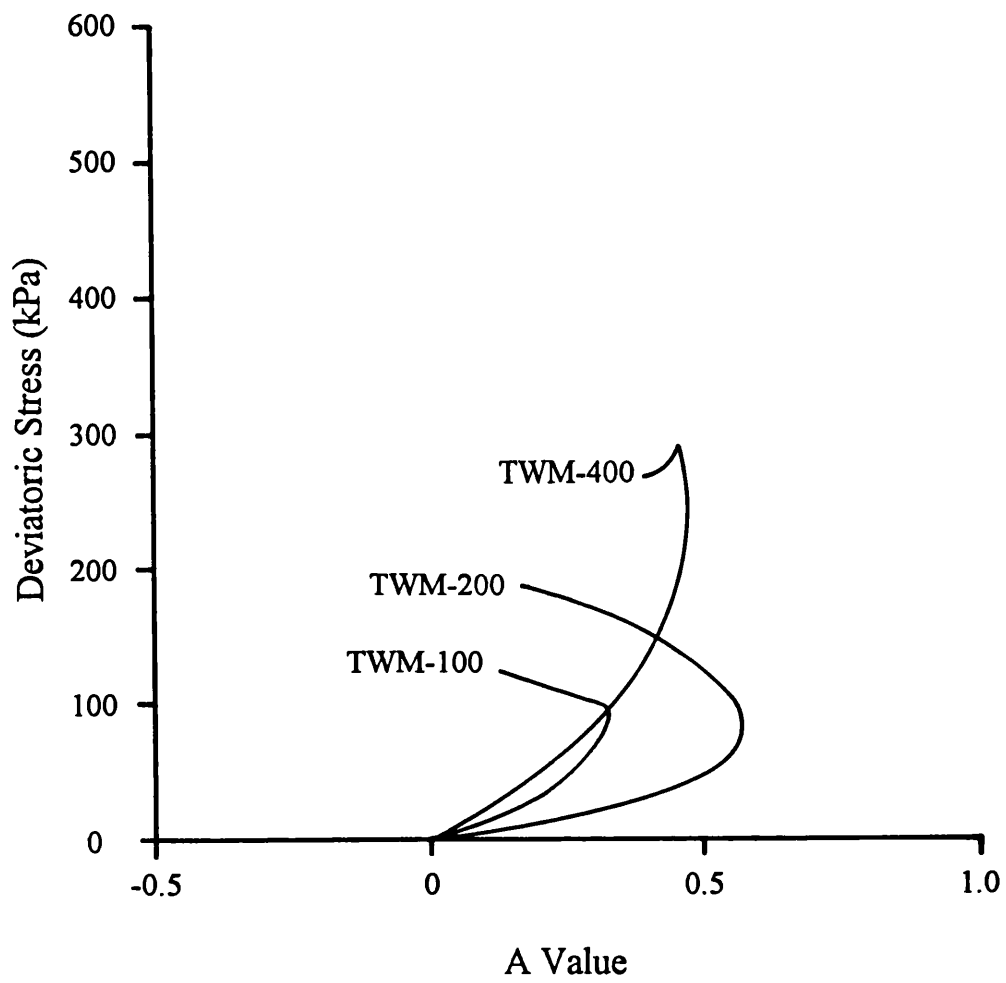


Figure 5.5.18 Deviatoric stress-Skempton pore pressure parameter A relationships for TWM experiments

5.5.2.3 Summary of the mechanical behaviour of the Lichi Mélange scaly clay

The change in undrained loading behaviour of the Lichi Mélange scaly clay between different weathering horizons is similar to that observed for the Joe's River Formation scaly clay. Generally speaking, the results of the TWL and TWS experiments show characteristics of heavy overconsolidation; that of TWP experiments heavy to moderate overconsolidation with characteristics of both clay and sand; and that of TWM experiments moderate to light overconsolidation. In terms of the shear resistance, the TWL and TWS samples have similar magnitude of strength. The strength increases when the material turns into its partially weathered state. This is believed to be due to weathering restructuring the material leading to the absence of the original scaly surfaces, which act to facilitate the development of shear failure plane and increased grain size. An increase in shear resistance is the result. If weathering continues, the restructuring propagates throughout the entire mass which effectively remoulds the material and consequently the strength of the material decreases appreciably.

Chapter Six: Discussion and Conclusions

6.1 Introduction

In the preceding chapters the background of this research has been described and all the data have been introduced. These data are discussed and their significance with respect to the objectives of the present research are considered in this chapter. Through this discussion of physical-chemical characteristics and mechanical behaviour, it is hoped that a better understanding of the influence of tropical weathering on the deformation characteristics of scaly clays will be gained. In sections (6.2) and (6.3) the discussion is restricted to the comparison between the two locations in the sense of their physical-chemical characteristics and mechanical behaviour respectively, whereas in section (6.4) a summary of the similarities and differences with respect to the effects of weathering on the scaly clays from the two study localities is made and some conclusions are given. The chapter is ended by extending the discussion and conclusion to consider the evolution of the badlands topography in tropical scaly clay mélange terrains.

6.2 General discussion on the physical-chemical characteristics

6.2.1 Porosity

The gradually increasing porosity throughout both the Barbados and Taiwan profiles (Table 6.2.1) agrees with the suggestion of many other workers (Terzaghi, 1936; Chandler, 1969, 1972; Balasubramaniam *et al.*, 1978). The increase in pore volume is a consequence of the physical-chemical weathering processes as well as a change in mean effective stress. According to the Terzaghi's consolidation theory, the volume of a soil mass is solely a function to the effective stress it is subject to (Appendix I). A decrease in the effective stress will lead to an increase in the volume of the soil mass due to elastic rebound (swelling) of the material. In the complex weathering system, decrease in effective stress is caused by the removal of overburden resulting from the severe surface erosion and frequent landslides which characterise the scaly clay terrains in both study areas. Additionally, the study materials have experienced intensive physical-chemical weathering processes which will have resulted in modification of the material's structure. These processes play an important role in promoting volume change and fabric alteration of the clay materials.

Low permeability is one of the characteristics of clay rich sediments. In material such as the studied scaly clays the penetration of the surface water is therefore restricted to a shallow zone which also experiences heavy evaporation, especially in low latitude regions. As a consequence, materials at shallow depth experience a high frequency of alternate wetting and drying. It was described in Chapter Two that alternate wetting and drying will cause expansion and contraction resulting in the development of considerable local stresses within the rock. The rock responds by breaking along lines of weakness. The breakage does not cause the volume of mineral grains to increase, but leads to an increase in the pore volume, and therefore, the bulk volume of the rock increases. This is believed to be a very important mechanism which promotes an increase in the void space of the material in a weathering profile (Trudgill, 1983; Chesworth, 1992). An increase in moisture content and a decrease in bulk density are the result (Table 6.2.1).

The increase in porosity through the Taiwan profile is not as large as recorded in the Barbados profile (Table 6.2.1). The total increase in porosity recorded for the Lichi profile from the bottom horizon to the most weathered horizon is from 20% to 25.5%. The small increase in pore volume leads to a small increase in the water content, from 9% to 13%, and a insignificant decrease in the bulk density, from 2.37 g.cc^{-1} down to 2.19 g.cc^{-1} . Although these figures are not very large, they are significant. As mentioned above the increase in pore volume is a result of both the reduction in effective stress due to the removal of the overburden and more importantly the structural modification by the weathering processes. The small pore volume change of the Taiwan material is probably because that the Lichi Mélange scaly clay is less permeable than the Joe's River Formation clay. This can be seen when conducting triaxial consolidation tests. Most of the Taiwan samples had to either use the side drainage technique or reduced sample size, or both, to complete laboratory consolidation in a reasonable time period. The extremely low permeability of the material seems to protect the underlying layers from weathering by restricting the penetration of surface water to a very shallow depth. This, in turn, restricts the disturbance and alteration resulting from water migration. Less structural alteration and a smaller increase in the pore volume is the result.

Leaching is also an important process causing an increase in pore space. Soluble and, perhaps, very fine grains are taken away by moving pore fluid, resulting in a decrease in volume of the mineral phase. Thus, there is a relative increase in the volume of the pore phase. Leaching seems, however, to be restricted to a very shallow depth in mudrocks by their low permeability because it requires fluid migration if it is to have a significant impact. Leaching is therefore of only minor importance as a contributor to pore enlargement in these cases.

Table 6.2.1 Summary of the porosity, natural water content and bulk density of the test materials

Sample location	Degrees of weathering	Porosity (%)	Moisture content (%)	Bulk density (g.cc ⁻¹)
Barbados Joe's River Formation	Least weathered	32.2	22.0	2.10
	Partially weathered	38.4	29.6	2.04
	Most weathered	47.7	32.3	1.91
Taiwan Lichi Mélange	Least weathered	20.0	9.0	2.37
	Slightly weathered	20.0	9.3	2.36
	Partially weathered	22.5	10.5	2.28
	Most weathered	25.5	12.9	2.19

There is hardly any change in porosity, moisture content and bulk density observed in the bottom two layers of the Taiwan profile. It seems that the changes start to occur at a specific depth of around 1 meter. This may indicate that there is a critical depth (1 m to 1.5 m) below which the influence of the surface conditions can not normally penetrate, and therefore samples from below that depth will have very similar physical properties. Above the critical depth the availability and the movement of water start to increase, thus, enlargements of the pore space and changes to the fabric occur.

In both the Joe's River Formation and Lichi Mélange scaly clays very little change in bulk chemical composition and mineralogy has occurred within the weathering profiles examined except for the ferric/ferrous iron ratio. Therefore it is difficult to determine the extent that the increase in pore volume is independent on chemical weathering. Particularly, as there is no evidence indicating that the change in pore volume of the scaly clay is generated from change in the bulk chemical composition and/or alteration of the mineralogy.

There is some mineralogical alteration observed in the upper parts of the Lichi profile. Kaolinite is absent in the lower three layers (TWL, TWS & TWP) but starts to appear in the most weathered horizon (TWM), and in the top layer (TWT) the kaolinite peak becomes stronger and the mica-2M and chlorite peaks become much weaker in the X-ray diffraction traces (Figures 4.3.12 to 4.3.16). This mineralogical alteration may have exerted certain effects on the increase in the pore volume. However, if weathering causes the formation of this kaolinite, it would make some contribution to the pore enlargement only in the most weathered horizon (TWM) and the very top layer (TWT). The mineralogical alteration will be discussed later this section.

6.2.2 Particle size distribution

The particle size distribution curves for both the Barbados and Taiwan samples indicate a range from clay to fine gravel, which is one of the characteristics of *mélange* sediments. The curves in each case are very similar particularly with respect to the sand and coarser fraction of all horizons (Figures 6.2.1 & 6.2.2). Only minor differences were observed in the clay and silt fraction. This suggests that within the examined profiles weathering does not have a pronounced effect on particle size, with any changes in size restricted to the fine fraction.

It is noted, in both cases, that the particle size distribution data do not show sequential change along the weathering profile. This is best demonstrated in the Barbados material in which the least weathered sample (from the bottom of the profile, BDL) has highest amount of clay sized particles, whereas the partially weathered sample (the intermediate horizon, BDP) contains lowest proportion of clay sized particles. The particle size distribution curve of the most weathered sample (BDM) lies in-between the other two, closer to that of the least weathered sample. This may be explained by the formation of aggregations of fine particles during the onset of weathering. Similar aggregation has been observed in many other cases in tropical region (Dixon & Robertson, 1971; Wallace, 1973; Pandian *et al.*, 1993a 1993b). Fine particles aggregate to form larger sized grains causing a reduction in the proportion of clay fraction and an increase in the silt fraction. This is also supported because all three curves exhibit great similarity in the sand and larger sized portion. This suggests aggregations are pronounced only for fine particles (clay size) but not for large particles (sand size) because the suction pressure, which draws the fine particles together, is restricted by the resulting grain size.

The decrease in the content of clay sized particles during weathering is all the more surprising because the effect of alternative hydration/evaporation and the associated local stress change, might be expected to physically break grains leading to an increase in the fine fraction. The increase in fine grained content of the most weathered samples may be a result of this process.

All five particle size distribution curves of the Taiwan samples fall into a very narrow band (Figure 6.2.2). It is difficult to say definitely that the variation seen in the particle size distribution is a consequence of weathering because it may be simply due to sample variability considering that *mélange* sediment is such a mixture of a variety of different types of rock fragments and different sized particles. However, the curves of TWL, TWS and TWT have almost exactly the same distribution across the whole range of sizes and

differ from the TWP and TWM curves which are also similar with coarse particles. This non-sequential change may also be due to particle aggregation similar to those recorded in the Joe's River Formation clay although sample variability cannot be ruled out. Alternate wetting and drying is the most important mechanism for particle aggregation to occur (Pandian *et al.*, 1993a), and the extremely low permeability reduces the frequency. Therefore, particle aggregation should not be as pronounced as seen in the Barbados material.

The very top layer of the Taiwan profile does not necessarily have to be residual but possibly a temporary accumulation of sediments transported from the upper part of the slope by surface run-off. Consequently, the representativeness of this part of the weathering profile is more doubtful. The change seen in the particle size distribution curve of TWT may not be a consequence of weathering.

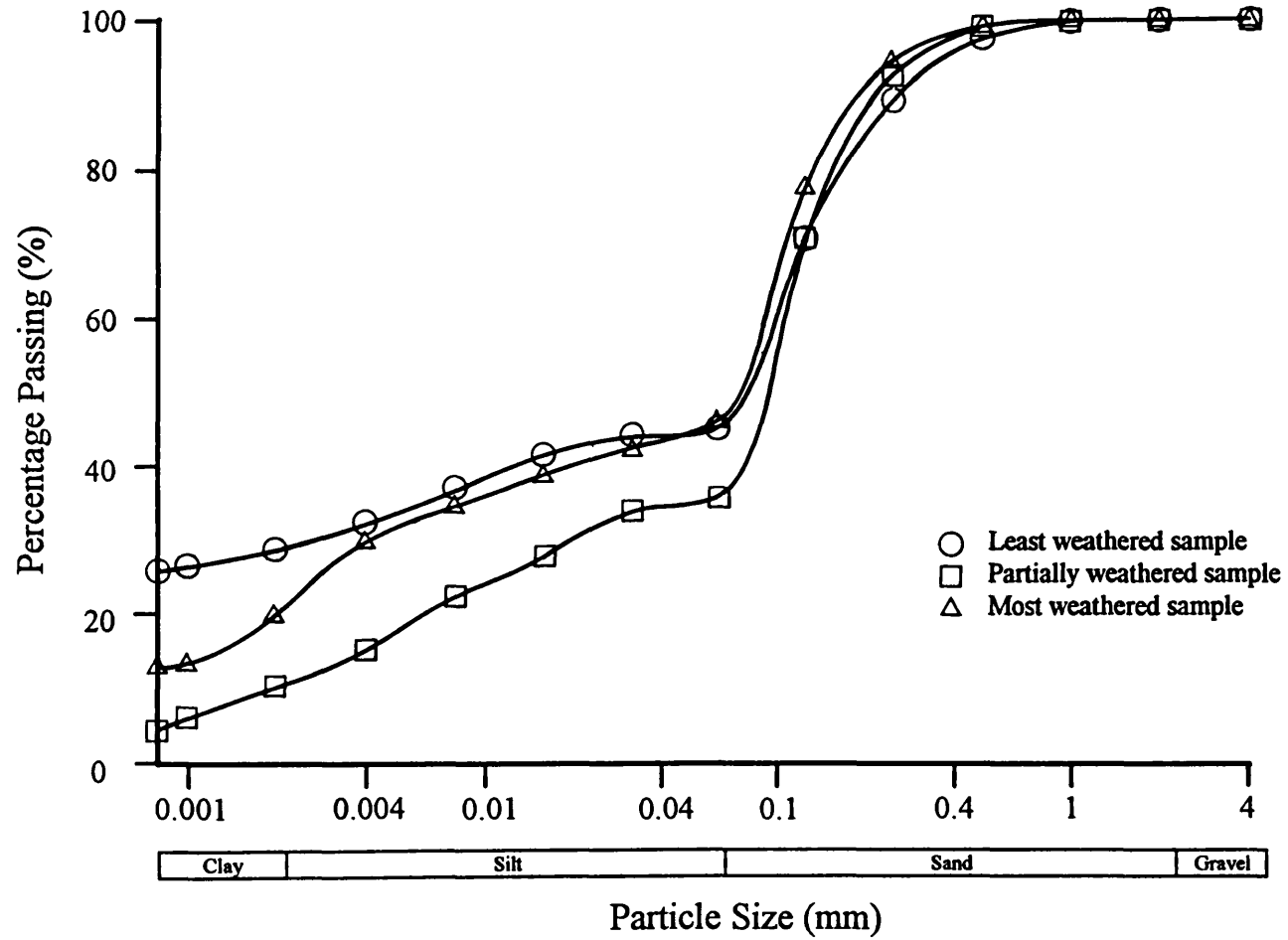


Figure 6.2.1 Particle size distribution curves for the Barbados samples

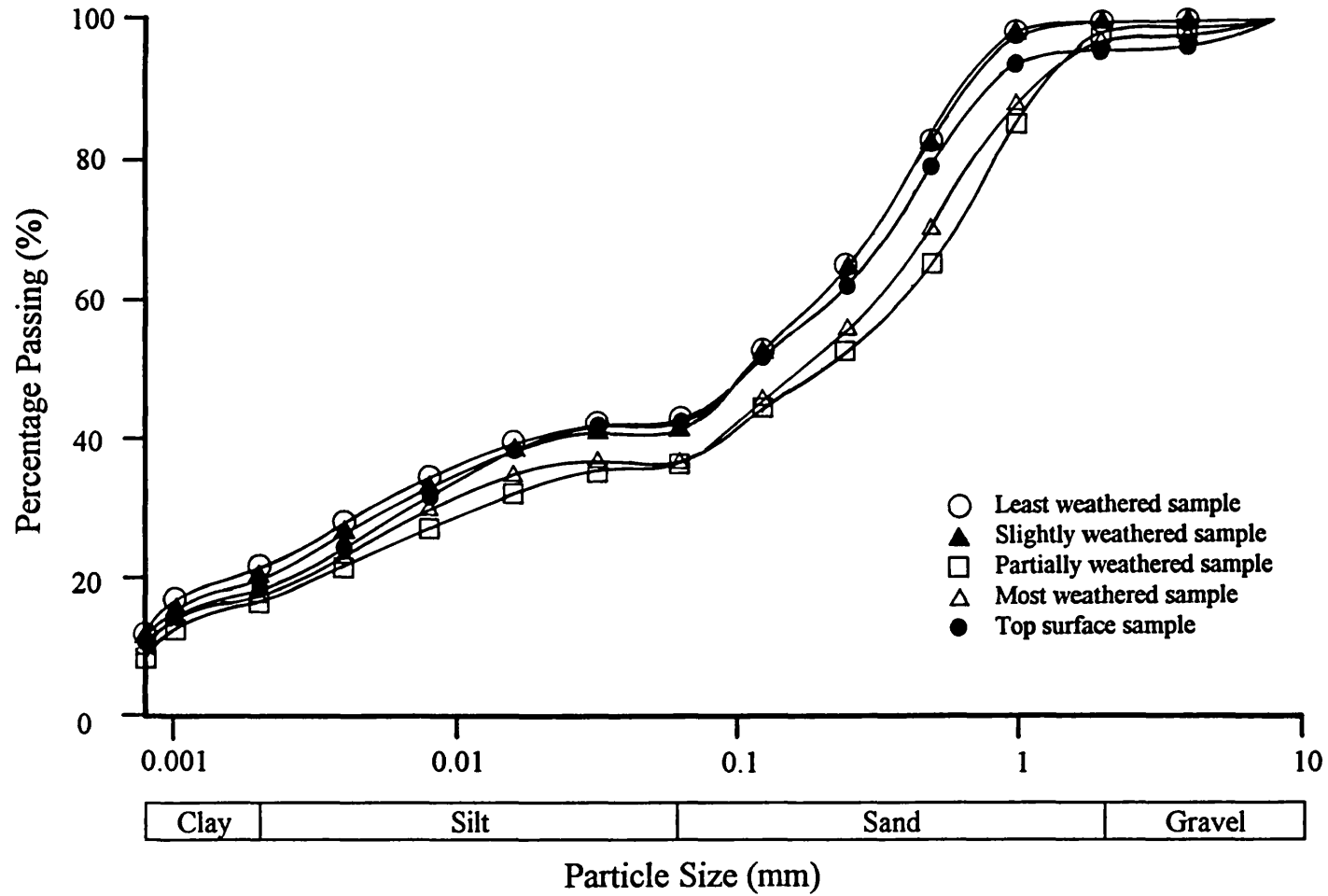


Figure 6.2.2 Particle size distribution curves for the Taiwan samples

6.2.3 Atterberg limits

Atterberg limits (liquid limit, plastic limit and plasticity index) reflect the mineralogy of a soil (Skempton, 1953). If soil samples have a similar mineralogical composition, their plasticity index properties will then be largely dependent on the particle size present in the samples (Lambe & Whitman, 1979). This is because it is the surface area that determines the extent to which water will bond to the surface of particles. The surface area of unit mass of a soil with more fine particles will be greater than that for a soil with larger particles. As a consequence, the one with the greater surface area will have more water attached to the particle surfaces at a given state, and thus will exhibit higher Atterberg limits.

These typical characteristics are demonstrated by the index property data of the studied materials. In the Barbados material all three horizons appear to have very similar mineralogical composition but slightly larger variations in their particle size distribution. Both liquid limits and plastic limits of the samples agree with the particle size distribution curves exhibiting a non-sequential change along the weathering profile. The partially weathered sample which contains a smaller amount of clay has liquid and plastic limits of 29.3% and 19.4% respectively, whereas the other two samples with similar particle size distribution curves have liquid and plastic limits of around 40% and 20% respectively. All three samples have a similar plastic limit of about 20%, and any differences in plastic limit may pertain to sample variability. However, it is obvious that the partially weathered sample has a distinctively low value of liquid limit, and this is thought to be a consequence of the low content of clay sized particles.

The Lichi M \acute{e} lange clays, on the other hand, exhibit similar particle size distribution curves but seem to have a larger variation in their mineralogical composition along the weathering profile. It is noted that the partially weathered sample exhibits a highest liquid limit of 35% (Table 6.2.2), and the top surface material shows a lowest value of 27% (Table 6.2.2). The former case may be explained as the sample having the strongest inter-layered smectite-mica peak at $7^{\circ} 2\theta$, indicating a greater capability for absorbing water and the latter case is, perhaps, a result of the presence of kaolinite with its low capacity for water absorption (Figures 4.3.12 to 4.3.16). Nevertheless, these variations in the index properties are small. This indicates that although there is some alteration in the mineralogy through the profile the change is responsible for only small variations in the plasticity index of the Lichi clays.

Table 6.2.2 Liquid limits, plastic limits and plasticity index of samples examined

Sample locations	Degrees of weathering	Plastic limits (%)	Liquid limits (%)	Plasticity index (%)
Barbados Joe's River Formation	Least weathered	22.8	42.8	20.0
	Partially weathered	19.4	29.3	9.9
	Most weathered	20.3	40.3	20.0
Taiwan Lichi Mélange	Least weathered	19.2	32.2	13.0
	Slightly weathered	19.3	31.5	12.2
	Partially weathered	20.3	34.9	14.6
	Most weathered	20.1	31.0	10.9
	Top surface layer	18.4	27.3	8.9

6.2.4 X-ray diffraction study

Generally speaking, in both cases the mineralogical alteration caused by chemical weathering is not pronounced. No formation of new mineral is recorded in the Barbados samples and only small amount of kaolinite may have been formed during weathering in the Taiwan profile. The X-ray diffraction data of the Lichi clay show that kaolinite starts to appear from the TWM horizon upwards (Figures 4.3.14, 4.3.15 & 4.3.16). The intensity of the kaolinite peak reaches its strongest at the surface layer (TWT). As mentioned in Section 2.3.3 kaolinite is one of the most common clay minerals and can be formed from any silicate rock or mineral if suitable conditions are sustained for a sufficiently long period of time (Weaver & Pollard, 1975). The XRD data suggest that weathering promotes the formation of kaolinite. However, the generally consistent mineralogy within the weathering profiles seems unusual because chemical weathering is expected to be most active in places where temperatures are high and water is readily available. The study areas, Barbados and southern Taiwan, should therefore experience a pronounced rate of chemical weathering and more changes in mineralogy might have been expected at shallow depth.

There are a few possibilities to explain the lack of change in mineralogy. First, the mineral composition of the examined clays may have been such that they were stable in the near surface environments. As mentioned in section 2.2, chemical alteration occurs when materials are not chemically in equilibrium with the new set of environmental conditions. Chemical weathering will, therefore, not be so significant if the original material is chemically stable. Secondly, the investigated materials are clay dominant sediments which are highly impermeable. The low permeability restricts the penetration of the surface water into the subsurface horizons as well as the fluid migration within the

material, therefore, chemical alteration is not as pronounced as expected. Thirdly, the study areas are highly dynamic where the rates of surface erosion and mass wasting processes are so high that the time between exposure of fresh clay to chemical weathering and removal from the surface may not allow appreciable mineralogical alteration to occur.

It is noticed in the XRD data for the Joe's River Formation samples (Figures 4.3.4, 4.3.5 & 4.3.6) that there is an apparent reduction in the intensities of the quartz & mica peak at $27^\circ 2\theta$, mica-2M peak at $9^\circ 2\theta$ and inter-layered smectite-mica peak at $7.5^\circ 2\theta$. This may suggest that chemical weathering does change the mineralogy in terms of concentration. There are two possibilities to elucidate this. One is that the weathering changes one phase to another which is already present in the material. It is difficult to detect this from the XRD traces without accurately measuring the quantity of each mineral present in the sample mixture. The second possibility is that it is usual for chemical weathering to alter the crystal structure of clay minerals converting the minerals into a non-crystalline form, known as amorphous clay, which does not give X-ray reflections and therefore can not be detected in the XRD analysis. However, the X-ray traces for the three Barbados samples are in general very similar suggesting that changes in concentration of any of the phases is generally small.

There are some quantitative variations in the intensities of chlorite and mica-2M peaks at 6° and $9^\circ 2\theta$ respectively recorded in the Lichi samples (Figures 4.3.12 to 4.3.16). These two peaks reach their highest intensities at the TWP horizon. This should not be interpreted as a consequence of weathering because mica and chlorite are not usually products of weathering (Deer *et al.* 1966). In addition, the other chlorite and mica-2M peaks do not exhibit any great change in their intensities. This indicates that the actual amount of mica and chlorite have not increased during the early stage of weathering but is simply diffracting more strongly at those particular angles for some reason.

6.2.5 Chemical analyses

In neither the Barbados nor the Taiwan samples has any correlation been detected between the bulk chemical composition and the depth from which the samples were extracted (Tables 4.3.4 & 4.3.8). The ferrous/ferric iron ratio in each case does, however, correlate nicely with depth in the weathering profile indicating that oxidation gets more severe towards the surface (Table 4.3.4 & 4.3.8). Similar correlations have been reported by other workers (e.g. Chandler, 1972). This is not surprising because the

availability of atmospheric oxygen (i.e. O₂) decreases downwards, and consequently, oxidation gradually decreases with increasing depth.

The ferrous/ferric iron ratio of TWL and that of TWS are very similar suggesting that these two horizons have experienced similar degrees of oxidation. The indication is that there is a critical depth below which the influence of surface conditions can not normally reach. This critical depth is dominantly controlled by the permeability of the material. The lower the permeability the material has, the shallower this depth will be. This also indicates that TWL and TWS are virtually the same and have not suffered significant weathering.

6.2.6 Micro-fabric study

The micro-fabric studies of the both clays indicate that weathering progressively destroys the scaly fabric. Scaly surfaces are a result of platy particles with a locally preferred orientation (Plate 6.2.1). This preferred orientation is restricted within a very thin layer. In places between scaly surfaces the particles are still randomly oriented (Plate 6.2.2). These scaly textures are thought to be formed during diagenesis and subsequent deformation of the sediment (Page & Suppe, 1981; Barber *et al.*, 1986). The effect of weathering is essentially to homogenise the materials and to modify the microstructure of the materials (Barden, 1972b). As one can expect, fluid migration (including water and air) within a low permeability material is largely controlled by the structure of the material and mainly through flow through discontinuities and fractures (Lambe & Whitman, 1979). Therefore, the surfaces of these fractures would be more heavily affected by the fluid flow than anywhere else. It can be postulated that when weathering commences more fluid flows through these fractures leading to a disruption of the particle arrangement at the fracture surfaces. This will result in a rearrangement of the particles which makes the original preferred orientation of platy particles become more randomly oriented. Thus, the scaly fabric is destroyed. This is a progressive and continuous process. In partially weathered samples some preferred orientation still exists (Plate 6.2.3), but this is much less obvious when compared with the fabric of the least weathered material.

It is also noted from the micro-structural study that the pore structure and volume changes and increases as weathering progresses (Plate 6.2.4). This has been discussed earlier. The SEM photographs provide a visual image demonstrating how the pore enlargement and alteration proceed. During the onset of weathering structural changes

mainly occur along the scaly surfaces where particles had preferred alignment. There is no remarkable change in structure or change in pore size away from the scaly surfaces. As weathering continues (i.e. more water and air available and more active) the pore enlargement progressively prevails until the entire rock is completely affected.

Micro-structural studies of the Taiwan samples reveal that the original preferred orientation of the clay particles has been little modified by weathering. The particles have been re-arranged to some extent. This conforms with the porosity data. There is, after all, only a 5% difference from the least weathered to the most weathered state.

As described previously this insensitivity of the fabric to weathering is a result of the extremely low permeability of the Lichi scaly clay sample. Because the material is practically impermeable below a very shallow depth the movement of water beneath that depth is highly confined resulting in very limited soil structure alteration. Therefore, the extent of the modification in fabric in the lower part of the profile is very restricted. Nearer to the surface more pore water becomes free to move which promotes the pores to open and facilitates some re-arrangement of particles.

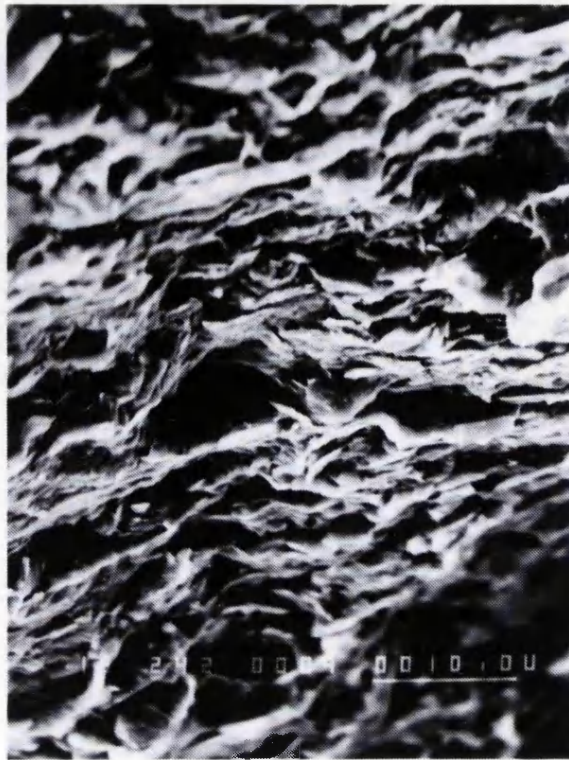


Plate 6.2.1 Photograph demonstrating strongly preferred orientation of clay particles along the scaly surface

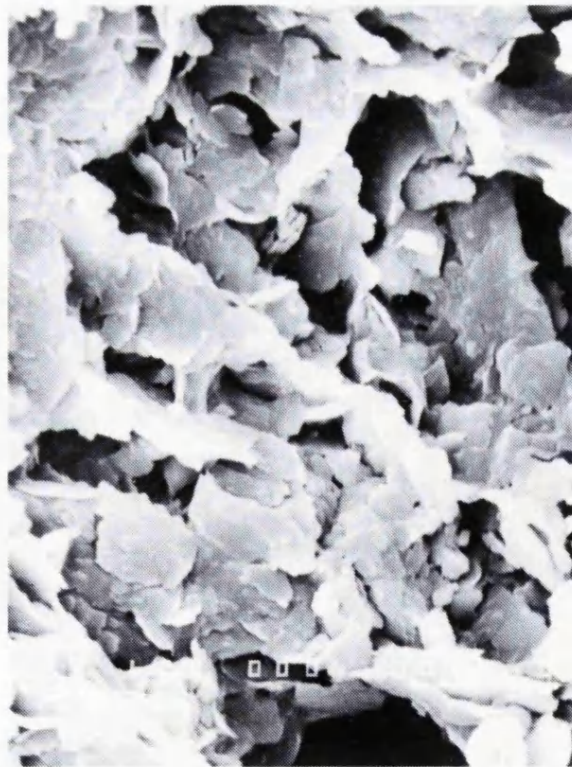


Plate 6.2.2 Photograph showing random arrangement of clay particles away from the scaly surface

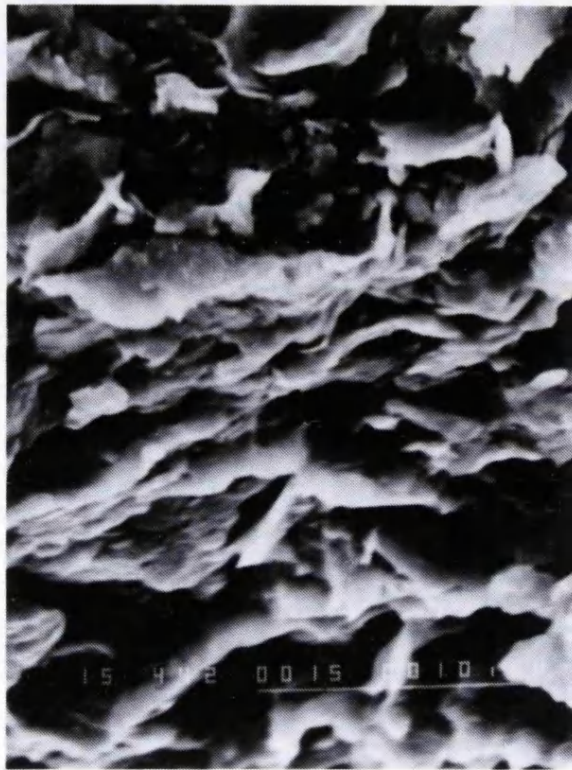


Plate 6.2.3 Photograph demonstrating some original preferred particle orientation in the partially weathered scaly clay

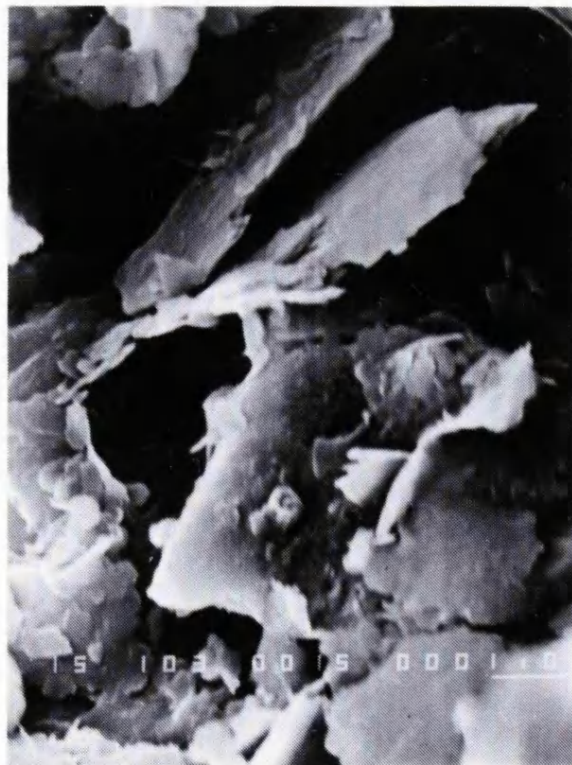


Plate 6.2.4 Photograph demonstrating pore enlargement in the highly weathered scaly clay

6.3 General discussion on the mechanical behaviour

Mechanical behaviour of a soil material is the observed response of the material to change of stress state, and is determined by its inherent properties such as pore volume, particle characteristics and soil micro-structure. If weathering imposes changes in grain size, micro-structure and/or pore volume, as discussed above, then commensurate change in mechanical behaviour should occur.

The geotechnical performance of the studied scaly clays changes remarkably through each weathering profile because the weathering alters the inherent properties of the material. As discussed in Chapter Five, the consolidation behaviour and undrained compression characteristics of the materials exhibit obvious differences for the materials from the different horizons. This section gives detailed discussion of the changes in mechanical behaviour induced by the prevailing weathering processes.

6.3.1 Consolidation behaviour

From the literature survey, it is the considered opinion that both of the unweathered scaly clays are heavily overconsolidated clays which have experienced a much greater stress during their previous geological history. This overconsolidation characterises the behaviour of the least and partially weathered samples where volume changes during laboratory consolidation are small. This can be demonstrated by the consolidation data of the Barbados experiments. Figures 6.3.1 & 6.3.2 are the consolidation paths for the three highest confining pressure experiments of the Joe's River Formation clay. Both BDL and BDP samples appear to have similar consolidation paths with very gentle slopes indicating that they are overconsolidated and the pressure range used in the laboratory testing is far less than their pre-consolidation pressure.

With increased weathering the structure and fabric of the material starts to be modified. Destructuring accompanied by particle re-arrangement propagates from the limited scaly surfaces, and eventually prevailing the entire mass. This completely changes the original structure of the material, and therefore its mechanical performance. The pore volume has been enlarged and the scaly textures have been destroyed and loosened by the weathering processes. Consequently, more volumetric strain is recorded during the consolidation processes resulting in the consolidation paths of the BDM experiments exhibiting greater slope gradients (Figure 6.3.2). This suggests that the most weathered samples are now behaving in a manner similar to a normally consolidated material. The unloading-reloading path recorded during experiment BDM-200 (Figures 5.4.23 & 5.4.26) provides

a good evidence that BDM sample has been effectively remoulded by the weathering processes.

Although both BDL and BDP samples exhibit similar gradients in their laboratory consolidation paths a slightly larger volume change is recorded during the experiment BDP-400 (8.5%) when compared with that for experiment BDL-400 (7%). It was described earlier that weathering would begin at the scaly surfaces and disrupt the preferred orientation of the particles. This disruption may result in a slight increase in pore volume in the vicinity of the surfaces. However, in places away from the scaly surfaces structures still remain unaffected or very little affected and possess overconsolidation characteristics. As a result, the consolidation curves of the BDP samples remain similar in slope to those of BDL samples. The excess volume change recorded during consolidation is likely to be the result of the slight increase in pore space in the vicinity of the scaly surfaces.

It was described in Chapter Five that one of the Barbados experiments was performed using a naturally remoulded sample (BDR-100). A comparison between the undisturbed sample experiments (BDL-100, BDP-100 & BDM-100) and this remoulded clay test (BDR-100) at the same confining pressure is made (Figures 6.3.3 & 6.3.4). The difference between BDM-100 and BDR-100 is most interesting because, as discussed previously, the BDM sample is thought to have been effectively remoulded by the weathering processes and the BDR sample is regarded as a remoulded material (Chapter Five, section 5.4.1.4). It is seen very clearly that the consolidation path for experiment BDR-100 exhibits a completely different form from that of BDM-100 sample (Figure 6.3.3 & 4). The volume change and the slope gradient of the BDR-100 sample are much greater than those of BDM-100 sample suggesting that although the most weathered clay (BDM) has been effectively remoulded by the weathering processes there are still some remnant original soil structure characteristics (e.g. overconsolidation) that exist in the BDM material. A gradual change in gradient can be seen in the four consolidation paths (Figure 6.3.4). This indicates that weathering can be regarded as a remoulding process which is a progressive process and modifies the original soil structure resulting from the diagenesis and compaction history.

The consolidation data of the Lichi clay samples do not illustrate such a good correlation through the weathering profile as those of the Joe's River Formation samples because of the unavoidable inconsistency in the testing procedure due to the extremely low permeability of the material. In the four sets of consolidation data presented in Chapter Five, the volume changes of TWL-400 and TWS-400 samples are larger than those of

TWP-400 and TWH-400 samples. This should not be interpreted as TWL and TWS samples being less stiff and less resistant to consolidation than TWP and TWM materials but may be attributed to the difference in the testing procedure or to the non-uniformity in the sampled material. This has already been discussed in Chapter Five.

From the above discussion it is seen that weathering tends to change scaly clay materials from structured heavily overconsolidated clays to partially remoulded less overconsolidated states by promoting enlargement of the pore space and modifying the internal structure of the material. In the following section the undrained deformation behaviour of the scaly clays from different weathering horizons is discussed. By combining consolidation and shear behaviour a better understanding of the effects of weathering on the material characteristics can be gained.

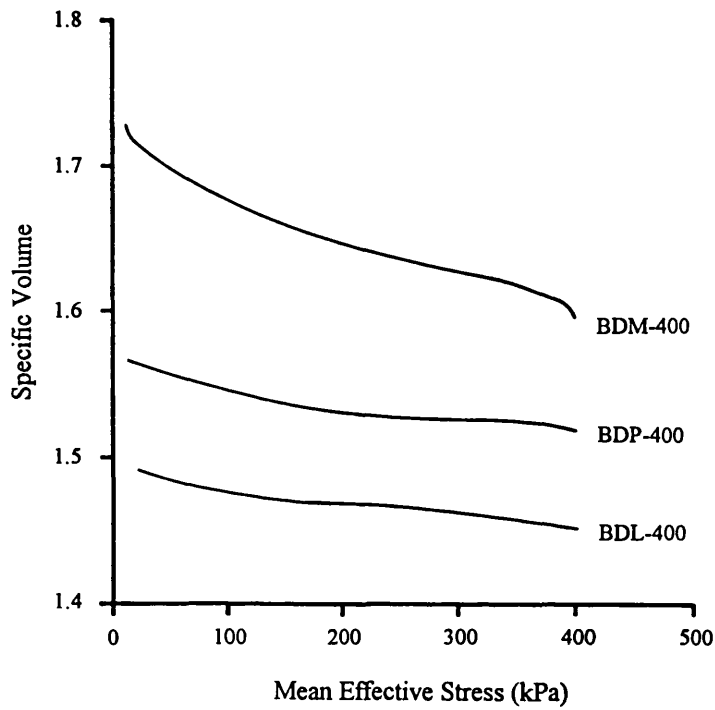


Figure 6.3.1 Consolidation path for experiments BDL-400, BDP-400 and BDM-400 (in linear scale, taken from Figure 5.5.1)

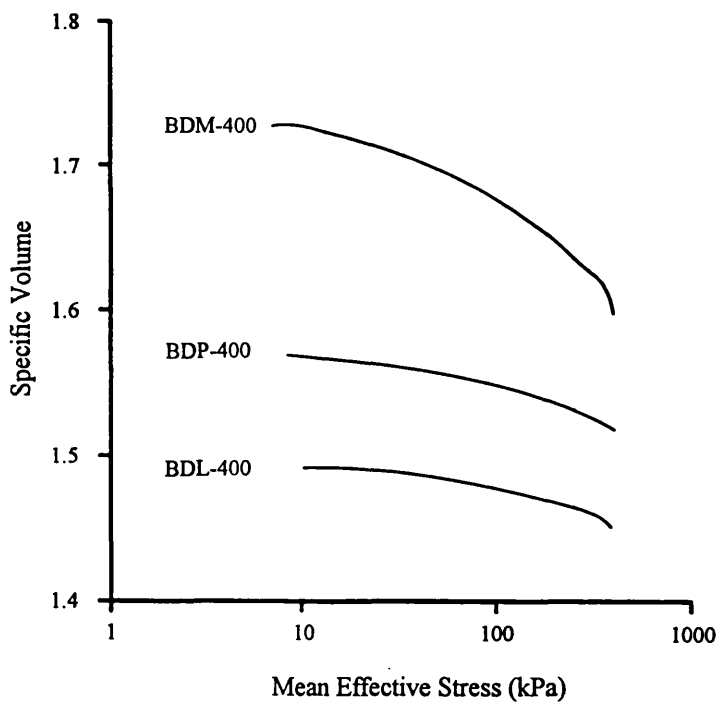


Figure 6.3.2 Consolidation path for experiments BDL-400, BDP-400 and BDM-400 (in logarithmic scale, taken from Figure 5.5.2)

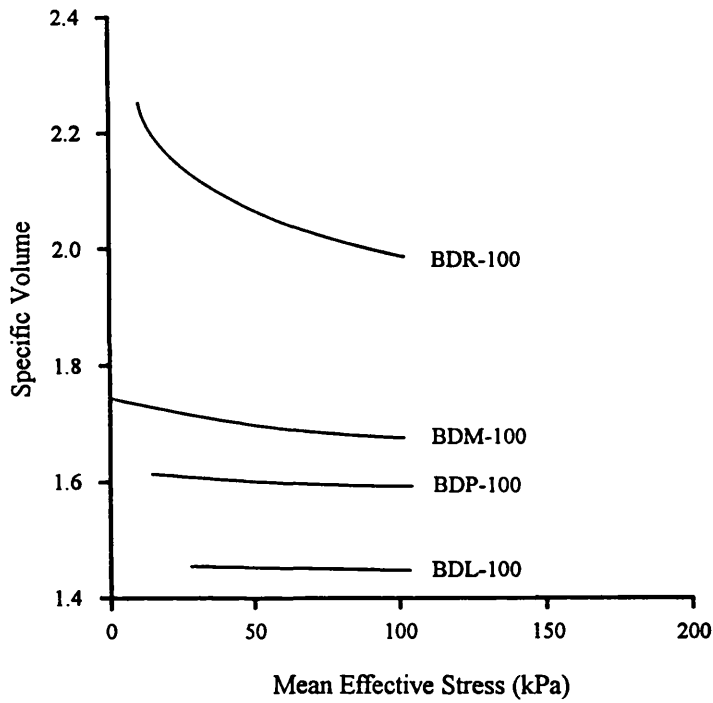


Figure 6.3.3 Consolidation path for experiments BDL-100, BDP-100, BDM-100 and BDR-100 (in linear scale)

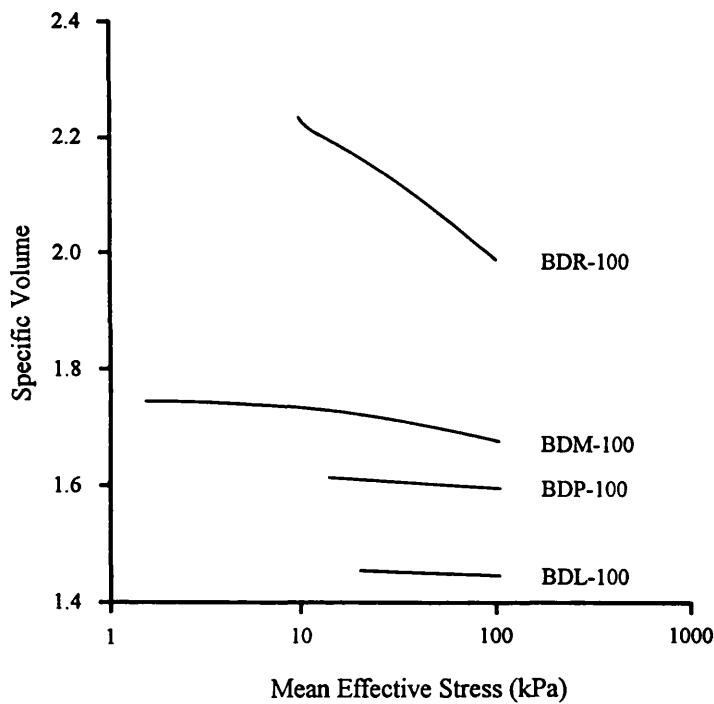


Figure 6.3.4 Consolidation path for experiments BDL-100, BDP-100, BDM-100 and BDR-100 (in logarithmic scale)

6.3.2 Undrained triaxial deformation characteristics

The undrained deformation behaviour for both the Joe's River Formation and the Lichi Mélange clays demonstrates obvious differences with change in the degree of weathering. It is revealed by inspecting the two families of stress path data (Figures 6.3.5 & 6.3.6) that after consolidation was completed although the samples were subject to undrained deformation, the development of pore fluid pressure is restricted, especially in the partially weathered samples. The least weathered samples show significant stiffness at the beginning of loading with the stress path rising almost vertically until a yield point has been reached. The stress paths then curve towards higher mean effective stresses and approach the failure envelope. The restriction of pore fluid pressure development becomes more pronounced in the partially weathered samples resulting in stress paths that slope notably to the right from the onset of axial loading. This indicates that the sample is dilating strongly as it deforms. In contrast, the most weathered materials show stress paths that curve towards lower mean effective stresses resulting from the more appreciable development of pore fluid pressure which indicates that weathering had caused a loss of soil stiffness in the most weathered samples. This reflects the observed change in soil structure with weathering.

As introduced in Chapter Five, the idealised form of stress paths for undrained tests for overconsolidated and normally consolidated materials with various degrees of overconsolidation are illustrated in Figure 6.3.7 (Atkinson & Bransby, 1978). The idealised stress paths for homogeneous soils start from the $q = 0$ plane of the yield figure and rise almost vertically to the state boundary surface where yielding occurs. Yielding continues as the stress path traverses the state boundary surface until failure occurs when the critical state line is reached. Natural, undisturbed soil samples are, however, generally heterogeneous in detail and the failure of an overconsolidated material often occurs prematurely, probably soon after the state boundary is reached (Farmer, 1983). The behaviour exhibited by the least weathered materials is very similar to those heavily overconsolidated materials described by Atkinson & Bransby (1978). The difference is that the failure of the least weathered samples occurred before the state boundary was encountered. Nevertheless, it seems to be reasonable to interpret the behaviour exhibited by the least weathered materials as being primarily due to overconsolidation, which is, presumably, a result of the fairly rapid and considerable geological unloading (Chapter Three, section 3.2).

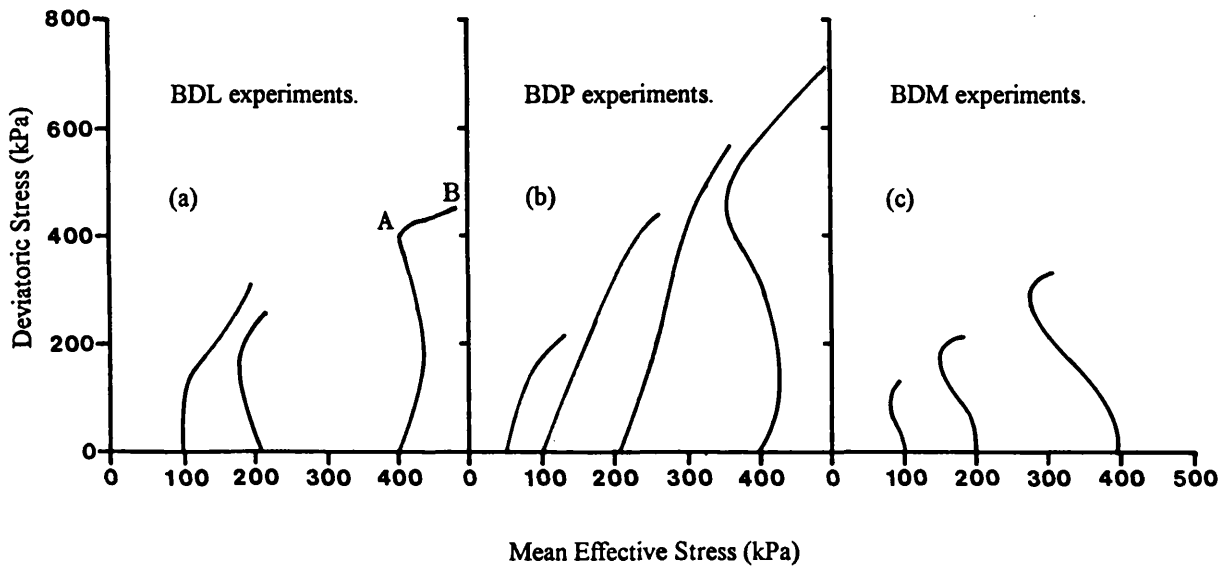


Figure 6.3.5 Three families of stress paths for samples from Joe's River Formation scaly clay, Barbados

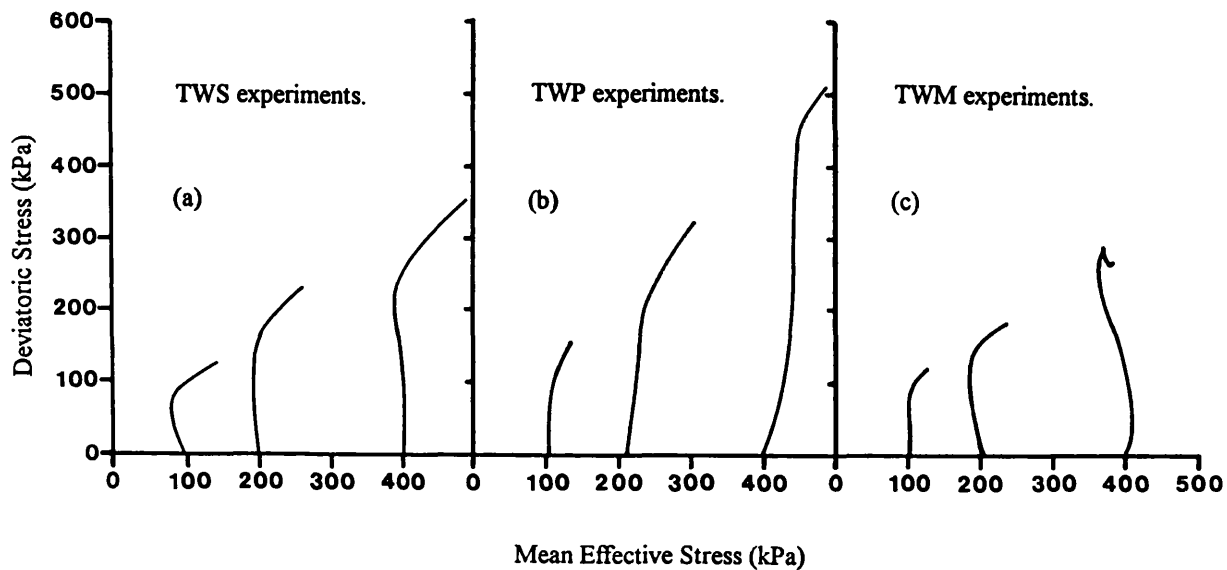


Figure 6.3.6 Three families of stress paths for samples from Lichi Mélange scaly clay, Taiwan

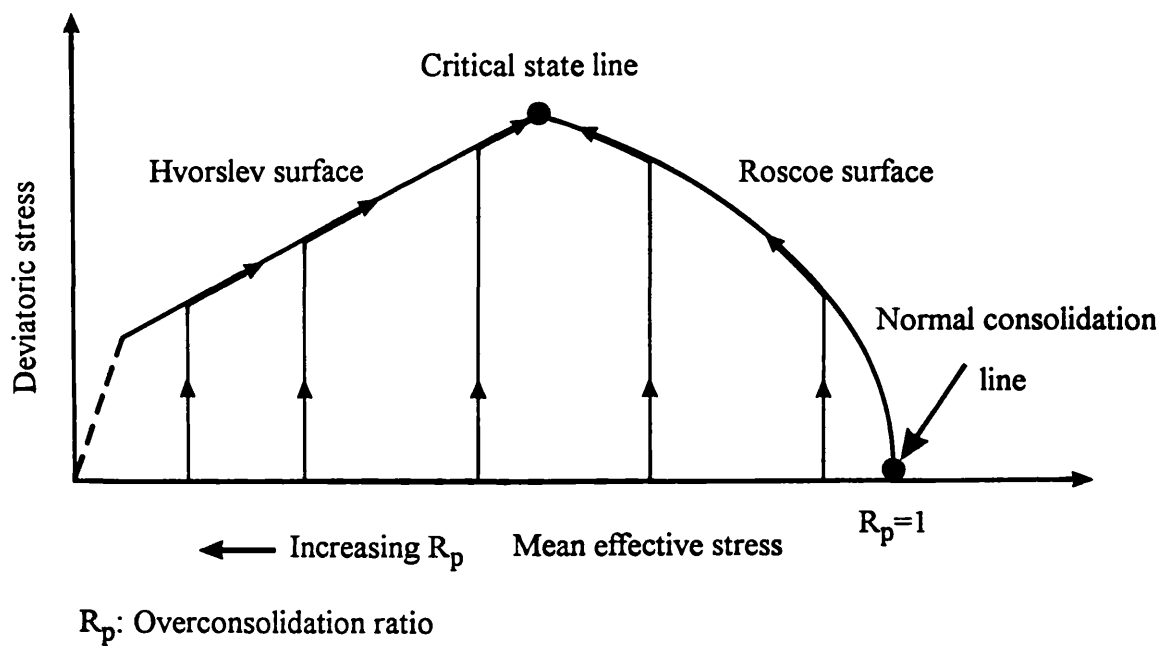


Figure 6.3.7 Expected undrained test paths for samples at different degrees of overconsolidation (overconsolidation ratio), (after Atkinson & Bransby, 1978)

The presence of the scaly surfaces in the least weathered material also exerts considerable effects on the failure behaviour. The surfaces facilitate the early formation of shear failure planes during undrained deformation, in particular in experiment BDL-200 which was terminated at an axial strain of 7% to prevent puncturing of the membrane. Among the three BDL experiments, only the BDL-400 managed to reach the state boundary surface (Figure 6.3.5a). In Figure 6.3.5a the line AB is interpreted as the stress path traversing the Hvorslev surface towards the critical state line. As explained earlier, heavily overconsolidated materials are likely to develop failure planes prematurely before the critical state is reached due to their inherent structure and brittleness (Farmer, 1983). The behaviour of the BDL samples is such an example.

The partially weathered materials also exhibit characteristics of overconsolidation, but in a different way from that of the least weathered samples. The overconsolidation behaviour exhibited by the partially weathered samples is characterised and controlled primarily by dilation. Dilation usually accompanies shear deformation of dense (e.g. overconsolidated) soil materials. During dilation the sample tends to expand which restricts pore fluid pressure generation and therefore the stress path rises towards to a higher mean effective stress. This indicates that the partially weathered samples have lost some of the original stiffness and soil structure during weathering enabling them to dilate as they deform. Large pore fluid pressure development is only seen in the highest confining pressures experiment because only at high effective stress can dilation be prevented. There is only an appreciable pore fluid pressure response in these samples (Figure 6.3.5b). This effect is absent in the least weathered materials.

It was mentioned in Chapter Five that the deformation behaviour of the partially weathered samples is in some way similar to the behaviour of sand with the samples exhibiting strong dilation during undrained deformation. The cause of this phenomenon, as discussed earlier in section 6.2, appears to be aggregation of fine particles to form larger grains during the onset of weathering. These large aggregate grains are held together by relatively strong bonds so that during shear deformation they tend to roll around each other causing the observed dilatant behaviour rather than breaking-up in response to the deformation. Similar observations have been made by other workers (Dixon & Robertson, 1971; Wallace, 1973; Pandian *et al.*, 1993a b) for various materials and the BDP and TWP samples appear to agree with this behaviour acting as if a mixture of both clay and sand. In the experiment BDP-400 (Figure 6.3.5), the increased confining pressure during isotropic consolidation appears to have broken the bonding holding the particles aggregate together. This has led to the loss of dilatancy and instead, positive pore fluid pressure was generated during undrained loading as the sample developed a

contractive style of shear behaviour. However, as the stress path approaches the failure envelop the sample starts to dilate, but in this instance the dilatant behaviour is a characteristic resulting from overconsolidation and not from particle aggregation.

As weathering continues the undrained deformation behaviour of the most weathered samples exhibits further changes. This is best demonstrated by the BDM experiments. In general, all of the most-weathered samples show the greatest pore fluid pressure generation during undrained deformation, but in these experiments the effect is most pronounced in the samples deformed under the largest confining pressures (400 kPa). Hardly any stiffness is mobilised during shear and in each case a large excess pore fluid pressure developed almost from the outset of undrained deformation. This leads to a reduction in the mean effective stress facilitating the development of shear failure. Pore fluid pressure development ceases when a clearly defined failure plane has developed. Subsequently, the pore fluid pressures continue to either slightly decrease or remain constant whilst the deviatoric stress continues to increase gradually (Figure 6.3.8). This response is known as dilation and is sustained until the ultimate state has been achieved. The large pore fluid pressure generation suggests that the samples are no longer as heavily overconsolidated as the least weathered and partially weathered samples and behave in a manner similar to a lightly overconsolidated or normally consolidated material.

A more comprehensive picture of the effect of weathering on the mechanical behaviour of scaly clay can therefore be developed. This is best illustrated by the stress paths for the Barbados experiments (Figure 6.3.9). The failure envelop for each weathering horizon is drawn on the stress paths diagram. It is found that the intersection of the failure envelopes with the deviatoric stress axis, which reflect the degree of intergranular bonding (or cohesion), decreases as the degree of weathering increases (Figure 6.3.9). This confirms the suggestion that soil structure is gradually lost during weathering leading to a change in the undrained loading behaviour. During the onset of weathering part of the original soil structure of the scaly clay is destroyed so the clay loses some of the stiff overconsolidation characteristics observed for the least weathered clays as well as loses some bonding/cohesion (lower failure envelop/deviatoric stress axis intercept value) (Figure 6.3.9). The alteration to the soil structure due to partial weathering appears to be mainly the formation of aggregate grains which are resistant enough to deformation so as to cause the soil to strongly dilate during shear. It was stated earlier that this behaviour is akin to the deformation behaviour of dense sand/granular soil. Further weathering of the scaly clay results in not only a further decrease in bonding/cohesion (an even lower failure envelop/deviatoric stress axis intercept value)

but also a loss of stiff, structured soil/ dense granular soil characteristics. For these most weathered scaly clays (e.g. BDM samples) there is less resistance to deformation causing significant pore fluid pressure generation during undrained loading. This type of material behaviour is similar to a normally consolidated soil.

The angles of the failure envelopes also show differences with change in the degree of weathering (Figures 6.3.9 & 6.3.10, Table 6.3.1). The angle of the failure envelope is related to the angle of internal friction of the soil. The least weathered sample appears to have the smallest angle of failure envelope. This is thought to be due to the presence of the scaly surfaces. As described previously, the scaly surfaces are a result of local preferred orientation of clay particles and a lower angle of internal friction along the surface is, therefore, expected. When weathering proceeds it disrupts the scaly fabric leading to a random orientation of clay particles and consequently an increase in the angle of friction is a reasonable conclusion to draw. This is also supported because further weathering does not significantly change the angle of the failure envelope suggesting that both partially and most weathered samples have similar randomly oriented particles and hence similar angles of internal friction (Figure 6.3.9). The slightly larger angle observed in the BDP samples may be due to its lower content of fine particles because of particle aggregation.

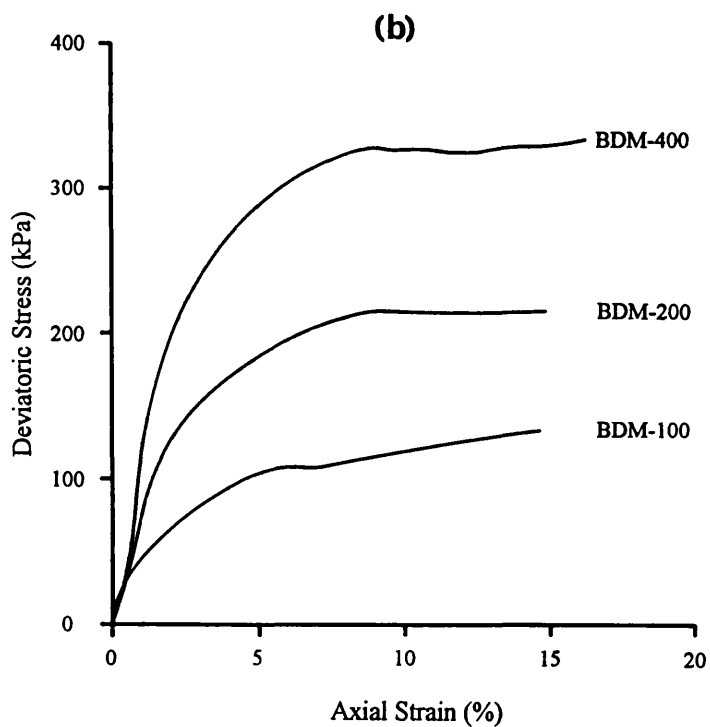
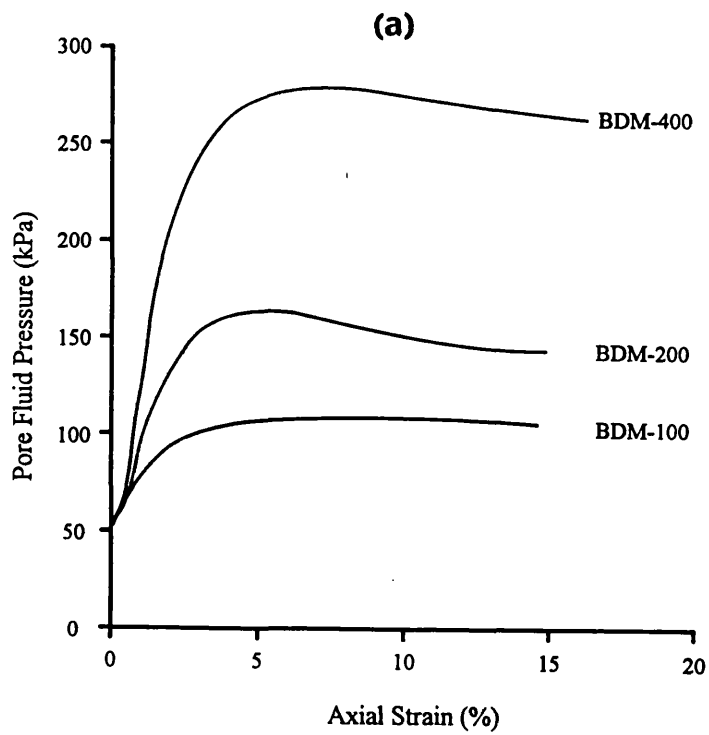


Figure 6.3.8 (a) Stress-strain behaviour of the BDM samples. (b) Pore fluid pressure development during undrained loading for the BDM experiments.

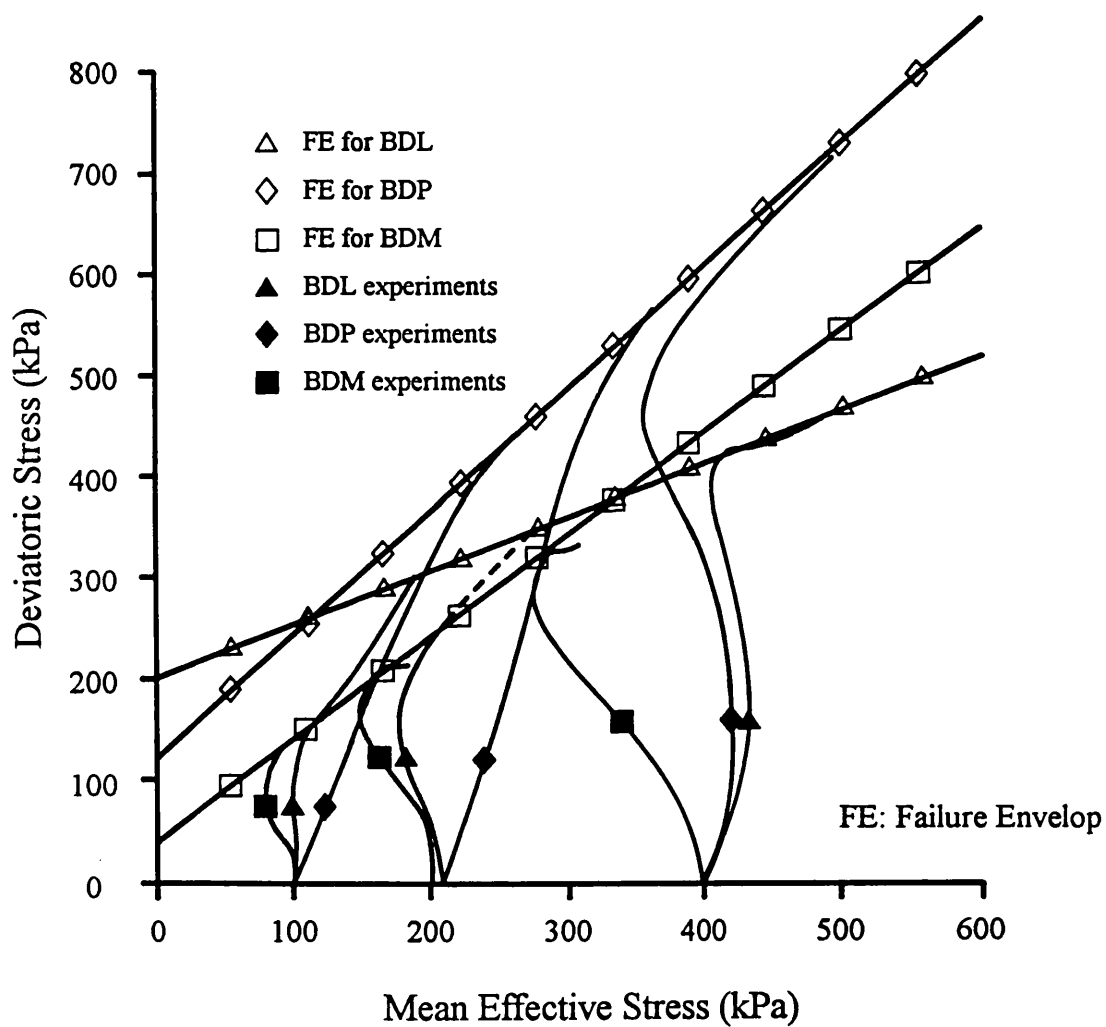


Figure 6.3.9 Stress paths and failure envelopes for the Barbados experiments

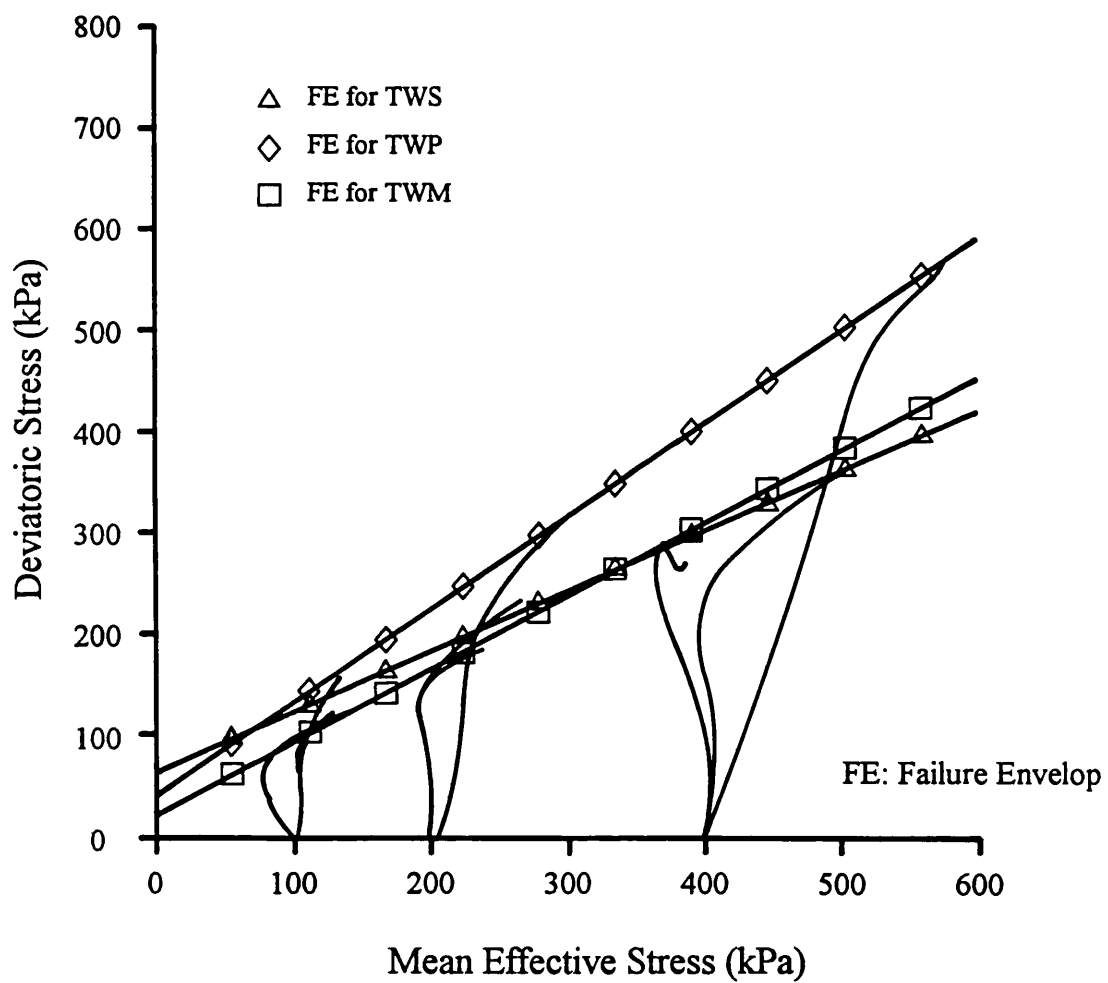


Figure 6.3.10 Stress paths and failure envelopes for the Taiwan experiments

It is noted that all three BDM experiments show some dilation behaviour at the end of each test (Figure 6.3.5c). This indicates that all of the original soil structure has not yet been completely destroyed. This can be demonstrated by comparing the results between the most weathered sample BDM-100 and the sample BDR-100 which is thought to have been remoulded (Figures 6.3.11 to 6.3.14). There are still differences between the two, such as the dilation behaviour and the strength. The stress path for experiment BDR-100 is typical for a normally consolidated soil which starts from the normal consolidation line and traverses along the Roscoe surface (see Appendix I) until it reaches the critical state line at which point sample strains at constant stress and constant volume (Figure 6.3.12 & 6.3.14). The stress path of experiment BDM-100 starts off similar to that of BDR-100 sample with a large pore fluid pressure development during undrained deformation. This continues until the pore fluid pressure reaches a maximum magnitude when the soil starts to dilate. The dilation continues until the experiment is terminated. The similarities in the development of pore fluid pressure, the shape of the stress path and the stress-strain behaviour indicate that weathering gradually remoulds the clay by destroying the original structure and by increasing its pore volume.

Insofar as discussed above, similar trends in mechanical behaviour can be seen for both the Barbados and Taiwan samples. However, there are slight differences with respect to mechanical behaviour in the upper part of the Taiwan weathering profile (i.e. from partially to most weathered state). Figure 6.3.15 shows the stress paths for the TWP and TWM experiments. It is noted that for the experiments conducted at low confining pressures, both TWP and TWM samples, follow almost the same stress path during the first part of undrained deformation until they start to dilate when, subsequently, the two stress paths bifurcate. In the experiments conducted at higher confining pressure (200 kPa) more pore fluid pressure is developed in the TWM experiment resulting in the TWM stress path lying to the left of the TWP path. At this stage the TWM sample still exhibits characteristics of overconsolidation in which the stress path rises nearly vertically towards the failure envelop until late stage dilation occurs. In the highest confining pressure tests the TWM sample generates even more pore fluid pressure during undrained loading and therefore the stress path curves towards the left indicating that the sample is now behaving in a manner similar to a normally consolidated or a lightly overconsolidated material. The indication is that the TWM sample is not as stiff or resistant to deformation as the TWP sample suggesting that weathering has destroyed some of the original soil structure, e.g. the overconsolidation characteristics. This can only be seen in the higher confining pressure experiments because in low pressure ranges they both exhibit stiff overconsolidation characteristics and it is difficult to distinguish the difference between the two.

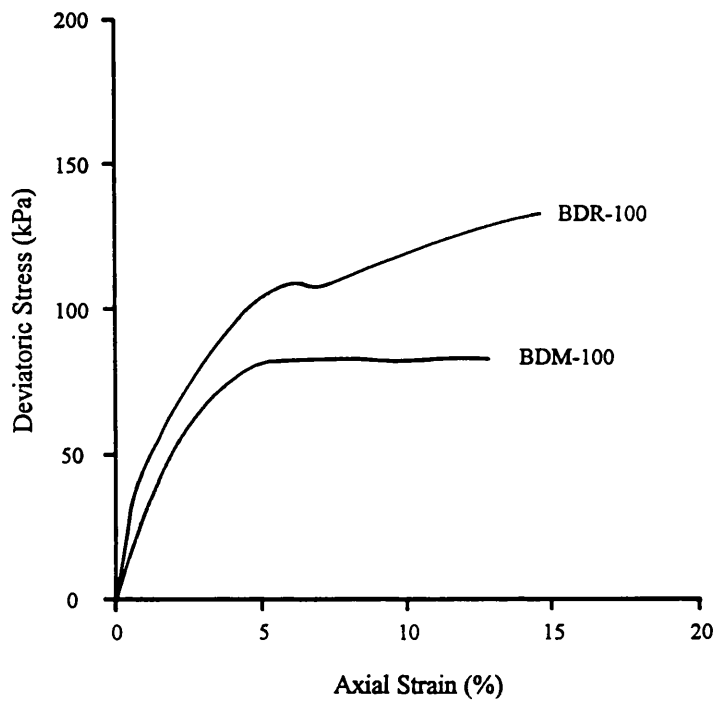


Figure 6.3.11 Comparison between the stress-strain curves from experiments BDM-100 and BDR-100

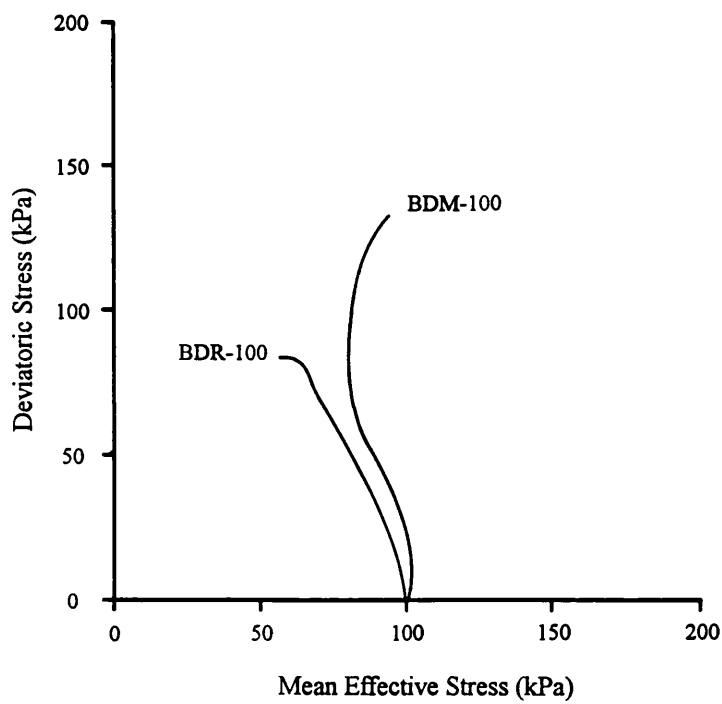


Figure 6.3.12 Comparison between the stress paths from experiments BDM-100 and BDR-100

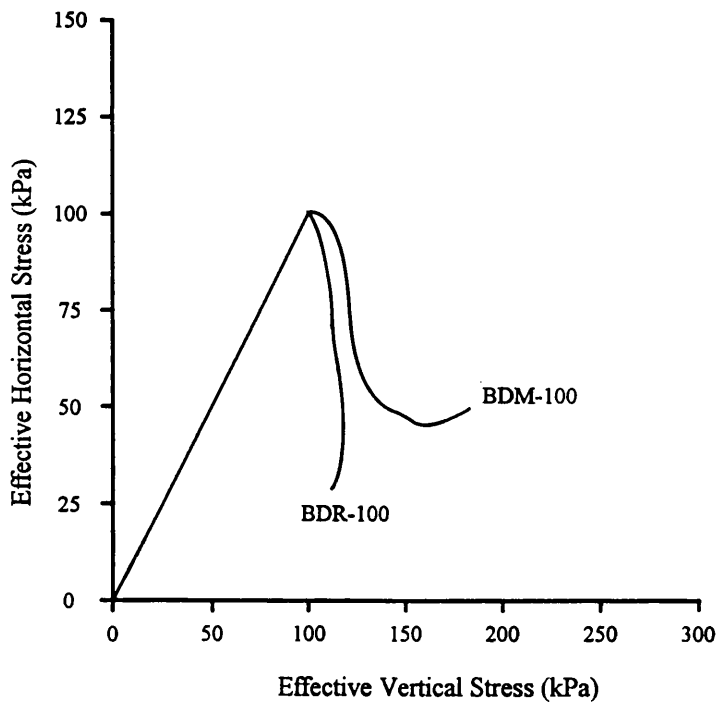


Figure 6.3.13 Comparison between the effective horizontal-vertical stress relationship from experiments BDM-100 and BDR-100

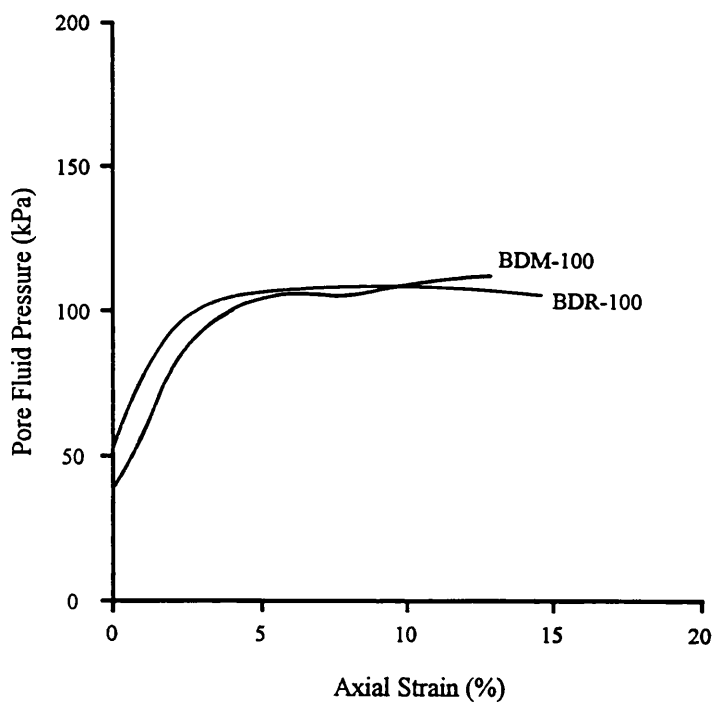


Figure 6.3.14 Comparison between the pore fluid pressure development during undrained compression from experiments BDM-100 and BDR-100

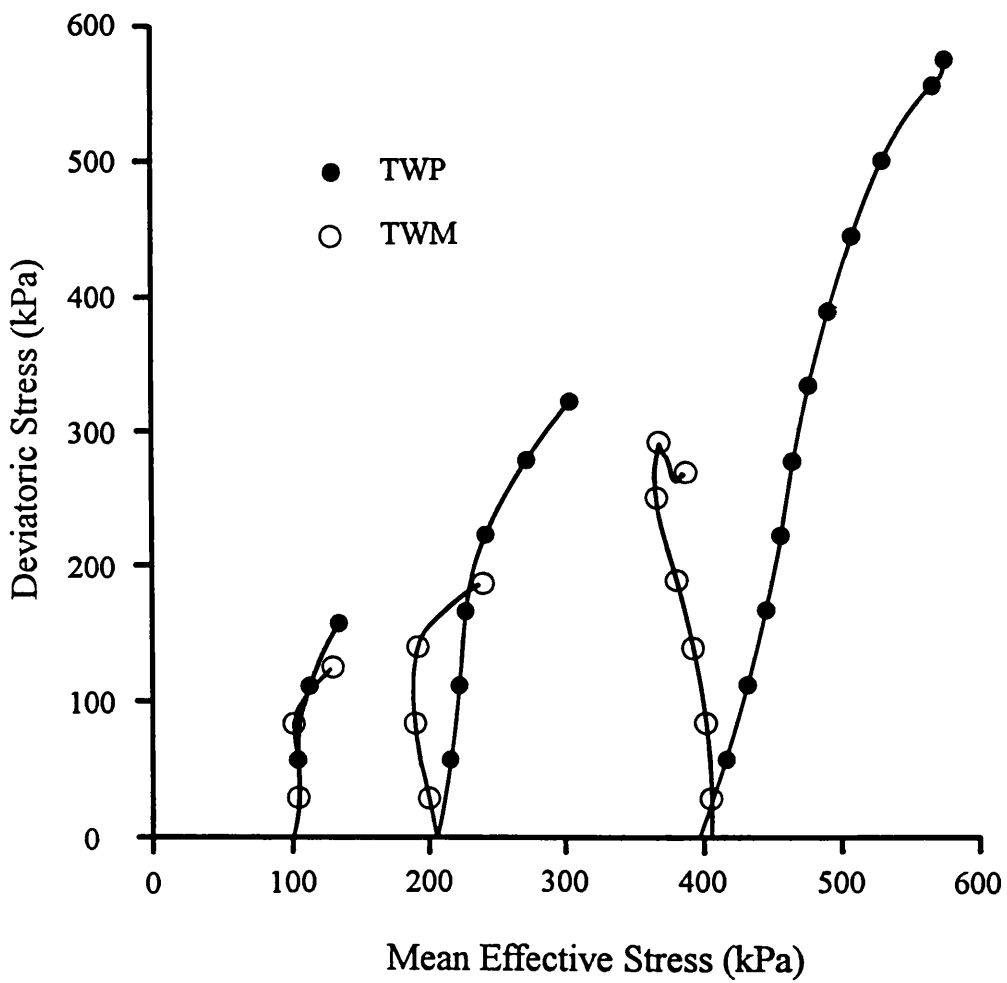


Figure 6.3.15 Stress paths for TWP and TWM families

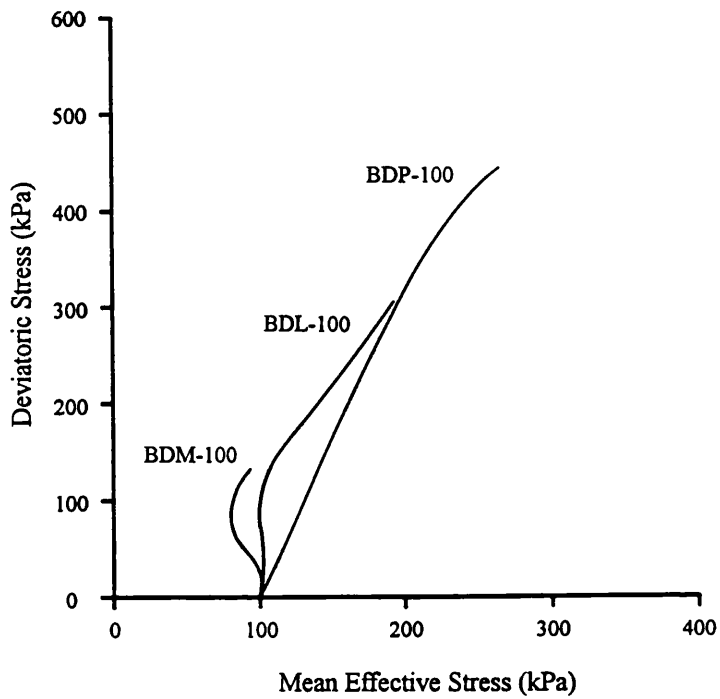


Figure 6.3.16 Stress paths for the three Barbados experiments at effective confining pressure of 100 kPa

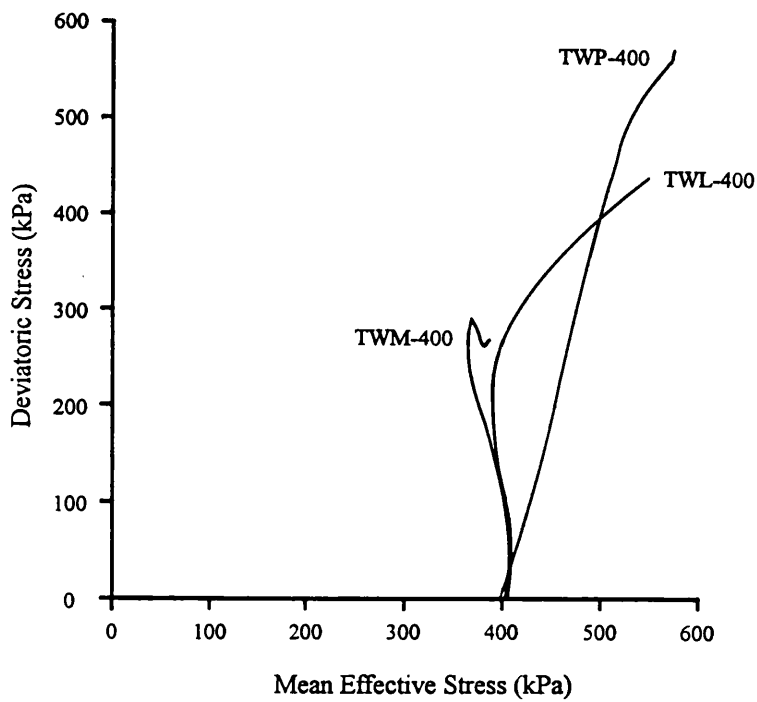


Figure 6.3.17 Stress paths for the three Taiwan experiments at effective confining pressure of 400 kPa

A comparison is made between Figure 6.3.16 and Figure 6.3.17 in which the stress paths of the Barbados experiments at 100 kPa effective confining pressure and those of the Taiwan experiments at 400 kPa effective confining pressure are plotted respectively. The similarities that can be observed in both sets of data are that the least weathered sample exhibits characteristics of heavy overconsolidation, partially weathered sample shows strong dilation behaviour and the most weathered material behaves closely akin to a lightly overconsolidated soil. It is therefore reasonable to believe that weathering imposes similar effects on the mechanical behaviour of the two scaly clays. The comparison also indicates that some higher pressure tests may be needed for the Lichi clay to see the same change in behaviour as that seen in the Joe's River Formation experiments.

Table 6.3.1 Some strength parameters for materials with various degrees of weathering

Degree of weathering	Shear strength at 100 kPa effective confining pressure	Shear strength at 200 kPa effective confining pressure	Shear strength at 400 kPa effective confining pressure	Intersection of FE with deviatoric stress axis	Angle of the FE appear in stress path diagram (degree)
BDL	310 kPa	260 kPa*	460 kPa	200 kPa	21.8
BDP	440 kPa	560 kPa	710 kPa	120 kPa	42.5
BDM	120 kPa	220 kPa	330 kPa	40 kPa	40.7
TWL	110 kPa		440 kPa		
TWS	110 kPa	220 kPa	350 kPa	60 kPa	24.5
TWP	150 kPa	320 kPa	565 kPa	40 kPa	34.8
TWM	120 kPa	180 kPa	260 kPa	20 kPa	28.6

FE: Failure Envelop. *: This experiment was subject to an early termination.

Other than the significant difference in the mechanical behaviour it is also noted that, in both cases, the shear strength of the partially weathered samples is much higher than that of the least weathered samples. It has been calculated from Table 6.3.1 that the shear strength of the BDP samples is approximately 50% higher than that of the BDL samples and an average of 45% increase in the shear strength is recorded between TWL and TWP samples. The unusual strengthening effect from least to partially weathered state is thought to be generated by the onset of weathering in scaly clay materials due to two reasons. First, the scaly surfaces which existed in the least (and slightly) weathered sample(s) and acted as an array of interconnected surfaces of low shear strength facilitating early failure have been progressively destroyed by the weathering processes. As these low strength surfaces are exposed to physical and chemical weathering, the

preferred orientation of the particles along the surfaces become restructured leading initially to an increase in the friction along these surfaces. This is reflected by the greater shear strength mobilised as these partially weathered clays deform.

Secondly, the change in particles size will also make some contribution to cause the strengthening effect seen in the partially weathered samples. During the onset of weathering some fine particles aggregate to form larger peds and clusters due to generation of suction between particles through, perhaps, wetting and drying. The partially weathered samples will, therefore, have deformation characteristics similar to a sand or granular soil. The shear resistance mobilised by sand-sized particles is greater than that of platy clay particles because of the fact that the sand size grains have to rotate around each other in order to accommodate the imposed deformation. This results in an increase in material strength as well as significant dilation during shear. As a consequence, the scaly clay with enhanced grain sizes will tend to exhibit greater shear strength.

Following the strengthening is an appreciable weakening effect as the clays change state from partially weathered to highly weathered. In both cases, this strength reduction is larger than the initial increase, especially in the largest confining pressure tests. The reduction in strength is between 75% and 50% for the Joe's River Formation samples and an average of 42% for the Lichi clay. This is similar to the substantial difference in strength between an undisturbed intact sample and a remoulded sample. The decreased strength is attributed to the destruction of the intact overconsolidated structure of the clay and the enlargement of the pore space. With increased weathering, restructuring of the clay fabric of the clay particles continue and the scaly fabric is largely eradicated from the material. These structural changes are akin to a partial remoulding of the clays and thus cause a loss of material stiffness. This results in a behaviour close to that of a normally consolidated material, and the material is observed to have a reduced strength. The most weathered samples have thus been effectively remoulded to some extent by weathering.

It was described in section 6.2 that neither profile shows significant changes in mineralogy although in the most weathered horizon of the Lichi profile kaolinite starts to appear. Whether the presence of kaolinite contributes to the strength reduction or to changes in material behaviour is not clear. This may need further investigation. However, the amount of kaolinite present in the TWM horizon is very small. Even if the kaolinite does exert influence on the mechanical behaviour, it should be a minor effect in this case.

Dilation behaviour has been observed in all the Barbados and Taiwan experiments conducted in the study except two tests, experiments BDR-100 and TWM-400 (Figures 6.3.5, 6.3.6 & 6.3.12). As suggested earlier, the Taiwan experiments, particularly TWP and TWM experiments, do not show obvious difference in the low stress regime, and therefore the discussion here is focused mainly on the Barbados experiments. Attention is drawn on the differences between the BDL and BDM samples because, as discussed earlier, the BDP sample possesses characteristics similar to a sand due to particle aggregation, and therefore, exhibits strong dilation from the beginning of undrained loading. The least weathered samples start exhibiting dilation at an axial strain in the range 2%-4% (Figure 6.3.18), whereas in the most weathered samples dilation does not occur until about 5%-7% axial strain (Figure 6.3.19). This is due to the effective remoulding of the sample by weathering. Canestrari & Scarpelli (1993) described that dilation appears to be a function of the specific volume (v) of the sample and the mean effective stress (p'). Dilation increases when the specific volume and mean effective stress decrease. In the cases discussed here where the mean effective stress is the same at the start of undrained deformation, the specific volume will then govern the observed late stage dilation behaviour. Dilation of the BDM samples is less strong and occurs later than that of the BDL samples because of the increased specific volume in the BDM samples and the loss of the original soil structure.

Generally speaking, the changing mechanical characteristics through the weathering profile at the Taiwan site are similar to those of the Barbados' profile. The original stiff behaviour of the material has been modified by weathering changing from a heavily overconsolidated style of behaviour to a normally consolidated or lightly overconsolidated style of behaviour in its most weathered state.

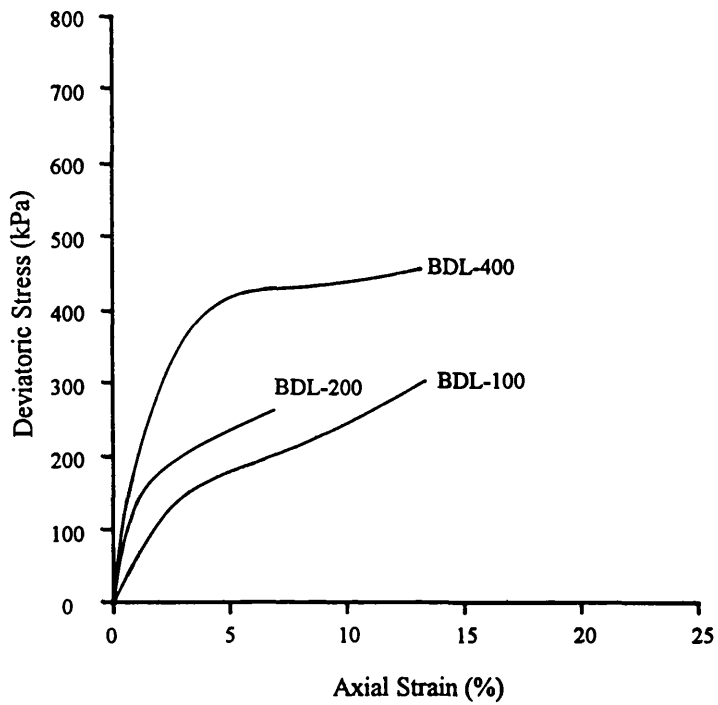


Figure 6.3.18 Stress-strain curves for BDL experiments

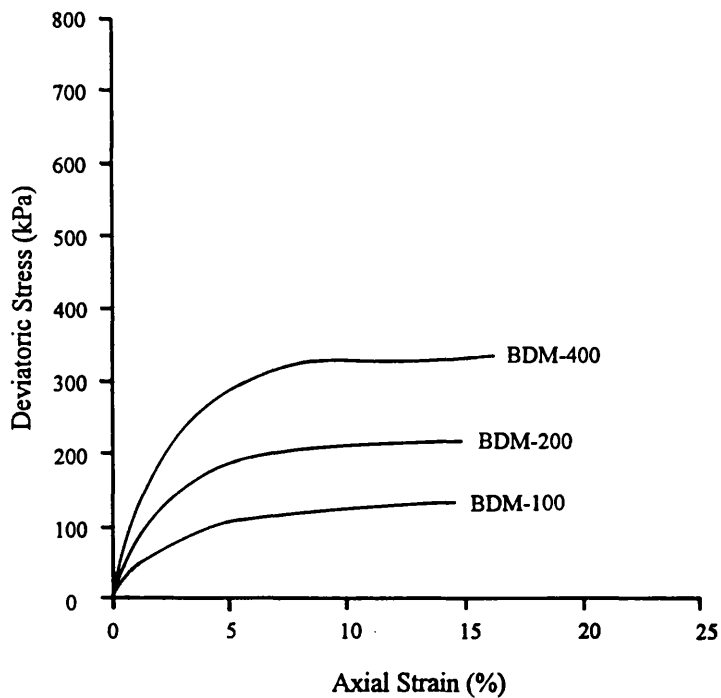


Figure 6.3.19 Stress-strain curves for BDM experiments

6.4 Summary of the similarities and differences

It is one of the substantial aims of the study to establish a general pattern or trend of how tropical weathering influences the physical, chemical and mechanical properties of scaly clay. The studied materials are from two different parts of the world which are characterised by tropical climates with warm temperatures and high humidity. It would not be surprising if there were differences between these two localities because weathering is such a complicated process involving many unquantifiable variables. Consequently, no two natural environments have exactly the same weathering scheme. However, the two selected study areas are similar in many aspects and it is hoped that by comparing the similarities and differences exhibited by the physical, chemical and mechanical properties of the two materials at different degrees of weathering that a better understanding of the general behaviour will be gained.

6.4.1 Similarities

- *The increasing porosity and moisture content, and the decreasing bulk density of the materials are a consequence of weathering.*

This suggests that when the material weathers the pore volume is progressively enlarged. This is a result of fabric alterations which are believed to be due to pore fluid migration within the material. Often, this alteration is accompanied by restructuring (or destructuring) of the material which leads to the scaly fabric being progressively destroyed.

- *The partially weathered material appears to have more coarse grains than the least and the most weathered samples.*

It is seen in both cases that the clay fraction is lower in the partially weathered horizon. The increase in particle size is attributed mainly to aggregation of fine grains which is not unusual in tropical regions. Further and more intense weathering results in establishment of stress within particles which leads to particle degradation.

- *No correlation between bulk chemical composition and depth has been observed.*

The bulk chemical composition does not show any significant change through the weathering profiles. This is thought to be due partly because the materials are chemically stable and partly because the severe surface erosion. The small differences between

horizons should not be interpreted as a consequence of weathering but may be simply due to sample variation.

- *Oxidation increases as weathering proceeds.*

The changing Ferric/Ferrous ratio indicates that oxidation is increasing towards the ground surface. Oxidation depends on the availabilities of oxygen and water which are the two most important factors influencing weathering. Oxidation is most severe at the surface and ceases below a certain depth. This depth is strongly controlled by the permeability of the material.

The triaxial test results show that the mechanical behaviour of the scaly clay from both locations is strongly influenced by the impact of weathering.

- *Overconsolidation style of behaviour exhibited by the material decreases as it weathers.*

A sequential change in the overconsolidation style of behaviour can be seen from the least weathered to the most weathered samples. It is therefore reasonable to believe that weathering progressively converts the stiff structured (heavily overconsolidated) scaly clays to a less structured, less stiff material state. In other words, weathering is progressively remoulding the materials.

- *Strengthening occurs during onset of weathering. Further weathering leads to an appreciable decrease in the strength of the materials.*

Unlike the overconsolidation behaviour, the strength does not follow a sequential change as the materials weather. The triaxial undrained deformation experiments illustrate that in both cases the partially weathered clay is by far the strongest. These strengthening effects, seen in the deeper parts of the weathering profiles are not present in the behaviour of the samples from the upper part of the profile. The most weathered materials appear less stiff and behave as lightly overconsolidated or normally consolidated soils and this change in characteristic is accompanied by an appreciable reduction in strength, with respect to the partially weathered materials.

6.4.2 Differences

- *No mineralogical change has been detected in the Barbados profile, but formation of kaolinite is found in the top most two layers of the Taiwan profile.*

X-ray Diffraction analyses show that the weathering does not significantly alter the mineralogy of the Barbados material. All the samples from the three horizons have similar X-ray Diffraction traces, suggesting that either the original mineralogy of the material is chemically stable in the near surface environment, or that the time taken for the material to pass from the least weathered to most-weathered state is insufficiently long for considerable mineral alteration to occur.

On the other hand, kaolinite has been found in the upper part of the Taiwan profile. Kaolinite peak starts to appear at the most weathered horizon and becomes stronger in the top surface layer. As the kaolinite gradually appears, it is seen that both mica-2M and chlorite peaks show decrease in intensity. It is therefore reasonable to presume that the formation of the kaolinite is associated with the change in the intensities of mica-2M and chlorite peaks. The detailed mechanism of this transformation is not known but it is not unusual for kaolinite to be formed from other silicates providing the conditions are suitable.

- *The Atterberg limits of the Barbados materials show a distinctive feature in the partially weathered sample, whereas in the Taiwan materials this is absent.*

The partially weathered sample from Barbados exhibits a distinctively low value of liquid limit. This is because the partially weathered sample has the lowest content of fine particles which leads to an decrease in the surface area, and thus has less water attached to the particle surface compared with the other two horizons.

In contrast, the plasticity index properties of all Taiwan samples are fairly similar. Although the partially weathered sample appears to contain slightly less fine particles but this is not shown in the index properties in the same way as that of the Barbados material. The slightly decreasing index properties (PL, LL & PI) of TWM and TWT may be due to the presence of kaolinite which has lower capability of water absorption.

- *Consolidation behaviour of the Barbados samples exhibits a correlation with weathering, whereas that of the Taiwan samples does not.*

This difference is largely caused by the extra treatment needed to accelerate the consolidation process for the Taiwan samples. There is a large change in the slopes of the recorded consolidation paths from BDP to BDM (Figure 6.4.1). This usually represents a change in the overconsolidation ratio of the material. The difference between TWP-400 and TWM-400 is largely in the shape rather than in the gradient of the consolidation path. TWP-400 exhibits a large volumetric strain at the beginning of consolidation without increasing the mean effective stress (Figure 6.4.2). Subsequently, the mean effective stress starts to increase with an appreciably less steep consolidation path. In contrast, TWM-400 exhibits less volumetric strain while the stress is low, and subsequently the path becomes steeper after the mean effective stress of 40 kPa is reached (Figure 6.4.2). As discussed in Section 6.2, the abnormal shape of the consolidation path of TWP-400 is thought to be due to its low permeability and should not be interpreted as its real consolidation behaviour.

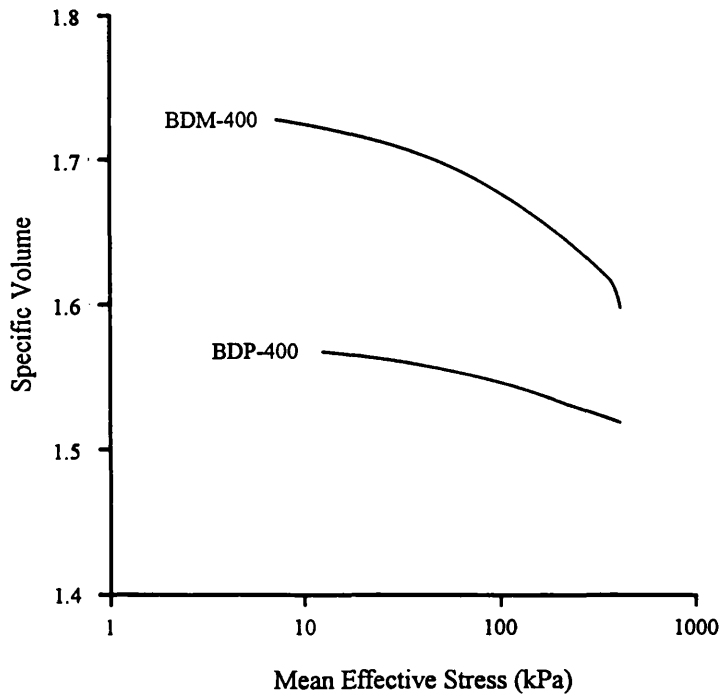


Figure 6.4.1 Consolidation paths for experiments BDP-400 and BDM-400 (in linear scale)

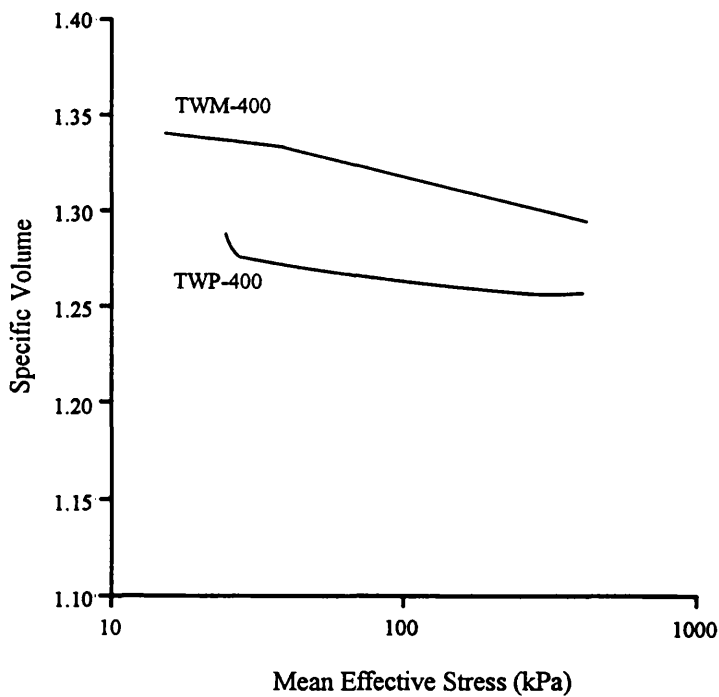


Figure 6.4.2 Consolidation paths for experiments BDP-400 and BDM-400 (in logarithmic scale)

6.4.3 Conclusion

To conclude the experimental findings of the study, Table 6.4.1 and Figure 6.4.3 are provided to describe the effects of tropical weathering on the physical-chemical and mechanical characteristics of scaly clay.

Table 6.4.1 Effects of tropical weathering on the physical-chemical and mechanical characteristics of scaly clay

Properties	Unweathered state	→	Partially weathered state	→	Highly weathered state
Porosity			<i>increase</i>		<i>increase</i>
Particle size			<i>increase</i>		<i>decrease</i>
Formation of kaolinite			<i>increase</i> (?)		<i>increase</i>
Scaly fabric			<i>decrease</i>		<i>decrease</i>
Material characteristics	Stiff, heavily overconsolidated clay	→	Dense sand	→	Lightly overconsolidated or normally consolidated clay
Shear strength			<i>increase</i>		<i>decrease</i>
Intergranular bonding			<i>decrease</i>		<i>decrease</i>

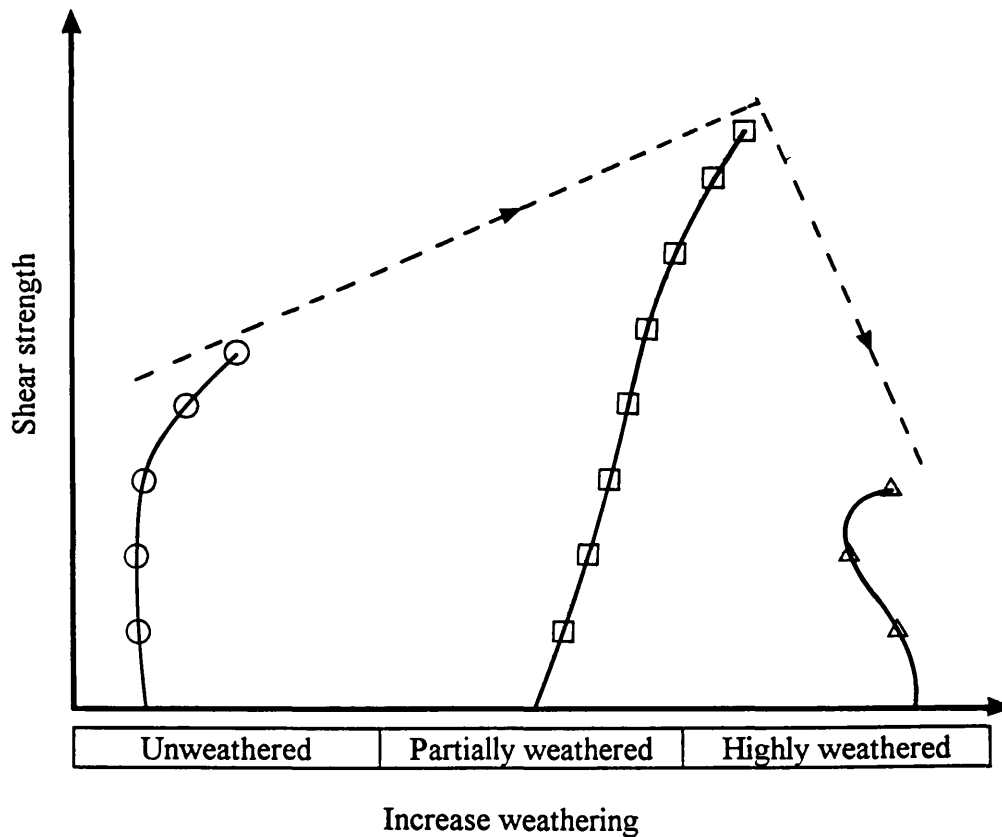


Figure 6.4.3 Diagram illustrating the effect of weathering on the mechanical behaviour of scaly clay

6.5 Implication on the evolution of badlands topography

The underlying primary objective of the study was to discover the links between the scaly clay, weathering processes and the development of the unique badlands topography that typifies scaly clay outcrops. Thus, it is necessary to combine the quantitative experimental data with the qualitative description of the landscape developing on the scaly clay sediments which was observed in the field. In both the Barbados and Taiwan sites, the outcrops of scaly clays are characterised by rapidly degrading slopes. A widespread, deeply incised gully system has developed in the scaly clay outcrop slopes (Plate 6.5.1). As weathering proceeds, the material properties are severely altered leading to a rapid and frequent down-slope transfer of sediment. The down-slope mass movement is partly surface erosion and overland debris flow process and partly shallow to medium depth landslipping. Fertile soils and vegetation have great difficulty developing in such a highly dynamic environment with its high frequency of mass wasting. As a result, badlands form largely during tropical rainstorm when intensive surface run-off becomes localised into the developing gullies.

A model for the evolution of badlands topography can therefore be suggested from the combination of the experimental data and the field observation (Figure 6.5.1). The starting point is fresh scaly clay uplifted and exposed to tropical weathering processes. As weathering commences, pore volume will start to increase and the scaly fabric begins to disappear. The destructuring of the scaly fabric is associated with the re-orientation of the platy particles and, perhaps, the aggregation of fine grains. This result in an increase in the material strength. No surface mass movement or landslide occurs at this stage.

As weathering continues, pore enlargements become more severe and the original structures no longer exist, a new, looser structure replaces the old one. The increase in void space and the change in structure are accompanied by an increase in moisture content as water now permeates into the sediment more easily. A layer of highly weathered, clay is formed on top of the partially weathered horizon. The strength of the material at this stage is far less than that of partially weathered state, and therefore the material becomes unstable.

When scaly clay transforms to its highly weathered state external climatic conditions will then control the subsequent evolution. If a heavy storm event occurs, it tends to trigger shallow landslides which remove the highly weathered horizon from the slope and leave the partially weathered scaly clay exposed to the atmosphere. If no heavy rain has occurred for a period of time then a thin cap of residual soil can be developed. When the

slope is again affected by heavy rain, this would be washed away from the slope by surface run-off and leave the highly weathered horizon exposed to the atmosphere. Because of the manner in which weathering changes the properties of scaly clay, mass movements are ubiquitous across any outcrop but are restricted to the upper most part of the soil profile. The combination of high uplift rates, and the continuous repetition of the weathering - mass wastage cycle means that soil development is severely restricted on exposed slopes so that they remain vegetation free with numerous gullies and the development of badlands. These badlands areas tend to increase in area continually rendering even more land unfit for agricultural use.



Plate 6.5.1 Photograph showing widespread gulley system in badlands area

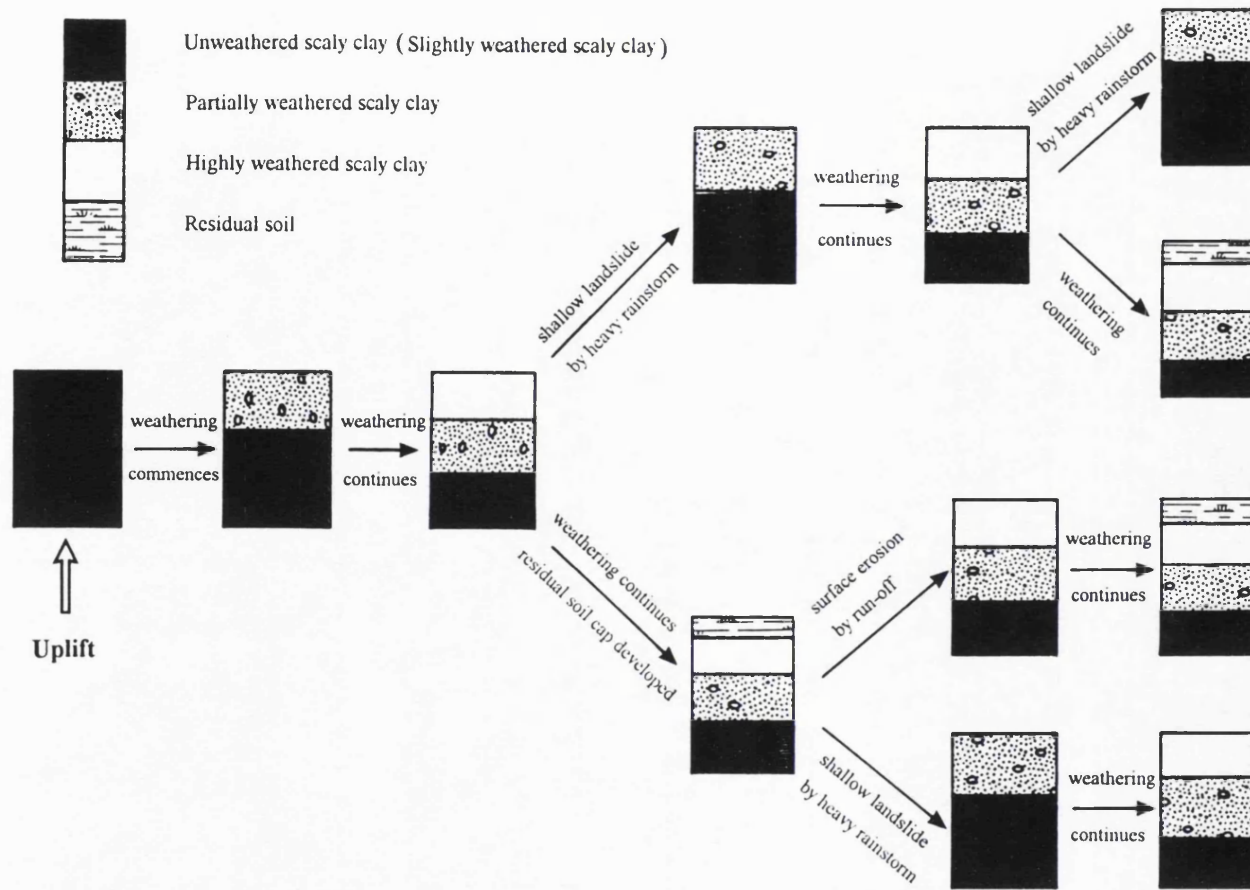


Figure 6.5.1 Suggested model for badlands evolution

References

- Addis, M.A. & Jones, M.E. 1989. Mechanical behaviour and strain rate dependence of high porosity chalk. Proc. Int. Chalk Sym., 4-7th September, 1989, Thomas Telford Ltd., London, pp. 111-116.
- Aires-Barros, L. & Mourza-Miranda, A. 1989. Weathering and weatherability of rocks and its significance in geotechnics. In Balasubramaniam, K.S. (Ed.): Weathering: its products and deposits, Theophrastus, Athens, pp. 605-645.
- Atkinson, J.H. & Bransby, P.L. 1978. The mechanics of soils: An introduction to critical state soil mechanics. McGraw-Hill, London.
- Aversa, S.; Evangelista, A.; Leroueil, S. & Picarelli, L. 1993. Some aspects of the mechanical behaviour of "structured" soils and soft rocks. In Anagnostopoulos *et al.* (Eds.): Geotechnical Engineering of Hard Soils-Soft Rocks. Balkema, Rotterdam, pp. 849-856.
- Balasubramaniam, A.S., Hwang, Z-M., Uddin, W., Chaudhry, A.R. & Li, Y.G. 1978. Critical state parameters and peak stress envelopes for Bangkok Clays. Q. Jour. Engng. Geol., Vol. 11, pp.219-232.
- Barber, A. J. 1981. Structural interpretations of the island of Timor eastern Indonesia. In The geology and tectonics of eastern Indonesia: Geol. Res. Dev. Centre Spec. Publ. 2, pp. 183-197.
- Barber, A. J.; Tjokrosapoetro, S. & Charlton, T. 1986. Mud volcanoes, shale diapirs and mélanges in accretionary complexes, Eastern Indonesia. Bull. Am. Asso. Petro. Geologists, 70, pp. 1729-1741.
- Barden, L. 1972a. The influence of structure on deformation and failure in clay soil *Géotechnique* Vol. 22, pp. 159-163.
- Barden, L. 1972b. The relationship of soil structure to the engineering geology of clay soil. Quar. Jour. Engng. Geol., Vol. 5, pp. 85-102.

- Barden, L. & Sides, G. 1971. The influence of weathering on the microstructure of Keuper Marl. Quar. Jour. Engng. Geol. Vol. 3, Technical note, pp. 259-260.
- Barrier, E. & Muller, C. 1984. New observations and discussion on the origin and age of the Lichi Mélange. Mem. Geol. Soc. China, No. 6, pp. 303-325.
- Bedian, M.P. & Khera, R.P. (1993) Direct simple shear tests on overconsolidated Anderten clay. In Anagnostopoulos *et al.* (Eds.): Geotechnical Engineering of Hard Soils-Soft Rocks. Balkema, Rotterdam, pp. 375-381.
- Bell, F.G. 1992. Engineering properties of soils & rocks. Third Edition. Butterworth-Heinemann Ltd.
- Berner, R. A. 1970. Behaviour of iron during weathering, sedimentation and diagenesis. In: Handbook of geochemistry, section 26G, Springer, Berlin, pp. 1-8.
- Bertuccioli, P. & Lanzo, G. 1993. Mechanical properties of two Italian structurally complex clay soils. In Anagnostopoulos *et al.* (Eds.): Geotechnical Engineering of Hard Soils-Soft Rocks. Balkema, Rotterdam, pp. 383-389.
- Biq, C. 1969. Role of gravitational gliding in Taiwan tectogenesis. Bull. Geol. Surv., Taiwan. No. 20, pp. 1-39.
- Biq, C. 1971. Comparison of mélange tectonics in Taiwan and in some other mountain belts. Petroleum Geology of Taiwan No. 9, pp. 79-106.
- Biq, C. 1973. Kinematic pattern of Taiwan as an example of actual continental-arc collision. Report of the seminar on Seismology, US-ROC Cooperative Science program 25, pp. 149-166.
- Biq, C. 1981. Collision, Taiwan style. Mem. Geol. Soc. China, No. 4, pp. 91-102.
- Biq, C. 1984. Present-day manner of movement of the Coastal Range, eastern Taiwan, as reflected by triangulation changes. Mem. Geol. Soc. China, No. 6, pp. 35-40.

Biju-Duval, B., LeQuellec, P., Mascle, A., Renard, V. & Valery, P. 1982. Multibeam bathymetric survey and high resolution seismic investigation on the Barbados Ridge complex (eastern Caribbean): A Key to the knowledge and interpretation of an accretionary wedge. *Tectonophysics*, Vol. 86, No. 1, pp. 275-304.

Birkeland, P.W. 1974. *Pedology, weathering, and geomorphological research*. Oxford University Press.

Birkeland, P.W. 1984. *Soils and geomorphology*. Oxford University Press.

Bishop, A. 1976. The influence of system compressibility on the observed pore pressure response to an undrained change in stress in saturated rock. *Géotechnique* Vol. 26, pp. 372-375.

Bishop, A.W. & Henkel, D.J. 1962 *The measurement of soil properties in the triaxial test*. 2nd ed., Edward Arnold Ltd., London.

Bishop, A., Kumpaley, N. & El-Ruwayih, A. 1975. The influence of pore water tension on the strength of clay. *Philosophical Transactions of the Royal Society of London. A. Mathematical and physical Sciences* 278 (1286), pp. 511-554.

Bishop, A. & Skinner, A. 1977. The influence of high pore water pressure on the strength of cohesionless soil. *Philosophical Transactions of the Royal Society of London*. 284, pp. 97-130.

Bjerrum, L. 1954. Geotechnical properties of Norwegian marine clays. *Géotechnique* 4, p. 49.

Bjerrum, L. 1967a. Engineering geology of Norwegian normally-consolidated marine clays as related to settlements of buildings. *Géotechnique* 17, pp. 81-118.

Bjerrum, L. 1967b. Mechanism of progressive failure in slopes of overconsolidated plastic clay and clay shales. *ASCE Jour. Soil Mech. Found. Div.* 93, SM5, pp. 3-49.

Blume, H. 1968. *The Caribbean Islands*. Translated by Maczewski, J. & Norton, A. 1974. Longman, London.

- Brenner, R.P., Nutalaya, P., Chilingarin, G.V. & Robertson, J.D. 1981. Engineering geology of soft clay. In Brand, E.W. & Brenner, R.P. (Eds), *Soft Clay Engineering*. Elsevier, Amsterdam, pp. 159-240.
- British Standard 1377, 1990. Method of test for soils for civil engineering purposes, British Standard Institution, London.
- Bromhead, E.N. 1986. *The stability of slopes*. Surrey University Press, Chapman and Hall, New York.
- Brown, K.M. & Westbrook, G.K. 1987. The tectonic fabric of the Barbados Ridge Accretionary Complex. *Marine and Petroleum Geology* 4, pp. 71-81.
- Brunsdon, D. 1979. Weathering. In: Embleton, C. & Thornes, J (Eds). *Process in Geomorphology*, pp. 73-129.
- Brunsdon, D. 1984. Mudslides. In Brunsdon, D. & Prior, D.B. (Eds.): *Slope instability*, Chichester, pp. 363-418.
- Burland, J.B. 1990. On the compressibility and shear strength of natural clays. *Géotechnique* 40, pp. 329-378.
- Caine, N. 1979. Rock weathering rates at the soil surface in an alpine environment. *Catena*, 6, pp. 131-144.
- Canestrari, F. & Scarpelli, G. 1993. Stress-dilatancy and strength of Ancona clay (Italy). In Anagnostopoulos *et al.* (Eds.): *Geotechnical Engineering of Hard Soils-Soft Rocks*. Balkema, Rotterdam, pp. 417-424.
- Carroll, D. 1970a. Clay minerals: A guide to their X-ray identification. *Geol. Soc. Am. Spec. Pap.* 126, Geological Society of America.
- Carroll, D. 1970b. *Rock weathering*. Plenum press, New York, London.
- Casagrande, A. 1932. Research on the Atterberg limits of soils. *Public Roads*, Vol. 13, No. 8.

- Casagrande, A. 1948. Classification and identification of soils. Proc. Am. Soc. Civ. Engng., Vol. 73 No. 6 Part 1.
- Case, J.E.; Holcombe, T.L. & Martin, R.G. 1984. Map showing major geologic provinces of the Caribbean region. Geol. Soc. Am. Mem. 162.
- Chandler, R.J. 1969. The effect of weathering on the shear strength properties of Keuper Marl. *Géotechnique* 19, No. 3, pp. 321-334.
- Chandler, R.J. 1972. Lias clay: weathering processes and their effect on shear strength. *Géotechnique* 22, No. 3, pp. 403-431.
- Chandler, R.J. & Apted, J.P. 1988 The effect of weathering on the strength of London Clay. Quar. Jour. Engng. Geol., London, Vol. 21, pp. 59-68.
- Chang, L.S. 1967. A biostratigraphic study of the Tertiary in the Coastal Range, eastern Taiwan, based on smaller foraminifera (I. southern part). Proc. Geol. Soc. China, No. 10, pp. 64-76.
- Chang, L.S. 1968. A biostratigraphic study of the Tertiary in the Coastal Range, eastern Taiwan, based on smaller foraminifera (II. northern part). Proc. Geol. Soc. China, No. 11, pp. 19-33.
- Chang, L.S. 1969. A biostratigraphic study of the Tertiary in the Coastal Range, eastern Taiwan, based on smaller foraminifera (III. middle part). Proc. Geol. Soc. China, No. 12, pp. 89-101.
- Chen, H. 1987. The stability and mechanical behaviour of colluvium slopes in Taiwan. Unpublished PhD Thesis, University of London.
- Chen, W.S. 1988. The evolution of the Coastal Range sedimentary basin, Taiwan, and its significance on the tectonics. PhD. thesis, National Taiwan University.
- Chesworth, W. 1972. The stability of gibbsite and boehmite at the surface of the earth. Clays, clay minerals, 20, pp. 369-374.
- Chesworth, W. 1992. Weathering system. In Martini, I.P. & Chesworth, W. (Eds.): Weathering, soils & paleosols. Elsevier, pp. 19-40.

- Chi, W.R. 1982. The calcareous nanofossils of the Lichi Mélange and the Kenting Mélange and their significance in the interpretation of plate-tectonics of the Taiwan region. *Ti-Chih*, 4(1), pp. 99-114.
- Clark, B.R. 1970. Mechanical formation of preferred orientation in clays. *American Journal of Science*, Vol. 269, pp. 250-266.
- Coop, M.R. & J.H. Atkinson 1993. The mechanics of cemented carbonate sands. *Géotechnique* 43: pp. 53-67.
- Coulthard, J.M. & Bell, F.G. 1990. The influence of weathering on the engineering behaviour of Lower Lias Clay. In: Cripps, J.C. & Moon, C.F. (Eds): *The Engineering Geology of Weak Rock*, Geol. Soc. Engng. Group, London, pp. 210-227.
- Coulthard, J.M. & Bell, F.G. 1993. The microstructure of, and fissuring in the Lower Lias Clay. In Anagnostopoulos *et al.* (Eds.): *Geotechnical Engineering of Hard Soils-Soft Rocks*. Balkema, Rotterdam, pp. 55-62.
- Cowan, D.S. 1984. Structural features at the deformation front of the Barbados Ridge Complex. Initial reports of the D.S.D.P. Leg 78A.
- Craig, R.F. 1992. *Soil Mechanics*. Fifth Edition (First published at 1974). Chapman & Hall, London, UK.
- Cripps, J.C. & Taylor, R.K. 1981. The engineering properties of mudrocks. *Quarterly Journal of Engineering Geology*. Vol. 14, pp. 325-346.
- Deer, W.A.; Howie, R.A. & Zussman, J. 1966. *An introduction to the rock forming minerals*. Longman.
- Dixon, H.H. & Robertson, R.H.S. 1970. Some engineering experiences in tropical soils. *Quar. Jour. Engng. Geol.* Vol. 3, pp. 137-150.
- Ebuk, E.J., Hencher, S.R. & Lumsden, A.C. 1990. The influence of structure on the shearing mechanism of weakly bonded soils. In: Cripps, J.C. & Moon, C.F. (Eds), *The Engineering Geology of Weak Rock*, Geological Society Engineering Group, London, pp. 242-253.

- El-Sohby, M.A., Mazen, S.O. & Aboushook, M.I. 1990. Deformational characteristics of some weakly cemented and overconsolidated soil formations In: Cripps, J.C. & Moon, C.F. (Eds), *The Engineering Geology of Weak Rock*, Geological Society Engineering Group, London, pp. 155-163.
- Enriquez-Reyes, M.P., Allison, R.J. & Jones, M.E. 1990. Slope stability in scaly clay terrains. In: Cripps, J.C. & Moon, C.F. (Eds), *The Engineering Geology of Weak Rock*, Geological Society Engineering Group, London, pp. 422-432.
- Enriquez-Reyes, M.D. & Jones, M.E. 1991. On the nature of the scaly texture developed in melange deposits. In Roegiers, J.-C. (Ed.): *Rock mechanics as a Multidisciplinary science*, Proceedings of the 32nd U.S. Symposium, pp. 713-722.
- Ernst, W.G. 1977. Olistostromes and included ophiolitic debris from the Coastal Range of eastern Taiwan. *Memoir of the Geol. Soc. of China*. No.2 pp. 97-114.
- Ernst, W.G. 1983. Mountain-building and metamorphism: a case history from Taiwan. In Hsu, K.J. (Ed.): *Mountain building*, Academic Press, London, pp. 247-256.
- Evans, L.J. 1992. Alteration products at the earth's surface - the clay minerals. In Martini, I.P. & Chesworth, W. (Eds.): *Weathering, soils & paleosols*. Elsevier, pp. 107-125.
- Fan, C-H., Allison, R.J. & Jones, M.E. 1994. The effects of tropical weathering on the characteristics of argillaceous rocks. In Robinson, D.A. & Williams, R.B.G. (Eds): *Rock weathering & landform evolution*. John Wiley & Sons, Ltd. Chichester.
- Fan, C-H. & Jones, M.E. 1994. The impact of tropical weathering on the mechanical behaviour of mudrocks. In Nelson, P.P. & Laubach, S.E (Eds.): *Rock mechanics: models and measurements challenges from industry*. Proc. 1st North Am. Rock Mech. Sym. Balkema, Rotterdam, pp. 867-874.
- Farmer, I. 1983. *Engineering behaviour of rocks*, 2nd ed. Chapman and Hall Ltd., London.
- Fookes, P.G.; Dearman, W.R. & Franklin, J.A. 1971. Some engineering aspects of rock weathering with field examples from Dartmoor and elsewhere. *Quar. Jour. Engng. Geol.*, Vol. 4, pp. 139-185.

- Frost, R.J. 1967. The importance of correct pretesting preparation of some tropical soils. Proc. South East Asian Reg. Conf. on Soil Engng., Bangkok, 1, pp. 43-53.
- Gerrard, A.J. 1988. Rocks and landforms. Academic Division of Unwin Hyman Ltd. London.
- Gillott, J.E. 1987. Clay in engineering geology. Elsevier.
- Glasser, L.S.D. 1977. Crystallography and its applications. Van Nostrand Reinhold (UK) Co. Ltd.
- Glenn, R.C. & Nash, V.E. 1964. Weathering relationships between Gibbsite, Kaolinite, Chlorite and expansible layer silicates in selected soils from Lower Mississippi coastal plain, In Bradley, W.F. (Ed.): Proc. 12th. National Conf. on Clays and Clay Minerals, pp. 529-548.
- Goldstein, M.N.; Misumsky, V.A. & Lapidus, L.S. 1961. The theory of probability and statistics in relation to the rheology of soils. Proc. 5th Int. Conf. Soil Mech., Paris, 1, pp. 123-126.
- Grainger, P. & Harris, J. 1986. Weathering and slope stability on Upper Carboniferous mudrocks in south-west England. Quar. Jour. Engng. Geol., London, Vol. 10, pp. 155-173.
- Hardy, R. & Tucker, M. 1988. X-ray powder diffraction of sediments. In Tucker, M (Ed.): Techniques in sedimentology. Blackwell Scientific Publ.
- Hawkins, A.B. 1984. Site investigation BS 5930. Geol. Soc. London Engng. Group, Spec. Publ. No. 2.
- Head, K.H. 1980. Manual of soil laboratory testing. Vol. 1, Pentech Press, London.
- Head, K.H. 1982. Manual of soil laboratory testing. Vol. 2, Pentech Press, London.
- Head, K.H. 1986. Manual of soil laboratory testing. Vol. 3, Pentech Press, London.

- Ho, C.S. 1975. An introduction to the geology of Taiwan, explanatory text of the geological map of Taiwan. The Ministry of Economic Affairs, R.O.C.
- Ho, C.S. 1977. Mélanges in the Neogene sequence of Taiwan. *Memoir of the Geol. Soc. China*. No.2, pp. 85-96.
- Ho, C.S. 1979. Geologic and tectonic framework of Taiwan. *Mem. Geol. Soc. China*, No. 3, 57-72.
- Ho, C.S. 1982. Tectonic evolution of Taiwan, explanatory text of the tectonic map of Taiwan. The Ministry of Economic Affairs, R.O.C.
- Ho, C.S. 1987. A synthesis of the geological evolution of Taiwan. *Mem. Geol. Soc. China*, No. 9, pp. 1-17.
- Hsu, T.L. 1956. Geology of the Coastal Range, eastern Taiwan. *Bull. Geol. Surv. Taiwan*, No. 8, pp. 39-63.
- Hsu, T.L. 1971. Mélange occurrence in Cyprus. *Proc. Geol. Soc. China* No. 14, pp. 155-164.
- Hsu, T.L. 1976. The Lichi Mélange in the Coastal range framework. *Bull. of the Geol. Surv. Taiwan*, No. 25, pp. 87-95.
- Huang, T.C.; Chen, M.P. & Chi, W.R. 1979. Calcareous nannofossils from the red shale of the ophilite-mélange complex, eastern Taiwan, *Mem. Geol. Soc. China*, No.3, pp. 131-138.
- Jenny, H. 1941. *Factors of soil formation*. McGraw-Hill, New York.
- Jones, M.E.; Kågeson-Loe, N.M.; Mortimore, R.N.; Willis, S. & Leddra, M.J. 1994. The influence of geological burial on the deformation characteristics of bonded carbonate rocks. In Nelson, P.P. & Laubach, S.E (Eds.): *Rock mechanics: models and measurements challenges from industry*. Proc. 1st North Am. Rock Mech. Sym. Balkema, Rotterdam, pp. 707-713.

- Kågeson-Loe, N.M.; Jones, M.E.; Petley, D.N. & Leddra, M.J. 1993. Fabric evolution during stress path testing of the chalk. Proc. 34th US Symp. Rock Mech., Madison. In int. J. Rock Mech. Min. Sci. & Geomech. Abstr. 30: 739-745.
- Kågeson-Loe, N.M. 1994. The strain behaviour of chalk. PhD. thesis, University of London.
- Keller, W.D. 1957. The principles of chemical weathering. Lucas, Columbia, Missouri.
- Kenney, T.C. 1967. The influence of mineral composition on the residual strength of natural soils. Proc. Geotech. Conf., Oslo, Vol. 1, pp. 123-129.
- Lambe, T.W. & Whitman, R.V. 1979. Soil mechanics, SI Version. John Wiley & Sons, Inc., New York.
- Laure, D.K. & Speed, R.C. 1984. Structure of the accretionary complex of Barbados. II: Bissex Hill: Geol. Soc. Am. Bull., Vol. 95, pp. 1360-1372.
- Leddra, M.J. 1989. Deformation of chalk through compaction and flow. Ph.D. thesis, University of London.
- Leroueil, S. & Vaughan, P.R. 1990. The general and congruent effects of the structure in natural soils and weak rocks. *Géotechnique* 40, No. 3, pp. 467-488.
- Lin, M.T. & Tsai, Y.B. 1981. Seismotectonics in Taiwan-Luzon area. Bull. Inst. Earth Sciences, Academia Sinica, Vol. 1, pp. 51-82.
- Lin, J. C. 1991. Landslides of the Coastal Range, eastern Taiwan. Unpublished PhD Thesis, University of London.
- Lindsay, J.F. 1992. Extraterrestrial soils-the lunar experience. In Martini, I.P. & Chesworth, W. (Eds.): Weathering, soils & paleosols. Elsevier, pp. 41-70.
- Liou, J.G.; Suppe, J. & Ernst, W.G. 1977. Conglomerates and pebbly mudstones in the Lichi Mélange, eastern Taiwan. Memoir of the Geol. Soc. of China. No.2, pp. 115-128.

- Liu, C. & Evett, J.B. 1984. Soil properties: testing, measurement, and evaluation. Prentice-Hall, Inc.
- Lo, H.J.; Chen, C.H.; Jouh, C.C. & Juan, V.C. 1978. A preliminary study of the exotic amphibolite in the Lichi Formation, east Coastal Range, Taiwan. Proc. Geol. Soc. China, No. 21, pp. 34-41.
- Loudon, P.A. 1967. Some deformation characteristics of kaolin. PhD. thesis, University of Cambridge.
- Macias, F. & Chesworth, W. 1992. Weathering in humid regions, with emphasis on igneous rocks and their metamorphic equivalents. In Martini, I.P. & Chesworth, W. (Eds.): Weathering, soils & paleosols. Elsevier, pp. 283-306.
- Meng, C.Y. & Chiang, S.C. 1965. Subsurface data from the wildcat SS-1, Shihshan, Taitung. Petrol. Geol. Taiwan, No. 4, pp. 283-286.
- Moore, G.S. & Kraig, D.E. 1980. Structural geology of Nias Island, Indonesia. Implications for subduction zone tectonics. Am. Jour. Sci., 280, pp. 193-223.
- Moore, C.J.; Roeske, S.; Lundberg, N.; Schoonmaker, J.; Cowan, D.S.; Gonzales, E. & Lucas, S.E. 1986. Scaly fabrics from Deep Sea Drilling Project cores from forearcs. Geological Society of America Memoir. Vol. 166, pp. 55-73.
- Morgenstern, N.R. & Tchalenko, J.S. 1967. The optical determination of preferred orientation in clays and its application to the study of microstructure in consolidated kaolin. I. Proc. Roy. Soc. A, 300, pp. 218-234.
- Motteshead, D.N. 1989. Rates and patterns of bedrock denudation by coastal salt spray weathering, a seven year record. Earth Surface Processes and Landforms, 14, pp. 383-398.
- Nahon, D.B. 1991. Introduction to the petrology of soils and chemical weathering. John Wiley & Sons, Inc.
- Ollier, C. 1984. Weathering. 2nd ed. Longman Inc., New York.

- Page, B.M. 1974. The Lichi mélange of eastern Taiwan: a preliminary report. *Mining Technical Digest (Taipei)*, 12, 11-14.
- Page, B.M. 1978. Franciscan mélange compared with olistostromes of Taiwan and Italy. *Tectonophysics* No.47, pp.223-246.
- Page, B.M. & Suppe, J. 1981. The Pliocene Lichi Mélange of Taiwan: Its plate-tectonic and olistostromal origin. *American Journal of Science*, Vol. 281, March, pp. 193-227.
- Pandian, N.S.; Nagaraj, T.S. & Sivakumar Babu, G.L. 1993a. Tropical clays I: Index properties and microstructural aspects. *Journal of Geotechnical engineering*, Vol. 119, No. 5. pp. 826-839
- Pandian, N.S.; Nagaraj, T.S. & Sivakumar Babu, G.L. 1993b. Tropical clays II: Engineering behaviour. *Journal of Geotechnical engineering*, Vol. 119, No. 5. pp. 840-861
- Pedro, G. & Sieffermann, G. 1979. Weathering of rocks and formation of soils. *Earth Sci.* 16, pp. 39-55.
- Peltier, L. 1950. The geographic cycle in periglacial regions as it is related to climatic geomorphology. *Ann. Assoc. Am. Geog.*, 40, pp. 214-236.
- Petley, D.N. 1994. Deformation of mudrocks. Unpublished PhD thesis, University of London, in press.
- Petley, D.; Leddra, M.; Kageson-Loe, N.; Jones, M.; Fan, C. & Stafford, C. 1993. Deformation and fabric change In weak fine grained rocks during high pressure consolidation and shear. In Anagnostopoulos *et al.* (Eds.): *Geotechnical Engineering of Hard Soils-Soft Rocks*. Balkema, Rotterdam, pp. 737-743.
- Pudsey, C.J. & Reading, H.G. 1981. Sedimentology of the Scotland Group, Barbados. *Geol. Soc. London Sp. Pub.* 10, pp. 291-308.

- Rampello, S. & Silvestri, F. 1993. The stress-strain behaviour of natural and reconstituted samples of two overconsolidated clays. In Anagnostopoulos *et al.* (Eds.): Geotechnical Engineering of Hard Soils-Soft Rocks. Balkema, Rotterdam, pp. 769-778.
- Roscoe, K.H., Schofield, A.N. & Wroth, C.P. 1958. On the yielding of soils. *Géotechnique* 8, pp. 22-53.
- Russell, D.J. & Parker, A. 1979. Geotechnical, mineralogical and chemical interrelationships in weathering profiles of an overconsolidated clay. *Quar. Jour. Engng. Geol.* Vol. 12, pp. 107-116.
- Schofield, A. & Wroth, C.P. 1968. Critical state soil mechanics. McGraw-Hill, London.
- Schoonmaker, J. 1986. Clay mineralogy and diagenesis of sediments from deformation zones in the Barbados accretionary wedge. *Geol. Soc. Am. Mem.* Vol. 166, pp. 105-116.
- Schwertmann, U. & Taylor, R.M. 1977. Iron oxides. In Dixon, J.B. & Weed, S.B. (Eds): Minerals in soil environments, Soil Sci. Soc. of Am. Madison, Wisc., pp. 145-180.
- Selby, M.J. 1993. Hillslope material and processes (2nd edition). Oxford University Press, Oxford.
- Senior, B.R. & Mabbutt, J.A. 1979. A proposed method of defining deeply weathered rock units based on regional geological mapping in southwest Queensland. *Jour. Geol. Soc., Australia*, 26, pp. 237-254.
- Senn, A. 1940. Paleogene of Barbados and its bearing on the history and structure of the Antillean Caribbean region. *Bull. Am. As. Pet. Geol.* 24.9, pp. 1548-1610.
- Seno, T. 1977. The instantaneous rotation vector of the Philippine Sea Plate relative to the Eurasian Plate. *Tectonophysics* No.42 pp. 209-226.
- Skempton, A.W. 1953. The colloidal activity of clays. *Proc. 3rd. Int. Conf. Soil Mech. Found. Engng., Zurich*, Vol. 1, pp. 57-61.

- Skempton, A.W. 1954. The pore pressure coefficients A and B. *Géotechnique* 4, pp. 143-147.
- Skempton, A.W. 1961. Discussion on Section 6 (Earth Dams, Slopes and Open Excavations). Proc. 5th. Int. Conf. Soil Mech., Paris, 3. pp. 349-350.
- Skempton, A.W. 1964. Long term stability of clay slopes. *Géotechnique* 14, pp. 77-101.
- Skempton, A.W. 1966. Some observations of tectonic shear zones. Proc. 1st Int. Conf. Rock Mech., Lisbon, 6, pp. 329-335.
- Skempton, A.W. & Bjerrum, L. 1957. A contribution to the settlement analysis of foundations on clay. *Géotechnique* 7, pp. 168.
- Skempton, A.W. & Petley, D.J. 1967. Strength along structural discontinuities in stiff, fissured clay. Proc. Geotech. Conf. Oslo, 2, pp. 3-20.
- Solé, A, Josa, R., Pardini, G., Aringhiere, R., Plana, F. & Gallart, F. 1992. How mudrock and soil physical properties influence badland formation at Vallcebre (Pre-Pyrenees, NE Spain). CATENA, Vol. 19, pp. 287-300.
- Speed, R.C. 1981. Geology of Barbados: implication for an accretionary origin. Oceanologica Acta, Proc. 26th Int. Geol. Cong., Geology of continental margins symposium, Paris (1980), pp. 259-265.
- Speed, R.C. 1983. Structure of the accretionary complex of Barbados, I: Chalky Mount. Geol. Soc. Am. Bull., Vol. 94, pp. 92-116.
- Speed, R.C. & Larue, D.K. 1982. Barbados: Architecture and implications for accretion. Jour. Geophys. Research, Vol. 87, No. B5, pp. 3633-3643.
- Stride, A., Belderson, R. & Kenyon, N. 1982. Structural grain, mud volcanoes and other features on the Barbados Ridge Complex revealed by Gloria side-scan sonar. Marine Geology, 49, pp. 189-196.
- Taylor, D.W. 1948. Fundamentals of soil mechanics. Chapman & Hall Ltd.

- Teng, L.S. 1981. On the origin and tectonic significance of the Lichi Formation, Coastal Range, eastern Taiwan. *Ti-Chi*, Vol. 2, pp. 51-61.
- Terzaghi, K. 1936. Stability of slopes of natural clay. *Proc. 1st Int. Conf. Soil Mech. Found. Engng.* 1, pp. 161-165.
- Terzaghi, K. & Peck, R.B. 1967. *Soil mechanics in engineering practice*. Wiley, New York.
- Thomas, M.F. 1974. *Tropical geomorphology. A study of weathering and landform development in warm climates*. MacMillan.
- Thomas, M.F. 1994. *Geomorphology in the tropics. A study of weathering and denudation in low latitudes*. John Wiley & Sons Ltd., Chichester.
- Toll, D.G. & Malandraki, V. 1993. Triaxial testing of a weakly bonded soil. In Anagnostopoulos *et al.* (Eds.): *Geotechnical Engineering of Hard Soils-Soft Rocks*. Balkema, Rotterdam, pp. 825-831.
- Torrini, R., Speed, R. & Mattioli, 1985. Tectonic relationships between forearc-basin strata and the accretionary complex at Bath, Barbados. *Geological Society of America Bulletin*, Vol. 96, pp. 861-874
- Trudgill, S.T. 1983. *Weathering and erosion*. Butterworth & Co Ltd.
- Vallejo, L.E.; Alaasmi, A. & Yoo, H. 1993. Behaviour under compression of stiff clays with multiple cracks. In Anagnostopoulos *et al.* (Eds.): *Geotechnical Engineering of Hard Soils-Soft Rocks*. Balkema, Rotterdam, pp. 825-831.
- Vaughan, P.R. 1985. Mechanical and hydraulic properties of in situ residual soils. *Proc. 1st Int. Conf. Geomechanics in Tropical Lateritic and saprolitic soils, Brasilia*, Vol. 3, pp. 231-263.
- Vaughan, P.R.; Maccarini, M. & Mokhtar, S.M. 1988. Indexing the engineering properties of residual soil. *Quar. Jour. Engng. Geol.* Vol. 21, pp. 69-84.
- Velde, B. 1985. *Clay minerals: A physical-chemical exploration of their occurrence*. Elsevier, Amsterdam.

- Vesic, A.S. & Clough, G.W. 1968. Behaviour of Granular materials under high stresses. Proc. Am. Soc. Civil Engrs., 94, SM3, 661-688.
- Vickers, B. 1978. Soil mechanics. Granada Publishing Ltd.
- Viggiani, G.; Rampello, S & Georgiannou, V.N. 1993. Experimental analysis of localisation phenomena in triaxial tests on stiff clays. In Anagnostopoulos *et al.* (Eds.): Geotechnical Engineering of Hard Soils-Soft Rocks. Balkema, Rotterdam, pp. 849-856.
- Wallace, K.B. 1973. Structural behaviour of residual soils of the continually wet Highlands of Papua New Guinea. *Géotechnique*, 23 (2), pp. 203-218.
- Wang, C.S. 1976. The Lichi Formation of the Coastal Range and arc-continent collision in eastern Taiwan. Bull. of the Geological Survey of Taiwan. No. 25, pp.73-6.
- Weaver, C.E. 1989. Clays, muds, and shales. Elsevier.
- Weaver, C.E. & Pollard, L. 1975. The chemistry of clay minerals. Elsevier.
- Westbrook, G.K. 1975. The structure of the crust and upper mantle in the region of Barbados and the Lesser Antilles. *Geophys. Jour.* Vol. 43, pp. 1-42.
- Westbrook, G.K. & Smith, M.J. 1983. Long décollements and mud volcanoes: Evidence from the Barbados Ridge Complex for the role of high pore fluid pressure in the development of an accretionary complex. *Geology*, Vol. 11, pp. 279-283.
- Wood, D.M. 1990. Soil behaviour and critical state soil mechanics. Cambridge University Press, Cambridge.
- Wu, B.; Marsden, J.R. & Hudson, J.A. 1990. Undrained mechanical behaviour of mudstones. In: Cripps, J.C. & Moon, C.F. (Eds): The Engineering Geology of Weak Rock, Geological Society Engineering Group, London, pp. 105-114
- Yassir, N.A. 1989. Mud volcanoes and the behaviour of overpressured clays and silts. Unpublished Ph.D. thesis, University of London.

Yen, F.S. & Chen, J.K. 1990. The relationships between the morphology and the weathering erosion behaviour of mudstone slope in the Southern Taiwan. *Ore Metallurgy* 34/3, pp. 80-93.

Yong, R.N. 1971. General Report to Session 5. Soil technology and stabilisation. Proc. 4th Asian Reg. Conf. Soil Mech. Found. Eng., Bangkok 2.

Appendix I: Soil Mechanics Theories

AI.1 Effective stress concept

In soil mechanics, the concept of effective stress is, perhaps, the most important Principle. The mechanical behaviour of a soil is largely influenced by the presence of pore fluid (Lambe & Whitman, 1979). When a soil is subject to a given total stress, the behaviour of the soil will be dependent on the magnitude of the pore fluid pressure (Atkinson & Bransby, 1978). Therefore, it is the interaction of total stress and pore pressure which controls the behaviour the soil, and this is the concept of the effective stress.

The principle of effective stress was first given by Terzaghi (1936). Terzaghi's statement consists of two parts. The first part defines the effective stress:

The stress in any point of a section through a mass of soil can be computed from the total principle stress σ_1 , σ_2 and σ_3 which act at this point. If the voids of the soil are filled with water under a stress u the total principle stresses consist of two parts. One part u acts in the water and in the solid in every direction with equal intensity. It is called the neutral stress (or the pore pressure). The balance $\sigma_1' = \sigma_1 - u$, $\sigma_2' = \sigma_2 - u$ and $\sigma_3' = \sigma_3 - u$ represents an excess over the neutral stress u and it has its seat exclusively in the solid phase of the soil. This fraction of the total principle stress will be called the effective principle stress.

from which the fundamental effective stress equation is derived as:

$$\sigma' = \sigma - u. \quad (\text{AI.1})$$

where

σ and σ' are the total and effective stress respectively,
 u is the pore fluid pressure.

The second part of the statement outlines the importance of the effective stress.

All measurable effects of a change of stress, such as compression, distortion and a change of shearing resistance, are exclusively due to changes in the effective stress.

Like many other principles, there are certain assumptions required to make the effective stress equation as simple as it shows,

1. the soil is homogeneous,
2. the soil is fully saturated,
3. the pore fluid is incompressible,
4. the grains are incompressible.

otherwise, more complexity has to be taken into account.

According to the principle of effective stress given by Terzaghi (1936), the consolidation of a sediment will only occur in response to changes in effective stress. Changes in total stress do not necessarily cause changes in the effective stress. If the pore fluid pressure changes by the same amount as total stress, the sediment will not receive any change in effective stress.

Since the effective stress concept was introduced, the validity of the principle has been assessed by various workers. Bishop (1976) examined the equation and took the compressibility of grains into account,

$$\sigma' = (\sigma - u) + (C_s/C)u \quad (\text{AI.2})$$

where,

C_s = compressibility of solid material forming grains, and

C = bulk soil compressibility for relevant stress range.

For clay material, C_s has, however, been found to be very low within stress range up to 62 MPa (Bishop *et al.*, 1975). Bishop and Skinner (1977) examined the validity of the equation by conducting high pressure tests on a variety of materials and concluded that the effective stress equation is valid for stress up to 70 MPa. It is, therefore, of no doubt that the principle of effective stress is valid for the experiments conducted in the study.

AI.2 Consolidation theory

In the context of the principle of effective stress, the volume of a saturated soil will only change when the effective stress that the soil is subject to is changed. Since mineral

grains and pore fluid (water) are assumed to be incompressible in the stress range used, the volume strain of a saturated soil can only occur when pore fluid is expelled from or drawn into the pore space. As pore fluid is removed from a mass of soil the volume of the soil will change and so will the effective stress until the system reaches an equilibrium stress state. According to Darcy's law, which governs the fluid flow in the mass of soil, the dissipating process is time-dependent and is known as consolidation. Therefore, consolidation is governed by complex interactions between total and effective stresses, drainage, pore fluid pressure, and compressibility.

The consolidation process can be demonstrated by the simple system model illustrated in Figure AI.1. The system contains a water-filled cylinder with a close-fitting piston (with negligible weight and frictionless), a spring connecting the piston and the base of the cylinder, and a standpipe of negligible volume connected to the cylinder at the mid-height. The piston has a drainage lead which is fitted with a valve controlling the water flow. Among the components of the model, the spring represents the soil skeleton, and the full-filled water is the pore fluid in a saturated soil. The stiffness of the spring can be treated as soil compressibility, and the resistance that given by the valve to the flow of water and the degree of opening of the valve model the permeability of the soil. The use of the standpipe is to measure the pressure of the water in the cylinder (pore fluid pressure).

When a force σ is applied to the piston, which has a cross section area of unit, it generates a total stress of σ to the water-spring system. Assuming the water in the cylinder has a pressure of u , the stress taken by the spring has to be $(\sigma-u)$ to achieve a balance of stress. This $(\sigma-u)$ is equivalent to an effective stress σ' as introduced previously.

For material to consolidate (i.e. spring compresses, piston settles, and water dissipates) an extra force $\Delta\sigma$ is added to the piston resulting in an extra total stress $\Delta\sigma$. If the valve is closed at this stage (i.e. no drainage is permitted), the extra total stress $\Delta\sigma$ will be completely taken by the water because water is assumed to be incompressible, and lead to an excess pore pressure Δu equivalent to $\Delta\sigma$ (Figure AI.2). Now, open the valve allowing water to drain out through the lead, the excess pore pressure starts to decrease, the stress taken by the spring increases, and the piston begins to settle. After an infinite time, the excess pore pressure becomes zero and the extra total stress $\Delta\sigma$ transfers on to the spring (i.e. the effective stress becomes $\sigma'+\Delta\sigma$), a new equilibrium state is reached and the consolidation is completed (Figure AI.3).

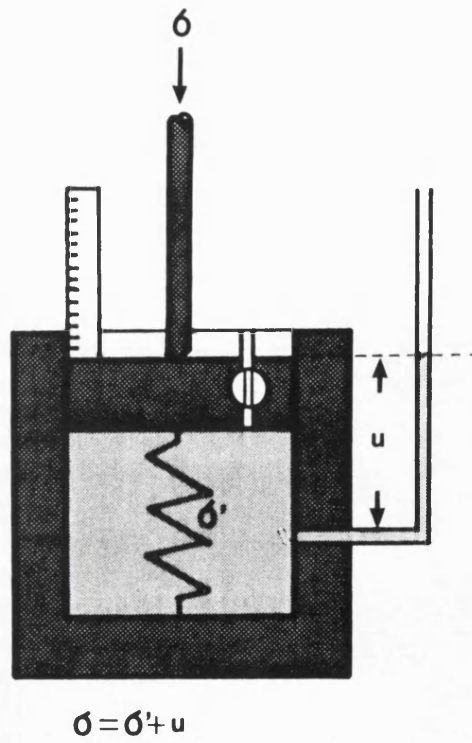


Figure AI.1 Consolidation model

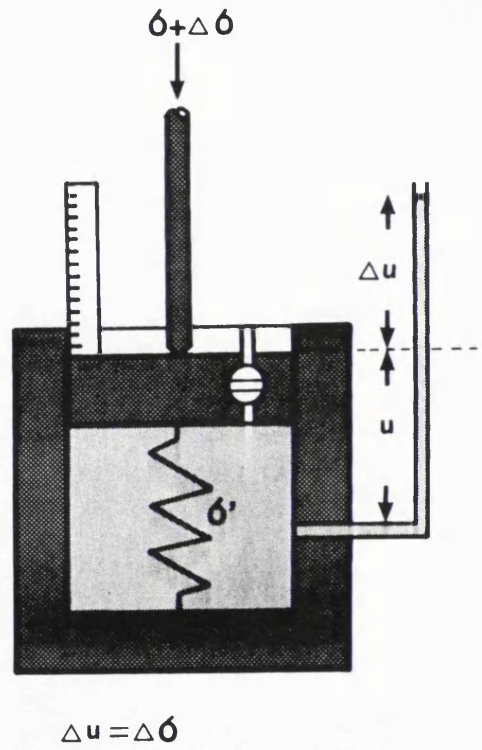


Figure AI.2 Undrained response to increase in total stress

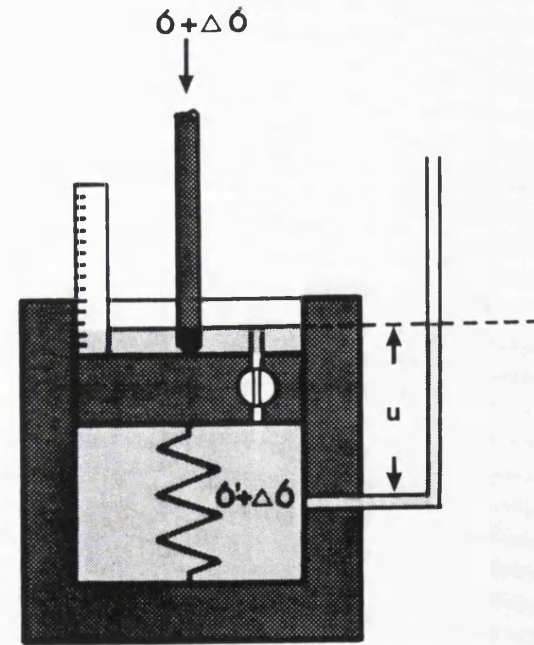


Figure AI.3 Consolidation as pore water drains and pore water pressure equilibrates

AI.3 Critical state model

The mechanical deformation behaviour of the studied materials from the standard Isotropic-Consolidation-Undrained-Shear test programme is interpreted based on a model, namely, the critical state model. The model was developed in 1960's and has been widely used in soil mechanics, which defines a series of state boundaries in q - p' - v space (deviatoric stress-mean effective stress-specific volume). These boundaries comprise two lines and two surfaces, and form a volume, inside which exist the only possible stress states for the material to achieve. The state boundaries can be determined by conducting a series of standard triaxial tests on materials of similar origin but with various overconsolidation ratios (Bishop & Henkel, 1962; Atkinson & Bransby, 1978; Wood, 1990). Different materials, in terms of either different origin or different compaction history, will have different performance in their stress paths, on the stresses-specific volume space. Therefore, by comparing the difference in the stress path between samples from various depth the effect of weathering on the mechanical behaviour of the materials can be understood.

The four state boundaries are described as follow:

1. The **NORMAL CONSOLIDATION LINE**: it is a stress path followed by a normally consolidated soil under isotropic compression, which means the path lies on the $q = 0$ plane (Figures AI.4, 5 & 6), and delineates the maximum specific volume that a material can be while it is subjected to a given mean effective stress. All materials, from normally consolidated to heavily overconsolidated, lie within this state boundary line.
2. The **CRITICAL STATE LINE**: it can be described as a ultimate state line existing in stress-specific volume space (Figures AI.7, 8 & 9) on which all the stress paths from triaxial compression test terminate, both drained and undrained. It exists as a point at a given specific volume where the material strains at constant volume without increasing stress. It is therefore necessary to conduct a series of tests on a particular material, at a range of initial confining pressures to be able to delineate the line.
3. The **ROSCOE SURFACE**: for those normally consolidated to lightly overconsolidated soils, the stress paths for both drained and undrained tests will trace out a curved surface which links the normal consolidation line with the critical state line in stress-void ratio space (Figures AI.10 & 11). This curved surface is termed the

Roscoe surface and the intersection of the test plane, either drained or undrained, for any test with the Roscoe surface, fixes complete test paths in stresses-specific volume space. Similar in characteristics to the normal consolidation line the Roscoe surface limits the stress state that a material of a certain specific volume can attain.

4. The **HVORSLEV SURFACE**: similar in concept to the Roscoe surface, applied to heavily overconsolidated soils there exists another state boundary surface which can be determined by a series of triaxial compression tests on heavily overconsolidated samples. This surface is termed the Hvorslev surface, which limits the states of heavily overconsolidated specimens within stresses-specific space. The Hvorslev surface (Figures AI.12, 13) is limited by the critical state line at one end and by the tension cut-off at the other, where the specimen will have tensile failure. In other words, the critical state line can diagrammatically be defined as the intersection of the Roscoe surface and Hvorslev surface, and these two boundary surfaces serve for both drained and undrained tests on normally consolidated and overconsolidated samples respectively.

Thus, a complete model can be obtained (Figure AI.14). Use the concept of the model the change in the material behaviour can be detected. The model, however, was developed assuming that the materials are homogeneous. In reality, this is very rare for those naturally occurred soils. Therefore, the results are seldom as simple as the model suggests and the model merely gives a guide line for the comparison between the materials with different degrees of weathering to be made.

In soil mechanics it is often for convenience purpose to distinguish samples by their initial water content. Soils are divided into two groups depending on whether their states lie above and to the right of the critical state line in v - p' space or lie below and to the left. The first group is termed *wet of critical*, for a sample in this category has a moisture content higher than that of the sample on the critical state line at the same value of p' , and the second group as *dry of critical*, (Figure AI.15). This classification is useful in that it group together samples with similar pore pressure and volume change behaviour. A simple description of these two terms is that wet of critical is equivalent to lightly overconsolidated to normally consolidated state and dry of critical is equivalent to moderately to heavily overconsolidated state.

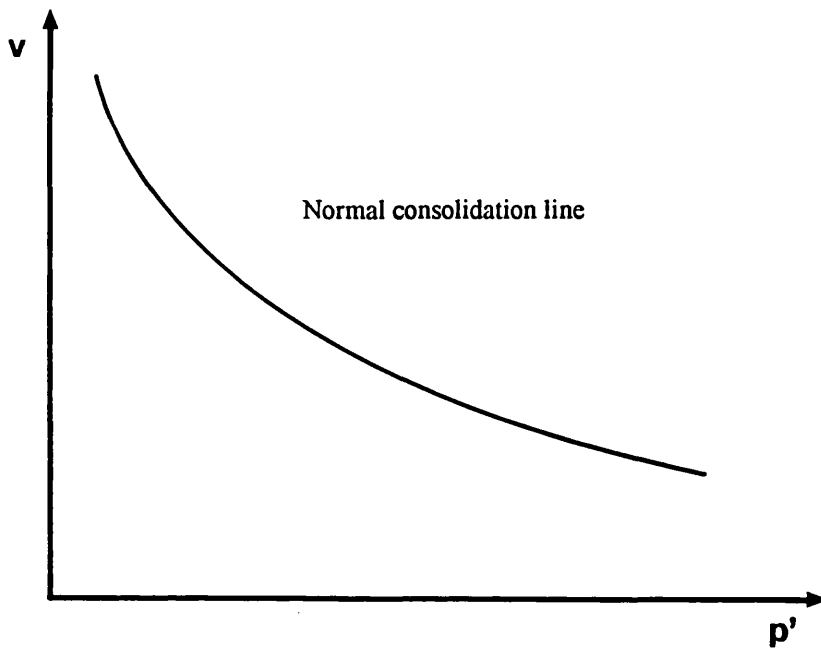


Figure AI.4 Normal consolidation line in $v - p'$ space

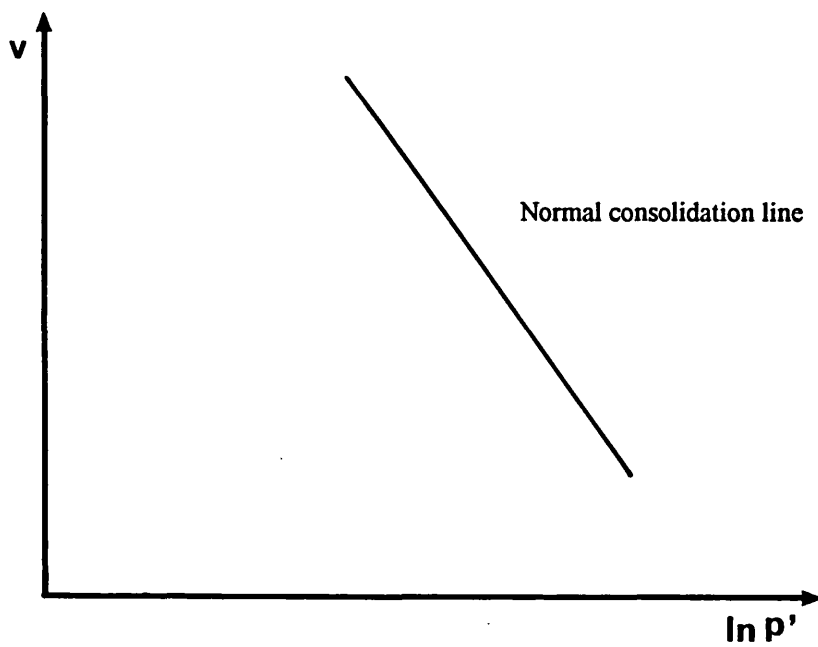


Figure AI.5 Normal consolidation line in $v - \ln p'$ space

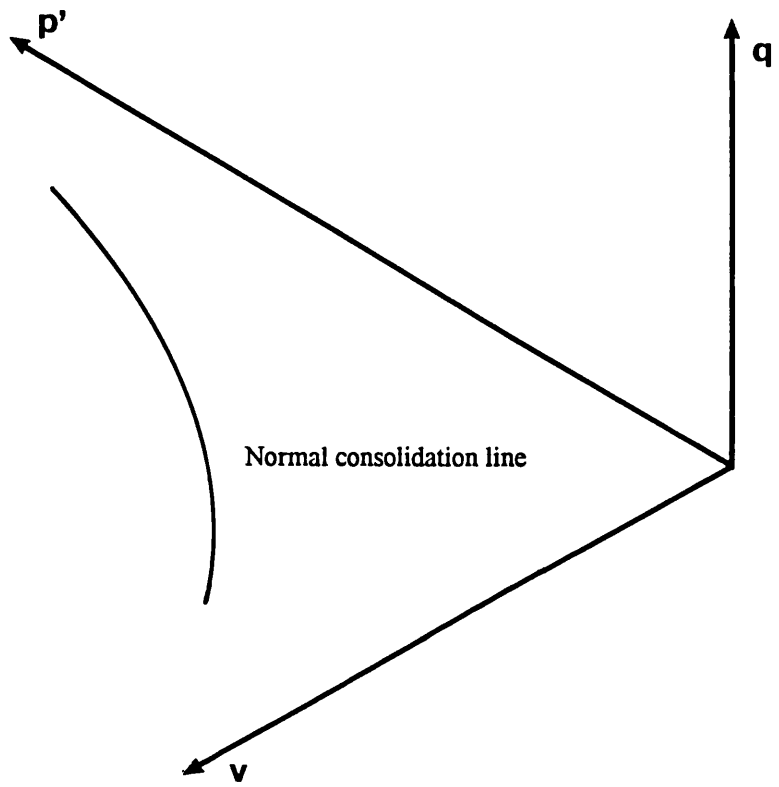


Figure AI.6 Normal consolidation line in $q - v - p'$ space

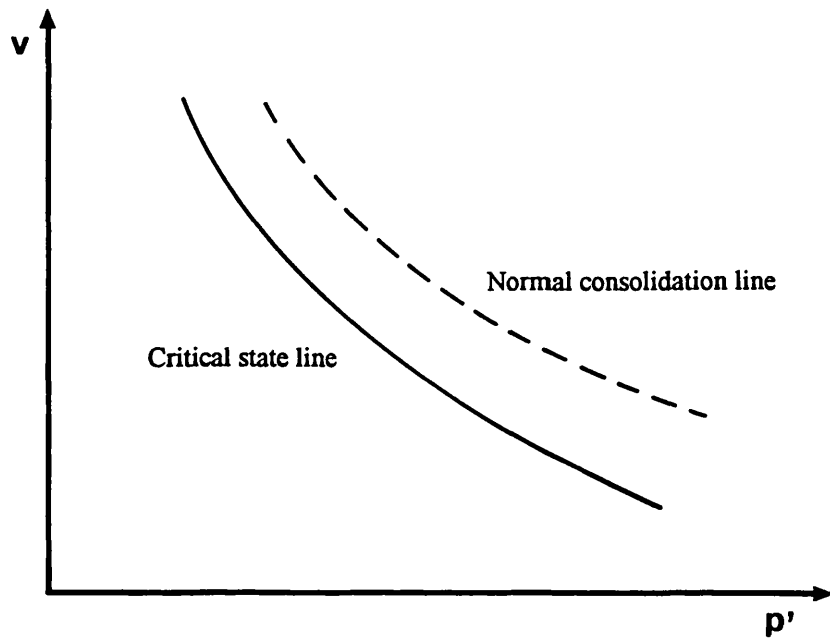


Figure AI.7 Critical state line in $q - p'$ space

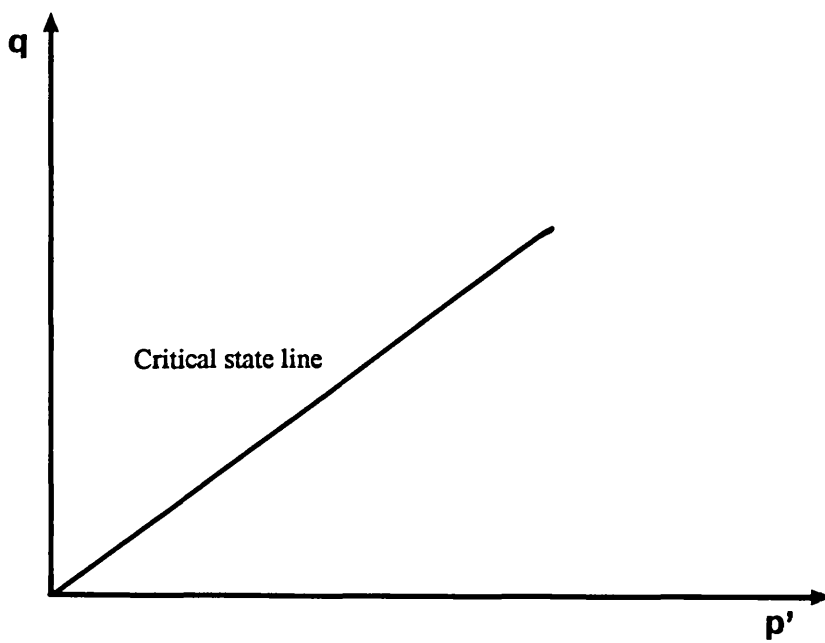


Figure AI.8 Critical state line in $v - p'$ space

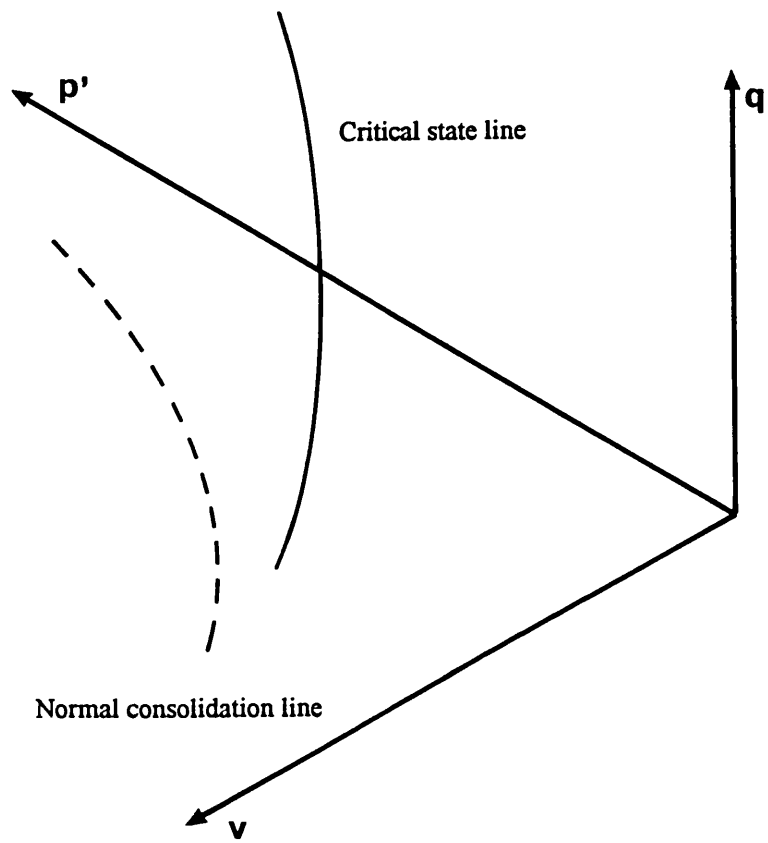


Figure AI.9 Critical state line in $q - v - p'$ space

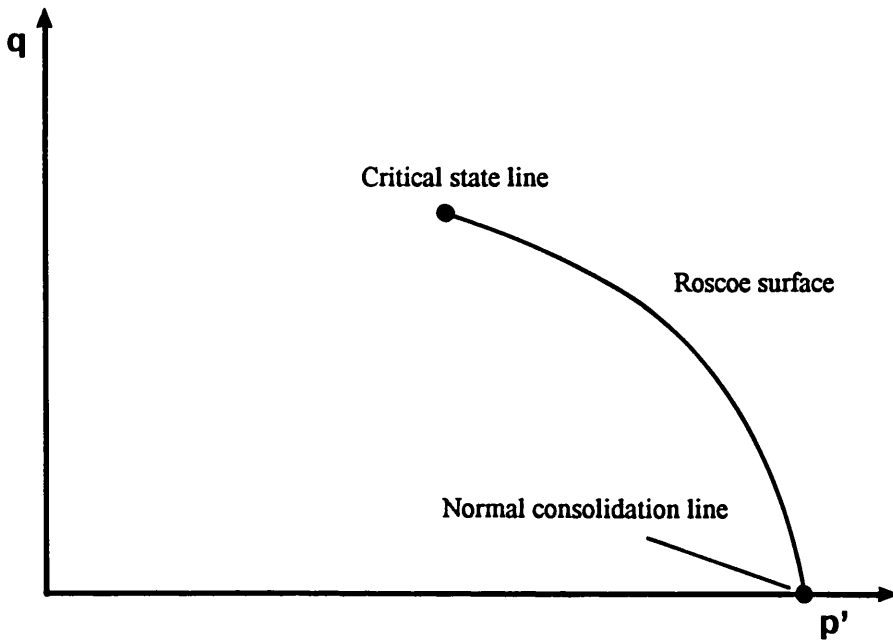


Figure AI.10 Roscoe surface in $q - p'$ space

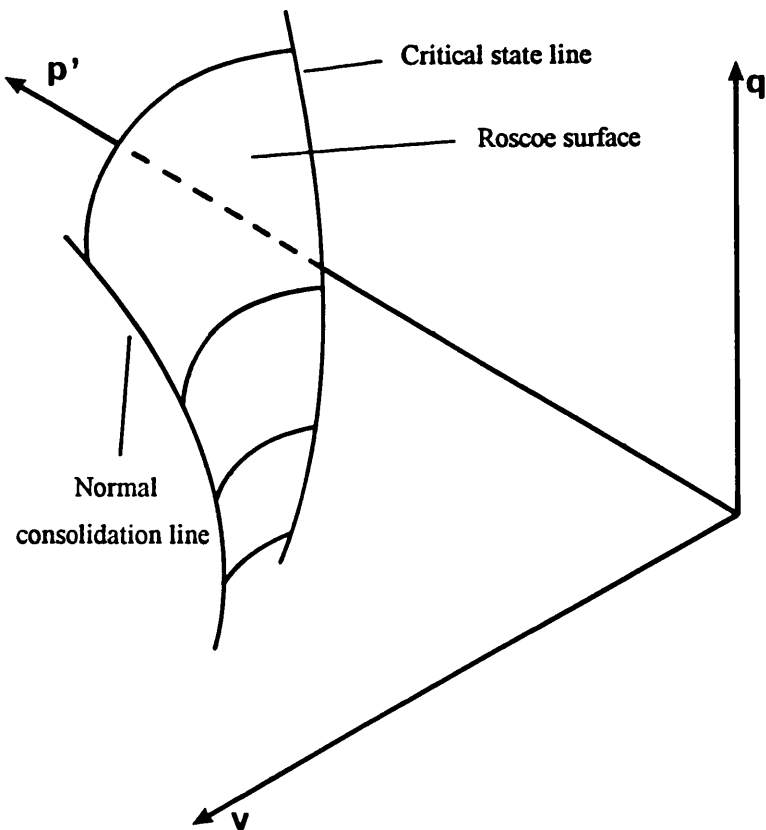


Figure AI.11 Roscoe surface in $q - v - p'$ space

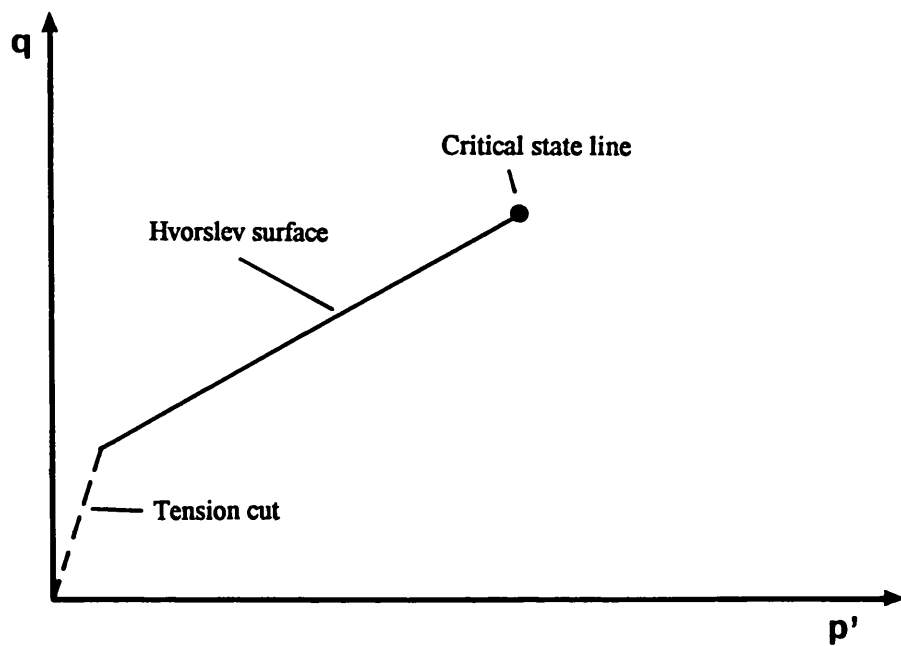


Figure AI.12 Hvorslev surface in $q - p'$ space

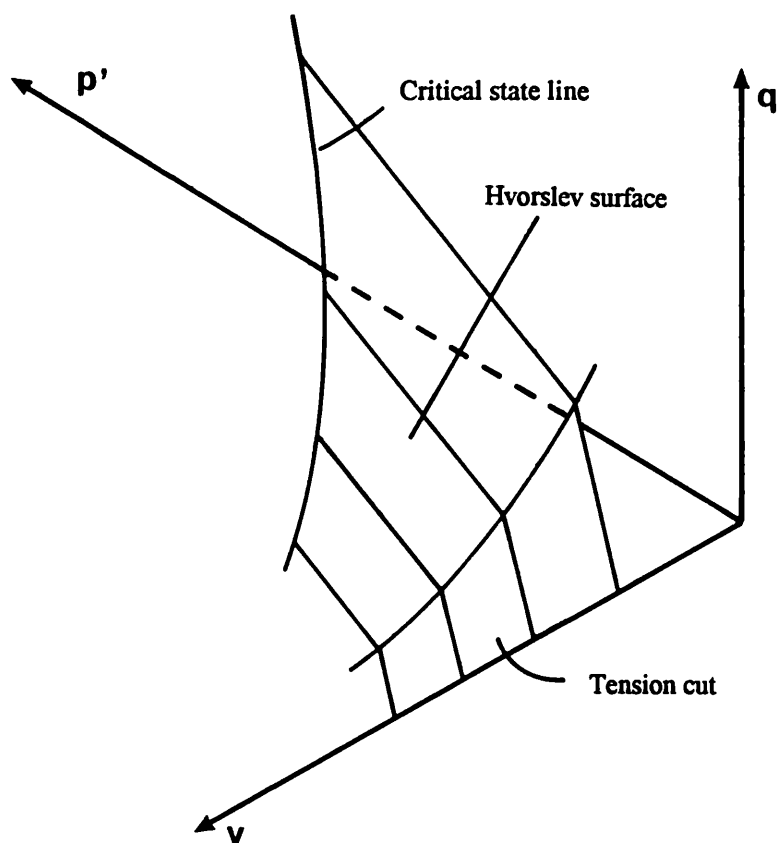


Figure AI.13 Hvorslev surface in $q - v - p'$ space

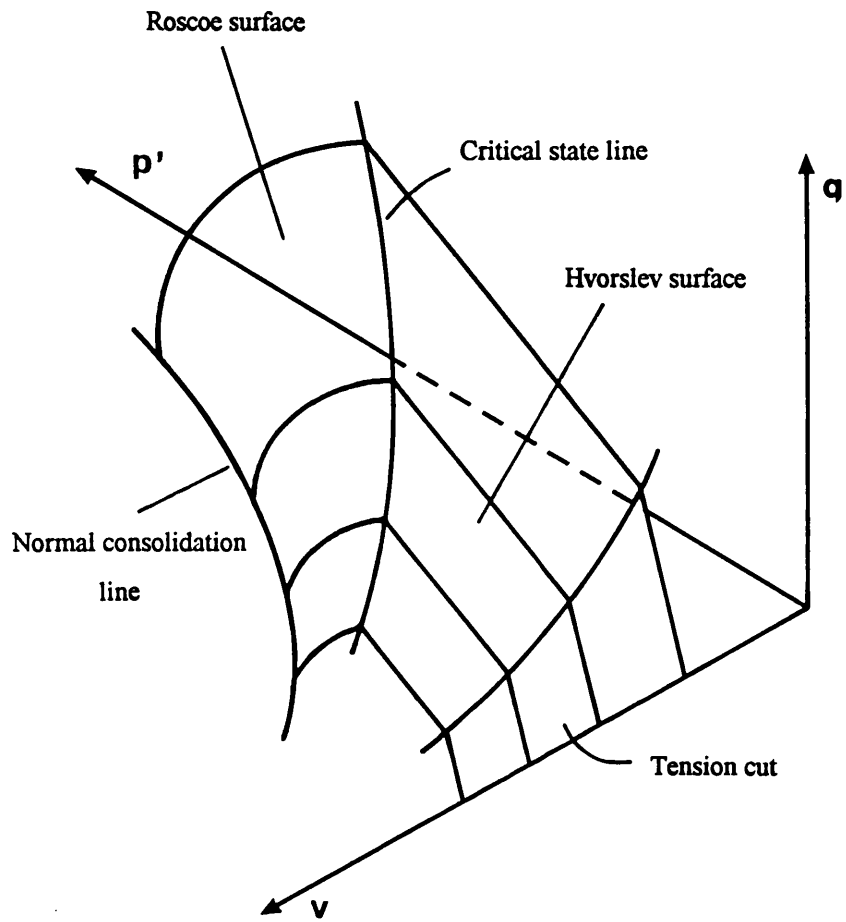


Figure AI.14 Complete critical state model

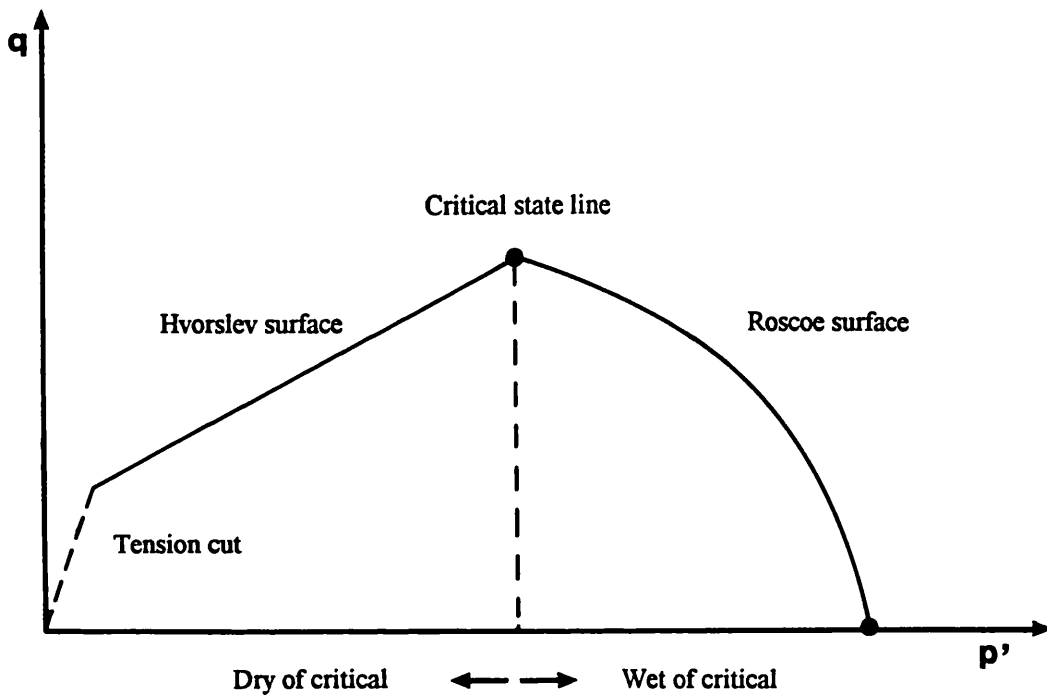


Figure AI.15 Diagram explaining wet & dry of critical

AI.4 Skempton's pore pressure parameters

The degree of pore pressure generation, resulting from an increase in either the horizontal or vertical total stress can be expressed in terms of a pore pressure parameter. Each pore pressure parameter relates the change in the pore pressure to a change in a particular stress (Skempton, 1954). Pore pressure parameters A and B are only valid for isotropically consolidated samples.

Pore pressure parameter A

This term relates a change in the pore pressure (Δu) to an increase in the total vertical stress ($\Delta\sigma_1$) in an undrained experiment where horizontal stress (σ_3) is held constant

$$A = \Delta u / \Delta\sigma_1 \quad (\text{eq. AI.3})$$

or, where the triaxial apparatus uses a balanced ram the change in σ_1 is equal to the change in deviatoric stress (Δq), as the cell pressure remains constant, thus,

$$A = \Delta u / \Delta q \quad (\text{eq. AI.4})$$

Pore pressure parameter B

This term relates pore pressure development to an incremental change in isotropic stress. B is considered to be equal to unit when sample is fully saturated.

$$B = \Delta u / \Delta\sigma \quad (\text{eq. AI.5})$$

Appendix II: SediGraph 5100, Sedimentation Theory

The finer part of the particle size distributions of the studied materials were obtained using the SediGraph 5100, a X-ray operated apparatus for determining particle size, at the Department of Geography, King's College London. The theoretical information about the SediGraph 5100 is described below.

The determination of particle size of SediGraph 5100 is based on the sedimentation theory, Stoke's law, in which the measured equilibrium velocity of a particle through a viscous medium, due to gravitational force, can be related to the size of the particle. The diameter of a spherical particle can be determined by the equation (AII.1) (Stoke's law).

$$D = Kv^{1/2} \quad (\text{AII.1})$$

where

D is the diameter of the spherical particle,

v is the equilibrium sedimentation velocity of the particle,

K is a coefficient which is relevant to the viscosity of medium and the densities of the particle and the medium.

The K value can be calculated using equation (AII.2)

$$K = [18\eta/(\rho-\rho_0)g]^{1/2} \quad (\text{AII.2})$$

where

η is the viscosity of the medium,

ρ is the density of the particle,

ρ_0 is the density of the medium,

g is the acceleration of gravity.

The Stoke's law, equation (AII.1), is actually defined to determine the diameters of spherical particles only but not for any other shapes. In reality, spherical particles are very rare, especially in clay sediment. However, it is generally accepted to specify the size of non-spherical particles using the diameter of a sphere of the same material that would have the same sedimentation velocity. This is because there is no single linear dimension can satisfactorily describe irregularly shaped particles at present day. Therefore, the diameter measured from equation (AII.1) is an effective diameter.

Data on the sedimentation velocity of suspended particles are obtained by measuring the concentration of particles remaining in suspension as a function of time. A dilute, dispersion of the fine particle material, which is obtained from sieving remaining in the < 63 μ tray, is stirred to make the mixture homogeneous. After stirring, allow particles to undergo sedimentation spontaneously and measure the time from the beginning of the sedimentation. A particle with diameter D will settle a distance h after a time period t, by which the equation (AII.1) can be re-written as:

$$D = K [h/t]^{1/2} \quad (\text{AII.3})$$

After a given time t_i particles larger than the corresponding diameter D_i will fall below the given distance h from the surface of the suspension. If the concentration of the particle is C_0 g cm⁻³ at the initial state and that at distance h after time t_i is C_i g cm⁻³, the weight percent of particles (P_i) finer the D_i can then be calculated by equation (AII.4).

$$P_i = 100 [C_i/C_0] \quad (\text{AII.4})$$

A particle size distribution curve can be plotted by measuring C_i after various times and calculating the corresponding values of P_i and D_i .

The above description is the way of determining particle size distribution using sedimentation method. It can be operated manually. The advantage of using the SediGraph 5100 is that all measurements are obtained by the apparatus without manual disturbance, and it is more accurate.

To obtain values of C_i , the SediGraph uses a finely collimated X-ray beam to penetrate the examined suspension. The transmitted intensity of the X-ray beam is determined by the clarity of the suspension, which is a function of the weight concentration of the suspension solid. The transmitted intensity of the X-ray beam through a sample container filled with examined liquid can be calculated by equation (AII.5).

$$I/I_0 = e^{-(a_1\phi_1 + a_2\phi_2)L} \quad (\text{AII.5})$$

where

I is the transmitted intensity,

I_0 is the incident intensity,

a_1 is the X-ray absorption coefficient of the liquid,

a_s is the X-ray absorption coefficient of the particulate solids,
 a_c is the X-ray absorption coefficient of the cell wall of the sample container,
 ϕ_l is the weight fraction of liquid present in the suspension,
 ϕ_s is the weight fraction of solid present in the suspension,
 L_1 is the internal cell thickness in the direction of irradiation,
 L_2 is the total thickness of the cell walls.

ϕ_l and ϕ_s have a relationship of $\phi_l = 1 - \phi_s$. A transmittance T is defined as the ratio of the transmission of the container when filled with studied sample dispersion to that when filled with pure suspending liquid. Therefore, it comes up with:

$$T = e^{-\phi_s(a_s - a_l)L_1} \quad (\text{AII.6})$$

which can also be written as

$$\ln T = -A\phi_s \quad (\text{AII.7})$$

where

A is a constant for a particular apparatus and suspension components.

Then, the T value can be used to calculate the weight percent of particles (equation AII.8) at a given depth h , by equation

$$P = 100 [\ln T_i / \ln T_0] \quad (\text{AII.8})$$

where

T_0 is the transmittance of the suspension at the initial state.

Appendix III: Chemical Analysis

General analysis:

1. Weigh sample (in powder) 1.5g (± 0.1 g)
2. Ignition
3. Calculate ignition loss
4. Weigh sample accurately 0.1g (± 0.0001 g)
5. Mix sample with 0.6g Lithium Metaborite (LiBO_2)
6. Heat sample on a meker burner for 30 minutes
7. Desolve the resulting glass in 900ml of deionized water
8. Add 15ml of Hydrochloric acid
9. Make it to 1000ml by adding deionized water

Analysis of the resulting solution was then undertaken using the ICP apparatus at Royal Holloway & Bedford College.

Ferrous iron determination

1. Weigh sample 0.5g in a Pd/Au crucible
2. Add 10ml of dilute H_2SO_4
3. Add 5ml of dilute HF
4. Boil the mixed sample solution in a Ni crucible using a Bunsen burner for 12 minutes and allow it to cool down
5. Make a solution with 300ml of distilled water, 10ml of 1:1 H_2SO_4 , 10ml of saturated Boric acid solution and 0.5ml of N-phenylanthranilic acid
6. Add the boiled sample to the made up solution
7. Titrate the mixture with N/20 standard potassium dichromate whilst stirring continuously. The end point is marked by the colour change of the solution from almost colourless to violet-red.

Use the formula to calculate the Ferrous iron in percentage:

$$F = (D * 3.5918) * 100\% / W$$

where F: Ferrous iron (%)

D: N/20 standard potassium dichromate used for titration (ml)

W: Sample weight (mg)

The total iron content can be obtained from the general analysis. Ferric iron can therefore, be calculated and so can the ratio of Fe⁺³ to Fe⁺² in the original sample.

Table AIII.1 The chemical composition of the Barbados samples (row data)

Chemical comp.	BD - I			BD - II			BD - III		
	1	2	3	1	2	3	1	2	3
SiO ₂ (%)	65.28	61.38	64.42	66.24	64.48	68.65	66.26	71.34	63.40
Al ₂ O ₃ (%)	15.92	18.68	17.03	17.40	20.37	16.27	16.35	14.10	17.34
FeO (%)	3.37	3.32	3.86	1.09	1.01	1.41	1.05	0.79	0.96
Fe ₂ O ₃ (%)	1.73	1.63	1.60	0.93	0.77	1.36	2.70	2.05	3.05
MgO (%)	1.10	1.12	1.10	0.31	0.32	0.47	0.87	0.63	0.84
CaO (%)	0.37	0.36	0.37	0.34	0.35	0.35	0.33	0.30	0.35
Na ₂ O (%)	0.18	0.19	0.18	0.20	0.33	0.18	0.50	0.46	0.39
K ₂ O (%)	1.86	1.86	1.85	0.92	0.92	0.91	0.92	0.94	1.84
TiO ₂ (%)	0.92	0.97	0.90	0.50	0.48	0.63	0.83	0.71	0.83
P ₂ O ₅ (%)	0.06	0.07	0.06	0.03	0.03	0.04	0.05	0.05	0.06
MnO (%)	0.05	0.04	0.04	0.02	0.02	0.03	0.03	0.02	0.03
Ignition loss (%)	6.92	6.77	7.10	8.28	7.83	9.00	7.81	6.12	8.11
Total (%)	97.76	96.39	98.51	96.26	96.91	99.30	97.70	97.51	97.20
Fe ⁺² /Fe ⁺³ ratio	1.95	2.02	2.41	1.17	1.31	1.03	0.39	0.38	0.32

Table AIII.2 The chemical composition of the Taiwan samples (row data)

Chemical comp.	I			II			III		
	TW 1	- 2	3	TW 1	- 2	3	TW 1	- 2	3
SiO ₂ (%)	59.16	57.76	56.90	59.04	58.34	59.17	60.04	58.25	57.20
Al ₂ O ₃ (%)	18.10	18.26	18.76	18.67	18.04	17.85	18.24	18.17	17.61
FeO (%)	4.41	4.76	4.67	4.38	4.60	4.49	3.36	4.06	4.07
Fe ₂ O ₃ (%)	1.44	1.62	1.54	1.61	1.57	1.42	1.46	1.87	1.90
MgO (%)	2.60	2.75	2.71	2.73	2.80	2.68	2.40	2.93	2.80
CaO (%)	0.66	0.80	0.78	0.75	0.91	0.81	1.08	1.08	0.96
Na ₂ O (%)	1.33	1.47	1.28	1.53	1.46	1.47	1.50	1.37	1.34
K ₂ O (%)	3.76	2.81	3.73	3.76	3.76	2.82	1.89	3.75	2.82
TiO ₂ (%)	0.87	0.85	0.86	0.87	0.84	0.85	0.78	0.85	0.87
P ₂ O ₅ (%)	0.08	0.08	0.09	0.08	0.08	0.08	0.09	0.09	0.08
MnO (%)	0.07	0.08	0.07	0.07	0.08	0.08	0.06	0.08	0.07
Ignition loss (%)	6.06	6.12	6.57	5.87	6.05	6.00	5.01	6.29	5.85
Total (%)	98.54	97.36	97.96	99.36	98.53	97.72	95.91	98.79	95.57
Fe ⁺² /Fe ⁺³ ratio	3.06	2.92	3.03	2.72	2.93	3.18	2.30	2.17	2.15

continue

Chemical comp.	IV			V		
	TW 1	- 2	3	TW 1	- 2	3
SiO ₂ (%)	55.92	57.15	56.60	58.00	58.24	56.67
Al ₂ O ₃ (%)	19.02	18.82	19.25	16.72	16.82	16.59
FeO (%)	4.14	4.05	4.24	2.64	2.86	2.65
Fe ₂ O ₃ (%)	2.91	2.74	2.66	3.47	2.99	3.54
MgO (%)	2.50	2.45	2.54	2.40	2.41	2.47
CaO (%)	0.97	0.91	0.87	2.54	2.20	2.40
Na ₂ O (%)	1.00	1.14	1.14	1.28	1.27	1.22
K ₂ O (%)	3.72	3.74	3.72	2.77	2.78	2.76
TiO ₂ (%)	0.90	0.88	0.89	0.84	0.89	0.87
P ₂ O ₅ (%)	0.09	0.09	0.09	0.10	0.10	0.11
MnO (%)	0.09	0.08	0.09	0.08	0.07	0.09
Ignition loss (%)	6.86	6.56	6.77	7.41	7.27	7.54
Total (%)	98.12	98.61	98.86	98.25	97.90	96.91
Fe ⁺² /Fe ⁺³ ratio	1.42	1.48	1.60	0.76	0.95	0.75

Appendix IV: Calibration of Transducers

The soil triaxial deformation cell used in the study is able to monitor the axial load, cell pressure (total confining pressure), both top and bottom pore pressures, axial displacement, and the volume of expelled pore fluid which can be back-calculated to get the volume strain of the specimen. All these measurements are measured using various type of transducers. The calibrations of the transducers are given below.

**Axial Load Proving Ring
Calibration Data**

**Applied Gauge
Stress Readings
(kN)**

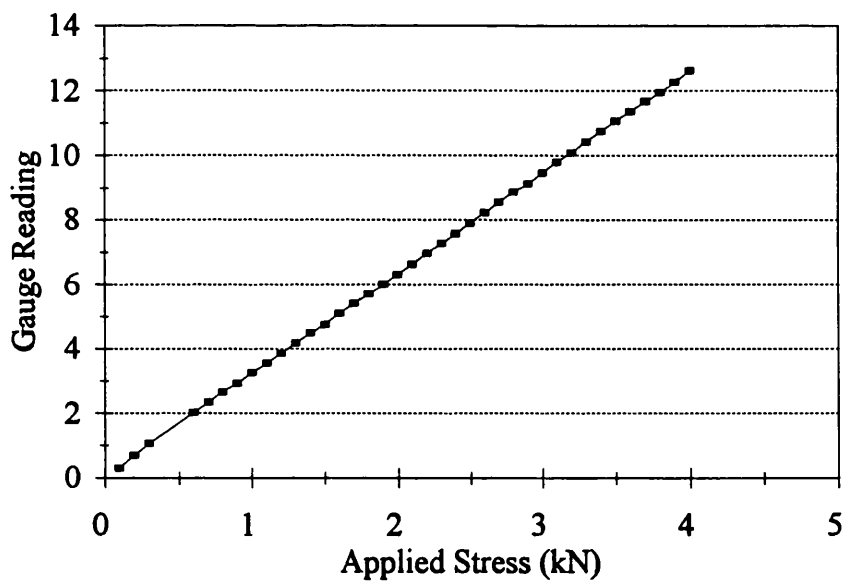
0.1 0.31
0.2 0.7
0.3 1.06
0.6 2.03
0.7 2.34
0.8 2.66
0.9 2.93
1 3.26
1.1 3.55
1.2 3.86
1.3 4.19
1.4 4.5
1.5 4.77
1.6 5.1
1.7 5.41
1.8 5.72
1.9 6.02
2 6.32
2.1 6.64
2.2 6.98
2.3 7.29
2.4 7.58
2.5 7.91
2.6 8.23
2.7 8.56
2.8 8.87
2.9 9.13
3 9.47
3.1 9.81
3.2 10.09
3.3 10.43
3.4 10.76
3.5 11.07
3.6 11.37
3.7 11.69
3.8 11.96
3.9 12.27
4 12.63

Regression Output:

Constant 0.103443
Std Err of Y Est 0.030263
R Squared 0.999993
No. of Observations 38
Degrees of Freedom 36

X Coefficient(s) 3.126253
Std Err of Coef. 0.004372

Calibration of the System Axial Load Proving Ring



**Axial Load Transducer
Calibration Data (Serial No. 1176)**

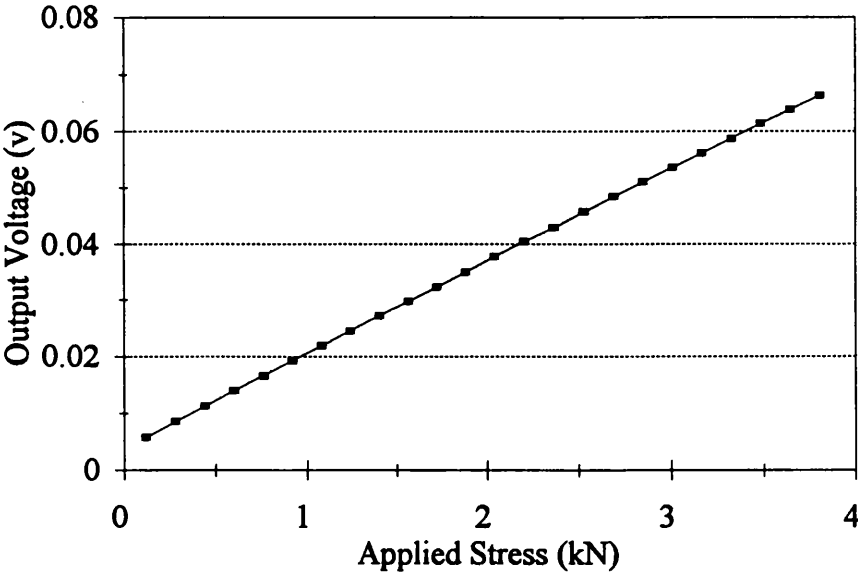
Applied Stress (kN)	Output Voltage (v)
------------------------------------	-----------------------------------

0.120783	0.0058
0.281087	0.00856
0.441391	0.01121
0.601695	0.01393
0.761998	0.01654
0.922302	0.01925
1.082606	0.02188
1.24291	0.02454
1.403214	0.0272
1.563518	0.02977
1.723822	0.03238
1.884126	0.03506
2.04443	0.03777
2.204733	0.04049
2.365037	0.04302
2.525341	0.04575
2.685645	0.04844
2.845949	0.05108
3.006253	0.05366
3.166557	0.05616
3.326861	0.05877
3.487164	0.06139
3.647468	0.0639
3.807772	0.0663

Regression Output:

Constant	0.004028
Std Err of Y Est	0.000141
R Squared	0.999945
No. of Observations	24
Degrees of Freedom	22
X Coefficient(s)	0.016464
Std Err of Coef.	2.6E-05

Calibration of the System Axial Load Transducer



Cell Pressure Transducer
 Calibration Data (Serial No. 57163)

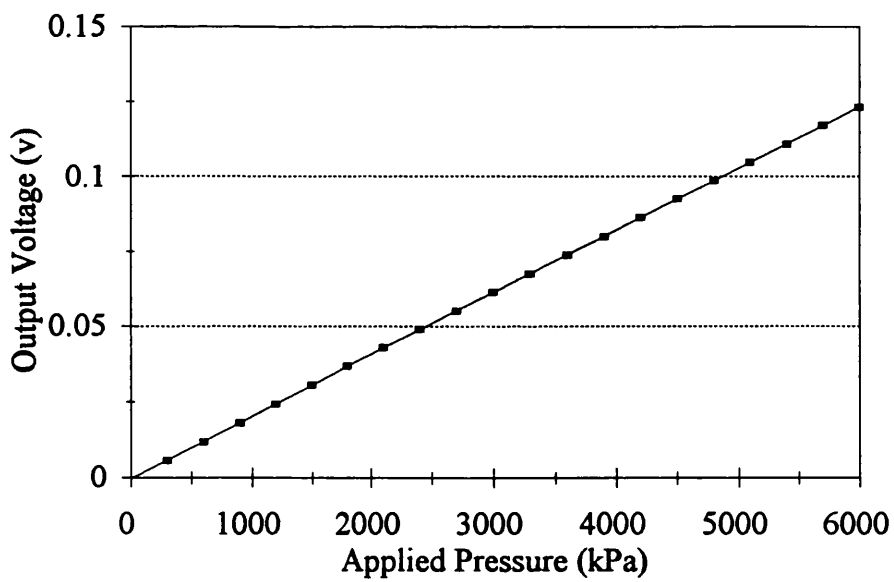
Applied Pressure (kPa)	Output Voltage (v)
------------------------------	--------------------------

0	-0.00043
300	0.00575
600	0.01193
900	0.01812
1200	0.02432
1500	0.03054
1800	0.03674
2100	0.04294
2400	0.04912
2700	0.05529
3000	0.06148
3300	0.06771
3600	0.07391
3900	0.08011
4200	0.08629
4500	0.09246
4800	0.09863
5100	0.10482
5400	0.11103
5700	0.11724
6000	0.1234

Regression Output:

Constant	-0.000434
Std Err of Y Est	2.05E-05
R Squared	1
No. of Observations	21
Degrees of Freedom	19
X Coefficient(s)	2.06E-05
Std Err of Coef.	2.46E-09

Calibration of the System Cell Pressure Transducer



**Top Pore Pressure Transducer
Calibration Data (Serial No. 38801)**

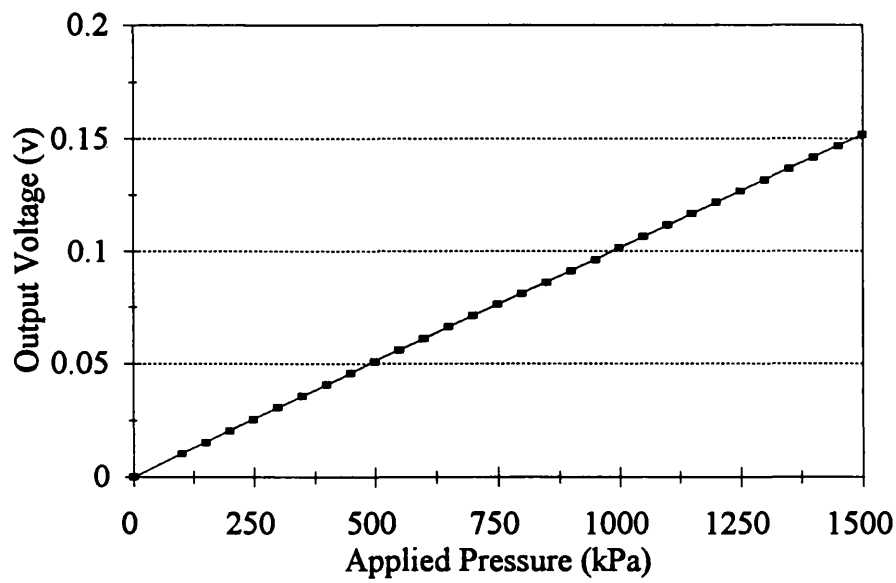
Applied Pressure (kPa)	Output Voltage (v)
---------------------------------------	-----------------------------------

0	0.0001
100	0.01031
150	0.01536
200	0.02043
250	0.0255
300	0.03057
350	0.03567
400	0.04073
450	0.0458
500	0.05087
550	0.05595
600	0.06103
650	0.06611
700	0.07118
750	0.07623
800	0.0813
850	0.08635
900	0.0914
950	0.09644
1000	0.10149
1050	0.10652
1100	0.1116
1150	0.11662
1200	0.12165
1250	0.1267
1300	0.13173
1350	0.13678
1400	0.14178
1450	0.1468
1500	0.15182

Regression Output:

Constant	0.000266
Std Err of Y Est	8.46E-05
R Squared	0.999997
No. of Observations	30
Degrees of Freedom	28
X Coefficient(s)	0.000101
Std Err of Coef.	3.54E-08

Calibration of the System Top Pore Pressure Transducer



**Bottom Pore Pressure Transducer
Calibration Data (Serial No. 57834)**

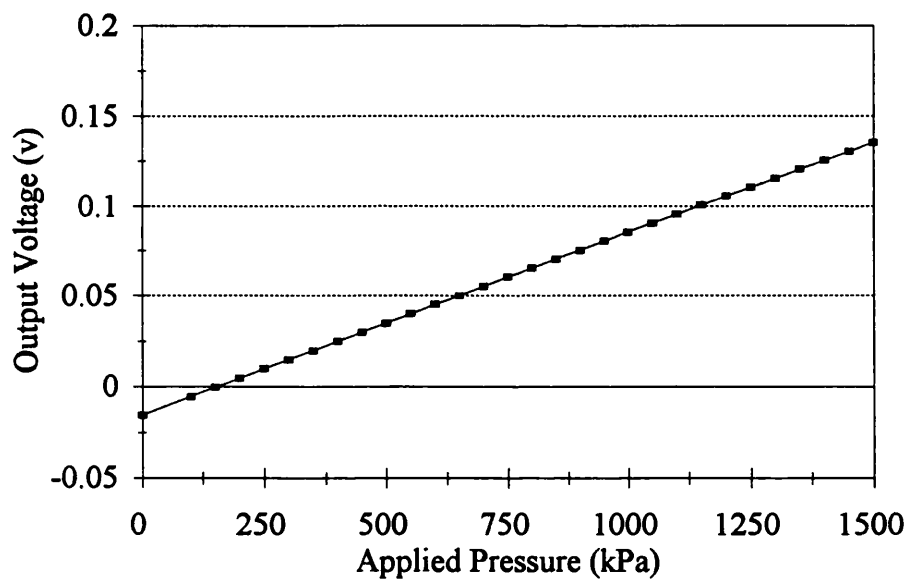
Applied Pressure (kPa)	Output Voltage (v)
---------------------------------------	-----------------------------------

0	-0.01536
100	-0.00522
150	-0.00018
200	0.00492
250	0.00996
300	0.01499
350	0.02004
400	0.02509
450	0.03014
500	0.03518
550	0.0402
600	0.04523
650	0.05026
700	0.0553
750	0.06034
800	0.06538
850	0.07041
900	0.07544
950	0.08048
1000	0.08553
1050	0.09057
1100	0.0956
1150	0.10064
1200	0.10566
1250	0.11066
1300	0.11563
1350	0.12064
1400	0.12564
1450	0.13063
1500	0.13562

Regression Output:

Constant	-0.015201
Std Err of Y Est	7.2E-05
R Squared	0.999997
No. of Observations	30
Degrees of Freedom	28
X Coefficient(s)	0.000101
Std Err of Coef.	3.02E-08

Calibration of the System Bottom Pore Pressure Transducer



Axial Displacement Transducer
 Calibration Data (Serial No. HS50/6968)

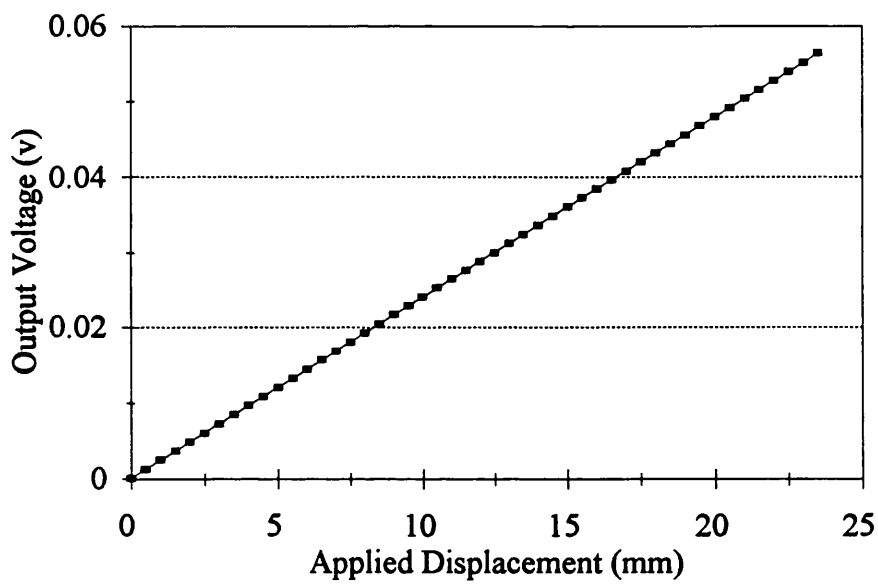
Applied Disp. (mm)	Output Voltage (v)
--------------------------	--------------------------

0	0.00014
0.5	0.00132
1	0.00252
1.5	0.00371
2	0.00491
2.5	0.00611
3	0.00731
3.5	0.00852
4	0.00971
4.5	0.01091
5	0.0121
5.5	0.0133
6	0.01451
6.5	0.01571
7	0.01691
7.5	0.0181
8	0.0193
8.5	0.0205
9	0.0217
9.5	0.02292
10	0.02412
10.5	0.02531
11	0.02651
11.5	0.0277
12	0.0289
12.5	0.03011
13	0.03132
13.5	0.03251
14	0.0337
14.5	0.0349
15	0.03609
15.5	0.0373
16	0.0385
16.5	0.0397
17	0.04089
17.5	0.04208
18	0.04328
18.5	0.04448
19	0.04569
19.5	0.04689
20	0.04807
20.5	0.04926
21	0.05046
21.5	0.05166
22	0.05286
22.5	0.05406
23	0.05525
23.5	0.05644

Regression Output:

Constant	0.000127
Std Err of Y Est	1.18E-05
R Squared	1
No. of Observations	48
Degrees of Freedom	46
X Coefficient(s)	0.002397
Std Err of Coef.	2.45E-07

Calibration of the System Axial Displacement Transducer

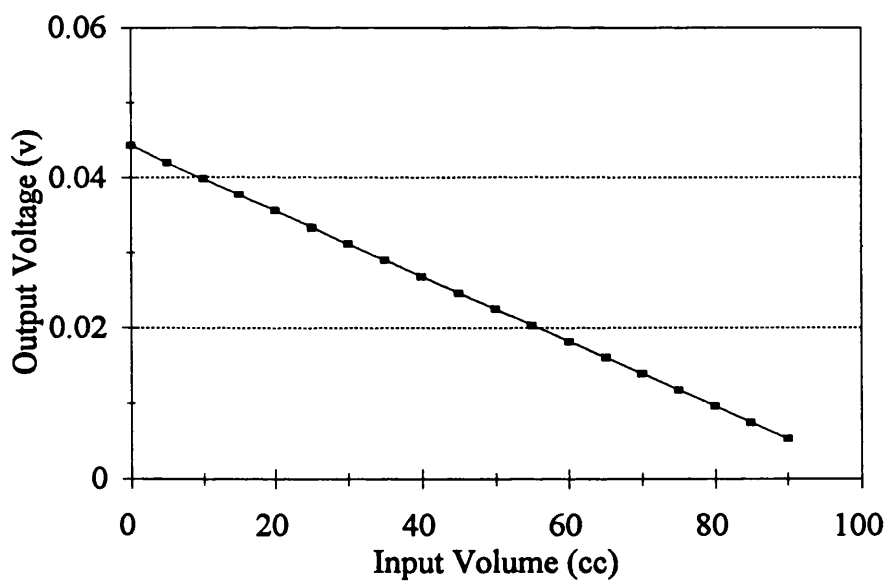


**Volume Gauge
Calibration Data (Serial No. 3077-25)**

Input Volume (cc)	Output Voltage (v)
0	0.04438
5	0.042
10	0.03982
15	0.03767
20	0.03554
25	0.03339
30	0.03123
35	0.02907
40	0.02691
45	0.02474
50	0.02256
55	0.0204
60	0.01823
65	0.01608
70	0.01393
75	0.01177
80	0.00962
85	0.00747
90	0.00531

Regression Output:	
Constant	0.044206
Std Err of Y Est	4.97E-05
R Squared	0.999984
No. of Observations	19
Degrees of Freedom	17
X Coefficient(s)	-0.000433
Std Err of Coef.	4.16E-07

Calibration of the System Volume Gauge



Appendix V: Undrained Deformation Process

A series of photographs have been taken while one of the Taiwan most weathered specimens was being subject to an undrained loading. This provides an idea visually of how the sample was deformed as well as the process of the shear plane development. Photographs were taken approximately every half percent axial strain.

